



UNIVERSITÀ DEGLI STUDI DI NAPOLI
FEDERICO II



PhD Thesis in

SCIENZE DELLA TERRA, DELL'AMBIENTE E DELLE RISORSE

XXIX Ciclo

**Integration of field investigations and remote
sensing techniques for the assessment of
landslide activity and damage**

Candidate:

Del Soldato Matteo

Advisor:

Prof. Pantaleone De Vita

Co-Advisors:

Prof. Domenico Calcaterra

Prof. Nicola Casagli

Prof. Roberto Tomás

PhD Coordinator:

Prof. Maurizio Fedi

Academic Year 2015/2016

“Ti sembra che tu stia facendo tante cose differenti, ma in realtà ne stai facendo solo una...ricerca sulle frane”

“It seems that you are doing several different things, but really you are doing only one...landslide research”

Cit. N.C.

Table of contents

LIST OF FIGURES.....	III
LIST OF TABLES	X
Abstract	1
1 Introduction	3
1.1 STRUCTURE OF THE THESIS.....	6
1.2 OBJECTIVES	7
2 Landslide definition and classification	8
2.1 LANDSLIDES	8
2.2 LANDSLIDE CLASSIFICATION.....	14
2.2.1 <i>Falls and topples</i>	15
2.2.2 <i>Slides</i>	17
2.2.3 <i>Spreads</i>	17
2.2.4 <i>Flows</i>	18
2.3 LANDSLIDE IN STRUCTURALLY COMPLEX FORMATIONS OF SOUTHERN APENNINE.....	21
3 Test areas.....	23
3.1 GEOLOGICAL AND GEOMORPHOLOGICAL FEATURES OF AGNONE (SOUTHERN ITALY)	23
3.1.1 <i>Available data</i>	26
3.2 GEOLOGICAL AND GEOMORPHOLOGICAL FEATURES OF VOLTERRA (CENTRAL ITALY)	30
3.2.1 <i>Available data</i>	34
4 Methodology.....	37
4.1 REMOTE SENSING ANALYSIS	37
4.1.1 <i>3D reconstruction of aerial images</i>	37
4.1.2 <i>Persistent Scatterer Interferometry</i>	45
4.1.2.1 <i>Radar</i>	45
4.1.2.2 <i>Synthetic Aperture Radar (SAR)</i>	47
4.1.2.3 <i>SAR Interferometry</i>	52
4.1.2.4 <i>Coherent Pixel Technique (CPT)</i>	54
4.1.2.5 <i>SqueeSARTM</i>	55
4.1.2.6 <i>Vertical (V_v) and Horizontal (H_v) velocity</i>	56
4.1.2.7 <i>Time series analysis</i>	60
4.2 FIELD INVESTIGATIONS	62

4.2.1	<i>Damage classification</i>	62
4.2.1.1	<i>Existing approaches</i>	62
4.2.1.2	<i>Burland (1977)</i>	63
4.2.1.3	<i>Alexander (1986)</i>	64
4.2.1.4	<i>Chiocchio et al. (1997)</i>	65
4.2.1.5	<i>Cooper (2008)</i>	66
4.2.1.6	<i>DPC (Baggio et al., 2009)</i>	68
4.2.2	<i>Global Position System (GPS) survey</i>	69
4.3	DAMAGE - DISPLACEMENT RELATIONSHIP	71
4.3.1	<i>Velocity projected along the slope (V_{slope})</i>	71
4.3.2	<i>Cumulated displacement projected along the slope (D_{slope})</i>	72
5	Application and results	73
5.1	NEW RANKING	73
5.2	AGNONE LANDSLIDE (MOLISE REGION)	79
5.2.1	<i>Reconstruction of evolutionary stages and monitoring of the landslide</i>	79
5.2.2	<i>Damage classification of facilities</i>	102
5.3	VOLTERRA LANDSLIDE (TUSCANY REGION)	125
5.3.1	<i>Evolutionary stages and monitoring of the landslide</i>	125
5.3.2	<i>Damage classification of buildings</i>	142
5.4	RELATIONSHIP DAMAGE-DISPLACEMENT	156
6	Discussion	170
7	Conclusions	179
8	Future research topics	181
9	List of publications	182
9.1	PROCEEDINGS	182
9.2	JOURNALS	182
10	Acknowledgments	183
11	References	184

List of figures

Fig. 2.1 - Spatial distribution of fatal single or grouped landslides (Petley, 2012)	8
Fig. 2.2 - Block diagram of ideal complex slide-earth flow (Varnes, 1978).....	9
Fig. 2.3- Topple profile section with the modified state of activity of landslide by WP/WPI (1993): a) active landslide; b) suspended landslide; c) reactivated landslide; d) dormant landslide; e) abandoned landslide; f) stabilized landslide; g) relict landslide. The state comprehended between d and g are considered inactive (WP/IWP, 1993).	12
Fig. 2.4 - Profile section showing different distribution of activity of a landslide, modified by WP/WPI (1993): a) advancing landslide; b) retrogressive landslide; c) enlarging landslide; d) diminishing landslide; e) confined landslide; f) moving landslide; g) widening landslide (WP/IWP, 1993).....	13
Fig. 2.5 - Scheme showing different landslide style activity: a) complex landslide; b) composite landslide; c) successive landslide; d) single landslide; e) multiple landslide (WP/IWP, 1993).	14
Fig. 2.6 -Example of evolution of a rock fall (Lynn Highland, http://blogs.agu.org/landslideblog/2011/10/13/a-gallery-of-landslide-images/) with explaining scheme of the phenomenon (b) (Hungre et al., 2014).	16
Fig. 2.7 - Example of rock topple (http://forums.hardwarezone.com.sg/japan-271/time-trip-report-16-oct-28-oct-tokyo-matsumoto-osaka-hiroshima-2550242.html) (a) with explanation of the possible Single and Multiple Topples evolution (b). (Hungre et al., 2014)	16
Fig. 2.8 - Rock slide occurred on the Highway 41 in Madera County on, Jan. 19, 2016 (http://www.fresnobee.com/news/local/article55419970.html).	17
Fig. 2.9 - Example of lateral spread (http://www.teara.govt.nz/en/photograph/8793/lateral-spread) at the locality known as Earthquakes, in the Waitaki Valley, North Otago(a) and scheme of the phenomenon (Hungre et al., 2014). ..	18
Fig. 2.10 - a) Rock flow of obsidian lava at Rock Mesa in Three Sisters Area, protected area Three Sisters Wilderness, Oregon, USA (https://commons.wikimedia.org/wiki/File:Rock_Mesa_obsidian_flow_in_Oregon_in_2011_(9)); b) Rock Avalanche occurred in Val Pola, upper Valtellina (Lombardy region, Italy) on July 28, 1987 (http://www.mergili.at/worldimages/picture.php?/7534).	19
Fig. 2.11 - Earthflow in Alaj, Kirghizistan (a) (http://www.panoramio.com/photo/12660372) and explanation of the ideal earth flow (b) (Hungre et al., 2014).	19
Fig. 2.12 - a) Debris flow occurred in the town of La Conchita, California, USA on January 2005. (http://www.geotimes.org/nov05/feature_landslides.html). b) Mudflow in 2014 in Mesa County, Colorado (http://blogs.agu.org/landslideblog/2014/05/28/grand-mesa-1/).	20
Fig. 2.13 - Categories of Structurally Complex Formations (Esu, 1977) (a); Italian Structurally Complex Formations outcrops and location of famous studied landslide in the geotechnical literature (D'Elia, 1991) (b).	22
Fig. 3.1 - Location of the Colle-Lapponi - Piano Ovetta landslide in the Agnone municipality.	23
Fig. 3.2 - Geological sketch map (Vezzani et al., 2004) of the area of interest in Agnone with the current contour of the landslide reported in red.	24
Fig. 3.3 - Geological section A-A' traced along the area of interest of the CL-PO landslide (ISPRA, 1971; Vezzani et al., 2004).	25
Fig. 3.4 - Engineering-geological interpretation of the data acquired in the boreholes S1, S2, S3 and S4, modified from	

Calcaterra et al. (2008) and Del Soldato et al., under review_a. A - hard rock fragments and clays; B - clays and sands; C - limestone level; D - marls and clays. 26

Fig. 3.5 -Picture and scheme of the inclinometer installed to monitor the displacement affecting the CL-PO landslide. 27

Fig. 3.6 - CL-PO landslide and location of the inclinometers. 27

Fig. 3.7 - CL-PO landslide and location of the Corner Reflectors. 29

Fig. 3.8 - Location of the municipality of Volterra (a) with the investigated area highlighted by the red box. b) The geological map of the whole municipality..... 31

Fig. 3.9 - Sectors of Volterra town. In red the two investigated sectors involved by a landslide are highlighted. 32

Fig. 3.10 - Geology of the SW area of the municipality of Volterra with the overlapped landslide and badland inventories (a) and two geological cross-sections (b). 1 - sandy detritus; 2 - clay detritus 3 - "Volterra limestone"; 4 - "Villamagna sand"; 5 - "Blue clay"; 6 - clay; 7 - sliding surface (GEOSER s.c.r.l. & GEOPROGETTI company)..... 33

Fig. 3.11 - Inventories of landslide (a) and badlands (b) affecting the municipal territory of Volterra. 34

Fig. 3.12 - Topographical map (1:5000) of the southwestern area of Volterra with the location of the drillings and the inclinometric investigations (GEOSER s.c.r. & GEOPROGETTI, 2010). 35

Fig. 3.13 - Details of the inclinometer used to monitor the landslide in Volterra. 35

Fig. 4.1 - Adapted workflow for 3D reconstruction by non-digital historical images. 39

Fig. 4.2 - a) Screenshot of the setting for the suitable alignment for historical aerial photos, when the camera position is unknown. B) Sparse cloud generated after the alignment of the images..... 41

Fig. 4.3 - a) Dense cloud of a Ligurian area where several Ground Control Points and Tie Points were added. b) Example of the table in which the errors of the inserted GCPs and TiePoints are shown. 42

Fig. 4.4 - a) Reshaping of the Box where the Dense Cloud will be generate. b) Setting of the Dense Cloud tool. 43

Fig. 4.5 - Setting to generate the Mesh (a) and the Texture (b). 44

Fig. 4.6 - Parameters for the DEM generation (a) and an example of DEM with 25 m contour (b). 44

Fig. 4.7 - Preferences to build the orthomosaic (a) for a region covered by three historical images with sufficient overlapping area (b) to generate it. The result is a big georeferred image (c) covering the entire area with enough overlapping to correlate the single shot..... 45

Fig. 4.8 - Image Radar geometry (Trivero and Biamino, 2010). 46

Fig. 4.9 - Relation between the LOS and the geometry for the incidence angle ϑ and for the local incidence angle ϑ_l (Rizzoli and Bräutigam, 2014). 47

Fig. 4.10 - The geometry and terms of the SAR systems (Ouchi, 2013). H_{SAR} : height of the SAR platform; c : velocity of the microwave; $r(t)$: slant-range distances at the azimuth time t ; R : slant-range distances at the azimuth when the antenna is nearest to the target at the origin of the ground coordinate system (x, y) 47

Fig. 4.11 - Microwave spectrum used for the SAR methods (Ouchi, 2013) related with the satellite constellation on which were mounted (past, present and future launches)..... 48

Fig. 4.12 - Geometric distortion effects (Farr, 1993): a) foreshortening (www.nrcan.gc.ca); b) layover (Xu and Cumming, 1996); c) shadowing (www.geo.uzh.ch). 50

Fig. 4.13 - Ascending and descending orbits (a) with right-looking satellite and the combination (b) of the orbit measurements to obtain the true vertical and east-west components of the motion (tre-altamira.com). 51

Fig. 4.14 - Two SAR images of the same area are acquired at different times recording, by means an interferogram, surface movements occurring between the two acquisitions (www.ga.gov.au). 52

Fig. 4.15 - Scheme of the spatial acquisition configuration by ascending and descending orbits and the composition in vertical and horizontal velocity components of an almost-vertical real motion (Bianchini and Moretti, 2015). 58

Fig. 4.16 - Flow-chart of the process to extract the Vertical and Horizontal components starting from PS of both ascending and descending geometries (Rosi et al., 2014)..... 59

Fig. 4.17 - GPS sensor (a) and an example of to application during a field campaign survey in Agnone (b)..... 70

Fig. 5.1 - Referring scheme of the damage which could affect structures and grounds in a landslide-prone area: a) thin and open vertical cracks; b) thin and open horizontal fractures; c) diagonal tension cracks; d) severe open damage; e) local crushing with or without loss of material; f) hairline fissure in plaster; g) loss of plaster enclosed by cracks; h) horizontal and vertical damage close to the intersection of walls; i) distortion of services as doors, windows or chimneys; j) unstable wedge in the intersection of walls severely affected by open cracks; k) bended roof; l) collapse of part of the structure (e.g. roof); m) open and thin fractures between the external façades and the sidewalk; n) open (sometimes filled by soil and grass) and thin parallel damage in sidewalk; o) open (sometimes filled by soil and grass) and thin perpendicular fractures in sidewalk; p) damage due to the propagation of the landsliding effects on horizontal structures; q) extensive ground cracking with minor and major scarps; r) fracture retracing the scarps of the landslide with tension cracks in soil; s) thin fissure in ground surfaces; t) piece of horizontal structure fractured and collapsed along the scarp of the landslide (from Del Soldato et al., under review_b). 74

Fig. 5.2 - Suggested recording scheme to survey damage on structures (Del Soldato et al., under review_b). 77

Fig. 5.3 - Precipitation graphs of two main reactivations that occurred in January 2003 (a) and between December 2004 and January 2004 (b) (Del Soldato et al., under review_a). 81

Fig. 5.4 - Displacement measured between 2006 and 2016 of some topographical benchmarks located inside the CL-PO landslide. The dimension and the orientation of the arrows reflect to the value of the displacement. 82

Fig. 5.5 - Visual evolution of the Colle Lapponi - Piano Ovetta landslide from 1945 to 2007 by means of the remote sensing analysis to realize the 3D models and some pictures shot from the same place..... 83

Fig. 5.6 - Localization of the inclinometers in the CL-PO landslide. 84

Fig. 5.7 - Graphic restitution of the inclinometric data. a) S6 in the crown of the landslide; b) S4 in the upper part of the body of the mass movement; c) S3 in the middle of the body landslide; d) S5 (ex S2); e) S1 in the toe of the landslide when it was installed..... 86

Fig. 5.8 - Visual evolution of the Colle Lapponi - Piano Ovetta mass-movement by means of two oblique terrestrial pictures taken during field surveys conducted in November 2015 (a) and in July 2016 (b)..... 87

Fig. 5.9 - Difference in volume between the reconstructed 3D Points Clouds of 1945 and of 2003 segmented on the boundary of the landslide that occurred in 2003 (a) and on the contour of the landslide traced in 2016 (b)..... 88

Fig. 5.10 - Orthomosaic of the CL-PO landslide referred to 1991 with highlighted in the red circle the fulfilled works between 1986 and 1991..... 89

Fig. 5.11 - Displayed displacement for the Corner Reflector located into the body of the CL-PO landslides map measured by means of GPS campaigns from 2010 to 2016. The dimension and the orientation of the arrows reflect the value of

the displacement.	90
Fig. 5.12 - Geomorphological map of the landslide area and its uphill region.	91
Fig. 5.13 - PS covers the CL-PO landslide acquired by ERS (a), ENVISAT (b) and COSMO-SkyMed (c) sensors.	92
Fig. 5.14 - Complete time-series merging the data of all sensors showing and confirming the most important period of movement due to the main reactivations that occurred between 2003 to 2007. Data are taken on the Build_01 located close to the landslide crown.	93
Fig. 5.15 - Areas where the time series were separately examined.	94
Fig. 5.16 - Categorization of the ERS ascending and descending PS time series of the surrounding of the CL-PO landslide.	95
Fig. 5.17 - Classification of ENVISAT ascending and descending PS time series of the surrounding of the CL-PO landslide.	96
Fig. 5.18 - Categorization of the COSMO-SkyMed ascending and descending PS time series of the surrounding of the CL-PO landslide.	97
Fig. 5.19 - Sample time series registered by the ERS1/2 (a) and COSMO-SkyMed (b) satellites on Area 1.	98
Fig. 5.20 - Sample time series registered by the COSMO-SkyMed satellites on Area 2.	99
Fig. 5.21 - Sample of a time series of the Area3 recorded by the ENVISAT sensors from 2002 to 2012.	100
Fig. 5.22 - Sample of the time-series recorded for the Area 3 by the COSMO-SkyMed sensors for the period 2012-2015.	100
Fig. 5.23 - Sample of a time series of the Area 4 recorded by the ENVISAT sensors from 2002 to 2012.	101
Fig. 5.24 - Sample of the time-series recorded for the Area 4 by the COSMO-SkyMed sensors for the period 2012-2015.	101
Fig. 5.25 - Localization of the structures of the Area 4 and their proximity to the closer landslide (a). Open cracks visible between two adjacent constructions (b).	102
Fig. 5.26 - Example of cracks and rupture identified on structures. a) hairline cracks on plaster of masonry wall; b) open crack on reinforced concrete walls; c) open crack of masonry building walls; d) open crack between wall and external sidewalk; e) open crack between external wall and ground surface; f) collapsed roof in a masonry building (Del Soldato et al., under review_a)	103
Fig. 5.27 - Fine (a) and open (b) cracks recognizable on pavement of sidewalks slab; hairline (highlighted by means of red arrows) and open fractures on concrete (c) and masonry walls (d).	104
Fig. 5.28 - Classification of the facilities close to the CL-PO landslide according to Burland, 1977.	105
Fig. 5.29 - Classification of the facilities close to the CL-PO landslide according to Alexander, 1986.	106
Fig. 5.30 - Classification of the facilities close to the CL-PO landslide according to Chiocchio et al. (1997).	107
Fig. 5.31 - Classification of the facilities close to the CL-PO landslide according to Cooper (2008).	108
Fig. 5.32 - Classification of the facilities close to the CL-PO landslide according to the DPC approach (Baggio et al., 2009).	109
Fig. 5.33 - Classification of the facilities close to the CL-PO landslide according to the Del Soldato et al. (NewApproach_under review) approach.	110
Fig. 5.34 -North façade (a) of the building (B01) located on the crown of the landslide with in front a several damage	

concrete sidewalk (b) partially collapsed (red circle).....	110
Fig. 5.35 - Classification of fracture and ruptures recognizable in soil and man-made surfaces by the methods proposed by Cooper (2008) (a) and Del Soldato et al. (under review_b) (b)	111
Fig. 5.36 - Building classification conducted based on the Velocity (a) and the cumulated displacement (b) recorded along the Line of Sight of the ascending orbit of ENVISAT sensor.....	113
Fig. 5.37 - Building classification conducted based on the Velocity (a) and the cumulated displacement (b) recorded along the Line Of Sight of the descending orbit of ENVISAT sensor.	114
Fig. 5.38 - Building classification conducted based on the Velocity (a) and the cumulated displacement (b) recorded along the Line of Sight of the ascending orbit of COSMO-SkyMed sensor.	116
Fig. 5.39 - Building classification conducted based on the Velocity (a) and the cumulated displacement (b) recorded along the Line of Sight of the descending orbit of COSMO-SkyMed sensor.	117
Fig. 5.40 - Building classification by means of the velocity projected along the slope and averaged assessed with ENVISAT sensors for each construction using DEM with 5-m cell resolution (a) and 10-m cell resolution (b).	119
Fig. 5.41 - Building classification using the cumulated displacement projected along the slope and averaged evaluated by ENVISAT sensors for each construction using DEM with 5-m cell resolution (a) and 10-m cell resolution (b).....	121
Fig. 5.42 - Building classification by means of the velocity projected along the slope and averaged assessed with COSMO-SkyMed sensors for each construction using DEM with 5-m cell resolution (a) and 10-m cell resolution (b)...	122
Fig. 5.43 - Building classification by means of the cumulated displacement projected along the slope and averaged evaluated by COSMO-SkyMed sensors for each construction using DEM with 5-m cell resolution (a) and 10-m cell resolution (b).	124
Fig. 5.44 - Landslide inventory in the studied southwestern portion of the municipality of Volterra.....	126
Fig. 5.45 - Evolution of the Le Colombaie and Fontecorrenti areas affected by both landslides (in red) and badlands (in dark blue) reconstructed 3D Point Clouds by means of the SfM techniques applied on historical aerial imagery of 1954 (a), 1965 (b), 1982 (c), 1986 (d) and 1995 (e). The boundaries of the landslides and of the badlands, derive from the inventories of the municipality strategic plan of Volterra (2005).....	127
Fig. 5.46 - Particular in Colombaie sector of the 3D reconstructions of 1965 (a) and 1995 (b) where new buildings uphill of a possible geomorphological shape, in red, were built.	128
Fig. 5.47 - Detection of changes of volume for Le Colombaie and Fontecorrenti areas affected by both landslides (in black) and badlands (in green). The orange circle indicates some buildings build between the 1954 and 1995 were visible as increase of volume.	129
Fig. 5.48 - ERS data in descending orbit bacscattered for the southwestern sector of Volterra town.	130
Fig. 5.49 - ENVISAT products acquired in the ascending (a) and the descending (b) geometries for the southwestern sector of Volterra.....	131
Fig. 5.50 - Localization of the inclinometers in the southwestern sectors of Volterra.....	132
Fig. 5.51 - Temporal sequences of inclinometer measures of five instruments located in the southwest sector of Volterra (GEOSER s.c.r. & GEOPROGETTI).	133
Fig. 5.52 - COSMO-SkyMed products acquired in the ascending (a) and the descending (b) geometries for the	

southwestern sector of Volterra.....	134
Fig. 5.53 - Study areas by means of the extraction of the time-series for each satellite that recorded data.....	136
Fig. 5.54 - Categorization of the ENVISAT ascending and descending PS time series of the whole southwester sector of Volterra town (a) and for the three area of interest (b).....	137
Fig. 5.55 - Classification of the COSMO-SkyMed ascending and descending PS time series of the whole southwester sector of Volterra town (a) and for the three area of interest (b).....	138
Fig. 5.56 - Sample of time-serises of ERS (a) and COSMO-SkyMed (b) sensors acquired in the Area1.....	139
Fig. 5.57 - Sample time-series of ERS data reflecting the situation of the Area2.....	140
Fig. 5.58 - Sample of time-series of ENVISAT (a) and COSMO-SkyMed (b) data of the Area2.....	140
Fig. 5.59 - Sample of time-serises of ERS sensor acquired in Area3 in Fontecorrenti sector.....	141
Fig. 5.60 - Sample of the time-series of ENVISAT (a) and COSMO-SkyMed (b) data of Area3.....	142
Fig. 5.61 - Le Colombaie (a) and Fontecorrenti sectors with the investigated buildings, the landslide and the badlands contours.....	143
Fig. 5.62 - Different types of damage (red and blue arrows) recognized during field surveys on buildings in the southwestern sector of Volterra. a) plaster cracks restored; b) weak and moderate fractures on plaster; c) numerous severe fractures; d) important cracks plunging about 45° and open fractures between the two structures; e) important tilting between two parts of the same buildings.....	144
Fig. 5.63 - Sample of the recording scheme (Del Soldato et al., under review_b) compiled (a), with two images (b and c) of the investigated buildings, used for the recognition of the damage affecting the several surveyed structures in the soutwestern sector of Volterra.....	145
Fig. 5.64 - Classification of buildings damage according to Cooper (2008).....	146
Fig. 5.65 - Classification of constructions damage according to Del Soldato et al. (under review_b).....	147
Fig. 5.66 - Buildings classifications based on the analysis of the velocity (a) and the maximum displacements (b) measured along the Line of Sight of the ascending orbit by ENVISAT sensors.....	148
Fig. 5.67 - Buildings classifications conducted considerin the velocity (a) and the maximum displacements (b) measured along the Line of Sight of the descending orbit by ENVISAT satellites.....	149
Fig. 5.68 - Structures categorization based on the velocity (a) and the maximum displacement (b) recorded along the Line of Sight of the ascending orbit of COSMO-SkyMed sensors.....	151
Fig. 5.69 - Buildings categorization according to the velocity (a) and the maximum displacement (b) measured along the Line of Sight of the descending geometry of COSMO-SkyMed constellation.....	152
Fig. 5.70 - Building classification conducted by the velocity (a) and the maximum displacement (b) projected along the slope and averaged for each construction, acquired by ENVISAT sensors.....	154
Fig. 5.71 - Constructions classification based on the velocity (a) and the maximum displacement (b) projected along the slope and averaged for each structure, acquired by COSMO-SkyMed satellite.....	155
Fig. 5.72 - Graphs between the values of velocity and maximum displacement acquired along the Line Of Sight in the ascending orbit of the ENVISAT sensors and the damage classification of buildings made by Cooper (2008) and Del Soldato et al. (under review_b) for the CL-PO in Agnone.....	157
Fig. 5.73 - Plots of values of the velocity and the maximum displacement reprojected, using a 5-m cell resolution DEM,	

along the slope recorded by ENVISAT satellites respect to the facilities damage ranks by Cooper (2008) and Del Soldato et al. (under review_b) for the CL-PO in Agnone. 158

Fig. 5.74 - Graphs showing the values of velocity and maximum displacement measured by ENVISAT satellites and reprojected along the slope using a 10-m cell resolution DEM, combined to facilities damage ranked by Cooper (2008) and Del Soldato et al. (under review_b) for CL-PO in Agnone. 159

Fig. 5.75 - Graphs showing the values of velocity and maximum displacement acquired along the LOS in the ascending orbit of COSMO-SkyMed constellation related to the damage classification of buildings conducted by Cooper (2008) and Del Soldato et al. (under review_b) for CL-PO in Agnone. 160

Fig. 5.76 - Plots of the values of velocity and maximum displacement acquired along the Line Of Sight in the descending orbit by COSMO-SkyMed satellites and the classes of damage recorded on buildings classified by the approach of Cooper (2008) and Del Soldato et al. (under review_b). 161

Fig. 5.77 - Graphs showing the values of velocity and maximum displacement value acquired by COSMO-SkyMed sensors, reprojected along the slope using a DEM with 5-m cell resolution, compared to the structures damage classified by Cooper (2008) and Del Soldato et al. (under review_b) for the CL-PO in Agnone. 162

Fig. 5.78 - Plots of velocity and maximum displacement reprojected along the slope using a 10-m cell resolution DEM values gathered by COSMO-SkyMed satellites related to the buildings damage ranked by Cooper (2008) and Del Soldato et al. (under review_b) for the CL-PO in Agnone. 163

Fig. 5.79 - Reliability categorization between the levels of damage recorded by Cooper (2008) and Del Soldato et al. (under review_b) and V_{slope} recorded by COSMO-SkyMed satellite for CL-PO in Agnone. 166

Fig. 5.80 - Categorization of the reliability of the V_{slope} of COSMO-SkyMed and the relieved damage for both classification of Del Soldato et al. (under review_b) (a) and Cooper (2008) (b) in the southwestern sectors of Volterra. 168

Fig. 5.81 - Classification of the reliability of the V_{slope} of ENVISAT and the relieved damage for both ranking of Del Soldato et al. (under review_b) (a) and Cooper (2008) (b) in the southwestern sectors of Volterra. 169

List of tables

Table 2.1 - Velocity landslide scale (Cruden and Varnes, 1996).	10
Table 3.1 - Characteristics of the used aerial photographs.	28
Table 3.2 - Main features of the PSI dataset used to study the CL-PO landslide. CSK indicates the COSMO-SkyMed sensor.	29
Table 3.3 - Characteristics of the historical aerial photographs.	36
Table 3.4 - Main features of the PSI dataset in the Volterra site. CSK indicates the COSMO-SkyMed sensor.	36
Table 4.1 - Definition of V_r direction depending on V_v and V_H values (from Rosi et al., 2014).	60
Table 4.2 - Classification of damage according to Burland (1977) modified by Boscardin & Cording (1989).	64
Table 4.3 - Classification of damage according to Alexander (1986).	65
Table 4.4 - Classification of damage according to Chiocchio et al. (1997).	66
Table 4.5 - Classification of damage according to Cooper (2008).	67
Table 4.6 - Classification of damage according to the DPC (Baggio et al., 2009).	69
Table 5.1 - Summary of features of the existing classifications regarding landslide-induced damage.	73
Table 5.2 - New proposed approach (Del Soldato et al., under review_b) for the classification of observable damage affecting facilities and ground surfaces. It was developed based on the scheme of Burland et al. (1977), Alexander (1986), Chiocchio et al., (1997), Cooper (2008) and DPC (Baggio et al., 2009).	75
Table 5.3 - Table of conversion from the level of damage recognized on each sector of the facilities to the classification of the entire structures (Del Soldato et al., under review_b).	78
Table 5.4 - Ground Control Points precision carried out by the reports of Photoscan.	80
Table 5.5 - Temporal sequence of the inclinometric measurements (GEOSERVICE).	84
Table 5.6 - Summary of the GPS measurements conducted for the CL-PO landslide.	90
Table 5.7 - Example of buildings located in different place respect to the landslide that show a low average annual velocity (V_{slope}) but reach noticeable cumulated displacements. The same results were carried out using both the DEM with 5-m cell resolution and 10-m cell resolution.	120
Table 5.8 - Reliability categories of the relationship between absolute value of V_{slope} and surveyed levels of damage.	164

Abstract

The aim of the PhD thesis was to look for a relationship between the landslide-induced damage recorded on structures and facilities based on the results of several field campaigns and kinematic parameters quantitatively estimated by remote sensing techniques. Investigations were developed on two test sites: a deep-seated landslide in Colle Lapponi-Piano Ovetta in municipality of Agnone (Molise region, southern Italy) and the landslides affecting the southwestern sector of Volterra (Tuscany region, central Italy).

First of all, a re-enactment of the evolution of both landslides were conducted, by means of 3D reconstructions based on historical aerial series of images and the analysis of Persistent Scatterers of ERS1/2, ENVISAT and COSMO-SkyMed satellites. The 3D Points Clouds and models were developed on several sets of aerial historical images dating from different years starting from 1945 and 1954 for Agnone and Volterra, respectively. To better understand the morpho-evolutionary stages, a qualitative assessment of changes of volume were made combining the oldest and the latest 3D reconstructed Points Clouds. This interpretation, even if qualitative and not quantitative, can be helpful for understanding possible effects of future reactivations and as a support to realize mitigation plans, susceptibility maps and other useful for the local administrators. The Persistent Scatterers were used to monitor the evolution in recent years, up to 2015.

Then, for both case studies, the damage was revealed on structures and facilities by several field surveys and classified by means of five literature damage categorizations. During their application, some drawbacks and benefits of the methodologies were carried out and a new approach to improve the categorization of the damage on structures, facilities and ground surfaces was developed. This was conceived in two subsequent phases: i) a classification to use during the field campaign to quantify the severity of cracks and fractures on structures, facilities and ground surfaces; ii) an *a posteriori* ranking to apply on the entire structure, involving the extension of damage classes, performed by a cell-grid matrix. Furthermore, a damage recording scheme, useful for the recognition of cracks and fractures during the field surveys, was proposed. A critical comparison between the results obtained applying the different classification approaches, then followed. Buildings and facilities, for both sites, were categorized using also kinematic parameters such as velocity and maximum displacement measured along the Line Of Sight, derived by A-DInSAR, and their absolute values re-projected along the steepest local slope. Once characterized and categorized all structures and facilities of both sites of interest, a correlation between the surveyed damage classes and the deriving parameters by satellite were looked for. The investigation was carried to understand the behaviour of entire structures, subject to displacements. The first analysis was conducted on the Agnone test site where for several constructions an upper regression line between damage categories and velocity reprojected along

the slope was recognized. Some outlayers were identified, mainly for low damage levels, then singularly investigated. To assess the reliability of all the structures, a matrix involving damage and velocity along the slope parameter acquired by ENVISAT and COSMO-SkyMed sensors was developed in order to obtain a classification. To validate the correlation and the reliability matrix the same procedure was applied to the Volterra site. Once asserted the validity of the relation between the velocity reprojected along the steepest slope and the classes of damage also for this area, the reliability matrix was applied on the constructions of the Volterra site. In this way, the relation between the displacement occurred during the period covered by ENVISAT and COSMO-SkyMed shows how the surveyed damage construction are related to the displacement. Some areas where damage occurred in the 2000 shows high reliability with ENVISAT recorded velocity, while others structures exhibits high reliability with COSMO-SkyMed data.

The results were interesting because they highlight the fact that for some construction there is correlation between velocity of displacement of the entire structure and affecting damage; for others, instead, the high damage is related to the differential settlement and not necessarily to a high rate of displacement velocity.

1 Introduction

Landslides are among the most important, natural or man-induced, gravity-controlled processes that worldwide represent one of the most widespread geological hazards. After earthquakes, landslides cause catastrophic effects with consequent fatalities and high socio-economic damages to man-built structures (e.g. replacement, repair or maintenance of damaged structures) with direct and indirect costs (and many others, difficult to evaluate, e.g. losses of service) (Schuster and Fleming, 1986; Schuster, 1996; Godt et al., 2000). Dimension and velocity of mass-movements, magnitude and typology of landslide mechanisms, involved lithologies, morphological features and consequences of anthropic activity are the main factors that determine the amount of total costs. Several predisposing and driving factors both natural and, sometimes worse, anthropic, e.g. deforestation or unsuitable urban planning (Wu and Qiao, 2009; Di Martire et al., 2012; Tofani et al., 2013b; Wu et al., 2015), can trigger mass-movements and determine their evolution.

The investigation of slope instability, mainly in urban areas affected by landslides, is an important issue for mitigation planning and landslide risk management. Physical vulnerability, defining the level of damage of lifelines and buildings, is a key parameter in risk estimation. Usually great attention is paid in planning strategies in order to prevent or reduce landslide disasters, to assess their impact and damage to understand the possible evolution. The assessment of damaging grade affecting buildings is useful to set countermeasures for avoiding future losses (Del Soldato et al., 2016a; Del Soldato et al., under review_a). Alexander (1986) demonstrated that the analysis of landslide-induced damage could help under several perspectives: administrative, planning, scientific and engineering design. Unfortunately it is common, in Italy as in other countries, that facilities, i.e. buildings, roads and infrastructures, are built on unstable areas where historically landslides have already occurred (Mansour et al., 2011), but at present the awareness of these events is lost. The continuous expansion of the urban fabrics, as a natural consequence of demographic growth (Rybár, 1997), induces people to occupy territories where dormant or old and forgotten active landslides caused ruinous events in the past. Moreover, the disregard of Italian laws and subsequent several amnesties for their infringement have facilitated the realization of structures and infrastructures in hazardous regions, such as volcanic or landslide-prone areas. Furthermore, the urban fabric expansion could cause modifications to hillslope morphology, inducing terrain remobilization and reactivation of previously dormant old slope instabilities, completely ignoring millennial knowledge of negative experiences (Chiocchio et al., 1997).

Among the methods applicable for the recognition of landslides state of activity, remote sensing encompasses a series of techniques that usefully helps the field monitoring of ground displacements (e.g. Colesanti et al., 2003; Colesanti and Wasowski, 2006; Dewitte et al., 2008; Bianchini et al., 2012; Bianchini et

al., 2013; Tofani et al., 2013b; Bianchini et al., 2015a; Hsieh et al., 2016). Such methodologies have become increasingly significant in the last two decades thanks to the technological progress that allowed the investigation, at regional or local scale, of the Earth's surface dynamics. To study "young" movements and their recent evolution, since the early nineties, radar satellite images, appropriately elaborated, allow the estimating of displacements and ground movements by means of interferometry and Persistent Scatterers (e.g. Metternicht et al., 2005; Tralli et al., 2005; Cigna et al., 2010; Del Ventisette et al., 2014). Concerning ground deformations that occurred prior to 1992, year in which the first radar sensor was launched, aerial photos still play a key role in the geomorphological and environmental analysis of natural processes (Carrara et al., 2003; Hapke, 2005).

Several methods to investigate historical aerial images, for instance software allowing the 3D vision by anaglyph glasses, 3D computer vision algorithm (Snavely et al., 2008; Westoby et al., 2012) or image-based modelling and reconstruction (Aliaga et al., 2002; Pollefeys et al., 2004) were developed surpassing the use of the obsolete stereoscopy technique. Furthermore, in the last decades the *Structure from Motion (SfM)* technique was developed to reconstruct buildings, monuments and archaeological sites in 3D (Furukawa and Ponce, 2010; Doneus et al., 2011; Verhoeven et al., 2012) as well as for unmanned aerial vehicles (UAV) applications (Turner et al., 2012; Lucieer et al., 2013; James and Robson, 2014) in order to produce Digital Elevation Models (DEMs). *SfM* technique can be applied on old aerial images to reconstruct 3D models in order to analyse the evolution in time of ground deformations and infrastructures (Riquelme et al., under review). Recently, further remote sensing techniques, like many different multi-temporal InSAR (Synthetic Aperture Radar Interferometry) techniques, e.g. Persistent Scatterer Interferometry (PSI) or SqueeSARTM (Ferretti et al., 2011), have been successfully and diffusely applied to assess ground deformations in order to support landslide studies over wide areas (e.g. Farina et al., 2006; Bianchini et al., 2012; Cascini et al., 2013) as well as to investigate building deformations and settlements at local scale by means (Ciampalini et al., 2014; Di Martire et al., 2014; Sanabria et al., 2014; Bianchini et al., 2015a). The correction to the regional trend, the reliability of the time series of Persistent Scatterers and an estimation of the date with abrupt changes were made by means of the PS Time approach (Berti et al., 2013) and the Notti et al. (2015) methodology.

Finally, spatial and kinematic characterization of landslides as well as the recognition and classification of landslide-induced damage effects on structures and infrastructures (Goetz et al., 2011; Guzzetti et al., 2012; Van Westen, 2013; Gullà et al., 2016), are fundamental to better delineate mass-movement boundaries. Furthermore, the same parameters allow to investigate the evolution of slope instability in time, in order to avoid repeated occurrences and to better plan mitigation measures (Del Soldato et al., under review_b).

The PhD thesis was developed on two sample areas affected by landslides where their geomorphological evolution was analysed and landslide-induced damage on buildings and facilities classified. Furthermore, the relationship between displacements affecting the structures and the related damage was analysed. A

comprehensive investigation of the two studied areas was conducted to analyse the evolution of occurred ground deformations, by means of remote sensing techniques.

The first investigated deep-seated landslide is located in the territory of the municipality of Agnone (Molise region, southern Italy) and it is an active landslide known since the beginning of last century (Almagià, 1910). The aerial images investigation allowed the interpretation of the evolution of the landslide starting from the 1940s to the present day, by means of the SfM technique and the analysis of the Persistent Scatterers (PS). The description and classification of damage occurred on buildings and facilities, mainly caused by the 2003 reactivation and the subsequent evolution, were conducted. Damage occurred on facilities and infrastructures in the landslide surroundings were surveyed during several field campaigns and classified with different methods existing in scientific literature (Skempton and MacDonald, 1956; Burland, 1977; Lee and Moore, 1991; Chiochio et al., 1997; Cooper, 2008; Mansour et al., 2011). Since each work presents some benefits and constraints (Del Soldato et al., under review_a), a new ranking for a quick landslide-induced damage evaluation (Del Soldato et al., under review_b) was developed and applied. From 2003 to 2015, the facilities were classified using several parameters elaborated by the remote sensing techniques. By means of velocity and displacement measured along each Line Of Sight geometry by the satellite and their reprojection along the slope, the structures were categorized. Furthermore, a relationship between these factors and the ranking of the damage affecting the structures was analysed and critically discussed. Finally, a matrix to investigate and validate the reliability of the relationship was developed and applied to each construction.

The second case of study is the southwestern sector of the municipality of Volterra (Tuscany region, central Italy), a partially urbanized area and affected by slope instabilities that threatens the urban fabric and its historical heritage. Here, several field surveys were conducted to recognize, describe and classify damage on each construction. Furthermore, as for the other investigated site, an analysis based on the reconstruction of multitemporal 3D models, by means of the *SfM* technique, and PS displacements was developed to understand the evolutionary stages of the phenomena. Moreover, classifications of damage on structures in the landslide-prone area by a method known in the scientific literature (Cooper, 2008) and the application of a new ranking approach were performed (Del Soldato et al., under review_b). As for the Agnone site, from 2003 to 2015 velocity and displacement measured by the PS derived from ENVISAT and COSMO-SkyMed for each orbit, as well as the velocity and the maximum displacement projected along the slope were used to classify structures kinematically. Finally, on the basis of the relationship found between the surveyed damage levels and kinematic characterization of structures by PS technique, as for the Agnone case study, investigations were carried out on structures and critically analysed and discussed by means of the matrix adopted for the reliability categorization.

1.1 Structure of the thesis

The thesis is divided in seven chapters.

The first chapter briefly depicts landslides related problems and provides the description of the purpose of the research project and the introduction to the PhD thesis.

The second chapter explains the basic knowledge on the landslides and them several typologies.

The third chapter illustrates the two investigated sites and the available data for each one.

The fourth chapter provides a general introduction to the SAR remote sensing techniques and a detailed description of the methodologies applied, both remote sensing applications and field investigations.

The fifth chapter shows the results of the evolution studies, the application of DInSAR and the relationship between the damage and the parameters of movement investigated for the two studied sites (Agnone and Volterra).

The sixth chapter contain the discussion on the results obtained providing a critical analysis of these results.

The seventh chapter illustrates some conclusions and identifies possible future studies to apply in order to improve the knowledge on the developed issues.

Finally, in the Appendix the contributions in congresses and the papers, accepted and under review, produced during the PhD period.

1.2 Objectives

The continuous expansion of the urban fabric, as natural consequences of the demographic growth (Rybár, 1997), induces people to occupy territory of which the evolution is unknown. For this reason and for the spread of slope-movements affecting territories of several countries, it is necessary advancing the knowledge on reconstruction of landslide evolutionary stages.

The final objective of this PhD thesis was to develop an integrated procedure between remote sensing techniques, ancillary data and field surveys to help land management authorities to best focus and perform mitigation works to avoid further landslide occurrences in the future. To this purpose the reconstruction of evolutionary stages, by multi-temporal aerial images, and movements of Persistent Scatterers, detected by DInSAR, of two landslides were investigated allowing to produce geomorphological map, velocity maps and deformation time series. Such results permitted evaluating extension and state activity of both landslides. Finally, the obtained results were compared with ancillary data, where available, to validate the remote sensing results and to allow a better interpretation of the phenomenon. The landslide-induced damage on buildings were categorized and some correlations between displacements affecting structures, namely measured velocity and damage, were researched and critically discussed. In order to prevent future important damage the reliability of a found relationship between the displacement and the cracks, affecting some sample buildings in the two studied sites, were investigated. Furthermore, to better develop the issue of the PhD dissemination, a new approach to assess the landslide-induced damage on facilities was developed as well as a methodology to reconstruct 3D models of areas starting from physical historical aerial images was tested.

Two test sites were chosen as cases of study:

- a deep-seated dormant complex landslide occurring in the Agnone municipality (Molise region, southern Italy) with an important reactivation in 2003 and other intermittent movements in the subsequent period, which affects facilities staying in its surroundings with relevant damage;
- a landslide area affecting some constructions and the historical heritage of a partially urbanized area in the southwestern sector of Volterra (Tuscany region, central Italy).

2 Landslide definition and classification

2.1 Landslides

The term '*landslide*', as simply denoted by Cruden (1991), refers to 'the movement of a mass of rock, debris or earth down a slope'.

Every year the Centre for Research on the Epidemiology of Disasters (CRED) published the "Annual Disaster Statistical Review" regarding the situation of emergencies causing relevant impacts on human health. Worldwide, in 2015, 376 reported natural disasters provoked 22765 death, more than 100 millions of victims with a consequent amount of direct and indirect cost of damage. The number of reported natural disasters in 2015 (376) showed an increase of 13.9% compared to 2014's number (330). It is worthy noticing that causes of the events are divided in "hydrological", namely floods, landslides and wave actions, "meteorological", represented by storm and extreme temperatures, "climatological", includes drought and wildfires, and "geophysical" considers earthquakes and volcanic activities.

In 2015, the number of climatological events (45) was the highest since 2005, 42% above its 2005-2014 annual average (31.5) and the one of hydrological disasters (127) is near its annual average (124.5). The growth of the urbanized areas, with consequent increase of damage and relates direct and indirect costs, has intensified the impact of landslide events representing the most influential events affecting human activities. In this way, the exposure to this type of geohazard results significantly relevant.

The global spatial distribution of fatal landslide, i.e. events reporting loss of lives, exhibits a strongly heterogeneity (**Fig. 2.1**), even if some clusters are recognizable (e.g. along the Himalayan Arc and the southwestern Indian coast, Sri Lank and China, in central China, etc).

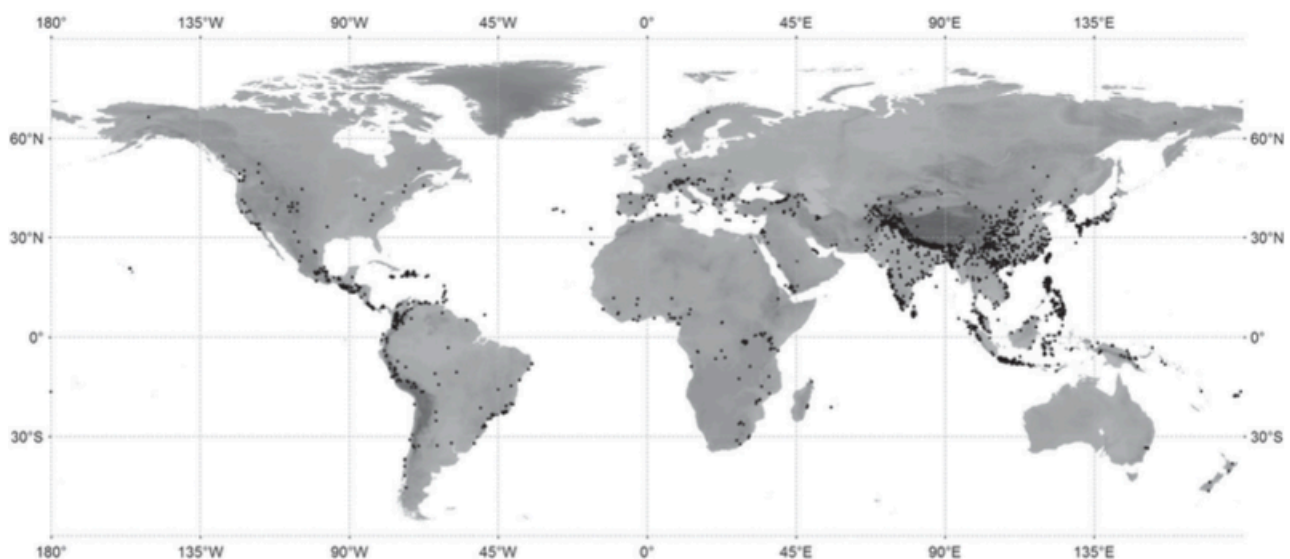


Fig. 2.1 - Spatial distribution of fatal single or grouped landslides (Petley, 2012)

The stability of a slope is controlled by the relationship between the driving forces and shear strength acting along the slope at the base of the unstable mass of geological material. Terzaghi (1950) divided the main causes of a landslide: external factors, due to an increase of the shearing stress caused by, for instance, geometrical changes, unloading of the slide toe, loading of the slope crest, shocks and vibrations, drawdown, changes in water regime; internal factors, decreasing the shearing resistance due to, for example, progressive failure, weathering or seepage erosion. Furthermore, the causal factors of landslides can be ranked according to their effect (preparatory or triggering) and their origin (ground conditions and geomorphological, physical or man-made processes).

Taking into account the significant numbers of devastating landslide events, the UNESCO Working Party on World Landslide Inventory (1993) claimed for establishment of details for classifying the rates of movements, their causes, the geology, the activity and the distribution of movement within the landslide merging the categorizations developed by several Authors.

In **Fig. 2.2** an ideal complex earth-slide flow is designed (Varnes, 1978) defining several components of a landslide. The ideal mass-movement consists of the crown area, defined by the undisplaced material in the upper part, two main lateral scarps and the toe, the lower part, usually characterised by a curved margin of displaced material farther than the main scarp. The main body of a mass movement is featured by two distinct regions: a portion where the elevation of the ground surface sinks due to landsliding; an accumulation area, where the elevation of the ground surface increases due to the deposition of displaced mass of material.

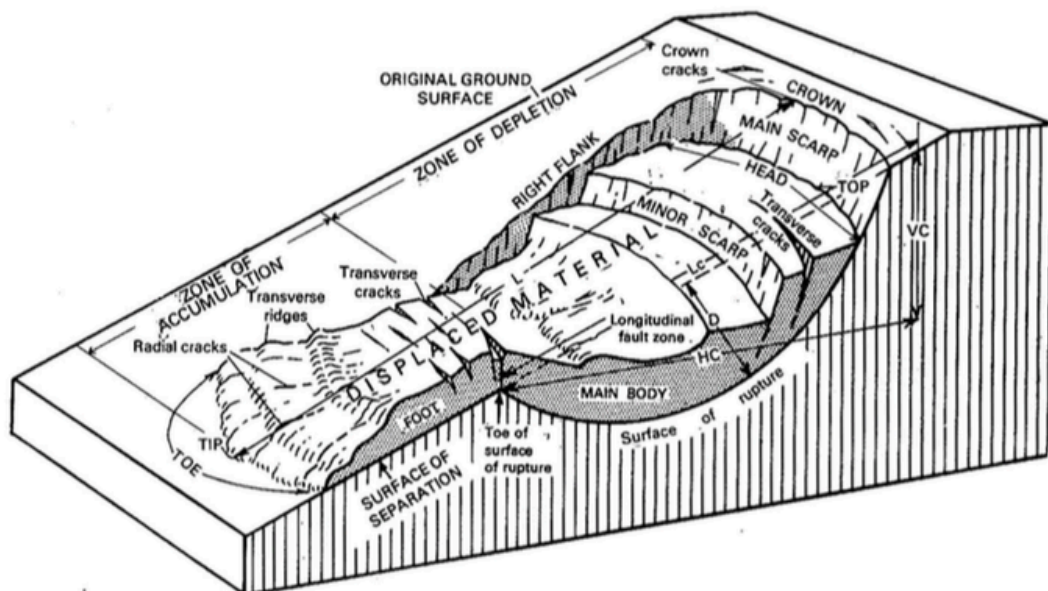


Fig. 2.2 - Block diagram of ideal complex slide-earth flow (Varnes, 1978).

An important parameter to categorize mass-movements and the related hazard is the velocity, generally representing a proxy for landslide intensity, the caused damage and the economic and human losses. In literature, it is known that small rapid debris avalanches or extremely rapid landslides can cause greater damage and casualties than larger slope movements with moderate or low velocities.

Cruden and Varnes (1996) ranked the velocity of mass-movement in seven classes from extremely slow to extremely rapid (**Table. 2.1**).

Table. 2.1 - Velocity landslide scale (Cruden and Varnes, 1996).

Velocity class	Description	Velocity (mm/sec)	Typical velocity	
7	Extremely rapid	$5 * 10^3$	5 m/sec	Catastrophe of major violence; buildings destroyed by impacted displaced material; many deaths; no escape
6	Very rapid			Some lives lost; velocity too great to permit persons to escape
5	Rapid	$5 * 10^1$	3 m/min	Escape evacuation possible; structures, possessions and equipment destroyed
		$5 * 10^{-1}$	1.8 m/h	Some temporary ad insensitive structures can be temporarily maintained
4	Moderate	$5 * 10^{-3}$	13 m/month	Remedial construction can be undertaken during movement; insensitive structures can be maintained with frequent maintenance work if total movement is not large during a particular acceleration phase
		$5 * 10^{-5}$	1.6 m/year	Some permanent structures undamaged by movement
3	Slow	$5 * 10^{-7}$	16 mm/year	Imperceptible without instrument; construction possible with precautions
2	Very slow			
1	Extremely slow			

The velocity of a slope movement, depending on landslide typology and characteristics can be measured by means of both several direct in situ investigations and remote sensing techniques. Some examples available to estimate and monitor the mass-movement velocities are stereo-photogrammetry (Jebara et al., 1999; Snavely et al., 2008; Maybank, 2012), GBInSAR (Ground-based Interferometric SAR) method (e.g. Tarchi et al., 2003; Antonello et al., 2004), several A-DInSAR (Advanced Differential Interferometric Synthetic Aperture Radar) techniques (e.g. Massonnet and Feigl, 1998; Ferretti et al., 2001; Farina et al., 2006; Hooper et al., 2012), the application of *Structure from Motion* (SfM) method (e.g. Pollefeys et al., 1999; Westoby et al., 2012; Lucieer et al., 2013) by means of the comparison of different reconstructed three-dimensional (3D) models, or the newly survey methods by means of unmanned aerial vehicles (UAVs) (Niethammer et al.,

2012). Instances of direct investigation methodologies useful to estimate the displacement in time of slope movements are the extensometers, inclinometers, GPS surveys (Brasington et al., 2000; Brückl et al., 2006) and terrestrial laser scanning (Razak et al., 2011).

A further fundamental parameter to well-define a landslide is the thickness of the implicated material (Segoni et al., 2012; Del Soldato et al., 2016b). If only the first 3 - 5 m of depth of the material are involved by mass-movements, they are considered shallow landslides with the possibility, depending on the involved material, to be transformed into rapidly moving debris flows (e.g. Campbell, 1975). Most of the shallow failures affect mostly colluvial material rather than bedrock formations. Statistically shallow landslides mainly occur on slopes showing steep angles, large unforested watersheds and in areas with concave transverse sections filled by colluvium deposits. The occurrences are not related to particular periods during the year, but the possibilities of triggering increase when the ground is nearly water-saturated.

Landslides with mechanical deformation occurring at considerable depth called *deep-seated* gravitational deformations are relatively rare phenomena (Petley and Allison, 1997), even if this typology was identified in many parts of the world. The geomechanical behaviour of a deep-seated landslide, particularly when exceeding thicknesses of 100 m, plays a key role. Despite mechanical characteristics and deformations affecting surficial deposits at the top of deep-seated mass movements can be significantly different from those of shallow landslides, no geomorphologist consider these differences during the investigations of large failures (Petley and Allison, 1997). Movement patterns in deep-seated landslides were extensively documented (e.g. Radbruch-Hall, 1978; Pasuto and Soldati, 1990) and two distinct main forms resulted evident. The '*creep*', commonly indicating the long-term displacement at low strain rate that may be subject to variations due to seasonal changes, is the first one. Some deep-seated landslides creep for long periods under normal gravitational forces, showing relatively constant rate. Minor fluctuations may be the result of small changes in the water-table altering the effective normal stress. The short period of creep is commonly linked to an increasing in displacement rate immediately prior to the rapid strain event. The second pattern appears when a short-term movement at very high rates of displacement causes a sudden failure.

Moreover, the state of activity, which describes what is known about the timing of movements and the temporal evolution characteristics (WP/WPI, 1993), are categorized in in eight different types through geomorphological information (**Fig. 2.3**).

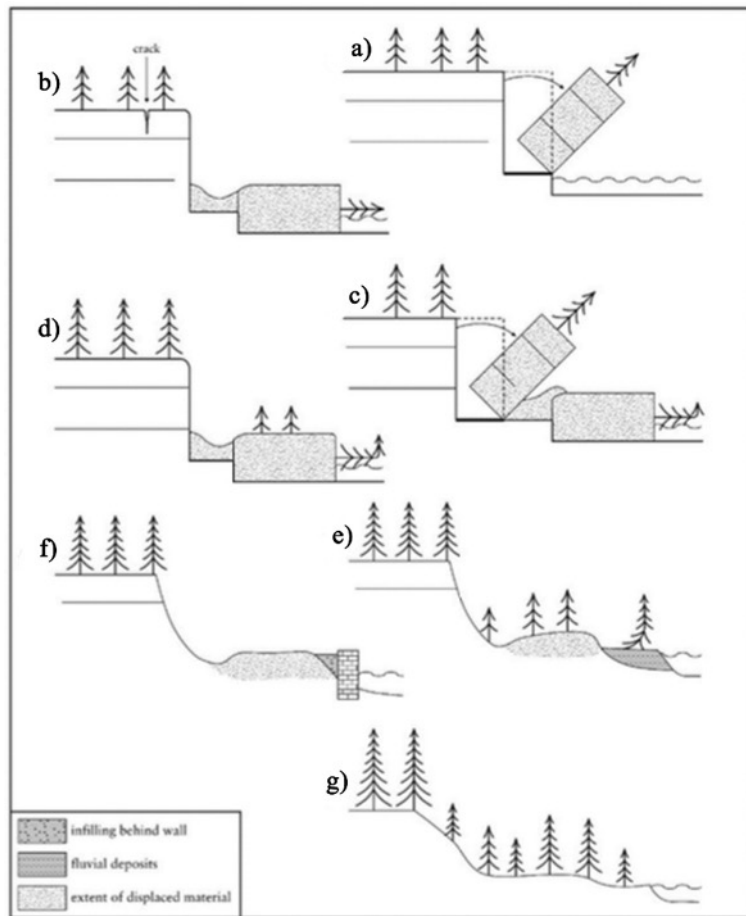


Fig. 2.3- Topples profile section with the modified state of activity of landslide by WP/WPI (1993): a) active landslide; b) suspended landslide; c) reactivated landslide; d) dormant landslide; e) abandoned landslide; f) stabilized landslide; g) relict landslide. The state comprehended between d and g are considered inactive (WP/IWP, 1993).

Active landslides are those where the movement is currently active, including first-time movements and reactivations due to erosion at the toe of the slope that causes blocks toppling. Landslides not moving at the present but that have shown movements within the last annual cycle of season are classified as suspended. Landslides that not exhibit movements since more than one annual seasonal cycle are described as inactive and they are subdivided in: dormant when reactivation are possible and tree cover and scarps modified by weathering take place on old displaced materials; abandoned in case of the displaced material is not influenced by its original triggers; stabilized if natural or anthropic protective measurements are adopted to protect the toe of the slope; relict for movements occurred in morpho-climatic settings actually extinct, i.e. masked by tree covers over slope.

Another important issue homogenized and delineated by the WP/WPI (1993) is the definition of the distribution of activity, referred to the localization and the typology of the movement affecting the landslide (Fig. 2.4).

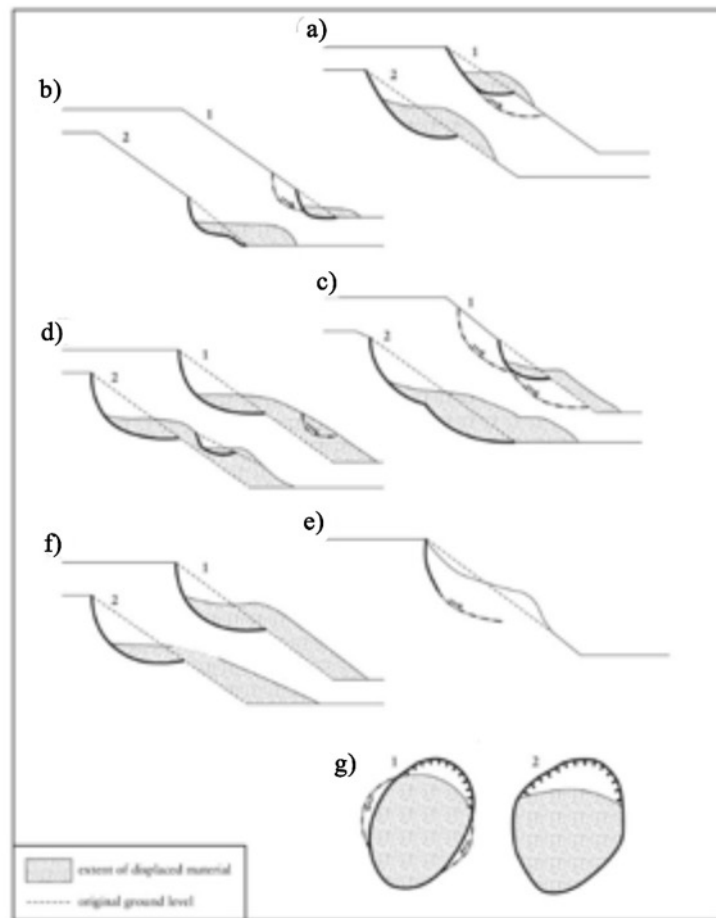


Fig. 2.4 - Profile section showing different distribution of activity of a landslide, modified by WP/WPI (1993): a) advancing landslide; b) retrogressive landslide; c) enlarging landslide; d) diminishing landslide; e) confined landslide; f) moving landslide; g) widening landslide (WP/IWP, 1993).

An advancing landslide shows the rupture surface aligned in the same direction of movement. The contrary happens for the retrogressive landslide where the movements is extending in the opposite direction respect to the displaced material. In case of expansion of the rupture surfaces in two or more directions, the landslide is defined as enlarging. Instead, if the volume of the mobilized material decreases the landslide is denominated as diminishing. In a confined landslide, scarps are visible, while no rupture surfaces are recognizable in the displaced mass. If the mobilized material continues to move without any visible changes in rupture surface and volume, the landslide is defined in moving. Landslide showing continue extension in rupture surfaces in one or both flanks the mass-movement is called widening landslide.

Finally, also the landslide activity style is defined and described. These parameters consist in the contribution of different movements within a single landslide and their relationship (**Fig. 2.5**).

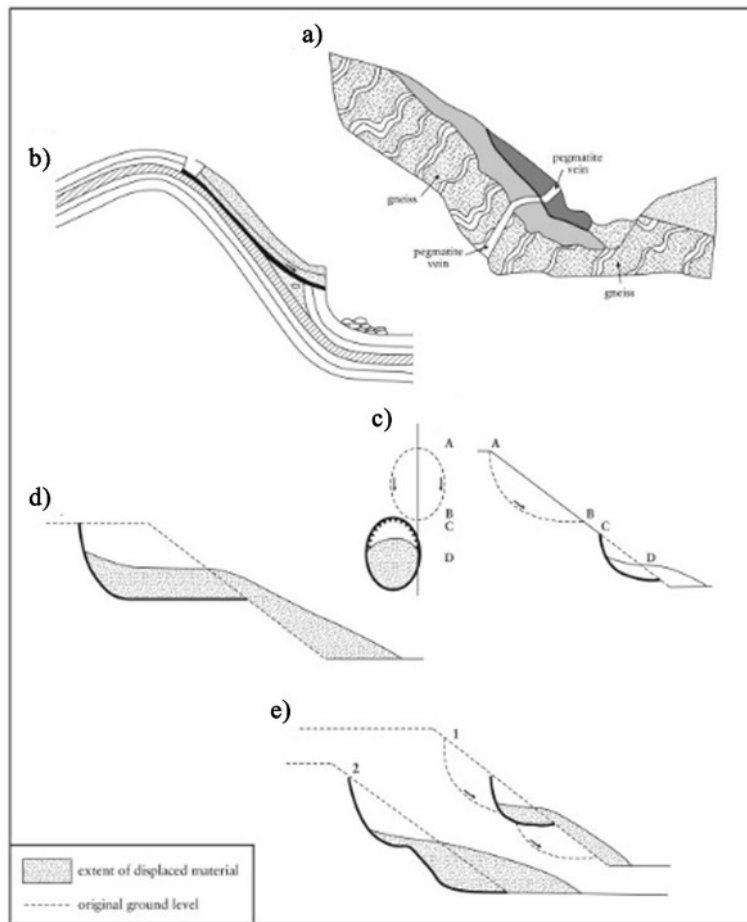


Fig. 2.5 - Scheme showing different landslide style activity: a) complex landslide; b) composite landslide; c) successive landslide; d) single landslide; e) multiple landslide (WP/IWP, 1993).

If a landslide exhibits at least two types of movement in temporal sequence, e.g. falling, toppling, sliding, spreading or flowing, is defined a complex landslide. While if at least two movements occurred simultaneously in different sector of the same mass-movement the landslide is named composite. A successive landslide is a similar type as a nearby, earlier landslide, but does not share displaced material or rupture surface with in. A single landslide is characterized by a single movement of displaced material and, if the same type movement is repeatedly shown, the landslide is defined multiple.

2.2 Landslide classification

The earliest landslide classification systems were developed in the Alpine countries (Baltzer, 1875) by the analysis conducted on the Swiss territory where the first categorization to distinguish different typologies of mass-movements in falls, slides and flows was carried out. In the following years, this ranking was increased with toppling and spreading classes. Subsequently, Almagià (1910), working on the Apennine territories severally affected by landslides, Heim (1932) and Zaruba and Ménécl (1969) focusing the attention on landslide types related with material facies described in geological terms, allowed to develop several landslide

typologies classifications. Stini (1910) and Bull (1964), instead, concentrated the investigation on debris flows and mud flows movements, respectively. In 1938, Sharpe introduced a three-dimensional classification system distinguishing type of movement, material and velocity of displacement. Varnes (1978) improved the knowledge and expanded the Sharpe's categorization. Hutchinson (1969, 1989) focused the attention on the propagation mechanism and based it on multiple elements such as material, water content, kinematics, morphology and displacement rate. In 1996, Cruden and Varnes proposed supplementary terms, such as advancing, enlarging, retrogressive, multiple or successive deformation, related to the typology of movement of failure. Furthermore, the classification was implemented with the post-failure activity of the mass-movement by means of dormant, abandoned, relict and re-activated.

Also the geotechnical material terminology plays a key-role in the description of the landslide and to improve the characterization of the mechanical behaviour (Hungr et al., 2014). Varnes (1978) takes into consideration "rock", "debris" and "earth". In case of transition between different textural classes the most significant term of the class influencing the physical behaviour has to be used. The term "earth", that not have a geological or geotechnical definition, is used, for instance, for names as "earthflow" or similar to describe a cohesive, plastic, clayey soil often mixed and remoulded.

Hungr et al. (2014) modified the Varnes' ranking system improving it by means of the recent development of landslide sciences. The increased categorization has thirty-two landslide types with a formal definition as much as possible compatible with the previously described Varnes' classification (1978). For complex landslides, not included as specific category in the ranking, the user can combine the type names to describe in the best way his case of study.

The following definitions are based on the classifications of Varnes (1978), Hutchinson (1989), Cruden and Varnes (1996) and Hungr et al. (2014).

2.2.1 Falls and topples

Falls (Fig. 2.6) are due to the detachment of soil or rock from steep slopes along surfaces characterized by little or no shear displacement. This movement mainly occurs by falling, bouncing or rolling of rock fragments or ice, and it may be also caused by tensile and buckling failures, sometimes preceded by small sliding or toppling that separate the displacing material from the undisturbed mass. The typologies of detachment are distinguished by the slope angle of the involved slope: above 76°, falling occurs; between 76° and 45°, bouncing arises; with slope angle values less than 45°, the mass movement is characterized by rolling. Usually the falls are movements involving a limited volume of rock occurring along steep slopes. The main triggers are differential weathering, excavations, stream erosions, vibrations or undercutting.



Fig. 2.6 -Example of evolution of a rock fall (Lynn Highland, <http://blogs.agu.org/landslideblog/2011/10/13/a-gallery-of-landslide-images/>) with explaining scheme of the phenomenon (b) (Hung et al., 2014).

Topples occur by the forward rotation or overturning of soil masses, rock columns or plates respect to the point of the centre of gravity. This type of movement may conduct to falls or slides depending on the geometry of the dislocating material, on the geometry of the surface of separation and on the orientation and extension of the kinematic active discontinuities. The main trigger factors are similar to falls in addition to the contribution of gravity, the probable water pressure and the possible ice filling cracks present in the rock-mass. The failure can involve little or important volumes on well-defined basal discontinuities characterized by slow initial displacement that can reach extremely rapid velocity during the event.

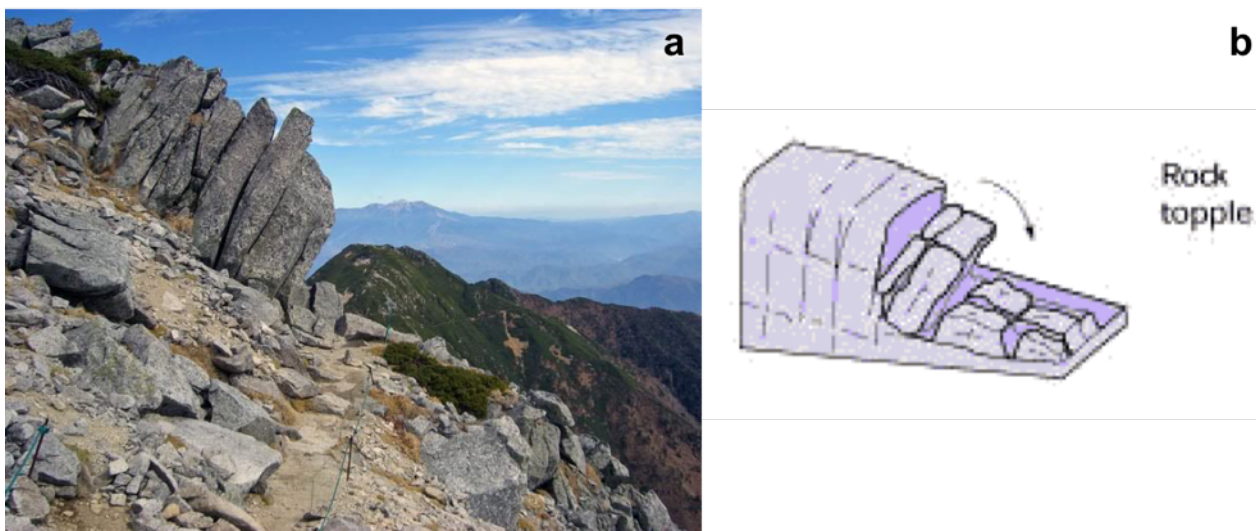


Fig. 2.7 - Example of rock topple (<http://forums.hardwarezone.com.sg/japan-271/time-trip-report-16-oct-28-oct-tokyo-matsumoto-osaka-hiroshima-2550242.html>) (a) with explanation of the possible Single and Multiple Topples evolution (b) (Hung et al., 2014).

2.2.2 Slides

Slides are featured by a downslope movement affecting soil and rock masses along one or more planar or curved rupture surfaces. The movement cannot be simultaneous for the entire involved mass but the volume of displacing material enlarges as it moves down from the area of local failure. Varnes (1978) distinguished two types of movement: rotational and translational slides. The first one moves along a curve and concave surface of rupture after a little, almost vertical, downward in head. The translation slide is characterized by a movement occurring along a planar or corrugate surface of rupture. The second type, if caused by a single discontinuity into a rock mass, is called *block slide* (Panet et al., 1969) or *planar slide* (Hoek and Bray, 1981). The velocity of these events depends on the type of material involved: slow or moderate velocity is usual for cases affecting; from slow to rapid for phenomena occurring in soils (Hungr et al., 2014).



Fig. 2.8 - Rock slide occurred on the Highway 41 in Madera County on, Jan. 19, 2016
(<http://www.fresnobee.com/news/local/article55419970.html>).

2.2.3 Spreads

Spread is a term introduced in the geotechnical engineering field by Terzaghi and Peck (1948) for describing an extension of rock mass or cohesive soil subsiding and subdivided in distinct and kinematically independent blocks due deformation of softer and ductile underlying strata. The movement is caused by liquefaction or flow of softer materials with consequent possible subsidence, translation, rotation, disgregation, liquefaction or flowing of the overhead cohesive material. The dominant mode of movement of spread phenomena is the lateral expansion accommodated by tensile or shear fractures (Varnes, 1978).

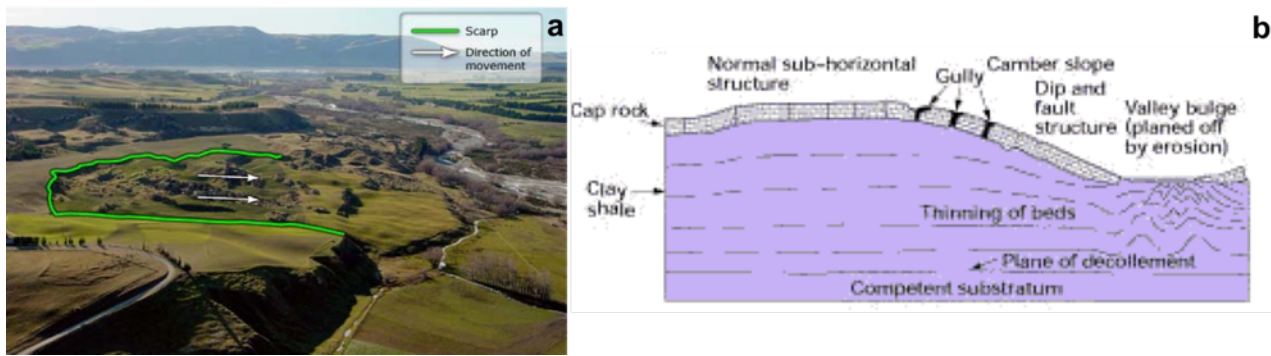


Fig. 2.9 - Example of lateral spread (<http://www.teara.govt.nz/en/photograph/8793/lateral-spread>) at the locality known as Earthquakes, in the Waitaki Valley, North Otago(a) and scheme of the phenomenon (Hung et al., 2014).

2.2.4 Flows

Flow is a spatial continuous movement describable by short-lived shear surfaces, closely spaced usually not preserved. The active surface is recognizable by differential movements and distributed velocities propagation within the moving mass similar to a viscous liquid. The huge deformation of the entire sliding-mass mainly allows differentiating flows from the other types of landslides in which the body mass-movement usually moves rigidly along the slip surface.

Different types of flows can be distinguished by means of the involved material, different velocity and triggering factors. Varnes (1978) used, for the first time, different terms to indicate several typologies of flows, subsequently increased by Hung et al. (2014). Furthermore, Authors grouped them in two principal categories: flows in rock and flows in soil.

The different flows in rock are divided in:

- ✓ Rock flow: movement in bedrock including deformations distributed among large or small fractures, or even microfractures, with no concentration of displacement along fractures. Vibration, undercutting, differential weathering, excavation or stream erosion, as for falls and topples, are the triggering factors.
- ✓ Rock avalanche: large rock disintegrates phenomena rapidly moving down forming a massive extremely rapid flow-like motion of fragment rock. These movements, named also “stürzstrom” (Heim, 1932), are characterized by an extremely rapid velocity mainly triggered by the pore-pressure until the fragmentation of the rock mass that provoke the generation of a very large space that drains the avalanche mass during motion.

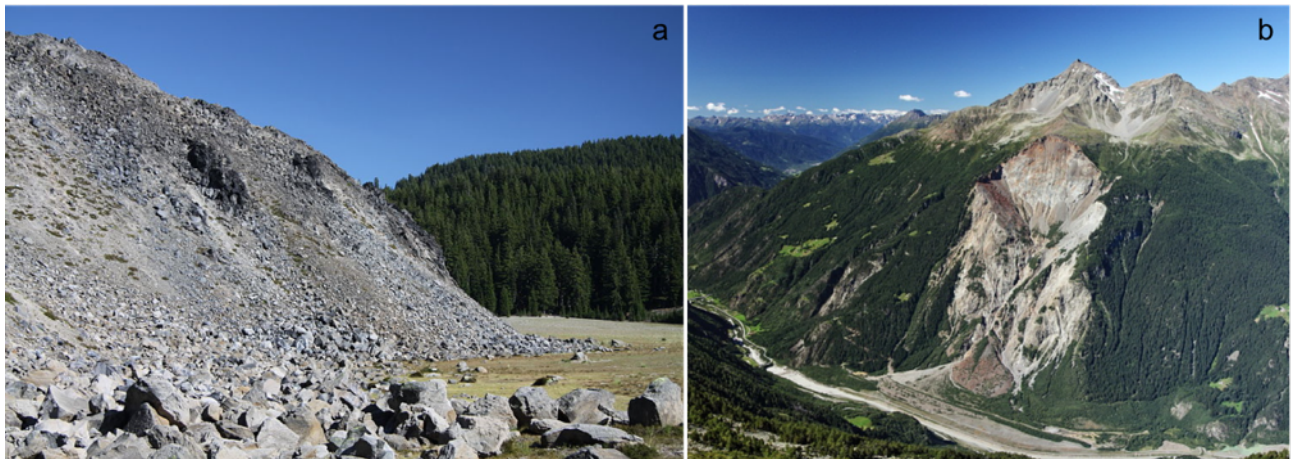


Fig. 2.10 - a) Rock flow of obsidian lava at Rock Mesa in Three Sisters Area, protected area Three Sisters Wilderness, Oregon, USA ([https://commons.wikimedia.org/wiki/File:Rock_Mesa_obsidian_flow_in_Oregon_in_2011_\(9\)](https://commons.wikimedia.org/wiki/File:Rock_Mesa_obsidian_flow_in_Oregon_in_2011_(9))); b) Rock Avalanche occurred in Val Pola, upper Valtellina (Lombardy region, Italy) on July 28, 1987 (<http://www.mergili.at/worldimages/picture.php?/7534>).

Flows involving soils are mainly triggered under saturation or near-saturation conditions affecting soils along slopes (i.e. from 5° until 45°). They are classifiable as follows:

- ✓ Earth flows: intermittent flow-like phenomena occurring in plastic, disturbed and mixed soils, with consistency close to their Plastic Limit¹. This typology of flow is favoured by a combination of multiple discrete shear surfaces and internal shear strains on which it slides. Furthermore, it may have more rapid “surges” alternated with long periods of relative dormancy. Earth flows develop where water-rich unconsolidated materials move by slumping and plastic flow.

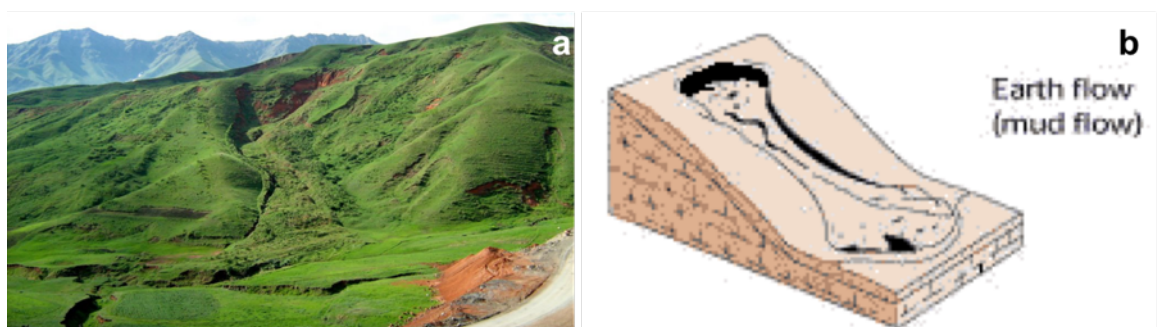


Fig. 2.11 - Earthflow in Alaj, Kirghizistan (a) (<http://www.panoramio.com/photo/12660372>) and explanation of the ideal earth flow (b) (Hungri et al., 2014).

¹ Plastic Limit is the water content inducing the loss of the plastic behaviour of the soil

- ✓ Debris flows: typology characterized by very rapid to extremely rapid flows of saturated non-plastic debris having low plasticity index² (lower than 5) and sliding mass with sandy to gravelly grain-size. Along the main track of the flow, it follows the direction of the channels which greatly allow the passage of the material. The runoff water that reaches the channels can increase the sliding mass speed and it can change the typology of the flow. The lateral confinement can affect the sliding body depth and the vertical velocity gradient, thus the vertical and longitudinal sorting of the material. The term *debris flow* was coined as a general form to describe rapid gravity-controlled mass movements of a mixture of granular, solid, water and air material (Costa, 1984). Subsequently, it was broadly used as a general term to describe many other types of flows like wet grain flows, lahars³, tillflows⁴, wet rock avalanches, and debris torrents.
- ✓ Mud flows: very rapid or extremely rapid flows road to steep channel. Saturated plastic debris and soils with significantly water contents related to the source material. These materials have a plasticity index higher than 5% and the rich plastic content of clay that allows the differentiation between this type of flow and a debris flow. Clay generates longer runout due to the dilution delay by water and drainage (Scott et al., 1992).

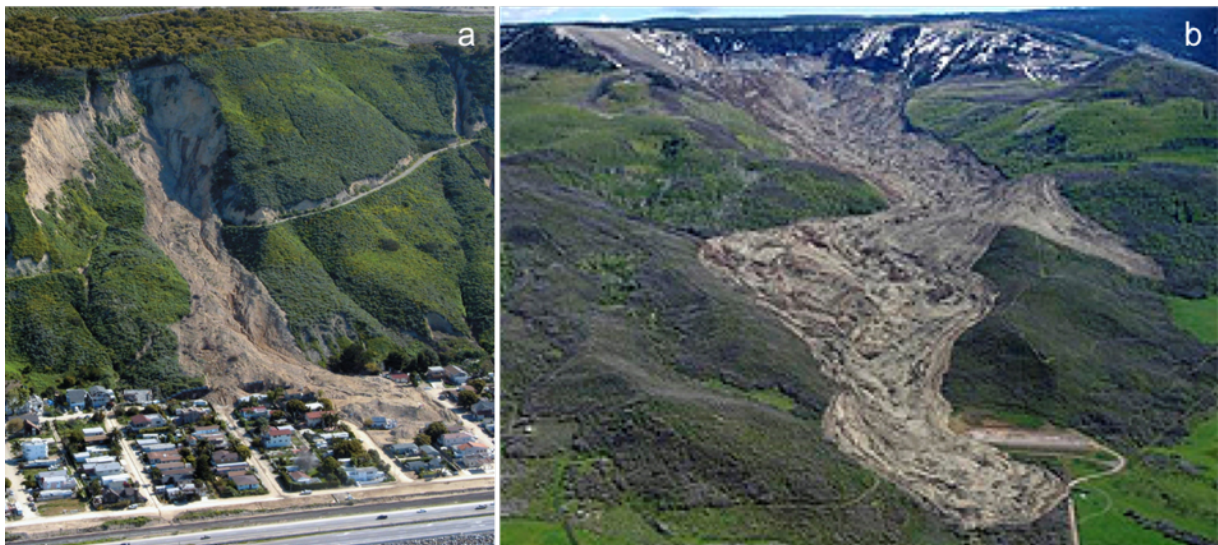


Fig. 2.12 - a) Debris flow occurred in the town of La Conchita, California, USA on January 2005. (http://www.geotimes.org/nov05/feature_landslides.html). b) Mudflow in 2014 in Mesa County, Colorado (<http://blogs.agu.org/landslideblog/2014/05/28/grand-mesa-1/>).

² The plasticity index is a measure of the plasticity of a soil. The plasticity index is the size of the range of water contents where the soil exhibits plastic properties.

³ A lahar is a volcanic mudflow similar to a pyroclastic flow, thus a fluidized masses of mixture of gases, water and rock fragments, downmoving rapidly caused by the high water contents and the gravity. Its consistency is viscous and the density is fluid when moving, solid at rest.

⁴ Tillflows are debrisflow originate in sediments deposited above the glacier that flows laterally into lower surfaces melted with glacier.

- ✓ Debris floods: very rapid important flows of mixtures of water and sediment, charged with debris and developed during extreme flooding in a steep channel. These flows are distinguishable from debris flows by means of the amount of solid concentration. The distinction of a mass-movement between debris-flow and debris flood is based on the threshold of 80% of soil concentration (Costa, 1984).
- ✓ Debris avalanches: shallow flows characterized by a very rapid to extremely rapid velocity with morphology comparable to snow avalanches. The material involved is partially or fully saturated debris down-moving on a steep slope, without confinement in an established channel. This typology of landslide can occur at all scales, starting as debris slide, associated with failure of residual, colluvial, pyroclastic or organic soil. The process of draining caused from the rock fall or rock slide can be a trigger factor of debris avalanches (Lacerda, 2007).

2.3 Landslide in Structurally Complex Formations of southern Apennine

The southern Apennine chain represents an African-vergent fold and thrust belt generated during the tectogenesis of the Neogene characterised by a deformation front direction of NW-SE subsequently migrated toward NE. The progressive thrusting and piling up of different tectonic units of different paleogeographic domains was due to several compressional tectonic phases (Patacca et al., 1990) associated with the collision between Africa and Europe occurred from the middle Miocene until the upper Pliocene. The important extensional tectonic phase, with a NE-SW extensional trend, caused a fragmentation of tectonic units in distinct blocks piled up in the Apennine chain and the development of counter-Appenninic regional transcurrent faults during the Quaternary.

The “*Structurally Complex Formations*” term describes geological materials that had suffered the above-mentioned geological evolution and it is characterized by large and scale-dependent heterogeneity in the lithological and structural features (Esu, 1977). Heterogeneity led to the development of a scaly-fabric with the alternation of “hard” (rock-like material) and “weak” horizons (soil-like material) featuring the geotechnical parameters (Picarelli et al., 2005).

Several landslides affecting the southern Italian Apennine were developed due to their particular geological, geotechnical and geomorphological features. These aspects and the mechanism of the occurring landslides result to be very complex and several studies analysed the general characters (Almagià, 1910; Cotecchia and Melidoro, 1974; Guida and Iaccharino, 1991; Di Maio et al., 2010). The stability conditions are conditioned by the morphological, geological and geotechnical characteristics that are depending on the genesis and the typology of involved material and on the geological process suffered by the succession that

modelled the landforms, mainly for Structurally Complex Formations (Esu, 1977).

Esu (1977) proposed a distinction of Structurally Complex Formations in three main categories, in turn, subdivided on the basis of the progressive chaotic structure (**Fig. 2.13**):

- ✓ A - fine-grained materials, lithologically homogeneous, with presence of structural discontinuities. This is subdivided in two classes based on the discontinuities represented by stratification and joints, or by tectonic stresses, respectively;
- ✓ B - heterogeneous material, as flysch, featured by the presence of two kind of soils with different mechanical features. It includes three subclasses based on the level of chaos of the structures.
- ✓ C - heterogeneous materials like rock or less weathered rocks in a clayey matrix with a completely disarranged fabric describing a typical of alteration blankets or landslide products.

Among the most famous landslides in SCFs studied during the last twenty years, are (**Fig. 2.13b**): Senerchia (Santaloia et al., 2001), Agnone (Calcaterra et al., 2008), Santo Stefano d’Aveto (Tofani et al., 2013a), San Fratello (Ciampalini et al., 2014), Montaguto (Giordan et al., 2013), and Cirò (Confuorto et al., 2014).

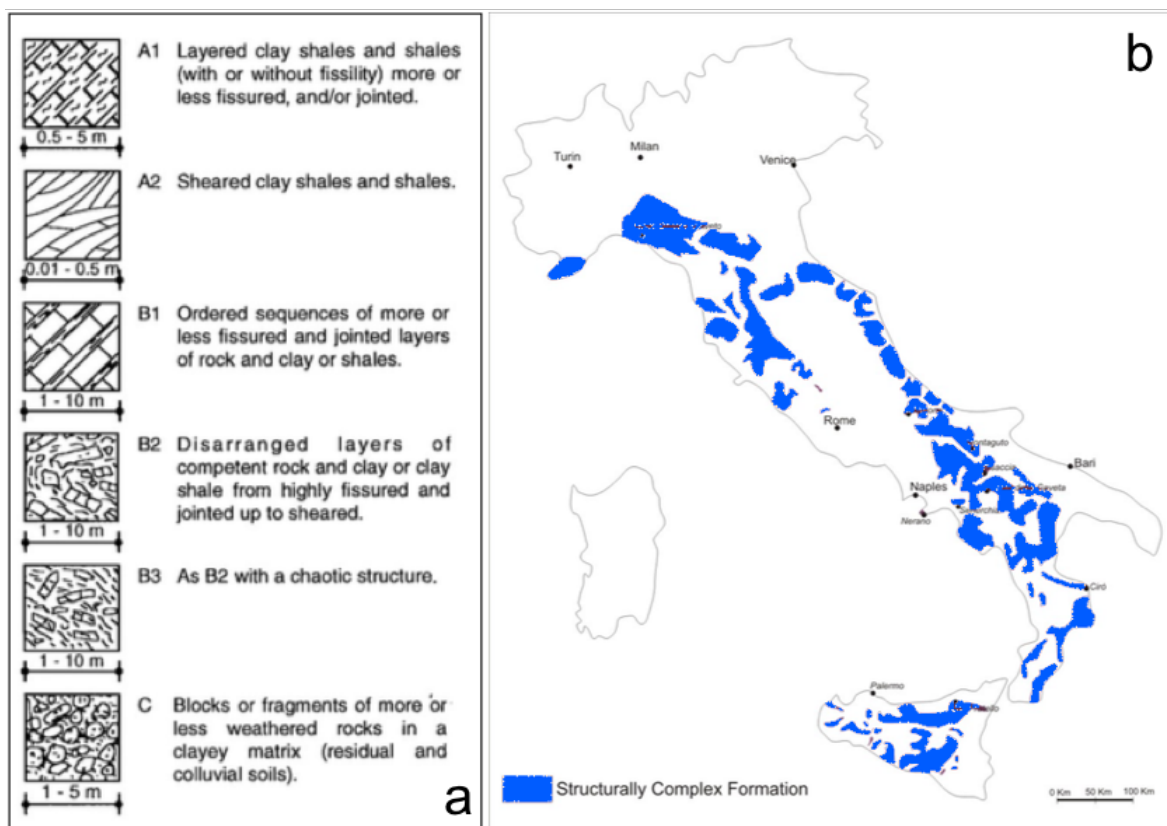


Fig. 2.13 - Categories of Structurally Complex Formations (Esu, 1977) (a); Italian Structurally Complex Formations outcrops and location of famous studied landslide in the geotechnical literature (D’Elia, 1991) (b).

3 Test areas

3.1 Geological and geomorphological features of Agnone (southern Italy)

The first analysed area is located in the western part of the Agnone municipality, Molise region (southern Italy), which is extended up to about 97 km². The climate of the region is temperate with alternation of rainy, sometimes snowy, and arid periods, in autumn-winter and spring-summer, respectively. The territory of this municipality, as the major part of this region, is strongly affected by landslides and erosional processes. In the western zone of the municipality, the Colle Lapponi-Piano Ovetta area (**Fig. 3.1**) in the catchment of San Nicola Valley, a tributary in the hydrographic right side of the Verrino Torrent, is affected by a large landslide. The continue evolution of the mass-movement, causing reshaping of the earth surface of the landslide, modify constantly the morphology of the area of interest.

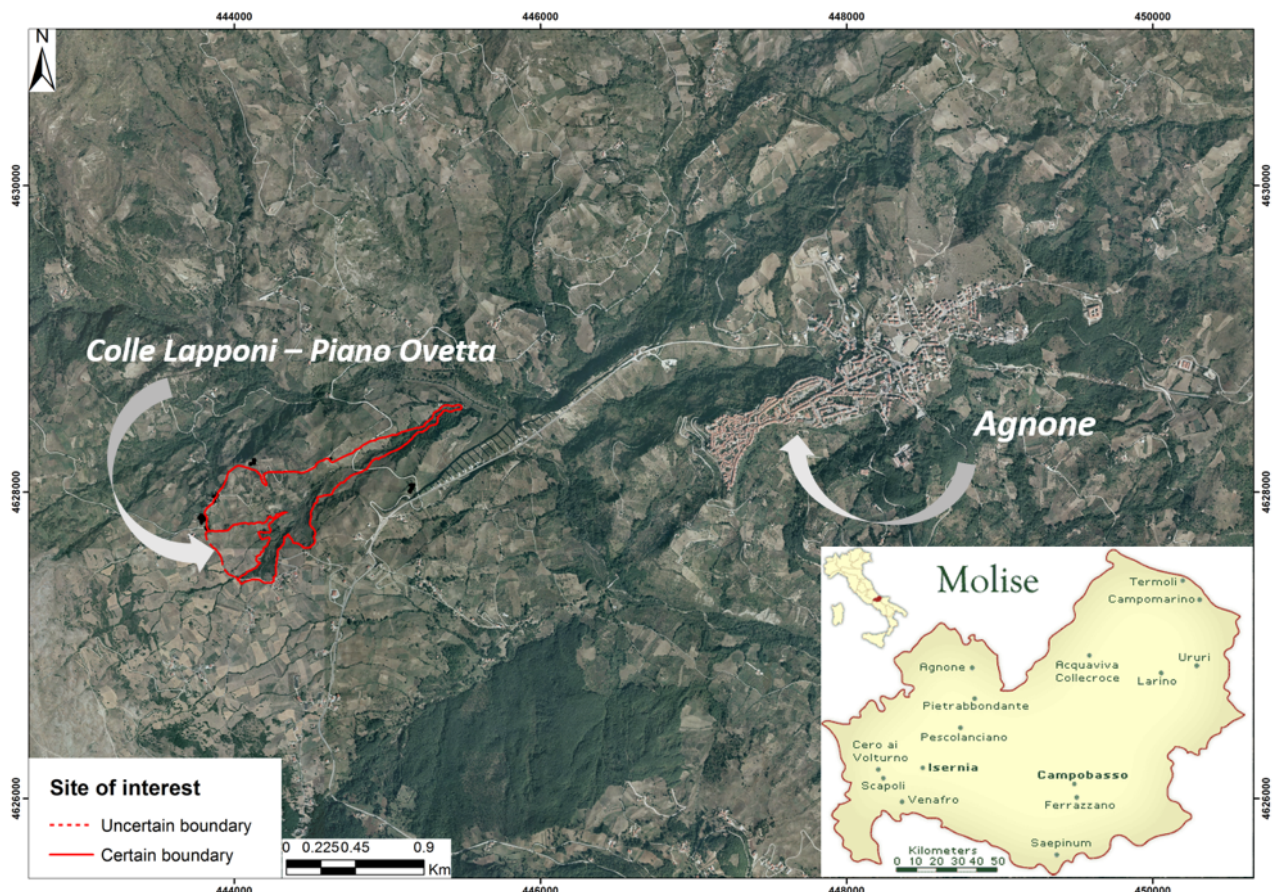


Fig. 3.1 - Location of the Colle-Lapponi - Piano Ovetta landslide in the Agnone municipality.

Geologically the area is characterized by the M. Pizzi-Agnone and Colle Albero-Tufillo unit showing the Agnone Flysch formation and a lower marly formation (**Fig. 3.2**). The geological setting of the Colle Lapponi -

Piano Ovetta landslide (CL-PO landslide hereafter) is characterized by the presence of two members of the Agnone Flysch, the Sannitico-Molisane Formation dated Upper Miocene (Vezzani et al., 2004), which can be considered a Structurally Complex Formation.

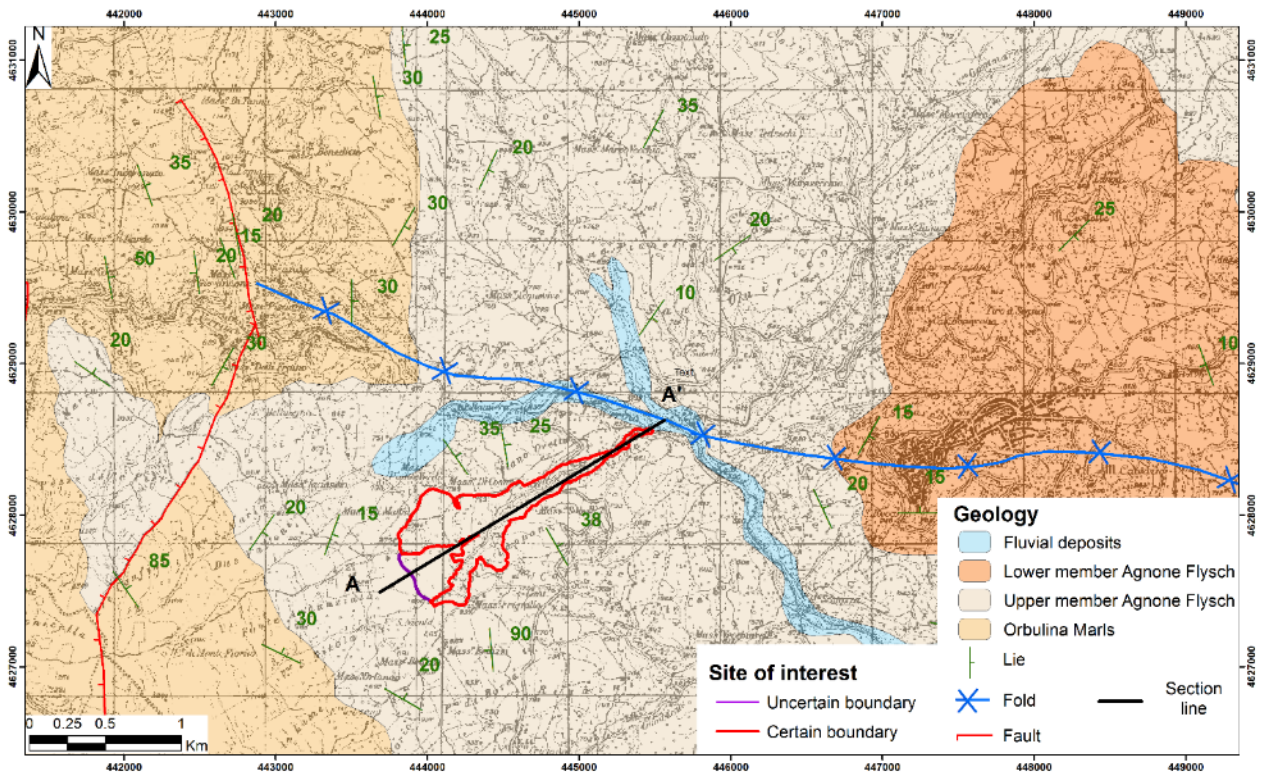


Fig. 3.2 - Geological sketch map (Vezzani et al., 2004) of the area of interest in Agnone with the current contour of the landslide reported in red.

The lower member of this formation is composed by alternations of marl limestones, marls and calcarenites in addition to turbidite silico-clastic deposits made of alternated thin layers of clayey sandstones, sandstones and arenites. The upper member of the Agnone flysch, involved in the CL-PO landslide as visible in the geological section A-A' traced along the landslide (**Fig. 3.3**), is constituted by an alternation of marly, semi-coherence clayey and subordinate greyish sandy levels with low mechanical resistance, diffuse alteration traces, and lithoid sandstones or calcareous intercalations with highly variable thickness. Some olistoliths of conglomeratic old material are present inside the Agnone formation (ISPRA, 1971; Vezzani et al., 2004; Filocamo et al., 2015). The territory characterized by this formation is mantled by a superficial regolith horizon composed of clays, silty clays and subordinate sand with diffuse alteration traces, abundant organic material and several clasts.

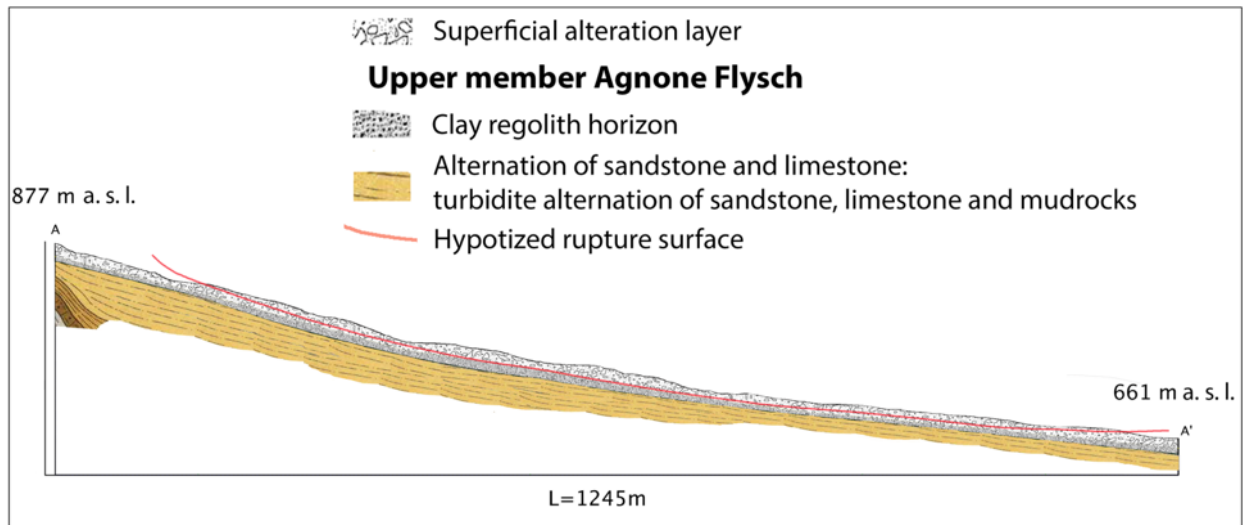


Fig. 3.3 - Geological section A-A' traced along the area of interest of the CL-PO landslide (ISPRA, 1971; Vezzani et al., 2004).

The ground morphology of the area surrounding the landslide is strongly controlled by the mass movement and by different lithotypes. Slopes showing higher topographical gradients, from 30° to 35°, corresponds to outcrops of the calcareous formations, while lower ones, from 5° to 10°, correspond to areas where the argillaceous Flysch units crop out. Areas affected by more significant erosional processes are characterized by slope angle values greater than 15° - 20°.

A geotechnical characterization of the landslide through several geological and geotechnical campaigns including the execution of four boreholes (**Fig. 3.4**) were conducted allowing the identification of four homogeneous layers described in the following, from the bottom to the top (Calcaterra et al., 2008):

Level D - marly clays, marls and clayey marls with silty and clay fractions. Soil fraction with a medium plasticity, effective peak friction of about 22° and effective cohesion of about 60 kPa.

Level C - calcareous levels with thickness variable from decimetres to meters.

Level B - grey clays, silty clays, sandy clay and silty sands with a medium plasticity, with effective peak friction angle of about 23° and effective cohesion of about 28 kPa.

Level A - resistant rock and mudstone fragments dispersed into a chaotic and plastic clayey matrix; this level was directly involved in the 2003 reactivation of the CL-PO landslide. Values of effective peak friction angle of about 19° and of effective cohesion of about 20 kPa were estimated by direct shear tests conducted on soil matrix samples.

The hard rock horizon is affected by weathering that causes consequences as discoloration, decomposition and weakening as well as the typical scaly structures.

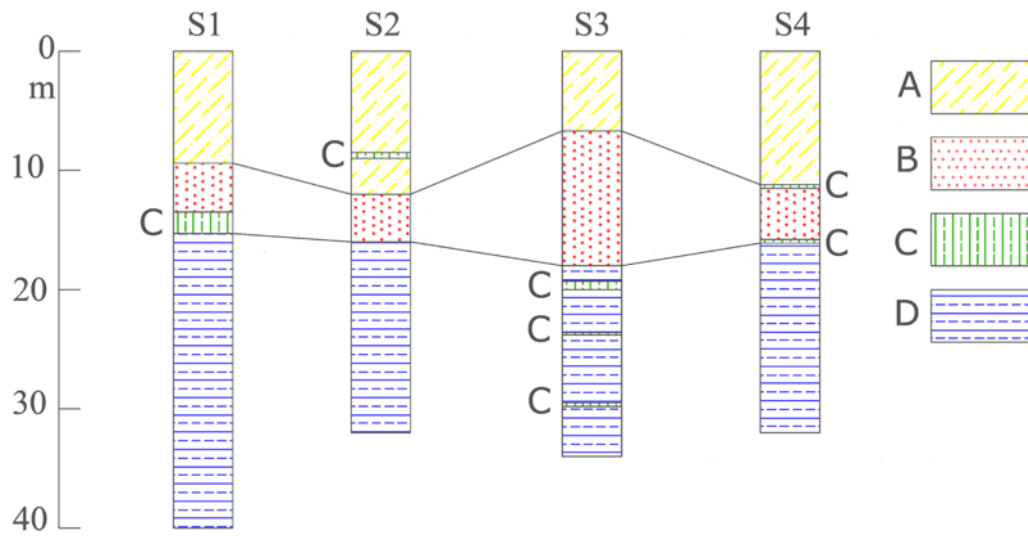


Fig. 3.4 - Engineering-geological interpretation of the data acquired in the boreholes S1, S2, S3 and S4, modified from Calcaterra et al. (2008) and Del Soldato et al., under review_a. A - hard rock fragments and clays; B - clays and sands; C - limestone level; D - marls and clays.

3.1.1 Available data

The available data for this area are ancillary, derived from remote sensing, direct investigations and instrumental monitoring. To characterize quantitatively the morphology of the investigated area, a series of maps derived from the 10-m cell size Digital Terrain Model TINITALY/ 01 DEM Project (Tarquini et al., 2012) were reconstructed, as for the *Aspect* and the *Slope* maps, using geographical tools of ArcGIS®. Furthermore, for the same area a DTM of the Molise Region with 5-m cell resolution was taken into account.

To monitor and analyse kinematically the landslide after the main reactivation, several instruments, both conventional, as inclinometers and piezometers, and remote sensing techniques, were used in addition to several field surveys and campaigns of GPS measurement.

Besides the four boreholes, to understand the local geology of the landslide, in 2006 five inclinometers were installed (**Fig. 3.5**) to monitor the movements occurring across the rupture surfaces of the landslide.

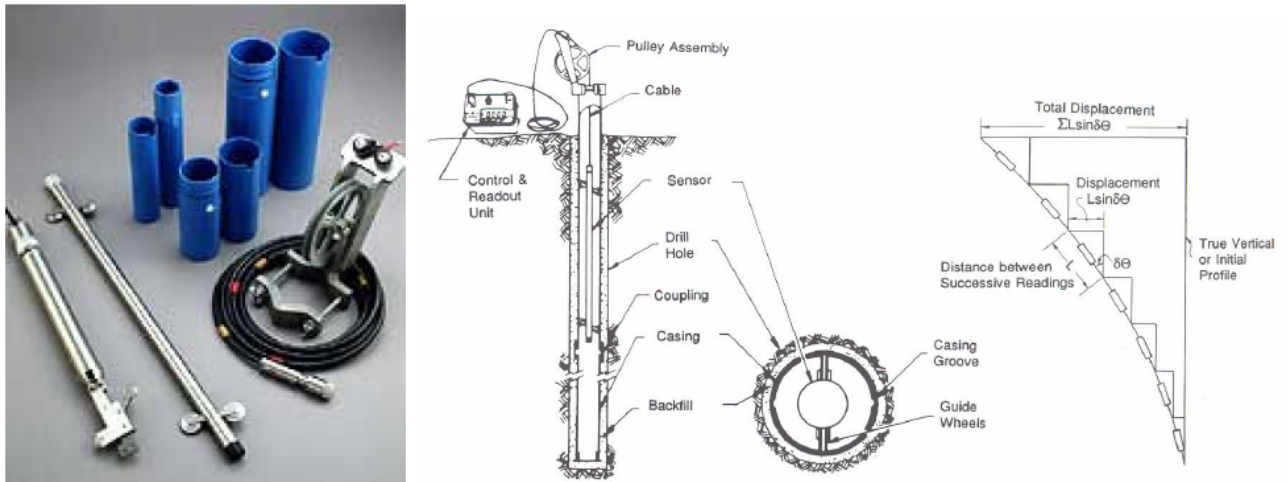


Fig. 3.5 - Picture and scheme of the inclinometer installed to monitor the displacement affecting the CL-PO landslide.

By means of the inclinometers, subsurface movements of a landslide can be determined with an accuracy of the measurement in the order of ± 0.02 mm each 3 m of depth (Borgatti et al., 2006; Bressani et al., 2008; Jongmans et al., 2008; Mihalinec and Ortolan, 2008; Yin et al., 2008). Despite the limitation due to the geometrical features of the inclinometer, which allow only the estimation of the displacement in a vertical plane (2D), the orientation of the displacement (respect to the North) is determined by two vertical logs carried out in the same borehole with a relative angular difference of 90° . From the visual analysis of both inclinometric logs the depth of the rupture surface(s) is determined.

As abovementioned, for the Agnone test sites, four inclinometers were installed within the landslide body (S1, S2/5, S3 and S4) and one beyond the 2006 crown zone, in an apparently stable area (S6) (Fig. 3.6).

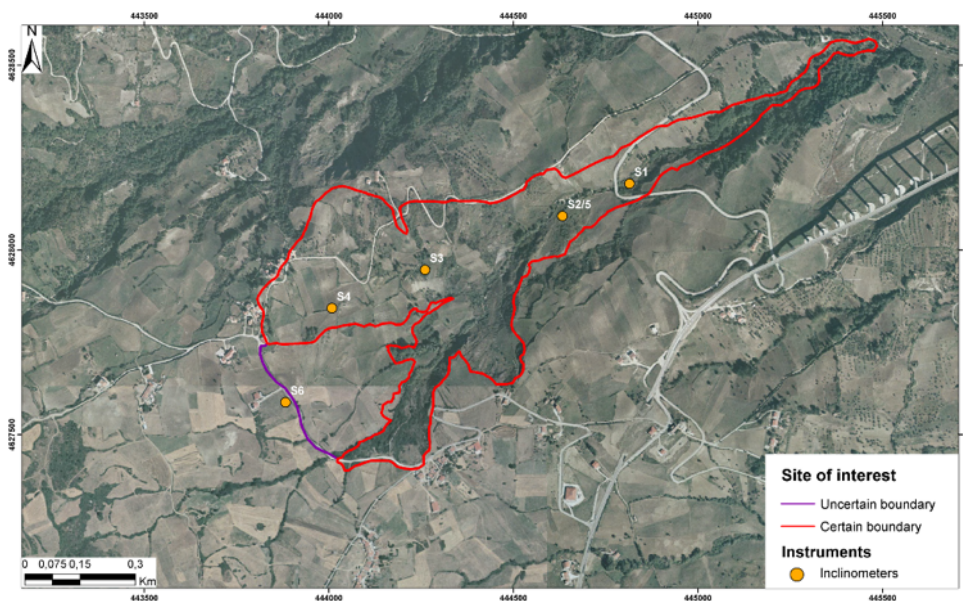


Fig. 3.6 - CL-PO landslide and location of the inclinometers.

Field data were integrated by the remote sensing techniques to investigate the evolution of the landslide by means of historical aerial photos and by the more recent A-DInSAR methodologies. To perform an investigation of the evolution of the landslide, a digital photogrammetric analysis was conducted. At the scope, six series of historical aerial photos of the landslide area, dated back from 1945 to 2003, in grey scale, were obtained by the Italian *Istituto Geografico Militare* (IGM) (**Table 3.1**). Furthermore, one set of colored pictures dated 2005 was provided by the municipal administrator of Agnone.

Table 3.1 - Characteristics of the used aerial photographs.

Acquisition year	Number of photos	Approximate scale	Time span (year)	Flying height (m)	Focal length (mm)
1945	4	1:55000	-	7500	137
1954	8	1:33000	9	6000	153.01
1981	5	1:30000	27	5200	152.55
1986	4	1:28000	5	5100	152.55
1991	6	1:36000	5	6070	153.22
2003	4	1:35000	12	5300	153.31

ERS1/2 and ENVISAT satellite images from 1992 to 2010 elaborated through the PSInSARTM technique by TRE (Telerilevamento Europa Company) were used. They were available from *Portale Cartografico Nazionale* (PCN) of the Italian Environmental Minister (<http://www.pcn.minambiente.it/>) thanks to a specific agreement with the Italian Ministry for the Environment, Territory and Sea (MATTEM).

Furthermore, a study conducted using COSMO-SkyMed images from April 2010 to February 2012 by means of the Announcement of Opportunity Project (ID n° 1460) - COSMO-SkyMed entitled "*Application of DInSAR technique for the slow moving landslides monitoring*", allowed to verify the suitability of DInSAR technique using SAR COSMO-SkyMed images for the Agnone site.

Given the low back scattering of the Persistent Scatterers due to vegetation, to investigate landslide movements in 2010, eight Corner Reflectors (**Fig. 3.7**) were installed with an arrangement consisting in two groups of four: the first placed for the ascending orbit and the second for descending ones. Furthermore, several campaigns of differential GPS measurements, starting from 2010, were carried out to monitor displacement of some specific points of the landslide body (CR1, CR2, CR3, CR4, CR5, CR6, CR7 and CR8) coinciding with the Corner Reflectors. The measurements were based on three stable points with coordinates known by the geodetic Italian network, located outside of the landslide area.

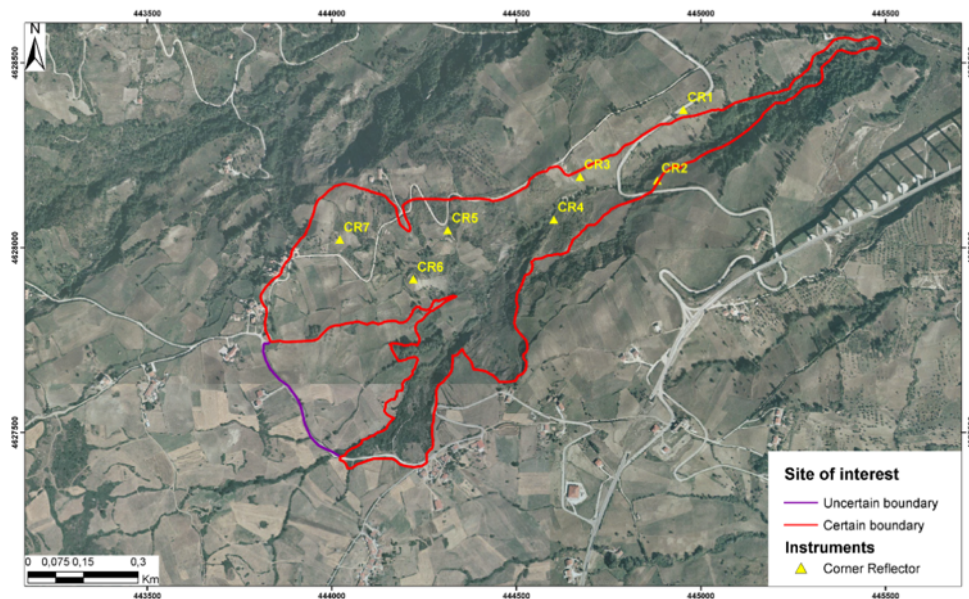


Fig. 3.7 - CL-PO landslide and location of the Corner Reflectors.

For the same area, after the analysis of the C-band products (ERS and ENVISAT sensors) and of 2010 - 2012 COSMO-SkyMed, a new application to a scientific call of the *Italian Space Agency* (ASI) (ASI ID Science 359 - P.I. Del Soldato Matteo) entitled “*Ground deformation monitoring of slow-moving landslides in Agnone (Molise region, Italy) for building damage assessment*” was made to obtain COSMO-SkyMed images. Accordingly, 88 images from 2012 to 2015, 41 in ascending and 47 in descending orbit, were obtained in order to monitor the landslide displacement for a longer period (**Table 3.2**).

Table 3.2 - Main features of the PSI dataset used to study the CL-PO landslide. CSK indicates the COSMO-SkyMed sensor.

Features	ERS	ERS	ENVISAT	ENVISAT	CSK	CSK
Wavelength	C (~5.6 cm)	C (~5.6 cm)	C (~5.6 cm)	C (~5.6 cm)	X (~3.1 cm)	X (~3.1 cm)
Incident Angle θ	~23°	~23°	~23°	~23°	26.6°	26.6°
Geometry	Ascending	Descending	Ascending	Descending	Ascending	Descending
PS cell resolution (m x m)	4 x 20	4 x 20	4 x 20	4 x 20	3 x 3	3 x 3
Revisit time	35 days	35 days	35 days	35 days	16 days	16 days
Temporal span (day/month/year)	25/04/1993 13/12/2000	08/06/1992 07/12/2000	29/11/2002 30/07/2010	07/11/2002 03/06/2010	15/10/2012 01/05/2015	13/02/2012 15/01/2014
Processing method	PSInSAR TM	PSInSAR TM	PSInSAR TM	PSInSAR TM	CPT	CPT
N° of images used	54	78	50	45	41	26

3.2 Geological and geomorphological features of Volterra (central Italy)

The municipality of Volterra, located in Pisa province (Tuscany region, central Italy), at an altitude from 460 to 500 m a.s.l., is extended over about 250 km² and delimited by the Era and Cecina river valleys (**Fig. 3.8**). The most relevant urbanized zones of the municipality are the Volterra urban area and Saline di Volterra, in the south-western sector. The local climate of the area is characterized by dry summer and rainfall concentrated in spring and autumn with a mesothermic, humid, Mediterranean features (Bazzoffi et al., 1997). According to the most recent available data (AMI 2011), the average annual precipitation ranges approximately between 760 and 800 mm per year.

The urban area of Volterra is located in a tectonic depression generated during the post-orogenic extensional stage (Neogene). The wide Pliocene graben-basin, known as Volterra basin, is NW-SE oriented and bordered by normal faults (Giannini et al., 1971). The formation cropping out in the northern area of Volterra municipality is mainly characterized by Miocene-Pliocene diffused clayey (“Argille Azzurre” - “Blue Clays”) and, in southern region, by a sandy marine formation (“Sabbie di Villamagna” - “Villamagna sands”). The top of the sequences is composed of Calcarenites and Limestones closing the marine sedimentary succession, overlapping the marine clays and sands, constituting the tableland on which Volterra city is located (Bianchini et al., 2015b) (**Fig. 3.8b**).

In the southern sector of the municipal territory chemical sedimentary deposits, such as travertine and gypsum levels (Miocenic evaporitic episodes) are present (Bazzoffi et al., 1997; Pascucci et al., 1999). Furthermore, fine and detrital coarse sediments developed in lacustrine/lagoonal or continental fluvial-deltaic environments, e.g. “Fosci Clays” and conglomerates and breccias, respectively, mantle the territory of the Volterra municipality. Sporadically, in the SE basin, some underlying Jurassic–Cretaceous ophiolitic rocks outcrops (i.e. serpentinites, basalts and gabbros) and marls and sandstones were formed by several sedimentary cycles. Finally, recent colluvial and alluvial deposits fill the valleys which are incised by rivers and streams over the whole area (Pascucci et al., 1999).

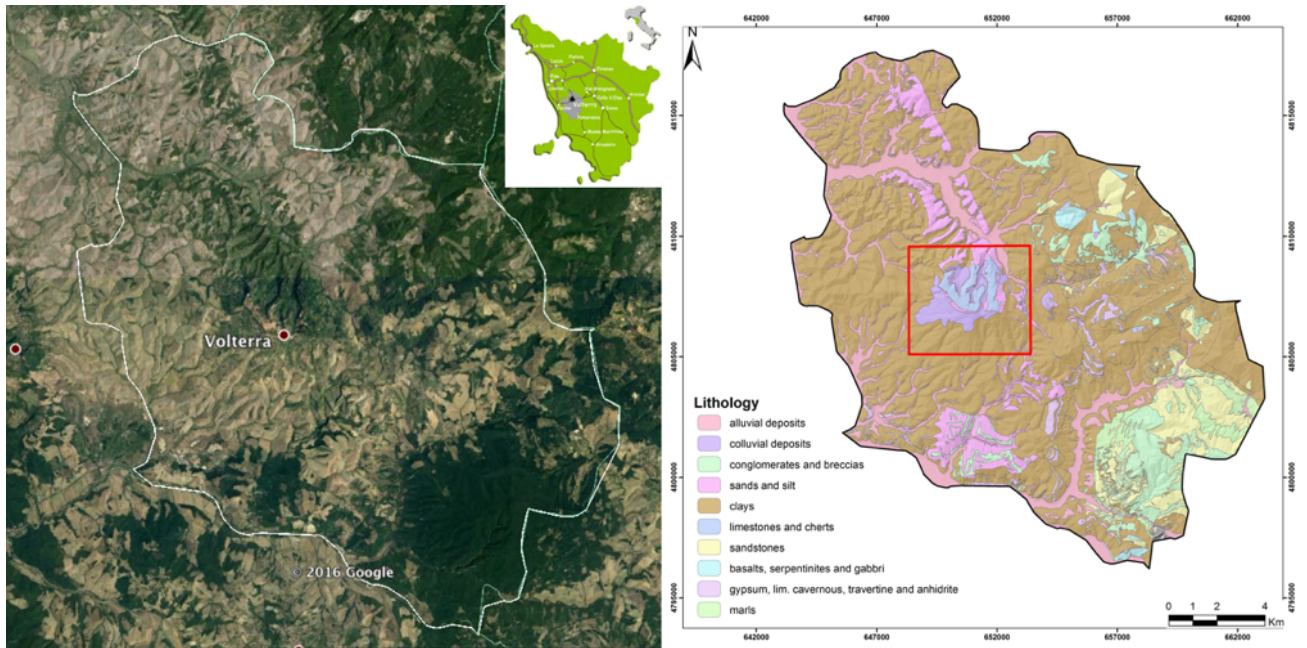


Fig. 3.8 - Location of the municipality of Volterra (a) with the investigated area highlighted by the red box. b) The geological map of the whole municipality.

The chosen test site in the municipality of Volterra, affected by slope instability, is located in the southwestern sector of the town (identified by the red colour in **Fig. 3.9**), characterized by a semi-urban and rural landscape and enclosed between the watersheds of Cecina, Arno, Botro and Pagliaro rivers. The buildings in the studies area are both masonry and concrete structures with different foundation types (e.g. direct foundations, bearing piles or continuous one), all realized after the 19th century.

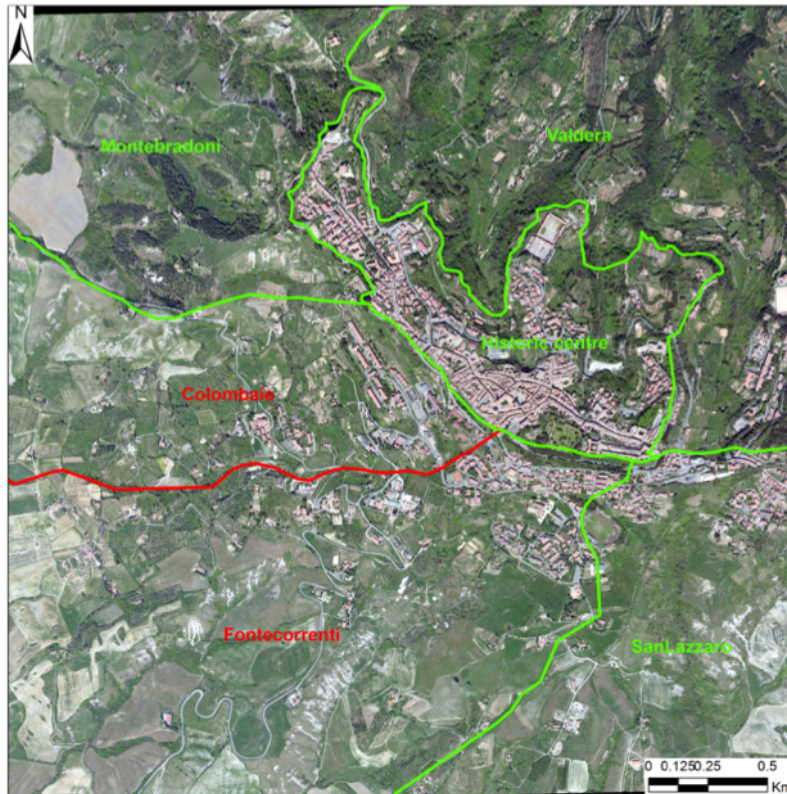


Fig. 3.9 - Sectors of Volterra town. In red the two investigated sectors involved by a landslide are highlighted.

The morphology of the studied area is typically hilly, with moderate relief and gentle slopes. The outcropping formations in this area retrace the main stratigraphic sequences present in the municipality with a level of marine “Blue Clays” overlapped by cemented “Villamagna sands” and the upper calcarenitic tableland, named also “Volterra limestone” (**Fig. 3.10a**). Moreover, in the area of interest they are mantled by shallow colluvial deposits, reaching locally thickness of 20 m, contributing to the ground instability whit diffuse superficial landsliding (Bianchini et al., 2015b; Pratesi et al., 2015). Sedimentary lithological units outcropping in the area of interest show a bedding with dip north-eastward between 2° and 10° (Terrenato, 1998; Sabelli et al., 2012) (**Fig. 3.10b**). The characteristic very steep, quite sub-vertical, cliffs around the Volterra tableland were caused by the different geotechnical properties between the upper well-cemented Volterra calcarenites, the overlapping erodible Villamagna sands and the lower impermeable clays.

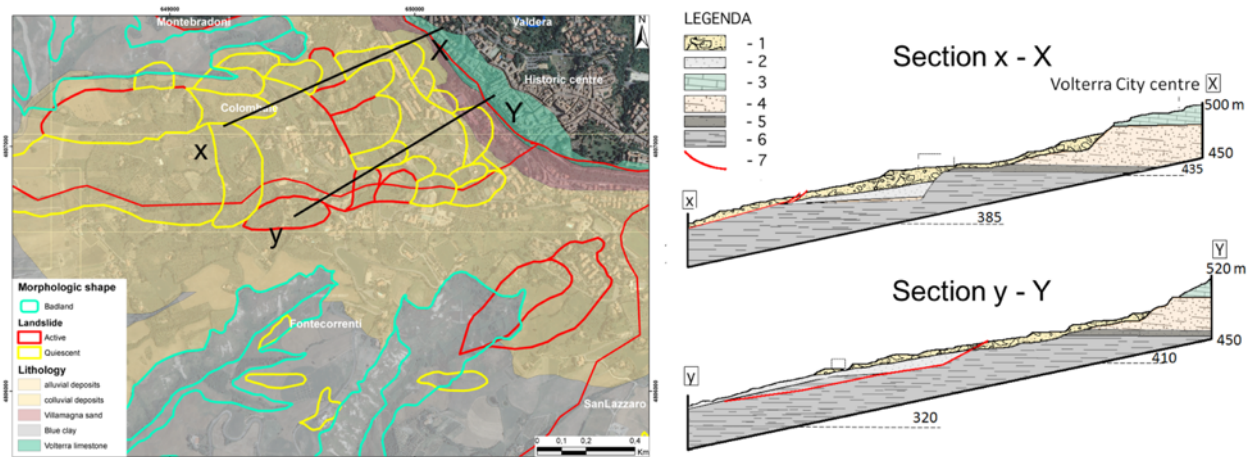


Fig. 3.10 - Geology of the SW area of the municipality of Volterra with the overlapped landslide and badland inventories (a) and two geological cross-sections (b). 1 - sandy detritus; 2 - clay detritus 3 - "Volterra limestone"; 4 - "Villamagna sand"; 5 - "Blue clay"; 6 - clay; 7 - sliding surface (GEOSER s.c.r.l. & GEOPROGETTI company).

The combination of hydrogeological features and setting of these formations caused the undermining of the basal clays of the Volterra hills with consequent retrogressive slope failures (Bianchini et al., 2016). In the entire municipal territory, more than one thousand of mass movements, categorized for their state of activity and typology of movement, were mapped (Fig. 3.11a) The main landslide typologies affecting this territory are represented by shallow transitional slides and soil erosion, according to the available landslide inventory map provided by the Tuscany region referred to 2012. Furthermore, the topography and the geological structure of the tableland influenced the spatial distribution and the typology of landslide involving the area (Bianchini et al., 2015b). Typical gullies in clayey soils characterize the southern slope of the Volterra hill where the "Blue Clays" mainly crop out (Fig. 3.11b), The two main types of *calanchi* are: "Type A", characterized by incised landforms with unvegetated and "knife-edged" ridge (Moretti and Rodolfi, 2000); "Type B", featured by shallow slides coexisting with concentrated water erosion (Rodolfi and Frascati, 1979).

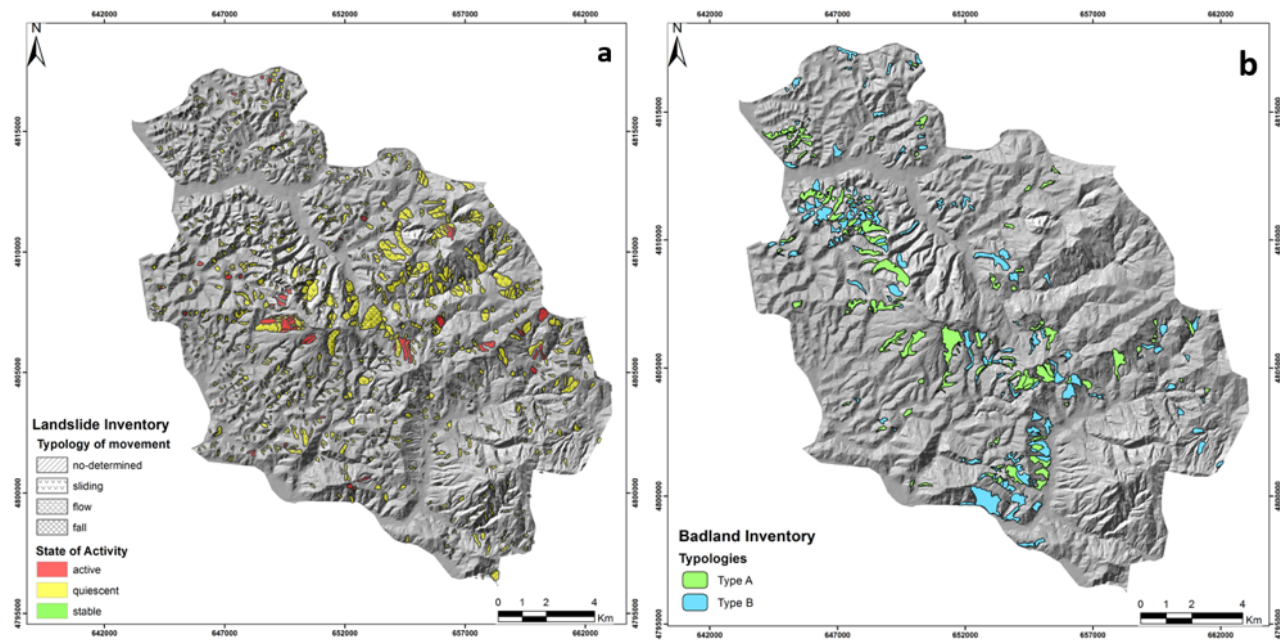


Fig. 3.11 - Inventories of landslide (a) and badlands (b) affecting the municipal territory of Volterra.

3.2.1 Available data

Data for analyses were obtained by remote sensing techniques, instruments located into and close to the landslide area, terrain calculations on Digital Terrain Model (DTM) data, with 10-m cell size resolution obtained from TINITALY/ 01 DEM Project (Tarquini et al., 2012), allowing the reconstruction carried out by ArcGIS® software of *Aspect* and *Slope* digital maps.

The lithologies of the southwestern region of Volterra affected by slope instabilities were investigated by means of twelve drillings by the GEOSER s.c.r.l. & GEOPROGETTI company (Fig. 3.12). Some of these were subsequently converted in piezometers and inclinometers (S1, S2, S4, S6, S7, S8 and S11) to monitor the depth of the water table and the movement of the landslide, respectively.

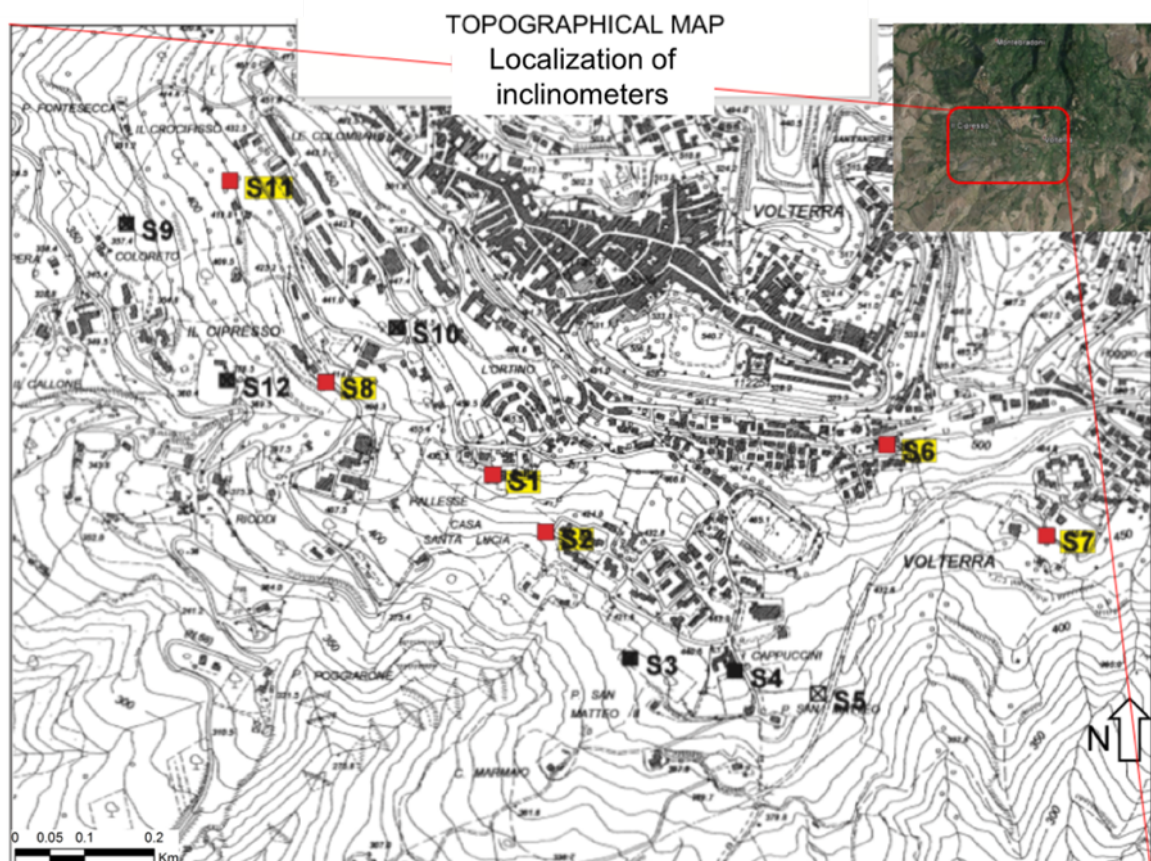


Fig. 3.12 - Topographical map (1:5000) of the southwestern area of Volterra with the location of the drillings and the inclinometric investigations (GEOSER s.c.r. & GEOPROGETTI, 2010).

The inclinometers installed in seven boreholes were system IN910 (Fig. 3.13) provided by SIM INSTRUMENT S.n.c. Company of Magenta, Milan (Lombardy province, north Italy). They were located as follows:

- S1, S2 and S4 in the *Fontecorrenti* area. The inclinometer S4 was destroyed and made useless;
- S6 and S7 in the *San Lazzaro* region;
- S8 and S11 in the *Le Colombaie* zone.

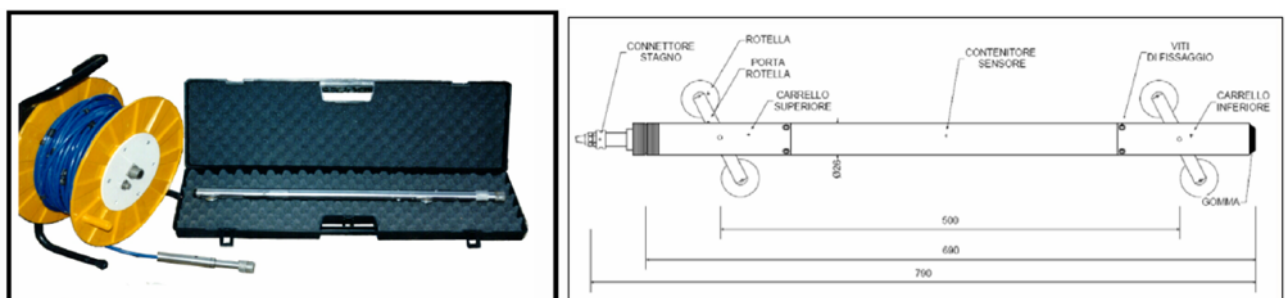


Fig. 3.13 - Details of the inclinometer used to monitor the landslide in Volterra.

In addition to conventional methods, remote sensing investigations by means of historical aerial images, analysed by the *Structure from Motion* technique, and Persistent Scatterers developed by the A-DInSAR methods were adopted to investigate the area of interest.

The available historical aerial images were requested to the Italian *Istituto Geografico Militare* (IGM) database and five series covering the area of interest from 1954 to 1996, in grey scale, were found and obtained (**Table 3.3**).

Table 3.3 - Characteristics of the historical aerial photographs.

Acquisition year	Number of photos	Approximate scale	Time span (year)	Flying height (m)	Focal length (mm)
1954	3	1:30000	-	5000	154.17
1965	4	1:22000	11	3000	152.35
1982	5	1:30000	17	4500	152.55
1986	3	1:32000	4	5000	152.55
1995	2	1:38000	9	5800	152.73
1996	2	1:40000	1	6200	153.22

ERS1/2 and ENVISAT Persistent Scatterers located in the investigated area were identified by the Portale Cartografico Nazionale (PCN) of the Italian Environmental Ministry (<http://www.pcn.minambiente.it/>). To investigate the deformation PS of C-band ERS1/2, acquired in the descending orbit, and ENVISAT, in both ascending and descending data, from 1992 to 2000 and from 2003 to 2010, respectively, were analysed. Furthermore, 57 COSMO-SkyMed X-band images were provided by the Italian Space Agency under request of the Italian Civil Protection Department to investigate the territory affected by hydrogeological problems during 2014, e.g. Volterra. These images covering the studied area from 2010 to 2015 (**Table 3.4**).

Table 3.4 - Main features of the PSI dataset in the Volterra site. CSK indicates the COSMO-SkyMed sensor.

Features	ERS	ENVISAT	ENVISAT	CSK	CSK
Wavelength	C (~5.6 cm)	C (~5.6 cm)	C (~5.6 cm)	X (~3.1 cm)	X (~3.1 cm)
Incident Angle θ	~23°	~23°	~23°	31°	26.6°
Geometry	Descending	Ascending	Descending	Ascending	Descending
PS cell resolution (m x m)	4 x 20	4 x 20	4 x 20	3 x 3	3 x 3
Revisit time	35 days	35 days	35 days	16 days	16 day
Temporal span (day/month/year)	24/09/1992 27/11/2000	26/08/2003 20/07/2010	10/02/2003 28/06/2010	24/02/2010 15/11/2013	28/01/2011 07/01/2015
Processing method	PSInSAR TM	PSInSAR TM	PSInSAR TM	SqueeSAR TM	SqueeSAR TM
N° of images used	41	41	35	25	41

4 Methodology

Both remote sensing analysis and field surveys were executed. In this chapter, the different methodologies applied to the two investigated areas are explained and described in detail.

4.1 Remote sensing analysis

Several techniques of remote sensing were applied for the scopes of the PhD research. The PhD investigations were developed with the contribution of the *Structure from Motion* technique, to reconstruct the 3D model of the study areas and landslide evolutionary stages. Moreover, Advanced-Differential Interferometry products, obtained by the elaboration of Synthetic Aperture Radar images in C- and X-band, were also used for the scopes of the research.

4.1.1 3D reconstruction of aerial images

Historically, “photogrammetrie” was a name coined by pioneers in the 1840’s who used cameras to estimate the shape of terrain through ground and aerial photographs (Jebara et al., 1999; Maybank, 2012). Digital photogrammetric analysis is a cost-effective and useful tool to pursue geomorphological studies (Lane et al., 1993; Chandler, 1999). Old aerial non-digital photos provide a two-dimensional (2D) sight and a three-dimensional (3D) vision only for the overlapped area by means of stereoscopy. Despite the use of old aerial photos shows several limitations, it still plays a key role to detect, map and monitor geomorphological and environmental evolution of natural processes affecting the territory (Carrara et al., 2003). For this reason, cost-effective methods for modelling and remote sensing approaches were spread and increased in importance in last decades (García-Ruiz et al., 2013). The analysis conducted by stereophotogrammetry using non-digital images, allows the observation of geomorphological evolution along several decades (Hapke, 2005). Currently, the use of a stereoscope is considered obsolete and a relatively old technique (Slama et al., 1980), while several free and commercial software packages allowing the 3D vision through the use of anaglyph glasses (glasses with one lens blue and the other one red) were developed. Formerly, historical aerial photos were used for producing Digital Elevation Models (DEMs) (Dewitte et al., 2008), to delineate geomorphological shapes and for analysing their evolution in time. Recently, the popularity of remote sensing techniques, such as *Structure from Motion* (*SfM* in the following) emerged in the late 1970s (Ullman, 1979), becoming more and more important since the last decade (Abellan et al., 2016). Digital models created through 3D laser scanning or LiDAR (Light Detection And Ranging) instruments can show the evolution between different acquisitions of data related to specific moments without the possibility to obtain digital

information of the past. Contrarily, *SfM* technique, allowing the reconstruction of a surface by means of digital photographs, can be used in order to investigate the situation of a site in several moments. Therefore, if historical digitalized images (non-digital scanned pictures) of a site were available, it is reasonable to consider that a digital model can be generated to reconstruct the geomorphological situation since the 40's (years of the first historical series available for many areas) in order to investigate the evolution of the recognizable phenomena.

Despite the algorithm was developed several years ago, the application of the *SfM* technique for geomorphological studies of the Earth surface evolution, and in the geosciences in general, is an emerging approach with basic tenets comparable to those of the stereo-photogrammetry (Snavely et al., 2008; Westoby et al., 2012). This approach allows to generate 3D point clouds (hereafter 3DPC) handling a set of overlapping digital photographs to represent, in a relative "image-space" coordinate system, the geometry and the structure of the scene (Hartley and Zisserman, 2003; Szeliski, 2010; Fisher et al., 2013). To project the object of interest in an absolute coordinate system, some Ground Control Points (GCPs) with known object-space coordinates have to be inserted in order to make useful this technique in the geosciences branch.

The *SfM* approach is widely used for applications of computer vision to recover 3D shape and appearance of objects in imagery (Szeliski, 2010; Doneus et al., 2011). In literature, several examples of 3D reconstructions of external façades of buildings and monuments (e.g. Snavely et al., 2008; Furukawa and Ponce, 2010) or archaeological sites (e.g. Doneus et al., 2011; Verhoeven, 2011; Verhoeven et al., 2012) are available. Moreover, the recent diffusion of Unmanned Aerial Vehicles (UAVs) allowed the application of *SfM* techniques to produce Digital Elevation Models (DEMs) (Turner et al., 2012; Lucieer et al., 2013; James and Robson, 2014).

Agisoft Photoscan Pro software exploits the *SfM* technique and it works using digital images and algorithms optimized for taking advantages of the graphic processing unit (GPU) (Lucieer et al., 2013). The *SfM* procedure and the parameters commonly adopted in Photoscan are described in Verhoeven (2011) and Doneus et al. (2011). To investigate the evolution of the two test areas, the common procedure to reconstruct in 3D on object has been adapted to generate 3D models from historical aerial non-digital images. The simply imagery processing workflow is summarized in **Fig. 4.1**.

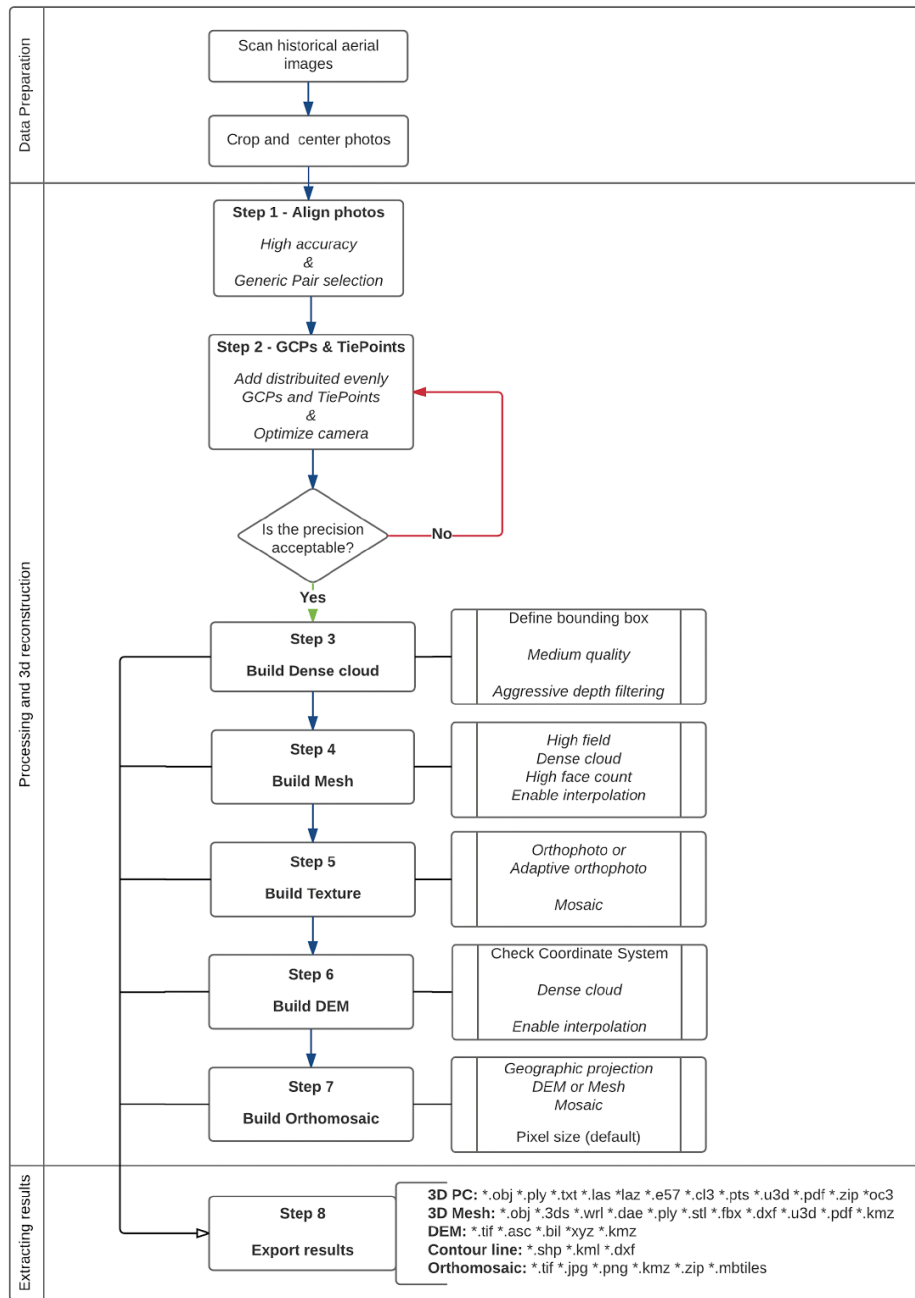


Fig. 4.1 - Adapted workflow for 3D reconstruction by non-digital historical images.

The proposed flowchart gives an easy overview of the processing, with the dedicated setting adopted for historical non-digital photos that could have relevant impact for the study of environmental evolution (Carrara et al., 2003). By means of the reconstruction of 3D models and the extraction of information for areas where, at least, two images took in the same time are partially overlapped, this approach offers an important opportunity to apply the *SfM* technique in the geosciences branch. Furthermore, these features permit to analyse the evolution of geomorphological features over wide areas by historical aerial pictures

available since, at least, the '40s.

First of all, the correct choice of the images covering the area of interest is fundamental. For example, one of the most important factors that determines a reliable reconstruction is the overlapping between, at least, two pictures of the investigated area. This condition plays a key role to develop the 3D reconstruction without bumping into errors and lacks of information in the restitutions. The available old source data are generally printed images and, given that the software works with digital imagery, raw data have to be digitalized through a scan process with close attention and appropriate resolution to preserve all the valuable information. It is worthy to note that photos, and consequently scanned images, can be degraded by time and even ruined by the users compromising some information. Secondly, the scanned images have to be cropped, preserving the central pixel coincident with the intersection of the optical axis in order to have exactly the same number of pixels to be processed by the software recognising all the images as shot by the same camera.

The first phase of the process is the alignment of the prepared images. Once that all images are loaded in a *chunk*⁵, the alignment process can be performed, in order to allow the software to automatically calculate the camera positions and orientations in the local “image-space” coordinate system and to correlate images each other. A big advantage of the *SfM* technique is the automatic reconstruction of the scene geometry, the camera pose and its orientation (Snavely et al., 2008), by means of a redundant iterative bundle adjustment procedure on features extracted from a set of overlapping digital imagery. In this way, the camera parameters are assessed and calibrated, and if the images are well prepared they have to be recognized as acquired by the same camera type, in order to apply the optimization processes and the lens calibration to all images simultaneously. This process allows to dramatically reduce the number of unknowns. The alignment step is performed using simple settings (**Fig. 4.2a**): *High accuracy, Generic pair selection*, suitable for unknown camera positions as for old aerial images.

The alignment procedure has to be conducted for each set of images, e.g. for each year of recording and for each area of interest. If the area of interest is close to water regions (e.g. big lake or sea), much attention has to be paid. It could happen that a large part of the overlapped area between the images under process falls into water areas and the alignment could be not allowed due to the lack of information. In case this occurs, a mask to “eliminate” the area with no, or not enough, information, e.g. water regions, can be created and the alignment has to be launched again.

The provided result of the first phase is a sparse point cloud of the overlapped area with the relative position in the “space-image” of the processed photos (**Fig. 4.2b**).

⁵ **Chunk**: box where set of photos could be split if in the same project different years are present concerning the same area or different areas of interest. The elaboration of the images is conducted separately.



Fig. 4.2 - a) Screenshot of the setting for the suitable alignment for historical aerial photos, when the camera position is unknown. **b)** Sparse cloud generated after the alignment of the images.

The re-projection of a sparse cloud from a local “image-space” coordinate system to an absolute coordinate system chosen by the operator is possible adding several GCPs and TiePoints (step 2 in **Fig. 4.1**). The handbook of Photoscan (2013) suggests to input at least 10 - 15 GCPs distributed evenly within the area of interest to obtain a good georeferencing. The accumulated experience had taught that the main important thing for obtaining a high precision is a good distribution of the GPCs in the whole area, increasing their number. In addition, Tie Points, points with no coordinates, but well-recognizable on each image, can be added to increase the correlation between the different overlapping images and to improve the correction of their distortion. The coordinates of the GCPs can be obtained by means of GPS campaigns during field surveys or they can be extracted from DEM or through official Web Map Services (WMS) available on web sites. Close attention has to be paid to recognize as accurate as possible the same location of points where the coordinates are taken on historical and currently available photos. Once that several GCPs are inserted on the aligned photos (**Fig. 4.3a**), the referring coordinate system has to be updated in that of the inserted points and the calibration process has to be launched. By means of the *Optimize camera* tool, error in meters and in pixels of each GPCs input is automatically calculated (**Fig. 4.3b**). The suggested parameter by the software can be used and an expected precision of the georeferencing were visualized in the bottom of the GCPs of the list. In case the obtained precision is not enough for the aim of the work, errors can be enhanced in several ways:

- a) switching off GPCs with excessive errors;
- b) checking the correct positioning of the GCPs and the correspondence of the TiePoints;
- c) improving the numbers of GCPs and covering areas in which they are scarce;
- d) adding some Tie Points to improve the alignment and the correlation between the overlapped images.

The calibration tool has to be launched each time that some GCPs or TiePoints are added, switched off or

modified, to update the georeferencing precision assessment.

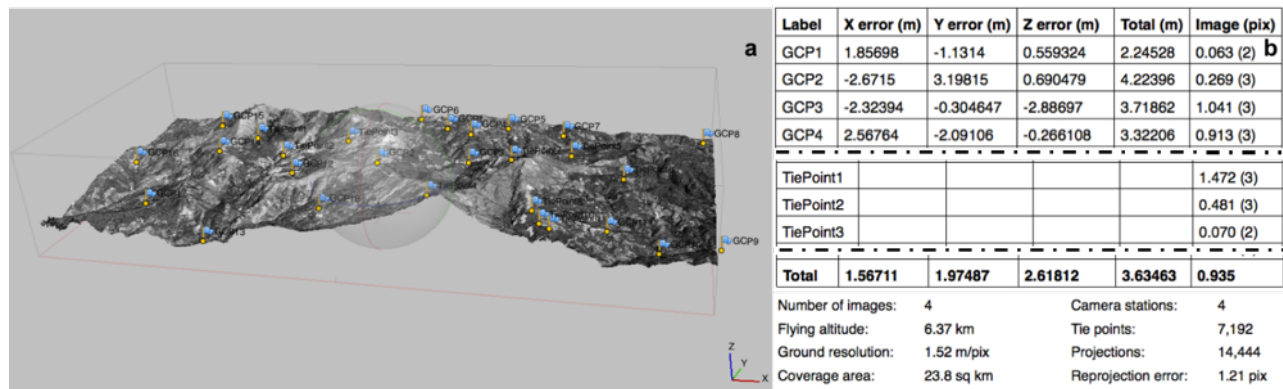


Fig. 4.3 - a) Dense cloud of a Ligurian area where several Ground Control Points and Tie Points were added. **b)** Example of the table in which the errors of the inserted GCPs and TiePoints are shown.

The 3D reconstruction is generated into a delineated space that can be sized and rotated to set the bounding box in which the 3D Point Cloud, and the subsequently products, will be generated. Attention has to be paid during the orienting phase of the ground plane, recognizable by means of the red colour (the lower surface of the box in **Fig. 4.4a**), under the model and parallel to the XY plane. This operation is important because it defines the reconstruction plane for the tool to calculate the height information from the terrain surface to be assigned to each point of the 3DPC. The 3DPC generation is conducted setting the *Quality* as *Medium* and the *Depth filtering* as *Aggressive* (**Fig. 4.4b**). The *Medium* quality is enough for the goal of the work considering that the reconstruction is conducted on digitalized historical images that not have high resolution. A higher quality would ask more time and a higher performance of the machine should be necessary, with high probability to obtain no better results since the cell of work considered by the algorithm would be smaller than the pixel resolution of the processed imagery (Photoscan, 2013). The depth filtering is set as *Aggressive* because this preference is suitable for areas with no meaningful detail and it allows to sort out most of the outliers, then it results adequate for the reconstruction of terrain from historical aerial images. Using other filters, areas with important slope changes are generally visualized as holes, thus showing areas with no information.

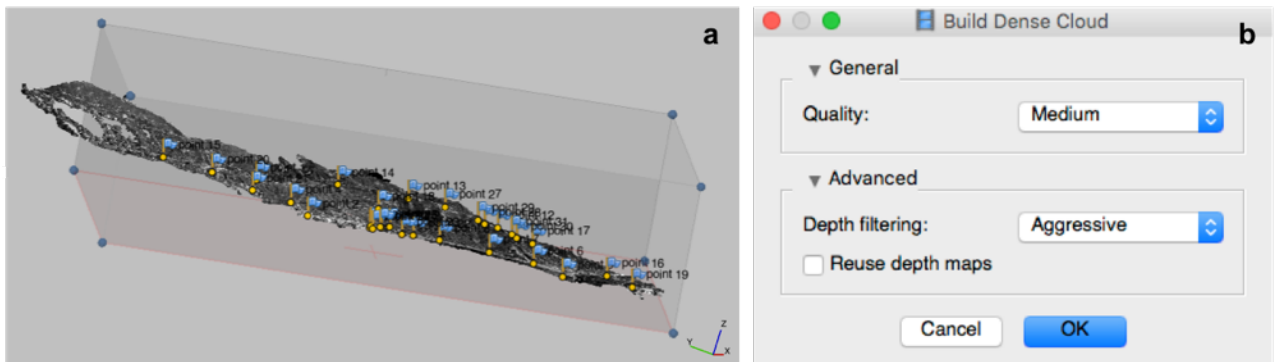


Fig. 4.4 - a) Reshaping of the Box where the Dense Cloud will be generate. b) Setting of the Dense Cloud tool.

The subsequent step envisages the reconstruction of the polygonal mesh from the 3DPC data previously generated. As settings in the tool window *High field as Surface type*, *Dense cloud as Source data* and *High Face count* configuration are chosen (**Fig. 4.5a**). *High field* as surface type is suitable for aerial images because it is optimized for modelling planar surfaces as terrains or basereliefs. The *Interpolation* preference allows three possibilities based on the aim of the study: *Enable (default)* creates the mesh closing holes, if present in the 3DPC, interpolating points close to them; *Disabled* leaves the holes also in the computed mesh; *Extrapolated* generates a mesh extrapolating it until the boundary of the box previously defined, even if bigger than the dense points cloud. In case some holes are present, they subsequently can be also closed editing the geometry by means of a tool that works in the same way, even if the mesh was generated.

Despite the creation of the texture is not mandatory, it can be built on the mesh data to further inspect the possible reconstruction of the area of interest before generating the model and exporting results. To perform the texture *Orthophotos* or *Adaptive Orthophotos* as *Mapping mode* and *Mosaic (default)* as *Blending mode* parameters have to be set (**Fig. 4.5b**). The choice between the *Orthophotos* or *Adaptive orthophotos* has to be taken based on the investigated area. *Orthophotos* and *Adaptive orthophotos* work with the same algorithm, but the second one, in addition, processes separately regions where vertical areas are present.

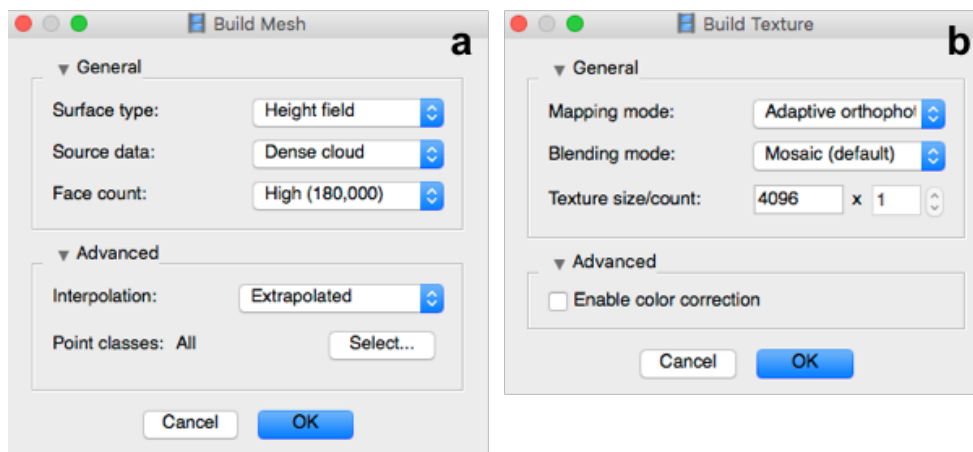


Fig. 4.5 - Setting to generate the Mesh (a) and the Texture (b).

At the end, Digital Elevation Model and the Orthomosaic of the whole area covered by images can be reconstructed. The DEM generation is based on the *Dense cloud* and as Coordinate System the one assigned during the input the GCPs is suggested by the software. The *Interpolation* setting (Fig. 4.6a) follows the same choices used for the Mesh generation (Step 4 in Fig. 4.1). Setting boundary by coordinates is not necessary because at default the used box dimensions are fixed during the phase concerning the generation of the 3DPC. Once performed the DEM, the contour lines can be set by the operator and automatically traced by the software according to chosen interval (Fig. 4.6b). Obviously, the quality of the generated model strongly depends on the available initial data and on the accuracy used during the input of GPCs and TiePoints.

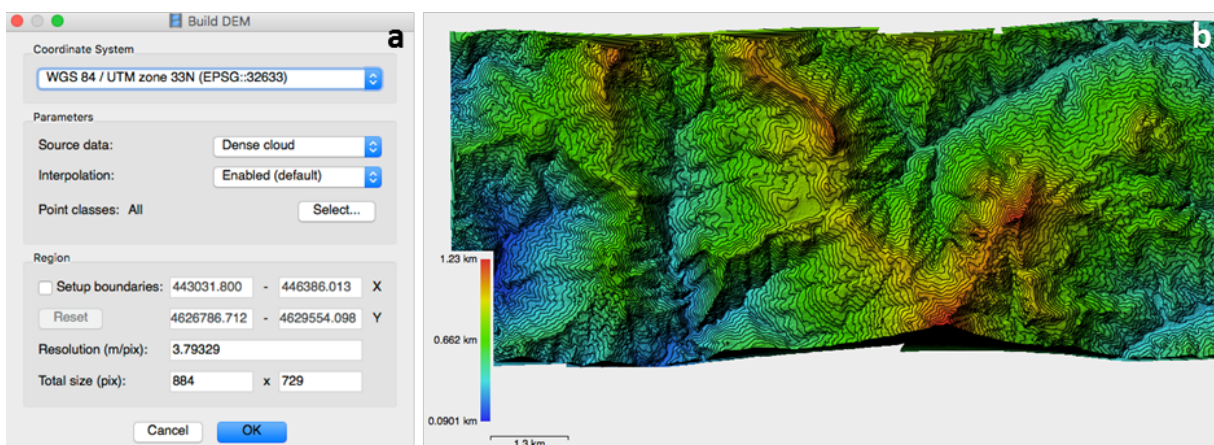


Fig. 4.6 - Parameters for the DEM generation (a) and an example of DEM with 25 m contour (b).

The *orthomosaic*, generated starting from the Digital Elevation Model or from the Mesh, allows to have a preliminary vision of the whole rebuilt and georeferenced area by means of the use of the historical aerial images. Also in this case, in the preferences dialog box it is possible to choice of the coordinate system of the product, the Geographical projection used in the previous stage is suggested, and the *Blending mode* at

default is set as *Mosaic mode* in the texture passage. The pixel size, shown in the bottom of the dialog box, is automatically set according to the resolution of the initial data, the developed processing and the size of the *orthomosaic*. As for the DEM, it is not necessary to set the boundary coordinates because they are carried out by the previous stages.

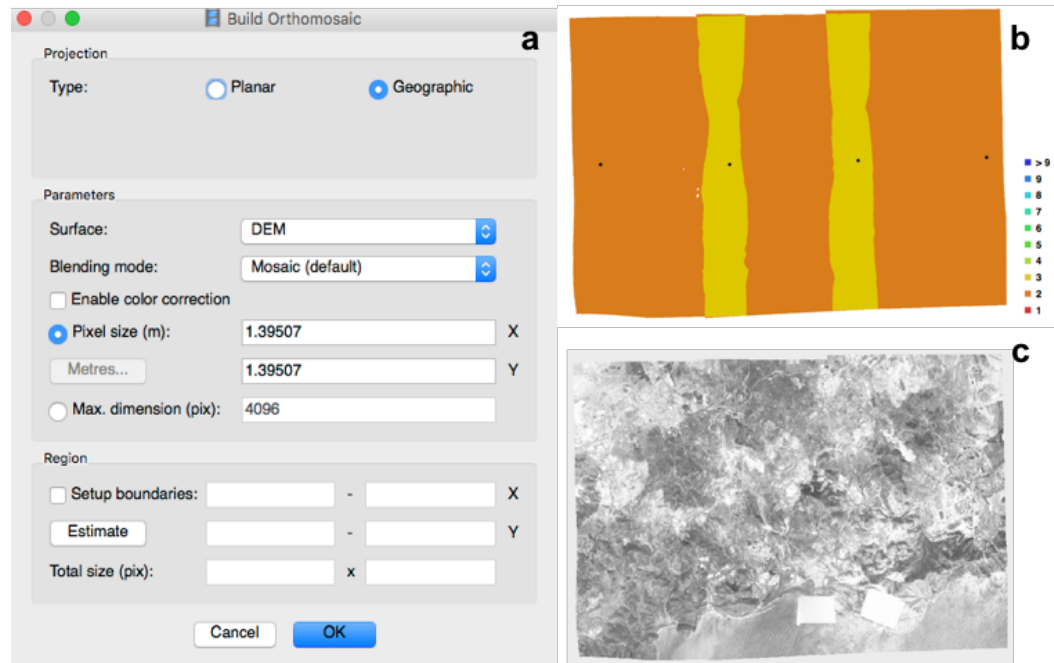


Fig. 4.7 - Preferences to build the *orthomosaic* (a) for a region covered by three historical images with sufficient overlapping area (b) to generate it. The result is a big georeferenced image (c) covering the entire area with enough overlapping to correlate the single shot.

4.1.2 Persistent Scatterer Interferometry

4.1.2.1 Radar

Radio Detection And Ranging, known as RADAR, is a technique based on the use of electromagnetic waves that allow to determine the position as well as the velocity of fix and moving targets with high precision. The radar technology works with a two-way travel time of pulses in radio wavelengths. The receiver is able to assess the echo of the back-scattered signal by the object inferring its intensity and physical quantity. The technique was born for military applications and only in the last decades was spread also for civil and scientific utilizations (Hanssen, 2001). The use of this type of sensors allows the acquisition of data independently of the weather conditions and illuminations getting it usable regardless during day and night. The application in geosciences gives big advantages for monitoring geomorphological evolutions, for instance, by means of the possibility to have overviews of wide regions of the Earth. Radar geometry (**Fig.**

4.8) is able to distinguish targets, differently from the optical instruments, by means of their reflected signal only based on the returning time of the emitted signal. Is it worthy to notice that, to perform this, the radar works using a *side-looking* shape to enlighten just one side of the ground range, generally the right-side.

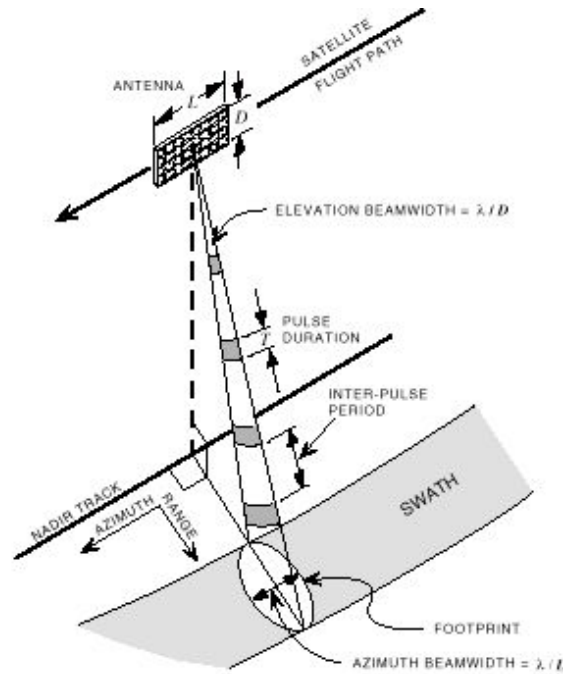


Fig. 4.8 - Image Radar geometry (Trivero and Biamino, 2010).

Swath is the area of the Earth surface enlightened by the microwave beam with a certain obliquity with respect to the nadir. The *azimuth range* or *along-track* is the direction along the trajectory of the sensor, while the *ground range* or *across-track* is the perpendicular way. The direction between the antenna and the object along the *Line of Sight (LOS)* is called *Slant range*. Given that the radar is side-looking, the *angle of incident* and the *angle of local incident* have to be distinguished (Fig. 4.9). The first one is the angle between the radar waves and the vertical ones, while the local incident is the angle formed between the radar waves and the normal with respect to the surface, subjects to changes according the ground slope.

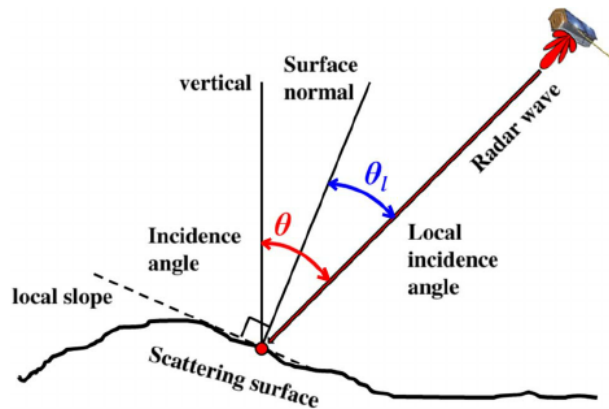


Fig. 4.9 - Relation between the LOS and the geometry for the incidence angle θ and for the local incidence angle θ_l (Rizzoli and Bräutigam, 2014).

4.1.2.2 Synthetic Aperture Radar (SAR)

The Synthetic Aperture Radar (SAR) is a technique in which the signal processing is used to improve the resolution “synthesizing” a very long antenna (Fig. 4.10). This permits to maintain an antenna with reasonable dimension reaching good resolution.

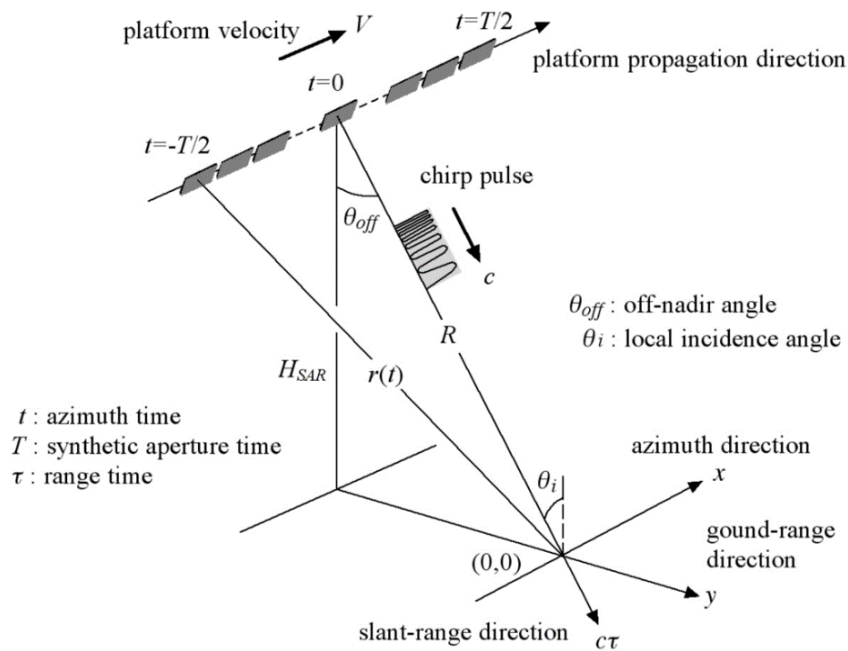


Fig. 4.10 - The geometry and terms of the SAR systems (Ouchi, 2013). H_{SAR} : height of the SAR platform; c : velocity of the microwave; $r(t)$: slant-range distances at the azimuth time t ; R : slant-range distances at the azimuth when the antenna is nearest to the target at the origin of the ground coordinate system (x, y) .

SAR sensors can work in different bands of the electromagnetic spectrum (Fig. 4.11) and, based on the length of the wavelength, the penetration of the signal changes. For instance, to have strong penetration

into the vegetation and soils the wavelength should be longer, then with low frequency (e.g. L-band).

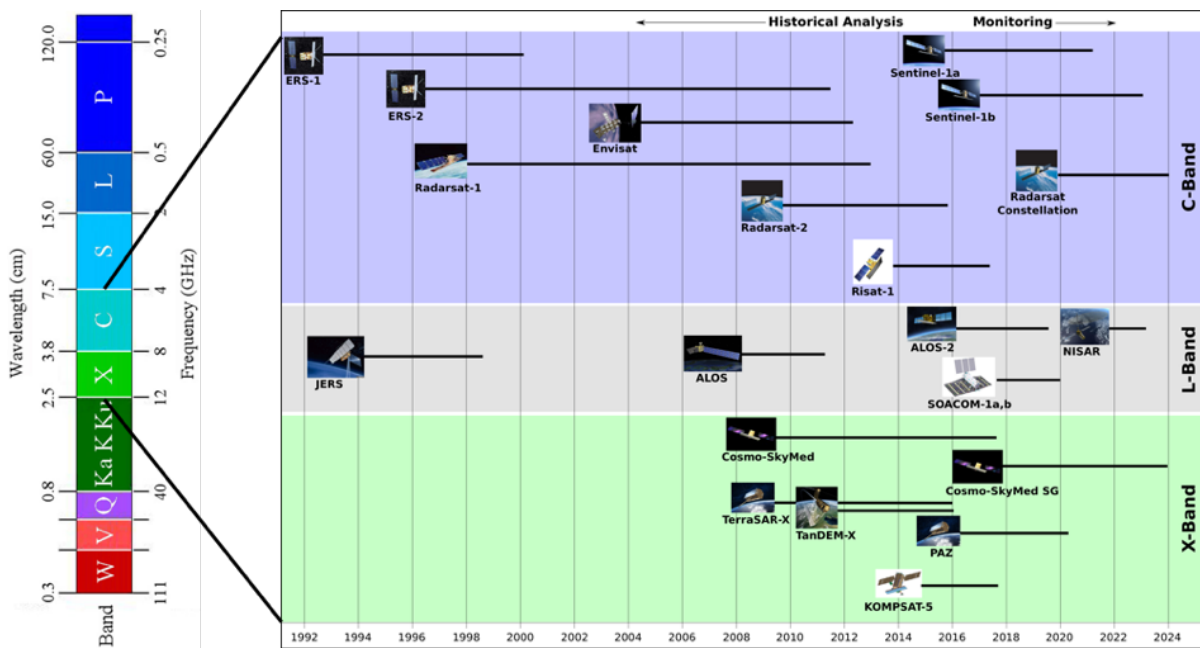


Fig. 4.11 - Microwave spectrum used for the SAR methods (Ouchi, 2013) related with the satellite constellation on which were mounted (past, present and future launches).

The images registered from the radar satellite sensors are affected by geometric and radiometric distortions. The geometric distortion is due to the relationship between the Line of Sight (LOS) of the satellite, function depending also on the flying line, and the topography of the scanned area. Objects close to the flying area (*near range*) appear compressed in direction of the ground range if compared with objects farther from the sensor (*far range*). Through the *slant-to-ground projection*, it is possible to approximate the real position of the sensors and better interpret the resulting images knowing the average height of the sensor with respect to the area. Three types of geometrical distortions affect the images captured from the side-looking satellites:

- **Foreshortening (Fig. 4.12a):** when the radar beam reaches the base of a tall feature tilted towards the radar (e.g. a mountain) before the top of it, the foreshortening effect occurs. The distance between these two points (A to B), from the radar measures distance in slant-range, appears compressed representing the length of the slope incorrectly (A' to B'). The severity of this effect depends on the angle between the hillside, or mountain slope, and the incidence angle of the radar beam. Maximum foreshortening occurs when the radar beam is perpendicular to the slope so that the base and the top of the slope are imaged simultaneously (A' and B' are projected in the same place), reducing the length of the slope close to zero in slant range. This geometrical distortion is recognizable in the acquired radar images by means of the white colour of affected areas.
- **Layover (Fig. 4.12b):** when the radar beam arrives at the top of a tall shape tilted towards the radar

(e.g. a mountain) before the base, the layover effect occurs. In this case the return signal from the top of the feature (B') is received before the signal from the bottom (A'). In this way, the top of the feature is displayed towards the radar from its true position on the ground, and it "lays over" the base of the feature (B' to A'). This effect on a radar image looks very similar to the foreshortening distortion and, also in this case, the layover is most severe for small incidence angles, the near range of a swath, and in mountainous terrain. Also in this case the layover effect is distinguishable in radar satellite images for white areas, but it has not to be confused with the foreshortening.

- **Shadowing (Fig. 4.12c):** when the radar beam is not able to illuminate, the ground surface the shadowing effect occurs. Shadowing affects areas in down range dimensions (i.e. towards the far range), behind vertical shapes and slopes with steep sides. Given that the radar beam does not manage to illuminate the surfaces, shadowed regions appear dark on the radar satellite images due to not enough energy to be backscattered. The shadow effect looks more obliquely as much as the incidence angle increases from near to far range. This geometrical distortion is recognizable in radar images as black area, paying attention to not confuse this effect with water areas.

To reduce the effect of the geometric distortion several techniques were developed based on, as instance, the use of several images to taking advantage of different view angles or by means of DEM to correct it.

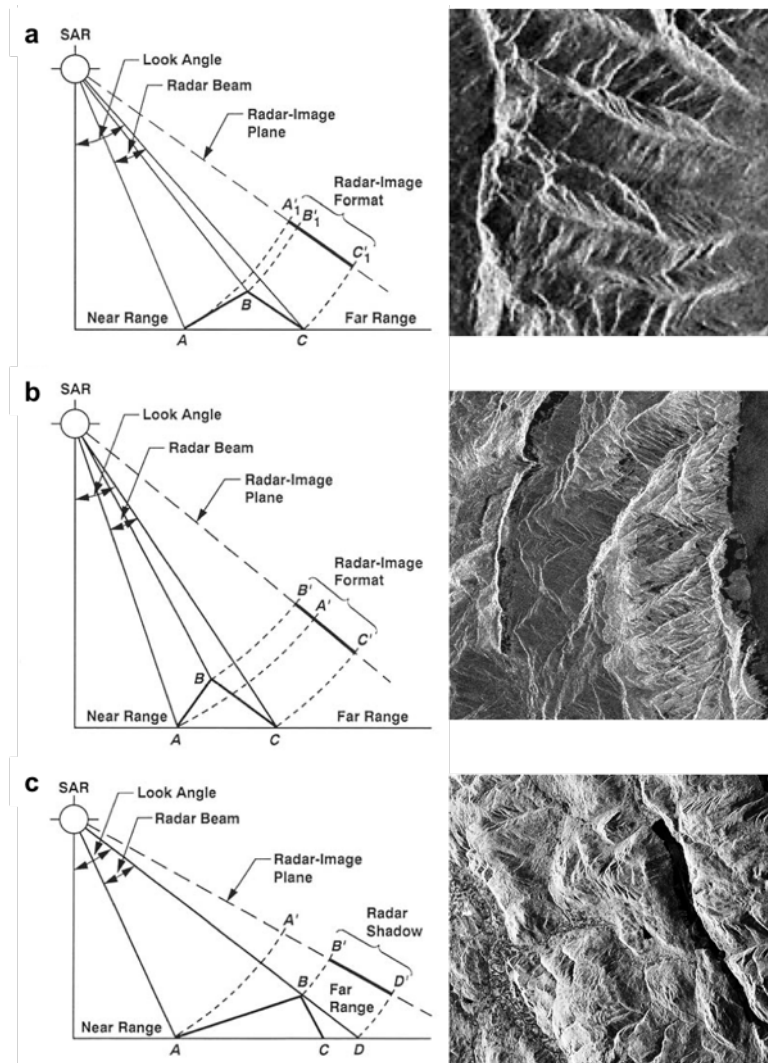


Fig. 4.12 - Geometric distortion effects (Farr, 1993): a) foreshortening (www.nrcan.gc.ca); b) layover (Xu and Cumming, 1996); c) shadowing (www.geo.uzh.ch).

The radiometric distortion influences the energy received to the sensors and often it is associated to the geometric distortion. For example, considering the foreshortening geometric effect, the sensor receives the backscattered energy stored in a smaller area than the real one absorbing intense reflected energy in few pixels. The main problem is that the effect of this distortion could not be adjusted without information derived from other sources to validate the results and understand the topography of the investigated area. Furthermore, the way in which SAR data are recorded should be understood to fully comprise this phenomenon.

Beside these negative effects, the use of the Radar system, through the Interferometry SAR (InSAR) technique, first described by Gabriel et al. (1989) and applied by Massonnet et al. (1993), lays the bases to analyse single or few interferences allowing to understand several Earth surface deformations. Successively, Ferretti et al. (2001) and Berardino et al. (2002) developed the multi-pass interferometric technique reaching good results on the quantitative assessment of the deformation along the LOS. SAR Interferometry (InSAR)

is an important branch of the remote sensing, playing a key role in active geological processes, such as landslide mapping and monitoring. The interferometric processing of the images works to provide the relative position changes of different points. Investigated deformations, for instance, take place on the ground surfaces survey caused by sudden events (e.g. earthquakes), slow natural events (e.g. landslides or glacier melting), or produced from anthropogenic activity (e.g. subsidence due to copious fluid extraction) (e.g. Schmidt and Bürgmann, 2003; Colesanti and Wasowski, 2006; Funning et al., 2007; Hooper et al., 2007; Herrera et al., 2009; Lagios et al., 2011; Bianchini et al., 2012; Lagios et al., 2012; Cigna et al., 2013; Tomás et al., 2013; Bianchini et al., 2014; Del Ventisette et al., 2014; Notti et al., 2014; Tomás et al., 2014). Satellite sensors are side-looking and the images are acquired in two different orbits: ascending or descending (Fig. 4.13a) following few degrees of shift with respect to the N-S direction and acquiring perpendicularly with respect to the Line of Sight (LOS). Sensors moving from south to north acquire in ascending orbit, satellites following the trace from north to south register in descending geometry. For this reason, movements respectively located on west-facing and east-facing slopes are better detectable while, using satellites that follow the polar orbits, landslides or ground displacements occurring along the north-south direction are difficult to identify and estimate. This is due to the natural rotation of the Earth and the side looking of the SAR antenna that enlighten only one direction during each orbit trajectory.

The combination of the ascending and descending acquisitions allows to eliminate the main effect of the spatial distortion abovementioned, even if finding two SAR images (from ascending and descending orbit) acquired at the same time and identifying the same target could be difficult. In case this could occur, the real displacement vector (Fig. 4.13b) can be obtained.

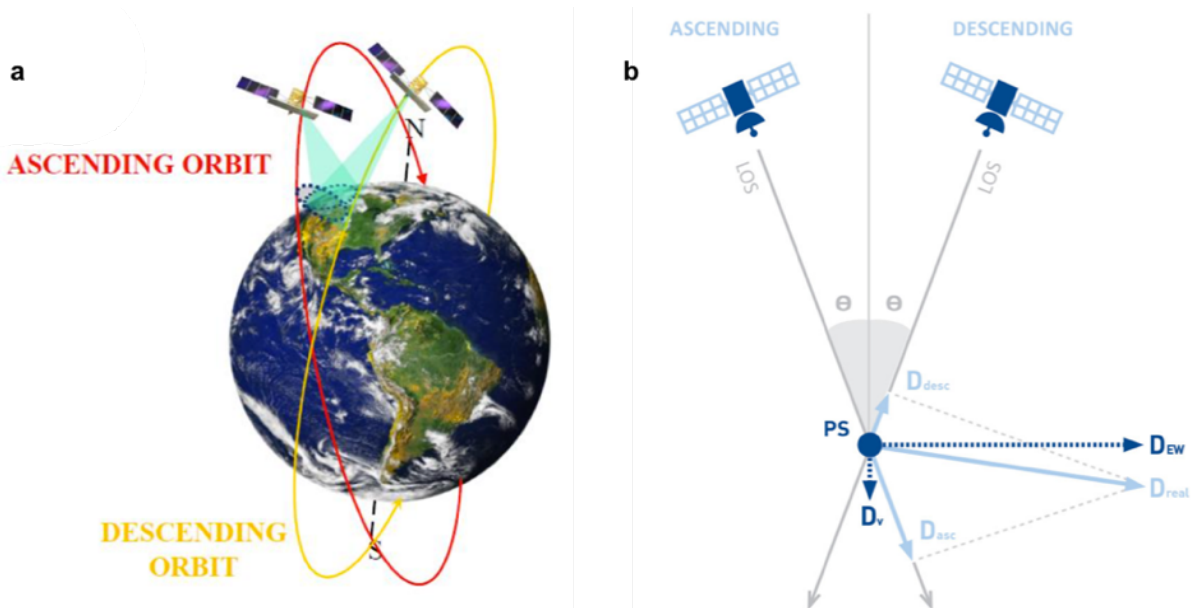


Fig. 4.13 - Ascending and descending orbits (a) with right-looking satellite and the combination (b) of the orbit measurements to obtain the true vertical and east-west components of the motion (tre-altamira.com).

4.1.2.3 SAR Interferometry

The SAR technique applied on studies of ground movement detection is focused on the Differential Interferometric SAR (DInSAR) approach (Fig. 4.14) (Massonnet and Feigl, 1998). Such methodology is often affected by atmospheric and temporal decorrelations (Massonnet and Feigl, 1998; Ferretti et al., 2001; Colesanti et al., 2003) that disturb the products. A possible solution to overcome these drawbacks is the use of the improved technique that takes advantage from multi-temporal radar acquisitions for reaching results allowing the investigation of PS displacement time-series. In this way the motion of each PS along the Line-Of-Sight (LOS), such as the Persistent Scattering Interferometry (PSI) (Kampes and Adam, 2006) can be exploited and carried out. For instance, by means of a specific analysis considering phase changes in a series of SAR images acquired at different times over the same region, a series of interferograms related to a “master” image can be provided. The PSI technique works a step further with respect to the conventional DInSAR correcting the atmospheric, orbital and topographical induced errors in order to derive velocity measurements and relatively precise displacements on specific ground target.

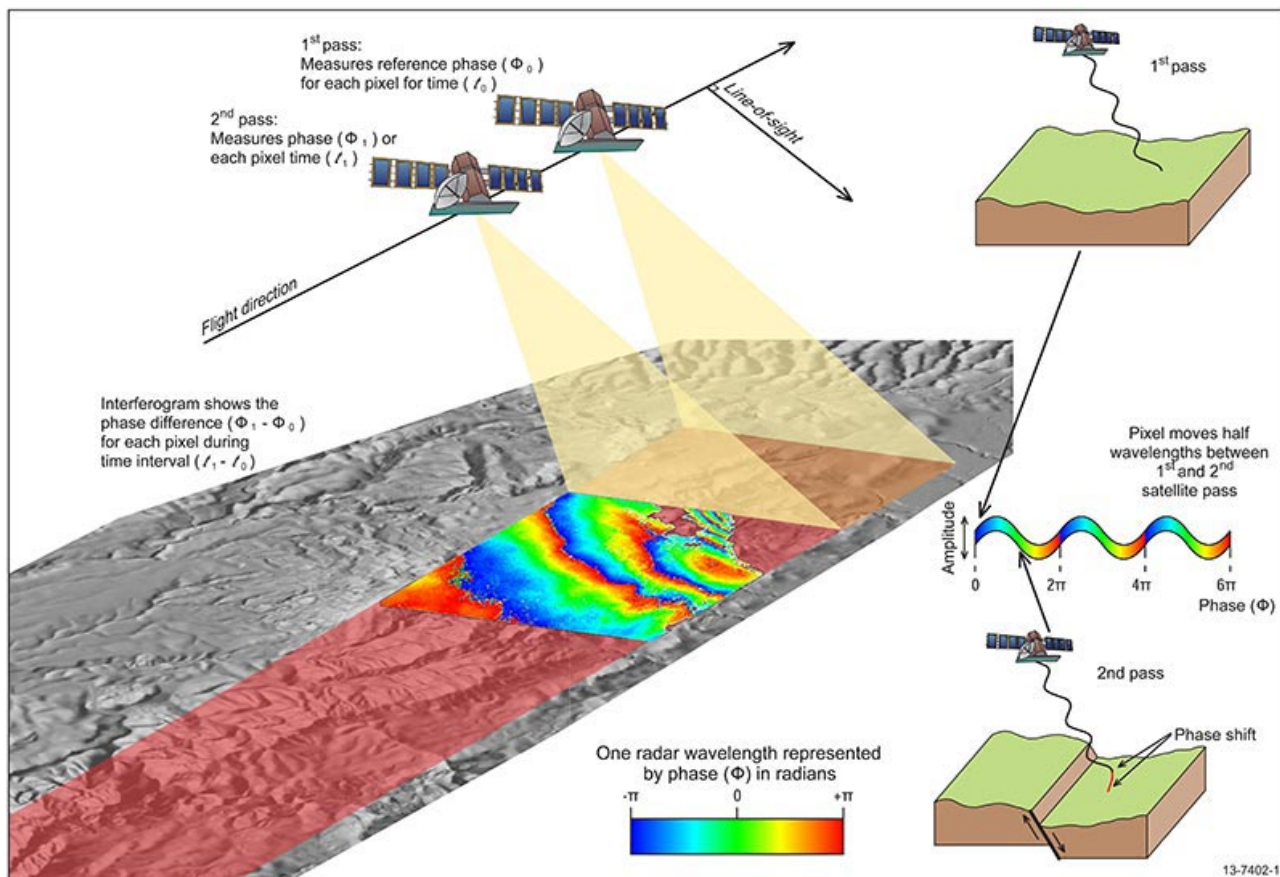


Fig. 4.14 - Two SAR images of the same area are acquired at different times recording, by means an interferogram, surface movements occurring between the two acquisitions (www.ga.gov.au).

The term PSI represents a specific class of DInSAR techniques and it is used to indicate several approaches to extract long-term stable benchmarks and high-reflective ground elements, namely Persistent Scatterers (PS) from several multi-interferogram analyses of SAR data. PSI name includes also the techniques based on the Distributed Scatterers (DS) and other hybrid methods (Crosetto et al., 2010):

- Persistent Scatterers Interferometry SAR (**PSInSARTM**) was the first approach to extract the PS developed by TRE, Italy, (Tele-Rilevamento Europa) spin-off company of Politecnico di Milano and Ferretti et al. (2000, 2001);
- Small Baseline Subset (**SBAS**) technique (Berardino et al., 2002; Lanari et al., 2004; Casu et al., 2006) was subsequently reviewed by Lanari et al. (2007) from CNR (Consiglio Nazionale delle Ricerche), Italy;
- Stanford Method for Persistent Scatterers (**StaMPS**) approach was developed at the Stanford University, USA, by Hooper et al. (2004) and improved by Hooper et al. (2007) to provide time series of deformation based on the spatially correlated nature of ground deformations using pixels with low phase variance;
- Coherent Pixel Technique (**CPT**) was grown at the Remote Sensing Laboratory (RSLab) of the UPC, Spain, (Universitat Politècnica de Catalunya) to take advantage from the separately use of amplitude- and coherence-based approach as selection criteria to obtain the components of non-linear deformations (Mora et al., 2003; Blanco-Sanchez et al., 2008);
- Interferometric Point Target Analysis (**IPTA**) developed from the GAMMA Remote Sensing, Switzerland, and presented by Werner et al. (2003) and Strozzi et al. (2006) to find persistent benchmark in low coherence regions, allows the use of large baselines for the phase interpretation;
- Stable Point Network (**SPN**) was strengthened by the Altamira group (Spain) to estimate the linear and non-linear components of deformation, to improve the use of adaptive filters and to implement the combination of temporal and spatial filters (Duro et al., 2004; Crosetto et al., 2008);
- **SqueeSARTM** is an implementation of the PSInSARTM technique proposed by Ferretti et al. (2011) to provide measurements also taking advantage of natural points over area of interest. This technique, developed by the TRE, Italy, (Tele-Rilevamento Europa), provides a point density much higher than the others.

PSI analysis integrated with auxiliary and ancillary data were useful in several cases for mapping and monitoring slow-moving landslides and to assess their state of activity (Notti et al., 2010; Righini et al., 2012; Herrera et al., 2013; Bianchini et al., 2015a).

The PS data interpreted and elaborated during this PhD Thesis were processed through PSInSARTM, CPT and SqueeSARTM techniques. All these methodologies are described in detail in the following subsections.

4.1.2.4 Coherent Pixel Technique (CPT)

Among the several methods to process and elaborate the radar satellite images, the *Coherent Pixel Technique* (CPT) algorithm implemented by Mora et al. (2003) and Werner et al. (2003) in a SUBSOFT processor at the Remote Sensing Laboratory (RSLab) of the Universitat Politècnica de Catalunya (UPC) was chosen for the investigated area of Agnone (Molise Region, southern Italy). CPT is an algorithm able to assess the deformation evolution from a stack of differential interferograms for wide areas for several SAR satellites such as ERS, ENVISAT, TerraSAR-X and COSMO-SkyMed.

First of all, images have to be co-registered before to develop the interferometric processing. This phase is a simple superimposing, in the slant range geometry, of two or more SAR images recorded in the same orbit and by the same acquisition mode. A coregistration is required for stacks of SAR images covering the same region on which some filters have to be applied. To correct rotational and scale differences or relative translational shifts, the spatial coregistration and a potentially resampling in case of different pixel size is required. Essentially, using the CPT algorithm, the coregistration consists in two subsequent phases: a *coarse registration* and a subsequent *fine registration*. The first step is dedicated to align the cropped images with an accuracy of a pixel for the whole scene and it is performed by means of the amplitude correlation of a portion of both images. The second one is finer reaching precisions of a fraction of pixel and it works processing pixel per pixel separately by means of a geocoding requiring an external DEM and the orbit information or correlating the amplitude of divided block of the images.

The processing scheme is composed by three main steps:

- generation of the best interferogram chosen among all the available images of the investigated area to identify the minimum number of interferograms needed to reach the maximum quality overall. The selection is made considering the *spatial baseline*⁶ (B_n), the *temporal baseline*⁷ (B_t) and the *Doppler frequency* (D_f). The estimation of the spatial (normal) baseline is based on a reference image, usually selecting the one used as reference already in the co-registered process. Subsequently, the interferogram selection works using the Delaunay triangulation⁸ of the available images in the $[B_n, B_t, D_f]$ to represent each interferogram by an arc connecting a pair of images.
- selection of the pixels within the area under investigation where terrain deformations can be detected on pixels with enough phase quality along acquisition. Several criteria based on the

⁶ *Spatial baseline*: the “distance” of the Slave acquisition respect to the Master images. It is also called “normal” baseline.

⁷ *Temporal baseline*: difference in time between the acquisitions.

⁸ *Delaunay triangulation*: kind of triangulation connecting neighbouring pixels, but not allowing the overlapping of triangles.

amplitude dispersion (Ferretti et al., 2001) and the coherence stability (Berardino et al., 2002) exist in order to select the better pixel.

- analysis to calculate the linear deformation by time series of pixels within the period of interest. The CPT approach relates the neighbouring selected pixels by means of a Delaunay triangulation to overcome the difficult to evaluate the phase of each pixel due to the occurrence of an offset among different interferograms. The connection between neighbouring pixels, assumed as nodes of a mesh, are linked setting a maximum length in order to reduce the atmospheric effect. In fact, the longest distance has been properly fixed to consider negligible the atmospheric term. To reach a good estimation of the node, then assuming their linear velocity and DEM error constant in the whole set of differential interferogram of the available data, it is possible to work on the phase model.

To obtain the velocity values for each pixel an integration process is necessary. Furthermore, a good distribution of control points, stable points affected by deformation and characterized by well-known linear velocity and height, helps to reduce the errors among zones badly connected. Blanco et al. (2006) implemented the multi-layer processing in order to provide larger pixel density preserving the suitability of the result and dividing the selected pixels in different layer according their quality. The multi-layer processing enhances the linear result and increases the pixel density due to the iteratively linear block executed starting from the high quality level and adding layers successively in order to preserve the high quality class and to improve the low quality levels.

4.1.2.5 SqueeSAR™

PSInSAR™ was recently improved and replaced by the SqueeSAR™ algorithm (Ferretti et al., 2011). This technique was applied by TRE-ALTAMIRA company to process the COSMO-SkyMed data available for the Volterra site (Tuscany region, central Italy) to provide a high density of points to analyse. SqueeSAR™ is a term that recall the concept of “squeezing”. In DInSAR application it is related to the association of information to coherent matrix in order to extract an optimum vector of phase values to use for interferometric analysis. SqueeSAR™ technique results to be a very effective tool for different scales, from regional to single building, to monitor with high precision displacements taking advantages of the typical remote sensing characteristics, the ability to cover wide areas and the possibility to assess displacements of few millimetres.

Generally, two big families of targets can be extracted by means of the InSAR processing on radar satellite images: Persistent Scatterers (PS), point-wise scatterers having the reflected energy of a single or a few connected pixels, and the Distributed Scatterers (DS) corresponding to a homogeneous area covering by

several pixels (e.g. forest, agricultural field). DS correspond to the return characteristics of several pixels “statistically homogeneous”.

The SqueeSAR™ algorithm was created to cover the necessity to combine the PS and DS improving the density of measured points (Hooper, 2008; Zebker and Shanker, 2008). Its aim was to increase the spatial distribution of points preserving the high quality reached by means of the PS technique. PSInSAR™ has some limitations about the density of points and the quality of the time-series in non-urban areas that DS, by means of a statistical description of the sensor parameters used and the kind of object illuminated, can overcome. The SqueeSAR™ can be considered as the second generation of PSI techniques that made visible targets from radar images identifiable by the PS and points recognizable by means of the spatially DS. Persistent Scatterers usually identified on man-made structures, and Distributed Scatterers, generally corresponding to uncultivated, desert or debris covered ground surfaces, are jointly processed without significant changes in the PSInSAR™ algorithm. Their combination allows results with a lower standard deviation with respect to the traditional PSInSAR™ algorithm (Ferretti et al., 2011; Lagios et al., 2013) thanks to the higher density of measured points and the wide spatial coverage.

An important improvement with respect to the other multi-interferogram algorithms is the use of all possible interferograms, following the theory that any interferogram could give significant information according to its coherence level. The SqueeSAR™ algorithm is based on the analysis made by means of a correlation matrix and, without taking into account the temporal and geometrical baseline, the generation of each possible interferogram correlated to its coherence value. Furthermore, an important innovation is due to the implemented filtering technique (DespeckS) that allows to preserve the information associated to a point-wise radar target (Ferretti et al., 2011). The results of the SqueeSAR technique for each measurement point includes the yearly displacement velocity value and the possibility to extract the displacement time history.

For further information about the SqueeSAR™ techniques see Ferretti et al. (2011) where the implementation on the PSInSAR™ algorithm is extensively explained.

4.1.2.6 Vertical (V_v) and Horizontal (H_v) velocity

As mentioned, radar satellites are able to acquire along two different polar orbits, ascending from south to north and descending from north to south. Images recorded by SAR sensors allow to measure the velocity along the Line of Sight (LOS), thus the displacement during time along a unit vector co-directional of the satellite. If both geometries data were acquired and are available, the real velocity of displacement affecting targets can be calculated as a vector \bar{V} as follow (Eq. 1):

$$\bar{V} = V_x \cdot \bar{s}_x + V_y \cdot \bar{s}_y + V_z \cdot \bar{s}_z \quad (1)$$

where V_x , V_y and V_z are the velocity components along the horizontal (E-W and N-S) and vertical directions (Z

component), while \overline{s}_x , \overline{s}_y and \overline{s}_z are the unit vectors of the three coordinate axes.

The combination of the velocities acquired by both ascending and descending orbits, provides the possibility to decompose the detected motion along the LOS into the horizontal and vertical components (Manzo et al., 2006; Notti et al., 2014). Using the mean velocity of the two available orbits a system with two formulas and three variables will be created as follow (Eq. 2):

$$\begin{cases} V_a = V_x \cdot h_{LOS,a} + V_y \cdot h_{LOS,a} + V_z \cdot e_{LOS,a} \\ V_d = V_x \cdot h_{LOS,d} + V_y \cdot h_{LOS,d} + V_z \cdot e_{LOS,d} \end{cases} \quad (2)$$

where $h_{LOS,a}$, $e_{LOS,a}$, $h_{LOS,d}$ and $e_{LOS,d}$ represent the LOS directional cosines for ascending and descending passes, respectively.

Eq. (2) can not be solved having too much unknowns, so the N-S horizontal components have to be considered negligible due to the characteristics of the geometrical acquisition (Notti et al., 2014). Considering the N-S component of the velocity to zero allow to solve the Eq. (2) and assuming the availability of both geometries, ascending and descending, the Horizontal (V_H) and Vertical (V_V) components of the motion can be derived by means of trigonometric rules (Eq. 3).

$$\begin{aligned} V_H &= \frac{((v_d/h_{LOS,a}) - (v_a/h_{LOS,a}))}{e_{LOS,d}/h_{LOS,d} - e_{LOS,a}/h_{LOS,a}} \\ V_V &= \frac{((v_d/e_{LOS,d}) - (v_a/e_{LOS,a}))}{h_{LOS,d}/e_{LOS,d} - h_{LOS,a}/e_{LOS,a}} \end{aligned} \quad (3)$$

where V_a and V_d represent the velocity measured by the satellite along the LOS direction in the ascending and descending passes, respectively, $h_{LOS,a}$ (Eq. 4), $e_{LOS,a}$ (Eq. 5) and $n_{LOS,d}$ (Eq. 6) are the LOS directional cosines for ascending and descending orbits, respectively.

$$h_{LOS} = \cos(\alpha) \quad (4)$$

$$e_{LOS} = \cos(1.571 - \alpha) * \cos \omega \quad (5)$$

$$n_{LOS} = \cos(1.571 - \alpha) * \cos \eta \quad (6)$$

$$\eta = 3.142 - \theta$$

$$\omega = 4.712 - \theta$$

The V_V computed by Eq. (3), corresponding to the vector V_{V1} in **Fig. 4.15** is the result of the combination between the ascending and descending LOS measurement; while if the available orbit is only one, indifferently ascending or descending, the vertical component of the motion is derivable only in case the real movement is nearby to the vertical. For instance, in case of availability of the ascending orbit only, the V_H is assumed as 0 and the vertical component is shown by the vector V_{V2} in **Fig. 4.15** and calculated by means of Eq. (7) (Bianchini and Moretti, 2015).

$$V_V = \frac{(v_d/e_{LOS,d})}{(h_{LOS,d}/e_{LOS,d})} = \frac{v_d}{h_{LOS,d}} = \frac{v_d}{\cos \theta} \quad (7)$$

where $h_{LOS,d}$ and $e_{LOS,d}$ represent the LOS directional cosines for the descending geometry and θ is the satellite incident angle.

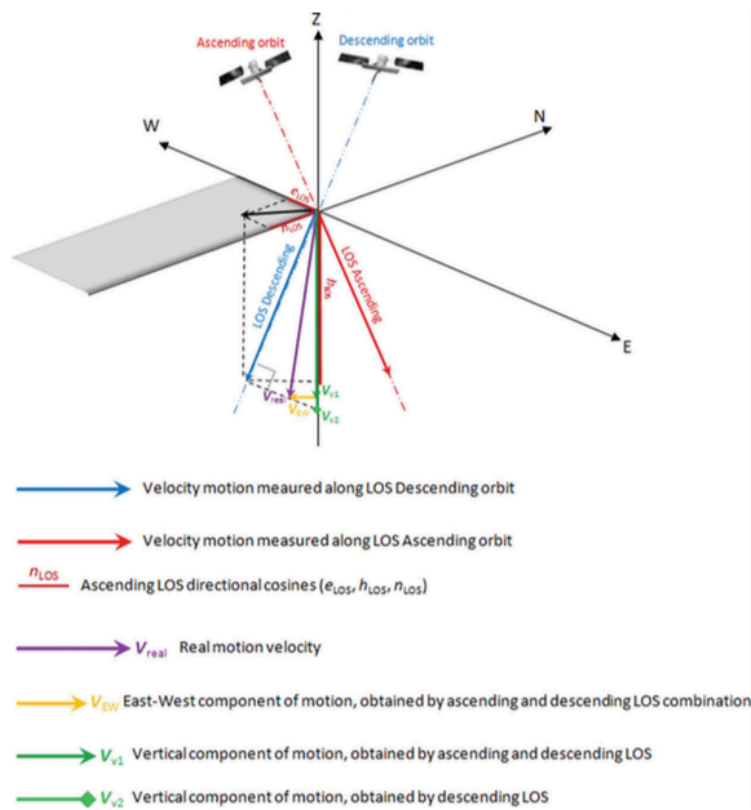


Fig. 4.15 - Scheme of the spatial acquisition configuration by ascending and descending orbits and the composition in vertical and horizontal velocity components of an almost-vertical real motion (Bianchini and Moretti, 2015).

To convert the velocity measured along the LOS into Vertical and Horizontal displacement, each single point of measure has to be recognized as a valid target in both geometries and synthetic PS, artificial Persistent Scatterers following a sampling grid, have to be created (Rosi et al., 2014). In this way, spatially regular series of synthetic PS were collected through a sampling grid with square cells in which to calculate the mean deformation velocity for both orbits. The process (**Fig. 4.16**) provides a distributed velocity deformation for ascending and descending geometries, and solving Eq. 2 the Vertical (V_V) and Horizontal (V_H) velocity can be extracted.

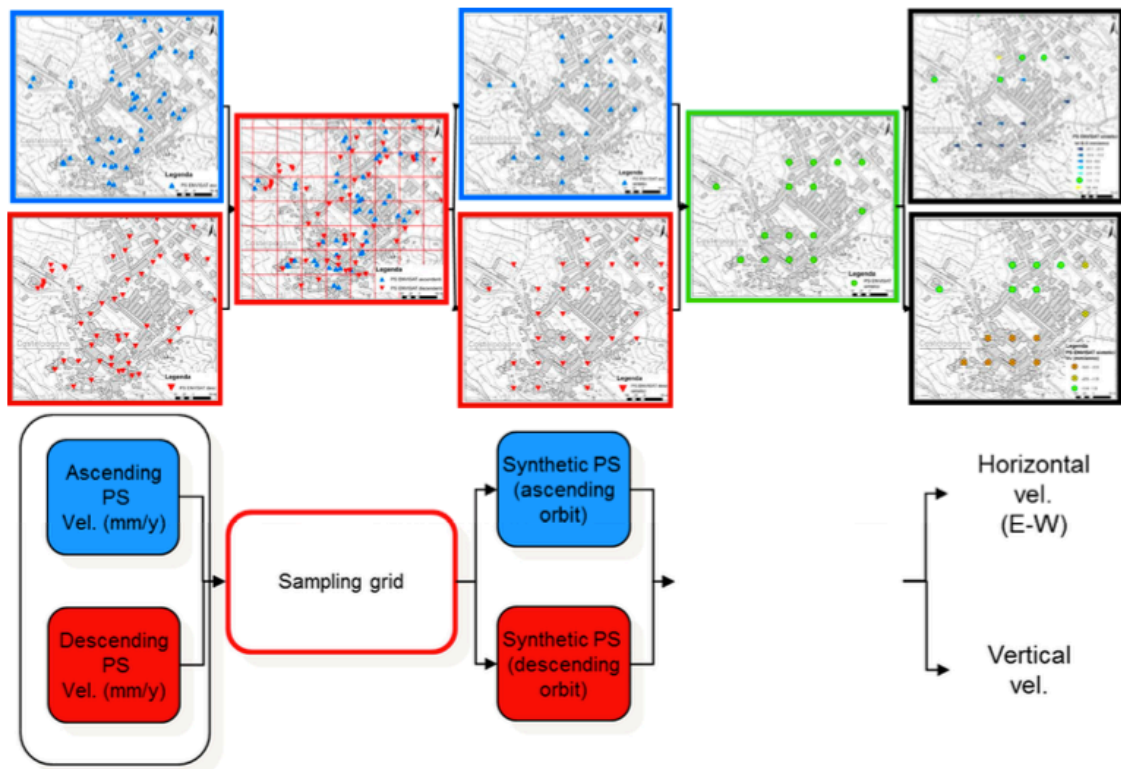


Fig. 4.16 - Flow-chart of the process to extract the Vertical and Horizontal components starting from PS of both ascending and descending geometries (Rosi et al., 2014).

The choice of the cell size to adopt for the conversion of PS in synthetic PS has to consider several parameters. It depends on the scale of the investigated site, the number and the distribution of the Persistent Scatterers in the area and, also, on the dimension of the investigated phenomena.

Once that the vertical and horizontal components of the vector are calculated, the main direction of ground deformation, the real velocity (V_r) can be calculated in order to discriminate areas affected by landslide or by subsidence. Given that the angle between V_H and V_V is 90° , it is possible to apply the Pythagoras theorem to calculate V_r (Eq. 8) based on the angle between the V_E and the V_r (α) or the angle between V_V and V_r (β) (Rosi et al., 2014).

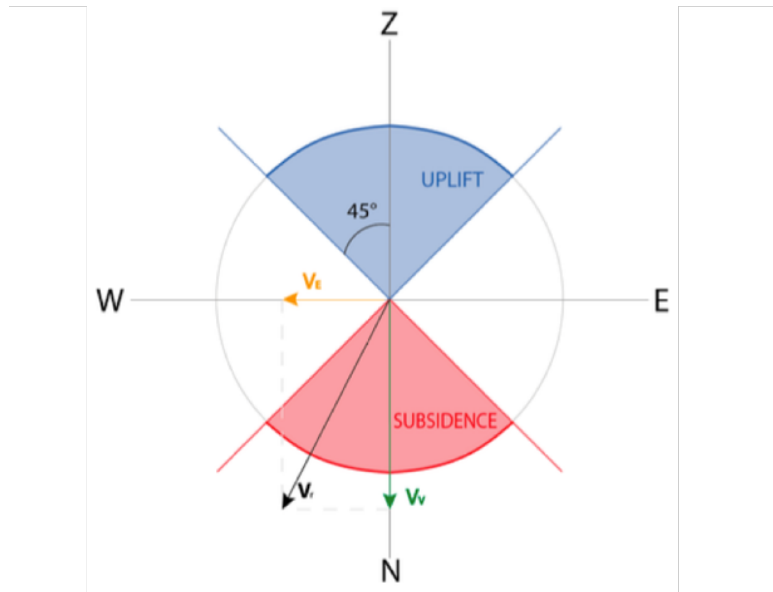
$$\sin \alpha = \frac{V_H}{V_r} \sin \delta \quad \text{or} \quad \sin \beta = \frac{V_V}{V_r} \sin \delta \quad (8)$$

where δ is 90° , the angle between V_V and V_H .

At the end to define the direction, thus the quarter in which the estimated V_r fall into, the sign of V_V and V_H have to be taken into account (Table 4.1)

Table 4.1 - Definition of V_r direction depending on V_V and V_H values (from Rosi et al., 2014).

V_V and V_H values	Quarter of V_r
both V_V and V_H positive	Z-E quarter
V_V positive and V_H negative	Z-W quarter
both V_V and V_H negative	N-W quarter
V_V negative and V_H positive	N-E quarter



4.1.2.7 Time series analysis

Recently, by means of the improvement of the processing techniques, the analysis on the capability of the DInSAR techniques was possible in the investigation of the evolution of natural processes (Calò et al., 2014). Furthermore, examining the time series of Persistent Scatterers, different trends can be automatically identifiable detecting distinct phases of the temporal evolution (Milone and Scepi, 2012; Cigna et al., 2012; Berti et al., 2013).

Notti et al. (2015), in order to properly characterize the temporal behaviour of the displacement, proposed and improved a methodology to analyse the time series with particular focus on landslide and subsidence phenomena. The authors suggested a wider improved post-processing of time series analyses to better observe the ground truth:

- *Removing noise and regional trends* - useful for time series affected by trends or anomalies not related to the ground motions. These can be identified selecting the PS in stable area, recognizable by LOS velocities comprise between ± 0.5 mm/y, and with high coherence (such as > 0.9). Once revealed the presence of a specific regional trend a *correct* time series can be computed removing the average stable time series to the original one.

- *Removing single date anomalies* - errors related to anomalous displacement diffuse to all dataset at certain date. To detect the errors, stable (± 0.5 mm/y) time series with high coherence (> 0.9) can be selected and if more than one-third of them show significant peaks at the same date, these data should be removed.
- *Detect and correct possible phase unwrapping errors* - this can occur when between two successive acquisitions or two close targets of the dataset are subject to a displacement bigger than a quarter of the radar wavelength (e.g. Crosetto et al., 2010). This error can occur especially investigating landslide-prone areas affected by possible sudden motions.

In this work, taking into account the available data, the time series investigated in the two site of interest, CL-PO landslide and southwestern sector of Volterra, were corrected by the regional trend in order to better analyse the displacement in time.

In 2013 Berti et al. developed a procedure based on a sequence of statistical characterization tests in order to classify the Persistent Scatterers Interferometry (PSI) time series according to their peculiar trends. This method overcomes such limitation of the Milone and Scepi (2011) clustering approach, allowing a classification of the PSI time series into six recurrent patterns:

- Type 0 "*uncorrelated*" - displacement that does not follow any pattern;
- Type 1 "*linear*" - displacement that linearly increases in time according to a constant velocity;
- Type 2 "*quadratic*" - time series characterized by a continuously variation of the velocity ion time;
- Type 3 "*bilinear*" - time series with a breakpoint with continuous function dividing two linear tracts with constant velocity;
- Type 4 "*discontinuous with constant velocity*" - time series segmented by a breakpoint with discontinuous function dividing two linear tracts with similar velocity;
- Type 5 "*discontinuous with variable velocity*" - time series segmented by a breakpoint with discontinuous function dividing two linear tracts with different velocity.

The classification of the time series can help the interpretation of physical processes related to slope instabilities. It is worthy noticing that the time series categorization is highly dependent on the quality of the used dataset.

4.2 Field investigations

Landslide mapping is an important tool to predict future evolution, assess the correlate risks and manage the landslide-territory (Wu et al., 1996). Several field surveys, both for the damage investigation and to recognize the geomorphological features to implement the remote sensing techniques, were conducted in the areas of interest.

4.2.1 Damage classification

Urbanized areas affected by landslide displacements often reveal ruptures and cracks on man-made facilities. These effects occur when the ground movements affecting buildings are greater than the tensions which structures are capable to absorb without showing deformations. The most rigid, or the weakest, constructive elements of facilities are the first elements that show suffering injures, e.g. walls and façades and joints, respectively (Bru et al., 2013). Damage and economic losses resulting from rapid landslides, such as debris flows, earth flows or rock falls (Cruden, 1991), are the most severe and therefore the most easily recognizable. Conversely, slow-moving landslides impacting on facilities, can be more difficult to detect despite leading to a total or partial disruption of their serviceability. Effects of slope movements can be also revealed by cracks and ruptures occurring on man-made infrastructures and anthropic or natural ground surfaces.

The investigation of landslide-induced damage can be motivated by a wide range of user purposes, as administrative (to declare restrictive rules such as the evacuation for no safe constructions), planning (to estimate direct and indirect costs and assess the needed restoration, reconstruction or relocation of structures), scientific (to study the phenomena, its extension and possible evolution) and engineering design (to arrange a reconstruction plan) (Alexander, 1986).

4.2.1.1 Existing approaches

A considerable amount of scientific literature dealing with damage assessment in landslide-prone and -affected areas already exists (Skempton and MacDonald 1956; Burland 1977; Lee and Moore 1991; Chiochio et al. 1997; Cooper 2008; Mansour et al. 2011). Each work presents some benefits and constraints, i.e. the choice of the relevant parameters to use, the lack of concern on some important features and the difficulty of applicability (Del Soldato et al., 2016a). Most of the existing damage classification methods consider different conflicting parameters without taking into account the relevance of damage investigations at ground surfaces. Furthermore, none of them takes into consideration the possibility of their applicability not only on buildings, but more generally on facilities. These pending issues do not allow a simple and univocal application and result, therefore a complete and easy-to-use methodology is required (Del Soldato et al., under review_a). The classification of the landslide-induced damage affecting different types of facilities

plays a fundamental role in order to assess their damage level related to the intensity of ground motion and impact severity, as well as indirectly to support a more precise mapping of landslide-prone areas (Ciampalini et al. 2014; Del Soldato et al., under review_a).

The first simple classification of building damage, based on the severity of the cracks affecting elements, even if without defining clear limits of evaluation, was employed by Skempton and MacDonald (1956). The Authors divided damage in three main categories: architectural, functional and structural damage. Architectural damage are referred to the appearance on the construction, e.g. fine cracks in finishes, floor or panel walls (wider than 0.5 mm), in plaster (wider than 1mm) and in rough concrete and masonry walls. Functional damage involve the use of the structure producing extensive cracks, tilting of floors and walls, falling plaster, obstructed doors and windows and other non-structural damage. Structural damage prejudice the stability of the construction manifesting ruptures and distortions in support elements (e.g. pillars, columns and load-bearing walls). In practice, damage affecting facilities are assessed performing field surveys highly conditioned by the criteria adopted and by the experience of the operators.

During the second half of the last century the scientific community developed some specific damage classifications for areas affected by natural catastrophic phenomena as earthquakes (e.g. Wood and Neumann, 1931; Medvedev, 1965; Grünthal, 1998; Baggio et al., 2009), subsidence (e.g. Howard Humphreys & Partners, 1993; Van Rooy, 1989; Freeman et al., 1994) and landslides (e.g. Burland, 1977; Alexander, 1986; Geomorphological Services LTD, 1991; Lee and Moore, 1991; Chiocchio et al., 1997; Cooper, 2008).

Here after, the five approaches existing in literature and one developed during the thesis applied to assess used to classify buildings and facilities of the two study sites are described.

4.2.1.2 Burland (1977)

Burland (1977) disseminated the first classification including a ranking scheme and some suggested values in order to limit the subjectivity of the operator. The Author presented a simple system derived from the cumulated experience by three previous works: a study of the economic consequences of the heave of construction on swelling clays where a simple categorization of the damage based on their restoration was conceived (Jennings and Kerrich, 1962); a simple classification based on wide experiences of damage caused by subsidence (National Coal Board, 1975); a ranking proposed by the Coal Board's recommendations (MacLeod and Littlejohn, 1974). The Burland (1977) classification (**Table 4.2**) consists of six classes of damage, including the width of cracks and their relationship with the facility of restoration. The provided values are related only to visible or aesthetic damage, observed corrosion and cracks permitting the penetration or the lacking of liquids or gases. For reinforced concrete, the approach to adopt should be more severe (Nawy, 1968).

Subsequently, Boscardin and Cording (1989) slightly modified the classification maintaining the same structure and correcting some approximations based on their experience.

Table 4.2 - Classification of damage according to Burland (1977) modified by Boscardin & Cording (1989).

Grades	Damage level	Crack width (CW in mm)	Description of damage
0	Negligible	< 0.1	Hairline cracks
1	Very Slight	< 1	Fine cracks and isolated generally restricted to internal walls finishes
2	Slight	< 5	Several slight fractures inside building; exterior cracks visible; doors and windows may stick slightly
3	Moderate	5 < CW < 15 or several > 3 mm	Several cracks; doors and windows sticking. Utility service may be interrupted; weathertightness often impaired
4	Severe	15 < CW < 25 depending on number of cracks	Windows and door frames distorted; floor sloping noticeably; Walls lean or bulge noticeably, some loss of bearing in beams; utility service disrupted
5	Very severe	> 25	Beams lose bearing; walls lean badly and require shoring; windows broken with distortion; danger of instability.

4.2.1.3 Alexander (1986)

In 1986, Alexander, after an important landslide event affecting Ancona (central Italy) in December 1982 (Alexander, 1983), presented an alternative intensity scale of damage. This methodology is referred to the landslide-induced damage observable on buildings and it was developed in order to compare visible damage on different structures involved in the same event. The ranking shows eight categories, two more than the previous one (Burland, 1977) to consider also the partial and total collapse as well as the possibility of the no damage: *none, negligible, light, moderate, serious, very serious, partial collapse* and *total collapse* (Table 4.3). They are based on the cracks observation on walls, their position and extension, their distortion of the rigid elements and on the settlement affecting foundations.

The classification of the building damage based on their description, includes the visual description of the internal and external damage and few referring values in centimetres, for the differential settlement, and in grades, for the inclination of the floor. Some missing features were spotted applying this method (Crescenzi et al., 1994; Iovine & Parise, 1995) such as the missing of the distinction between the construction materials of the structure in addition to the lacking of data about the opening and the number of the cracks. In spite of the very simple scheme, the Author suggested a checklist of suitable information to better describe the structure affected (e.g. typology of construction, description of building and foundations, if visible), the phenomenon occurred (e.g. type of ground movement and position of the structure respect to the landslide) and the specific damage (e.g. direction and magnitude of the movement, inclination of the elements and typology of cracking).

Table 4.3 -Classification of damage according to Alexander (1986).

Grade	Category of damage	Description of building damage
0	None	Building is intact
1	Negligible	Hairline cracks in walls or structural members, no distortion of structure or detachment of external architectural details
2	Light	Building continue to be habitable; repair not urgent. Settlement of foundation, distortion of structure and inclination of walls are not sufficient to compromise overall stability
3	Moderate	Walls out of perpendicular by 1° - 2° , or substantial cracking has occurred to structural members, or foundations have settled during differential subsidence of at least 15 cm; building requires evacuation and rapid attention to ensure its continued life
4	Serious	Walls out of perpendicular by several degrees; open cracks in walls; fracture of structural members; fragmentation of masonry; differential settlement of at least 25 cm compromise foundations; floors inclined by up to 1° - 2° , or ruined by soil heave; internal partition walls will need to be replaced; door and window frames too distorted to use; occupants must be evacuated and major repair carried out
5	Very serious	Walls out of plumb by 5° - 6° ; structure grossly distorted and differential settlement will have seriously cracked floors and walls or caused major rotation or swelling of the building (wooden buildings may have detached completely from their foundations). Partition walls and brick infill walls will have at least partly collapsed; occupants will need to be rehoused on a long-term basis and rehabilitation of the building will probably not be feasible
6	Partial collapse	Requires immediate evacuation of the occupants and cordoning of the site to prevent accidents with falling masonry
7	Total collapse	Requires clearance of the site

4.2.1.4 Chiocchio et al. (1997)

Chiocchio et al. (1997) defined a new classification of landslide damage induced on buildings (**Table 4.4**) which overcomes some of the drawbacks arisen in the abovementioned classification during some applications (Crescenzi et al., 1994; Iovine and Parise, 2002). The new approach was conceived thanks to an interdisciplinary involvement of geologists, geomorphologists and civil engineers.

For the first time the damage classification scheme was implemented by the distinction of two different typologies of structures (i.e. masonry and reinforced concrete) and quantitative reference values for some parameters were suggested. These improvements were relevant to analyse the fractures, to distinguish the meaning of similar cracks in different materials and to minimize the subjectivity of the survey. Damage was schematized in eight different grades and, additionally, some general recommendations for rehabilitation measurements were defined. Each level represents a state of the damage affecting the building: the first three levels correspond to negligible and weak damage; buildings affected by the fourth grade of damage exhibit some serious cracks and restoration strategies are suggested for them; the fifth grade is characterized by several failures affecting the construction and the surrounding area; the last two classes are for buildings in which the level of damage is so severe that the decision to renovate or relocate them has to be accurately evaluated (Chiocchio et al., 1997).

Table 4.4 - Classification of damage according to Chiocchio et al. (1997).

Grade	Damage level	Load-bearing structures	Rigid settlement	Cracking	Immediate measures
0	None	Masonry	0	None	None
		Reinforced concrete frame	0	None	None
1	Negligible	Masonry	0	Hairline cracks of the plaster	None
		Reinforced concrete frame	0	Hairline cracks of the plaster	None
2	Light	Masonry	2 - 3 cm	Small cracks through walls and partitions	None
		Reinforced concrete frame	2 - 3 cm	Small cracks through walls and partitions	None
3	Moderate	Masonry	10 - 15 cm	Open cracks in walls; walls disjunction; little deformation; badly working casings	Evacuation suggested
		Reinforced concrete frame	10 - 15 cm	Significant cracking in the beams; partition walls deformed and crumbling; badly working casing	Evacuation suggested
4	Serious	Masonry	15 - 20 cm	Considerable disjunction of walls; space deformation; partition walls collapsed; unusable casing	Evacuation & shoring
		Reinforced concrete frame	15 - 20 cm	Perimetric and partition walls partly collapsed; deformed structures; spread cracking	Evacuation
5	Very serious	Masonry	>25 cm	Open cracks in floor; partition walls totally collapsed; seriously ruined lintels	Evacuation & cordoning
		Reinforced concrete frame	>20 cm	u.d.	Evacuation & cordoning
6	Partial collapse	Masonry	u.d.	u.d.	Cordoning
		Reinforced concrete frame	u.d.	u.d.	Cordoning
7	Total collapse	Masonry	u.d.	u.d.	Cordoning
		Reinforced concrete frame	u.d.	u.d.	Cordoning

4.2.1.5 Cooper (2008)

Cooper (2008) conducted a study on several existing methods devised to categorize damage due to subsidence, earthquakes, mining and landslide phenomena. Moreover, the recording procedure and scheme of damage has to be popular, simple and easily to use by means of more practical parameters for field surveys. The Author found that many parameters, with slight differences, were commonly used to evaluate and classify the injuries. The affinity between several existing schemes for recording damage induced by landslides and subsidence permitted to generate a single classification scheme, independently of the causes (Cooper, 2008). This ranking divides the severity of the damage in seven classes, from very slight to total collapse, in addition to a negligible one. It is worthy to notice as the description of the damage not include details about cracks on foundations or on other subsurface amenities and the external visibility of the building cracks is added because the internal accessibility to the structures has not to be considered as necessary condition. The suggested ranking (**Table 4.5**) includes the characterization and classification of building damage and a description, and relative categorization, of the ground surface ruptures distinguished for the two causes. In fact, ground damage caused by landslides and subsidence were included considering

that most of the survey was performed studying the external façades of buildings and cracks on sidewalk and on natural surfaces can improve the capability of the assessment of the severity of damage.

Table 4.5 - Classification of damage according to Cooper (2008).

Grade	Typical building damage	Subsidence ground damage	Landslide Ground damage
0	Hairline cracking, widths to 0.1 mm. Not visible from outside	Not visible	Not visible
1	Fine cracks, generally restricted to internal wall finishes: rarely visible in external brickwork. Typical crack widths up to 1 mm. generally not visible from outside	Not visible	Not visible
2	Cracks not necessarily visible externally, some external repointing may be required. Doors and windows may stick slightly. Typical cracks widths up to 5 mm. difficult to record from outside	Not visible	Not visible
3	Cracks that can be patched by a builder. Repointing of external brickwork and possibly a small amount of brickwork to be replaced. Doors and windows sticking, slight tilt to walls, service pipes may fracture. Typical crack widths are 5-15 mm, or several of say 3 mm. Visible from outside	Slight depression in open ground or highway, noticeable to vehicle users, but may not be obvious to casual observers. Repairs generally superficial, but may involve local pavement reconstruction	No damage likely to be noticed in vegetated ground. Tight cracks in hard surfaces paths, roads, pavements and structures with no appreciable lipping or separation
4	Extensive damage that requires breaking-out and replacing section of walls, especially over doors and windows. Windows and doors frames distorted, floors sloping noticeably; some loss of bearing in beams, distortion of structure. Service pipes disrupted. Typical crack widths are 15-25 mm, but also depends on numbers of cracks. Noticeable from outside	Significant depression, often accompanied by cracking, in open ground or highway. Obvious to the casual observer. Small hole may form. Repairs to the highway generally require excavation and reconstruction of the road pavement	Slight stretching of roots, tension changes on wires and fences. Open cracks, distortion, separation or relative settlement. Small fragment falls cause slight damage to roads and structures. Remedial works not urgent
5	Structural damage, which requires a major repair job, involving partial or complete rebuilding. Beams lose bearing capacity, walls lean badly and require shoring. Windows broken with distortion. Danger of instability. Typical crack widths are >25 mm, but depend on the number of cracks. Very obvious from outside	Rotation or swelling of the ground or significant depression, often accompanied by cracking, in open ground or highway. General disruption of services in highways. Significant repair required	Widespread tension cracks in soil and turf. Ground surface bulged and/or depressed. Settlement may tilt walls, fracture of structures, service pipe and cables. Remedial work necessary
6	Partial collapse. Very obvious from outside	Collapse of ground or highway, significant open void, services severed or severely disrupted	Extensive ground cracking with minor scarps, ground bulging and soil rolls. Minor flows, falls and slide may affect roads and structures. Settlement causes cracks and distortion to structures and roads. Remedial work urgent
7	Total collapse. Very obvious from outside	Large open void	Extensive ground cracking with major scarps and grabens. Major debris, earth or mud flows, and slides and falls. Settlement causes rotation or swelling of ground, gross distortion and destruction of structures. Major remedial works may not be feasible

Furthermore, according to the Author, damage to roads and other facilities can be also evaluated and could be even surveyed and related to more severe classes of damage (above the third grade). The definition of the categories, the descriptions and the ranking of the landslide-induced damage affecting buildings and ground surfaces were carried out analysing the National Coal Board (1975), Alexander (1986), Geomorphological Service Ltd (1991), Freeman et al. (1994), the Institution of Structural Engineers (1994) and Chiocchio et al. (1997).

4.2.1.6 DPC (Baggio et al., 2009)

In Italy a further approach to classify damage affecting civil constructions and to evaluate the reliability of buildings to host safely its inhabitants after seismic events was presented by the Italian Department of Civil Protection (DPC hereafter) (Baggio et al., 2009). This method was conceived to survey damage after seismic events, in order to assess the fitting for human habitation of the buildings. Such approach is applicable also to landslides because, also in slope movements, damage is due to the effects of shear stress. Several field experiences of seismic events in Italy (e.g. Irpinia, Campania region in 1980, Abruzzo region in 1984, Basilicata region in 1990) was the base of this methodology, then it was tested in subsequent earthquakes (e.g. Umbria-Marche regions in 1997 and Pollino, Basilicata-Calabria regions, in 1998). The aim of this ranking scheme is to extract a judgment on the reliability of the structure to host safely its inhabitants.

The DPC approach was devised for quick survey and to classify the damage magnitude, even if the requested field analysis on the structure has been conducted with care. It was conceived to assess the reliability of the structure, it is more complete than others one, composed of several tables and schemes to be followed during the post-seismic events survey. Overall, the form to compile during the field campaign is composed of nine sections: three tables dedicated to the identification and description of the examined buildings; two sections referred to the structural and non-structural damage and the quickly performed measures; one part including the evaluation of the induced hazard for surrounding constructions; one section about the terrain and foundations; one section for the judgment of conformity to standards; the last one conceived to note down further information.

The assessment of the damage magnitude was realized in six grades of severity, but divided in four classes: *nothing* (no damage); *weak*; *moderate & serious*; *very serious & collapse*. The peculiarity of this approach is the introduction of the evaluation of the damage extension. It has to be evaluated in percentage, separating the categories by an interval of 33% or 66%, of the magnitude of damage divided in null (D0) for no damage, weak (D1), medium-severe (D2-D3) and very severe (D4-D5) (**Table 4.6**). To assess damage affecting structures, section by section, the extension of the cracks and their magnitude have to be taken into account considering the sum of the damage extension can not exceed 1, representing the entire building (e.g. 2/3 of D4-D5 + 1/3 of D2/D3).

Table 4.6 - Classification of damage according to the DPC (Baggio et al., 2009).

Grades	Damage level	Crack width (CW in mm)	General description of the damage
D0	Nothing	None	None
D1	Weak	≤ 1	Damage don't change significantly the resistance of the structure; slightly cracks (≤ 1 mm) in walls; limited separation of elements and dislocation (≤ 1 mm); limited distortion without separation or structural failure
D2/D3	Moderate & Serious	< 10 or 15	Damage that could change significantly the resistance of the structures without the collapse of elements; cracks with big entity than D1 with possible expulsion of material (≤ 1 cm or more close to the opening); symptom of crushing crack; important disjunctions; possible small collapse
D4/D5	Very Serious & Collapse	> 15	Damage that evidently modify the resistance of the structures; possible partial and total collapse

The DPC classification was realized to classify damage, not to categorize the whole structures, considering the original aim of the approach: the evaluation of the fitting of the human habitation of buildings affected by a seismic event. For this reason, a further elaboration was necessary to apply the method to the PhD cases of study. All the possible crossings between percentage of the extension of the level of damage and the four classes of cracks size were taken into account using a matrix to evaluate a whole unit. Several possible combinations were individuated, considering also the possibility that the entire building is affected by the same type of damage (100% in the same class). For each level of damage, a value was assigned and then, the values were grouped between 0 (negligible damage) and 7 (total collapse) to be comparable with the other above described classifications.

4.2.2 Global Position System (GPS) survey

To better understand the movement of several areas, sometimes not visible by remote sensing techniques, involved by a landslide and to monitor their evolution, a Global Position System (GPS) survey can play a key role. Furthermore, this approach can be applied over time repeating measurements in the same control points and allowing the evaluation of their displacement. A GPS sensor (**Fig. 4.17**) is composed of a console to manage the measured points and an antenna that has to put up on a rod with note height (i.e. one or two m). The system allows to perform occasional measurements, that have to be repeated over time, in addition to real-time measurement based on the aim of the studies, i.e. small or large scale analysis. This approach, with respect to the terrestrial instrumentations (e.g. terrestrial geodetic sensor) can work in any condition of visibility and weather. On the other hand, GPS requires a certain satellite "covering", at least four satellites have to be visible from the receiver, of the monitored area to reach good precision.

To reach good precision during the survey the console has to be connected to internet, by means of the use of a mobile phone, to calculate as good as possible the correct position by the triangulation method. In this way, it is possible to reach errors of ± 0.05 m. The three dimensional coordinates (latitude, longitude

and height) (Bonnard et al., 1996; Wasowski et al., 2004; Mills et al., 2005; Webster and Dias, 2006; Yin et al., 2008; Zhang et al., 2008) of various control points can be obtained for several readings and, by means of statistical evaluation on the reliability of the data, the displacement vector for each measured point can be assessed correlating the repeated measures.



Fig. 4.17 - GPS sensor (a) and an example of its application during a field campaign survey in Agnone (b).

4.3 Damage - displacement relationship

In order to understand and prevent human losses and decrease consequently economic disasters, a correlation between the surveyed and classified damage on the facilities and kinematic parameters obtained by the A-DInSAR technique were investigated.

4.3.1 Velocity projected along the slope (V_{slope})

This work was conducted using both ascending and descending geometries of the satellite because the slopes in both analysed cases of study are exposed to Southeast and West, respectively. In both cases, the combination between ascending and descending PS was allowed projecting the velocity measured along the LOS in velocity along the steepest slope. Notti et al. (2014) presented a formula (Eq. 9) subsequently modified by Colesanti and Wasowski (2006) and Plank (2014) to project the velocity measured along the Line-of-Sight (LOS) of the satellite along the slope.

$$V_{slope} = \frac{V_{LOS}}{C} \quad (9)$$

where V_{LOS} is the velocity measured by the satellite along the Line-Of-Sight and C represents the percentage of movement that the SAR sensor can register. This coefficient (Eq. 10) is calculated using parameters derived from the DEM of the investigated area and the direction cosine (Eq. 4, 5 and 6) of the LOS depending on the incident angle and the LOS azimuth in radians.

$$C = (n_{LOS} * \cos(S) * (\sin(A - 1.571))) + (e_{LOS} * (-1 * \cos(S)) * \cos(A - 1.571)) + (h_{LOS} * \sin S) \quad (10)$$

Where:

$$h_{LOS} = \cos(\alpha) \quad (5)$$

$$e_{LOS} = \cos(1.571 - \alpha) * \cos \omega \quad (6)$$

$$n_{LOS} = \cos(1.571 - \alpha) * \cos \eta \quad (7)$$

$$\eta = 3.142 - \theta$$

$$\omega = 4.712 - \theta$$

Using V_{slope} the evaluated velocity affecting the structures is closer to the real more than the measured one along the LOS. Furthermore, to calculate the velocity along the slope allows to combine both geometries to assess the movement affecting each building. On the other hand, the projection along the slope has some limitations due to, for instance, small variations in the slope orientation that provoke strong effect on the V_{slope} measurement. Notti et al. (2014) suggest some consideration to adopt in order to reduce the problems affecting the reprojecton of the velocity:

- discard the PS, or assume correct V_{LOS} , in case of positive V_{slope} values, i.e. indicating up movements along the slope (very difficult condition);
- project PS LOS velocity only on areas with more than 5° of slope because the occurrence of landslides in flat area is very rare and the movement could be caused by other reasons;

- set a maximum value of the coefficient C to reduce any exaggeration of the projection when this value tends towards 0. Notti et al. (2014) suggests, based on empirical experience, three categories $C = -0.2$ when $-0.2 < C < 0$ and $C = 0.2$ in case of $0 < C < 0.2$.
- C value varies strongly with the irregularity of the slope, then Notti et al. (2014) suggests to use a DEM with low resolution, or resampled, to smooth out small variation causing errors and uniform the coefficient into the entire landslide.

V_{slope} parameter was used to classify the buildings in order to investigate for a relationship with the damage. In this way the buildings were categorized based on a velocity of displacement close to the real one affecting them. PS are intersected with the buildings isolating PS only referred to the structures and, by means of *Summary Statistics* tool of ArcGIS® the mean V_{slope} was assessed for each construction. Considering that the process of velocity reprojection caused an increment of the “error” inducing to enlarge the range of stability from ± 2 mm/year or ± 1.5 mm/year, for C-band and X-band respectively, to ± 5 mm/year.

4.3.2 Cumulated displacement projected along the slope (D_{slope})

Another important parameter describing the movement of the landslide is the displacement. By means of the possibility to have available data on both ascending and descending orbits is possible to project the displacement, as the for the velocity, along the slope. Using the same coefficient C (Eq. 10) and the same precaution above mentioned, D_{slope} was calculated as follows (Eq. 11)

$$D_{slope} = \frac{d_{LOS}}{C} \quad (11)$$

where D_{LOS} is the maximum displacement measured for the examined period along the LOS and C is the quantity of registered movement (Eq. 9).

In this way it is possible to improve the number of PS for areas where they are scarce, allowing the merging between the two orbits, and to investigate the real displacement affecting the target.

Also for D_{slope} values were used to categorize the buildings in order to look for a correlation with the damage recorded on the structures. To categorize the buildings based on the displacement close to the real occurring on them, PS are intersected with the structure to take into consideration only the signal reflected by the constructions. Then by means of *Summary Statistics* tool of ArcGIS® the mean D_{slope} was extracted for each structure. Also for this parameter the process of the reprojection caused an increment of the “error” inducing to expand the range of stability from ± 2 mm/year or ± 1.5 mm/year, for C-band and X-band respectively, to ± 5 mm/year.

5 Application and results

5.1 New ranking

The applications of the considered methodologies to classify the landslide-induced damage on structures known in scientific literature (**Table 5.1**) show several benefits and constraints that were taken into account and critically examined to propose a new approach for a quick damage assessment. The aim of the method was to overcome eventual difficulties in damage survey, as well as to reduce the drawbacks revealed when applying the aforesaid methods. The developed approach is a well-structured simple method for the recognition and classification of damage with the final aim of providing a subsequent effective categorization of the entire affected structures.

Table 5.1 - Summary of features of the existing classifications regarding landslide-induced damage.

	<i>Burland et al.</i>	<i>Alexander</i>	<i>Chiocchio et al.</i>	<i>Cooper</i>	<i>DPC - Baggio et al.</i>
Year	1977	1986	1997	2008	2009
Number of classes	6	8	8	8	4
Distinction of structure	NO	NO	YES	NO	NO
Reference values	YES (mm)	NO	YES (cm)	YES (mm)	YES (mm)
Partition of the structure	NO	NO	NO	NO	YES
Applicability on ground surface	NO	NO	NO	YES	NO

As mentioned in Cooper (2008), a method for assessing landslide-induced damage on buildings should allow to assess damage on facilities and ground surfaces, it should be simple and rapid to apply and not requiring the accessibility of the interiors of the investigated constructions (e.g. often private dwellings). To such a scope, the proposed approach is divided in two main steps: firstly, recognition and classification of the severity of damage, supported by drawings, notes and pictures; secondly, the *a posteriori* categorization of the entire facilities affected by damage. The specific goal was to propose an easy and suitable methodology of damage survey which allows also to assess the level of criticality of the whole damaged facility and help in the characterization of the investigated area.

To simplify the recognition of damage during the damage assessment on structures, a visual description (**Fig. 5.1**) of the possible observable cracks and fractures affecting the facilities, by means of the scheme in **Table 5.2** derives from Baggio et al. (2009), improved by the experiences accumulated in field, was reported.

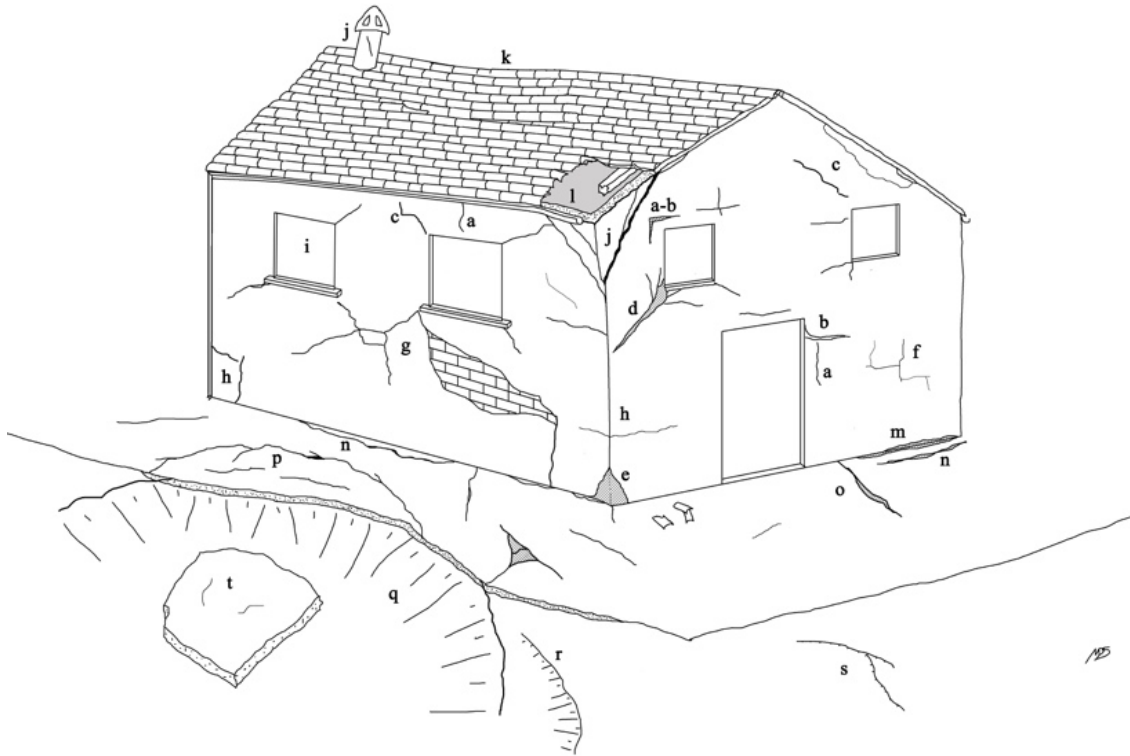


Fig. 5.1 - Referring scheme of the damage which could affect structures and grounds in a landslide-prone area: a) thin and open vertical cracks; b) thin and open horizontal fractures; c) diagonal tension cracks; d) severe open damage; e) local crushing with or without loss of material; f) hairline fissure in plaster; g) loss of plaster enclosed by cracks; h) horizontal and vertical damage close to the intersection of walls; i) distortion of services as doors, windows or chimneys; j) unstable wedge in the intersection of walls severely affected by open cracks; k) bended roof; l) collapse of part of the structure (e.g. roof); m) open and thin fractures between the external façades and the sidewalk; n) open (sometimes filled by soil and grass) and thin parallel damage in sidewalk; o) open (sometimes filled by soil and grass) and thin perpendicular fractures in sidewalk; p) damage due to the propagation of the landsliding effects on horizontal structures; q) extensive ground cracking with minor and major scarps; r) fracture retracing the scarps of the landslide with tension cracks in soil; s) thin fissure in ground surfaces; t) piece of horizontal structure fractured and collapsed along the scarp of the landslide (from Del Soldato et al., under review_b).

The proposed classification differentiates six levels (**Table 5.2**) from the non presence to the high severity of damage: no damage (G0), negligible (G1), weak (G2), moderate (G3), severe (G4) and very severe (G5). The distinction of five grades of damage, in addition to the no damage level (G0), derives from the classification of Burland (1977) and the merging with the DPC one (Baggio et al., 2009).

Table 5.2 - New proposed approach (Del Soldato et al., under review_b) for the classification of observable damage affecting facilities and ground surfaces. It was developed based on the scheme of Burland et al. (1977), Alexander (1986), Chiocchio et al., (1997), Cooper (2008) and DPC (Baggio et al., 2009).

<i>Damage level</i>	<i>Load-bearing structures</i>	<i>Crack width (CW in mm)</i>	<i>Cracking description</i>	<i>Ground damage</i>
G0 No damage	Masonry	-	Building is intact	Not visible
	Reinforced concrete frame			
G1 Negligible	Masonry	≤ 1	Fine or isolated cracks, generally in internal walls or finishes not influencing the resistance of the structure; no distortion. Not visible from the outside, rarely in brickwork. Restoring with normal redecoration	Not visible
	Reinforced concrete frame			
G2 Weak	Masonry	$1 < CW \leq 5$	Settlement of foundations, distortion and inclination not involving the stability. Several slight fractures on walls and partitions inside the buildings. Doors and windows may stick slightly. Repair not urgent, some external redecoration probably required. Difficult to record from outside.	Thin cracks in hard surfaces as roads, concrete pavements. No ruptures visible in vegetated ground. No separation or distortion in vertical structures
	Reinforced concrete frame			
G3 Moderate	Masonry	$5 < CW \leq 15$ or several > 3 mm	Open cracks in walls that could influence the resistance of the structure; walls disjunction and lintel deformation with sticking of doors and windows. Possible expulsion of materials and fracturing of service pipes. Visible from outside.	Change of tension in wires and fences. Open cracks, distortion, separation or relative settlement with falling of small fragment due to slight damage to road and structures. Remedial works not urgent
	Reinforced concrete frame			
G4 Severe	Masonry	$15 < CW \leq 25$ depending on number of cracks	Spread cracking and fractures in structural members conditioning the resistance of the structure. Considerable disjunction; floors inclined and walls out of perpendicular. Windows and doors too distorted to use, walls lean or bulge noticeably, service pipes disrupted. Evacuation and shoring. Noticeable from outside.	Ground surface bulged and/or depressed presenting widespread tension cracks in soil and turf. Settlement may tilt walls, fracture of structures, service pipe and cables. Remedial work necessary
	Reinforced concrete frame	$5 < CW \leq 20$ depending on number of cracks		
G5 Very severe	Masonry	> 25 depending on number of cracks	Partial collapse of floor and open cracks on structural parts hardly damaging the stability of the structure. Out of plumb walls, structure grossly distorted, seriously cracked floors and walls, doors and windows broken. Possible major rotation or swelling of the building and collapse of part of the structure. Evacuation and cordoning; Occupant will need to be rehoused. Partial or total rebuilding requires, probably not feasible. Very obviously from outside	Extensive ground cracking with minor and major scarps, ground bulging and soil rolls. Debris, earth and mud flows, falls and slide may affect man-made facilities. Settlement causes cracks, rotation and distortion to structures and roads. Remedial works urgent.
	Reinforced concrete frame	> 20 depending on number of cracks		

Comparing the proposed classification of damage level to the existing ranking it is possible to notice the absence of levels referred to the collapse condition, indifferently partially or totally. The choice was done to pursue the specific target of the ranking, thus the classification of cracks and fractures observed during field surveys. In this way the collapses can be categorized as *very severe* following the philosophy of Burland (1977)

and DPC (Baggio et al., 2009) recording schemes. The second column, concerning the typology of the load-bearing structure, takes inspiration from the approaches of Alexander (1986) and Chiocchio et al. (1997). The difference of behaviour between masonry and reinforced concrete frameworks were already touched upon by Nawy (1968). Steel and timber frames are not considered because their response to the movement can be assimilated to the reinforced concrete reaction (Grünthal, 1998). The width of the cracks, and their numbers are considered important parameters to group the visible fractures on facilities and the exhibited values are reported by Burland (1977) and Cooper (2008) categorizations in addition to the illustrations of the damage from Alexander (1986) and DPC (Baggio et al., 2009). The descriptions of damage were derived taking into account the main features of each abovementioned existing classifications. Some modifications, based on the accumulated experience, were made in order to adapt the characterizations to better recognize damage from the exterior of structures. It is important to highlight that fractures affecting foundations are not considered in the categorization because not easily recognizable without invasive investigations. The definitions of the ground damage was adopted from the Cooper (2008) classification and modified in the proposed approach by not taking into account interpretation of the severity but considering strictly a classification of cracks, as being not related with the consequences that could be elicited on the structures. In this way, the ground landslide-induced damage is classifiable from *weak* (G2), to *very severe* (G5) as for the visible cracks on facilities. To facilitate a methodical survey of the buildings a recording damage scheme (**Fig. 5.2**) was suggested in order to better compare all the surveyed constructions. By means of this support, the categorization of **Table 5.2** and the visual description shown in **Fig. 5.1**, a good classification of cracks and ruptures on facilities and on ground surfaces is possible. The suggested scheme requires several information about the structures, important not only to investigate damage, but also for the evaluation of their vulnerability or risk (Uzielli et al., 2015).




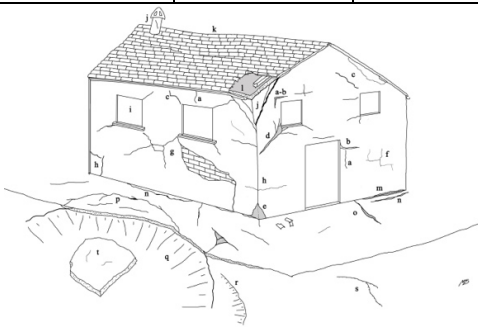
DAMAGE RECORDING SCHEME				 Universitat d'Alacant Universidad de Alicante				 UNIVERSITA DEGLI STUDI FIRENZE DST DIPARTIMENTO DI SCIENZE DELLA TERRA		
Data				ID						
Site		Corners coordinates			X	Y	Z			
Municipality		Prov.		N						
Type of construction				E						
Load-bearing material				S						
Date of construction				W						
Floors		Position respect to the landslide								
				Thin and open vertical, horizontal and diagonal cracks (a , b , c and d); local crushing with or without losing of material (e and g); fissure and cracks in plaster and intersection of walls (f and h); distortion of services (i); unstable wedge and bended or collapse roof (j , k and l); open and thin crack between the wall and sidewalk (m); open (sometimes filled) and thin parallel and perpendicular cracks in in horizontal structures (n and o); propagation of landslide crown (p); minor or major scarps (q); fractures and thin fissure in ground surfaces (r and s); piece of structure fall along the scarp (t)						
				Extension of the damage	G0	G1	G2	G3	G4	G5
				< 1/3						
				1/3 < damage < 2/3						
				> 2/3						
Description and sketch of the damage										
Observations:										

Fig. 5.2 - Suggested recording scheme to survey damage on structures (Del Soldato et al., under review_b).

The second part of the work consists in the assessment of the damage severity affecting the whole structure. This has to be carried out after the damage classification recognized by means of field surveys. The aim is the estimation of the stability of the entire structure considering the construction divided in sectors and taking into account the extension of damage. All possible crossings considering all grades of the proposed classification are shown and considered in **Table 5.3**. The empty cells represent the no possible crossings, while the colours show the severity of damage grouped into 8 levels of damage: *no damage, negligible, weak, moderate, severe, very severe, potential collapse* and *not-habitable*.

Table 5.3 - Table of conversion from the level of damage recognized on each sector of the facilities to the classification of the entire structures (Del Soldato et al., under review_b).

	> 2/3 G5	1/3 < G5 < 2/3	< 1/3 G5	> 2/3 G4	1/3 < G4 < 2/3	< 1/3 G4	> 2/3 G3	1/3 < G3 < 2/3	< 1/3 G3	> 2/3 G2	1/3 < G2 < 2/3	< 1/3 G2	> 2/3 G1	1/3 < G1 < 2/3	< 1/3 G1	> 2/3 G0	1/3 < G0 < 2/3	< 1/3 G0
> 2/3 G5	-	-	7.000	-	-	6.533	-	-	6.067	-	-	5.600	-	-	5.133	-	-	5.000
1/3 < G5 < 2/3	-	7.000	-	-	6.300	-	-	5.600	-	-	4.900	-	-	4.200	-	-	4.000	-
< 1/3 G5	7.000	-	-	6.067	-	-	-	5.133	-	4.200	-	-	3.267	-	-	3.000	-	-
> 2/3 G4	-	-	6.067	-	-	5.600	-	-	5.133	-	-	4.667	-	-	4.200	-	-	4.067
1/3 < G4 < 2/3	-	6.300	-	-	5.600	-	-	4.900	-	-	4.200	-	-	3.500	-	-	3.300	-
< 1/3 G4	6.533	-	-	5.600	-	-	4.667	-	-	3.733	-	-	2.800	-	-	2.533	-	-
> 2/3 G3	-	-	5.133	-	-	4.667	-	-	4.200	-	-	3.733	-	-	3.267	-	-	3.133
1/3 < G3 < 2/3	-	5.600	-	-	4.900	-	-	4.200	-	-	3.500	-	-	2.800	-	-	2.600	-
< 1/3 G3	6.067	-	-	5.133	-	-	4.200	-	-	3.267	-	-	2.333	-	-	2.067	-	-
> 2/3 G2	-	-	4.200	-	-	3.733	-	-	3.267	-	-	2.800	-	-	2.333	-	-	2.200
1/3 < G2 < 2/3	-	4.900	-	-	4.200	-	-	3.500	-	-	2.800	-	-	2.100	-	-	1.900	-
< 1/3 G2	5.600	-	-	4.667	-	-	3.733	-	-	2.800	-	-	1.867	-	-	1.600	-	-
> 2/3 G1	-	-	3.267	-	-	2.800	-	-	2.333	-	-	1.867	-	-	1.400	-	-	1.267
1/3 < G1 < 2/3	-	4.200	-	-	3.500	-	-	2.800	-	-	2.100	-	-	1.400	-	-	1.200	-
< 1/3 G1	5.133	-	-	4.200	-	-	3.267	-	-	2.333	-	-	1.400	-	-	1.133	-	-
> 2/3 G0	-	-	3.000	-	-	2.533	-	-	2.067	-	-	1.600	-	-	1.133	-	-	1.000
1/3 < G0 < 2/3	-	4.000	-	-	3.300	-	-	2.600	-	-	1.900	-	-	1.200	-	-	1.000	-
< 1/3 G0	5.000	-	-	4.067	-	-	3.133	-	-	2.200	-	-	1.267	-	-	1.000	-	-
No damage	1	Negligible	1 ÷ 1,499	Weak	2 ÷ 2,499	Moderate	3 ÷ 3,499	Serious	4 ÷ 4,499	Very serious	5 ÷ 5,499	Potential collapse	6 ÷ 6,499	Unusable	6,499 ÷ 7			
Safety																		
Inhabitable																		

The classification based on the characterization of damage severity considers six levels while the classification of the whole structure expects eight classes. By means of a mathematical value assigned to each level of damage, a numerical value is assigned to each crossing cell. First of all, for no damage (G0) the value 1 was arbitrarily designated in order to allow the division in portions. The thresholds between the classes of the categories of the whole constructions (i.e. seven) were defined correlating them with the numbers of the level of damage (i.e. five). Structures entirely affected by the same level of cracking have to be evaluated in two different parts to enter in the symmetric matrix (**Table 5.3**). The ground fractures classified with the scheme in **Table 5.2** have not to be contemplated in the second phase (**Table 5.3**), dedicated to rank damage on facilities.

5.2 Agnone landslide (Molise region)

5.2.1 Reconstruction of evolutionary stages and monitoring of the landslide

The investigated Colle Lapponi - Piano Ovetta landslide is a deep-seated mass-movement whose morphological features and effects on involved structures are the results of two important reactivations occurred in January 2003 and between December 2004 and January 2005, which were followed by other minor continuous movements.

The first evidences of a landslide affecting the investigated site were found in literature and dated back to the beginning of the XX century. Almagià (1910) described a phenomenon that occurred on March 1905 damaging the access bridge to the historical centre of Agnone caused by the combination of an intense rainfall period with the snow-melting. Other old reports are very rare to find, but it is known that the territory of the Agnone municipality was diffusely and chronically affected by landslides.

In order to investigate the evolution of the landslide, the historical aerial images taken by the IGM in different years since 1945 were analysed. By means of the application of the *Structure from Motion* technique, the 3D reconstructions of several years of the landslide area were realized in order to investigate the evolution of the landslide (**Fig. 5.5**). The precision of the models depends on the quality of the scan process used for the images and the source of the GCPs coordinates, in this case a DEM with 5-m cell resolution. In this way, all the reconstruction realized for the Agnone landslide resulted with a pixel dimension lower than 5 m (**Fig. 5.5**). For the analysis of the evolution of the CL-PO landslide, the 3D reconstructions were developed only on the landslide area and the surrounding region. Analysing the 3D reconstructions developed for seven historical sets of images, from 1945 to 2005, different stages of the mass-movement evolution affecting the Colle Lapponi - Piano Ovetta were recognized. It is interesting noticing that the first activation, or reactivation, of the landslide occurred before the 1945 involving only the western part of the valley (**Fig. 5.5a**) and damaging the access road to some buildings. The subsequent reconstructions made by means of aerial images of 1954, 1981 and 1986, shown as the evolution of the territory tried to remove the geo-morphological shapes determined by the landslide before 1945. In the model of 1954 no important enlargements of the investigated area were shown: only little advancing of material at the foot can be recognized. (**Fig. 5.5b**). The 3D reconstruction of 1981 do not show important differences too, even if a cloud on the right side of the valley covers part of the landslide area (**Fig. 5.5c**). The diffusion of several ploughed and cultivated areas allows to suppose that no new events occurred. This hypothesis can be confirmed by the model of 1986 where the signs of the landslide are almost totally obliterated by the time and by means of diffused agricultural practices (**Fig. 5.5d**). The changes recognizable in the abovementioned period, from 1945 to 1986, are due to very little events affecting the flanks or the

river, or due to the transportation of the beforehand mobilized materials. The reconstruction developed by means of the set of images shot in 1991 shows a continuous enlarging of the movement only on the natural embankments probably due to the erosion. Other important facets to highlight are the interventions operated along the Verrino Torrent (in the lower part of the reconstructed area) and along the river flowing into the CL-PO valley (**Fig. 5.5e**). These works were probably made to avoid the continuous span erosion and to control the runoff drainage, which in some cases are still visible in the lower part of the landslide, close to the spilling of the river into the Verrino torrent.

Table 5.4 - Ground Control Points precision carried out by the reports of Photoscan.

Year	X error (m)	Y error (m)	Z error (m)	XY error (m)	Total (m)	Image (pix)
1945	3.173	1.388	2.577	3.463	4.317	0.657
1954	2.721	1.594	2.010	3.154	3.740	0.873
1981	0.416	0.678	0.621	0.795	1.009	0.539
1986	1.373	1.367	1.732	1.938	2.599	0.521
1991	0.906	1.111	1.331	1.434	1.956	0.362
2003	0.989	1.414	1.125	1.725	2.060	0.392
2005	0.331	1.153	0.701	1.199	1.389	1.138

Guzzetti et al. (1994) edited the nationwide AVI project, by means of an archival and bibliographical landslides research, carrying out between the 1970 and 1998, more than 60 landslides affected the council territory of Agnone. Two important phenomena were reported in literature regarding the area close to the investigated Colle Lapponi - Piano Ovetta: a) a landslide involving two pylons of the State Road viaduct in February 1984, forcing its partially demolition (Guadagno et al., 1987); b) a mass-movement in 1994 involving the Colle Lapponi - Piano Ovetta valley causing the interruption of an important dirty road, connecting several houses. In 2008 ISPRA (*Istituto Superiore per la Protezione e la Ricerca Ambientale*) updated the landslide inventory and produced the IFFI project (*Italian Landslides Inventory Project*) in which for the whole Agnone territory recorded more than 450 events.

The following news about the CL-PO landslide were issued in 2003 when, between 23rd and 27th January, an intense rainfall event with more than 200 mm over 72 hours (**Fig. 5.3a**) provoked an important reactivation (**Fig. 5.5f** and **g**) of a historical dormant landslide, due to an unusual increase of pore pressures (Calcaterra et al., 2008). Nearby the territory involved in the mass movement, a cumulative precipitation of about 50 mm was measured and with high probability this was a main triggering factor of the deep-seated landslide. The mass movement involved the Agnone Flysch formation with a complex style consisting in a large roto-translational slide and an earth-flow (Cruden and Varnes, 1996). The consistent effects on the territory and

on facilities forced the municipality administration to adopt restrictive measures, i.e. the evacuation of 13 buildings, and relative 17 families living inside, located into and close to the area involved by the landslide. Owing to the severity of the situation, the municipal administrator earmarked funds to the fulfilment of some urgent interventions to improve the drainage in the upper part of the landslide body where the hydrogeological condition and the ponding of water could have been a possible dangerous triggering factor. For this reason, some excavations of trenches were realized in order to intercept and drain surficial water table as well as some re-shaping of the mass-movement were made. In spite of these remedial maintenances, the landslide continued to be active in the following years, increasing its dimension and carrying on to provoke several damage on facilities and buildings. Some testaments are due to the continuous problems occurring on the road sited on the crown on the landslide, repeatedly affected by cracks and sliding and continuously renovated by means of the use of natural engineering interventions, i.e. gabionades. From the 3D model of 2003 (Fig. 5.5f) the big entity of the displacement is not appreciable as well as by means of the picture (Fig. 5.5g). It is probable that they are not registered in the same period, but that the photo was shot some months later when the phenomenon was subject to a further evolution. For instance, on the 3D reconstruction the dirty road that crossed the landslide is yet recognizable, instead in the picture it is indistinguishable from the detritus.

Less than two years later the first important reactivation, a series of several rainfall events (Fig. 5.3b) activate again the CL-PO landslide, in March 2004 (Fig. 5.5h) and between December 2004 - January 2005 (Fig. 5.5i and j), extending the involved area until it reached an estimated total volume of $3.5 \times 10^6 \text{ m}^3$ (Calcaterra et al., 2008). Consequently, a new reshaping of the slope and 10 trench drains, were realized in order to avoid further damage on facilities and reactivations.

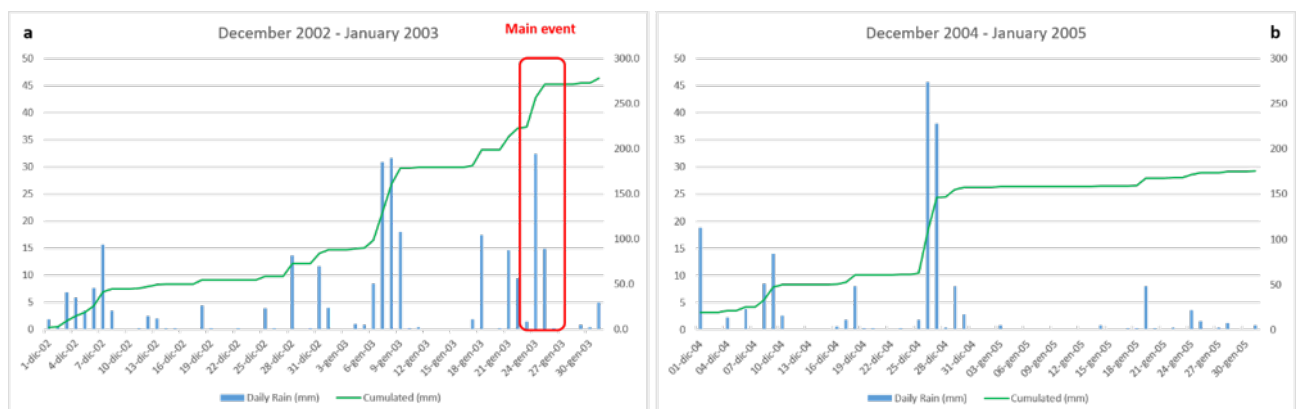


Fig. 5.3 - Precipitation graphs of two main reactivations that occurred in January 2003 (a) and between December 2004 and January 2004 (b) (Del Soldato et al., under review_a).

These actions allowed the stabilization of the mass movement in the middle-lower region. From 2004 onward, a set of topographic benchmarks were placed in unstable areas to monitor the ground movement of the landslide. By means of topographical measurements, the landslide enlarging was estimated about 350 m of advancing at the toe and about 270 m of retrogressing in the head sector, reaching a total length up to 1500 m. Some of them were measured again during the field campaign carried out in July 2016. Not all benchmarks were found because during the years some of them were destroyed during the realization of the drainage operations, lost for the continuous displacement affecting the territory or because too difficult to reach due to the intense vegetation, ground damage and some gates to contain the animals. The displacement calculated during the time span between the measurement carried out in 2006 and in 2016 are only for few benchmarks (**Fig. 5.4**).

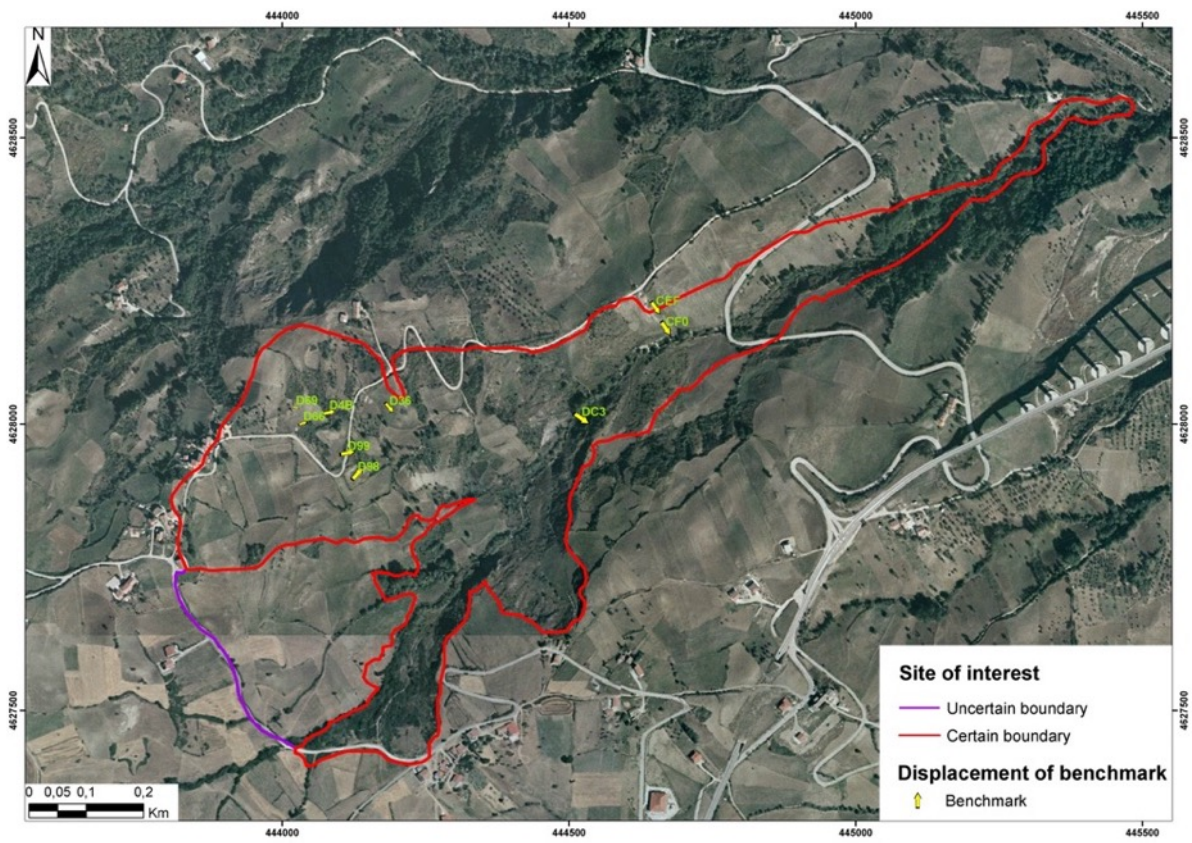


Fig. 5.4 - Displacement measured between 2006 and 2016 of some topographical benchmarks located inside the CL-PO landslide. The dimension and the orientation of the arrows reflect to the value of the displacement.

In the following period, until June 2006, the material involved in previous reactivation continued to move inside the landslide increasing its length of about 70 m in the foot region. Then between April 2006 and April 2007 an incessant lower displacement rate was recognized. The pictures shot from the same place of the previous one (**Fig. 5.5k**), focusing on the entire landslide, simplifies the recognition of the progressive increment of the involved area by the mass-movement and the displaced materials.

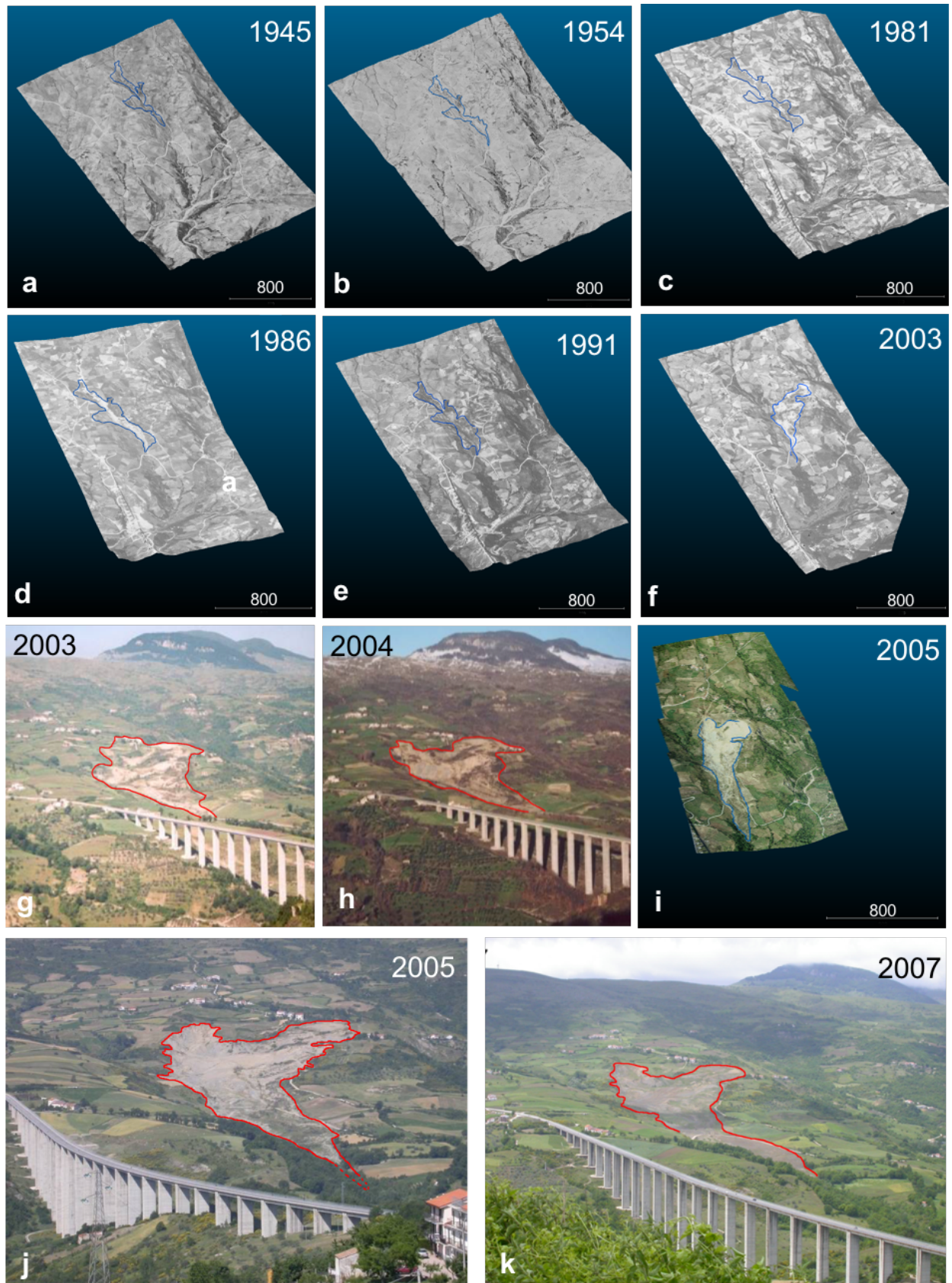


Fig. 5.5 - Visual evolution of the Colle Lapponi - Piano Ovetta landslide from 1945 to 2007 by means of the remote sensing analysis to realize the 3D models and some pictures shot from the same place.

The continuous slow movement was testified to the monitoring campaign carried out by the inclinometers (Fig. 5.6) from April 2006 (used as “read zero”) until July 2006 by means of three measurements (Table 5.3) after which the instruments were broken due to the large movement affecting the landslide.

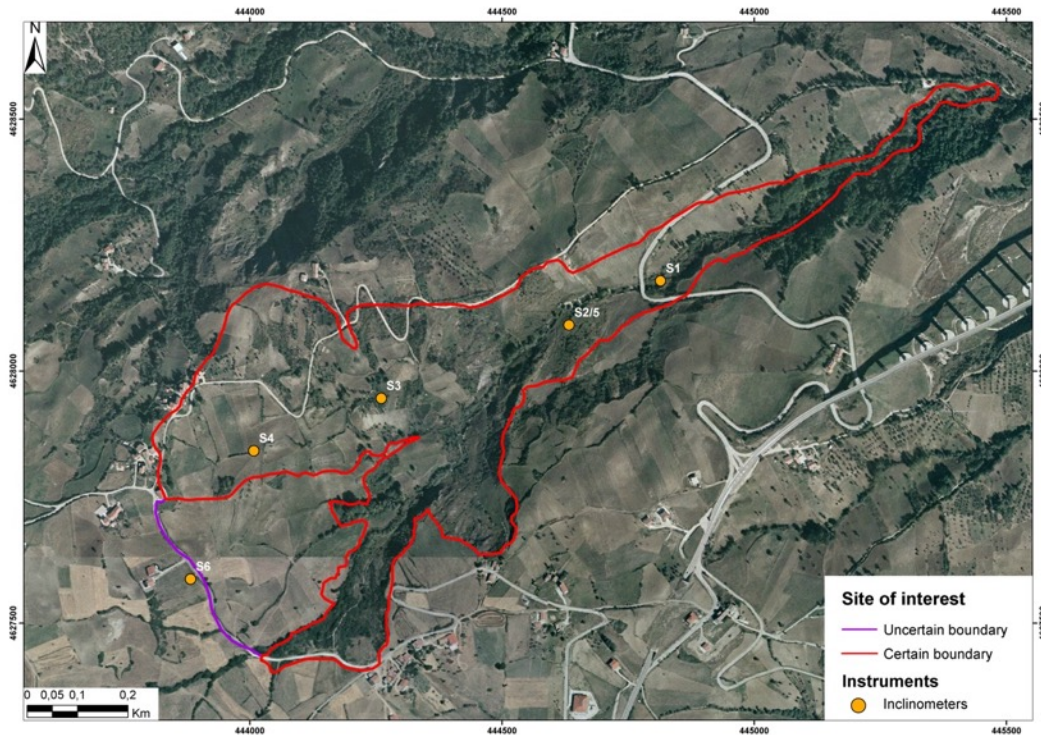


Fig. 5.6 - Localization of the inclinometers in the CL-PO landslide.

Table 5.5 - Temporal sequence of the inclinometric measurements (GEOSERVICE).

Inclinometers	S1	S2	S3	S4	S5 (ex S2)	S6
Installation	11/01/06	03/02/06	30/01/06	15/02/06	11/04/06	12/04/06-
Reading "0"	16/03/06	16/03/06	16/03/06	17/03/06	-	13/04/06
Reading "1"	13/04/06	lost	13/04/06	13/04/06	13/04/06	19/05/06
Reading "2"	19/05/06	lost	19/05/06	19/05/06	19/05/06	21/06/06
Reading "3"	21/06/06	lost	21/06/06	21/06/06	lost	19/07/06
Reading "4"	19/07/06	lost	19/07/06	19/07/06	lost	06/09/06
Reading "5"	06/09/06	lost	06/09/06	06/09/06	lost	04/10/06
Reading "6"	04/10/06	lost	04/10/06	04/10/06	lost	08/11/06
Reading "7"	08/11/06	lost	08/11/06	08/11/06	lost	06/12/06
Reading "8"	06/12/06	lost	06/12/06	06/12/06	lost	10/01/07
Reading "9"	10/01/07	lost	10/01/07	10/01/07	lost	lost

The measurements were recorded about once per month and plotted in the schemes shown in **Fig. 5.7**.

Starting from the landslide crown to the internal body:

- the inclinometer placed close to the boundary in the crown of the landslide, S6 (**Fig. 5.7a**), did not show important movement, even if some little displacements were visible recognizable as a possible retrograde increasing of the mass-movement;
- the instrument installed in the soil drilling S4 (**Fig. 5.7b**) showed movements of possible slip surfaces at 23 m depth;
- the inclinometer sited in the borehole S3 (**Fig. 5.7c**) was noisy, but at 12 m depth showed an evident surface of displacement between April and June;
- the instrument located in the hole S2/S5 (**Fig. 5.7d**) highlighted a slip surface with movement of centimetres to 9 m depth and an instability in the bottom of the hole at 18 m depth;
- the inclinometer placed in the toe of the landslide, at the time of the installation, S1 (**Fig. 5.7e**) presented a rupture surface at about 8m of depth corresponding to a movement started between March and May and remaining constant with a velocity of 3 mm per month.

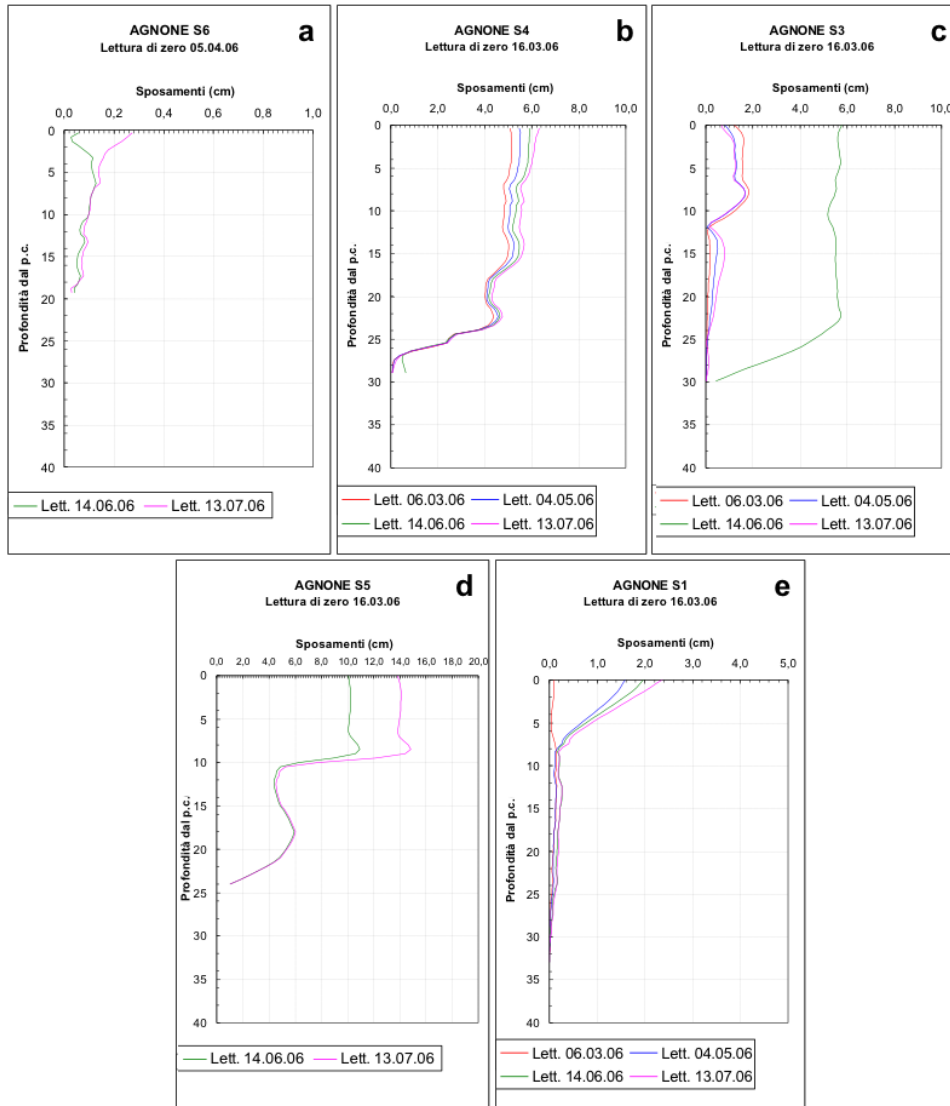


Fig. 5.7 - Graphic restitution of the inclinometric data. a) S6 in the crown of the landslide; b) S4 in the upper part of the body of the mass movement; c) S3 in the middle of the body landslide; d) S5 (ex S2); e) S1 in the toe of the landslide when it was installed.

The continuous movements of the slope led the local administrator to adopt new mitigation measures to eliminate another lake formed in the middle part of the landslide caused by a ground subsidence and by a drainage of the surface runoff. Ten trench drains 6.5 m deep and about 150 m long in addition to a reshaping of the slope were realized in order to stabilize the middle-lower region of the mass movement to avoid further down slope with possible formation of a dam in the Verrino torrent.

No more reports or news of important reactivations were reported, but the field surveys conducted in 2015 and 2016 highlighted as the movement of the landslide was not arrested (**Fig. 5.8a** and **b**). The dimension of the landslide area was recognized in a continuous enlargement by a series of geomorphological features, a continuous progression of important visible damage on facilities and buildings as well as the visual comparison of oblique terrestrial pictures taken during field campaigns.

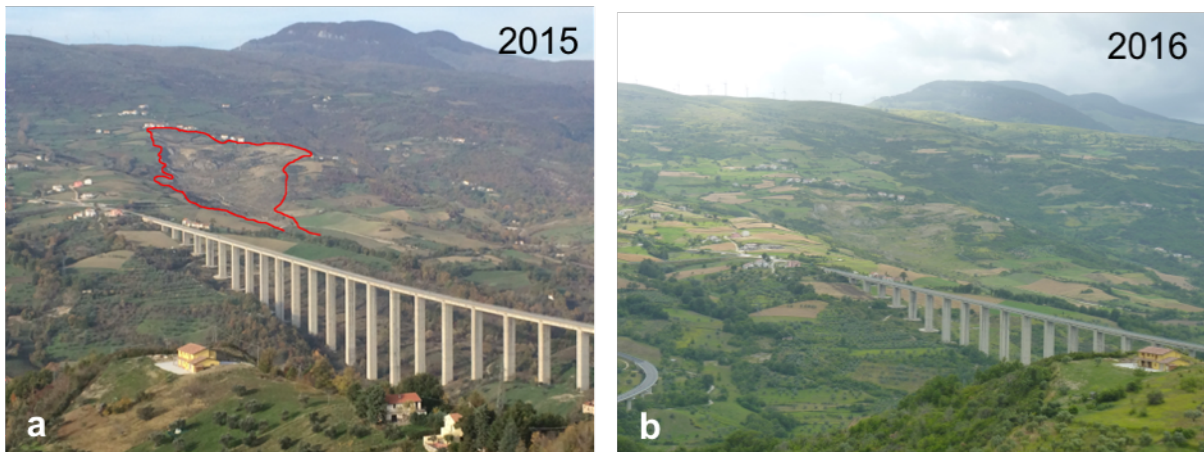


Fig. 5.8 - Visual evolution of the Colle Lapponi - Piano Ovetta mass-movement by means of two oblique terrestrial pictures taken during field surveys conducted in November 2015 (a) and in July 2016 (b).

From 3D terrain models generated by *SfM* technique applied to historical aerial images, a difference between the 3DPCs referred to 1945 and to 2003 was computed to assess the change of volume that occurred on the landslide region and surroundings by means of CloudCompare software (M3C2 plugin). This tool allows to carry out quantitative results, but the resolution of the input raw data and the elaboration process permits to evaluate volume changes. The M3C2 is an appropriate tool for Terrestrial Laser Scanning (TLS) and photogrammetric data in complex 3D environments using a grid of “core” points and the normal analysis (Brodu and Lague, 2012). It works directly on the point clouds, computing the 3D variation in local distance between two points along the normal surface and estimating a confidence interval for each distance measurement (Lague et al., 2013). In the application of CL-PO landslide the 1945 3D Points Cloud were used as *reference* cloud, while the 2003 3D Points Cloud were assumed as *compared* cloud. Operating the difference between the two Point Clouds a distribution of the changes of volume were carried out (**Fig. 5.9**). Investigating the area where the event of 2003 occurred (**Fig. 5.9a**), a region affected by an important loss of volume, in blue, and an accumulation zone, in red, were recognized. These zones are in accordance with the localization of the trigger area of the landslide and the zone where the run-out material were amassed, respectively. Besides the investigation involved the reconstructed 3D Point Clouds referred to 2003, the volume difference analysis was conducted also considering the traced landslide contour in 2016 by means of field surveys and supported by remote sensing techniques (**Fig. 5.9b**). It is worth noting the influence of the reactivation affecting the uphill area respect to the 2003 crown. In this region some areas in alternation red and in light blue are recognizable. These areas are identifiable as smooth tilted morphological shapes formed due to the landslide events.

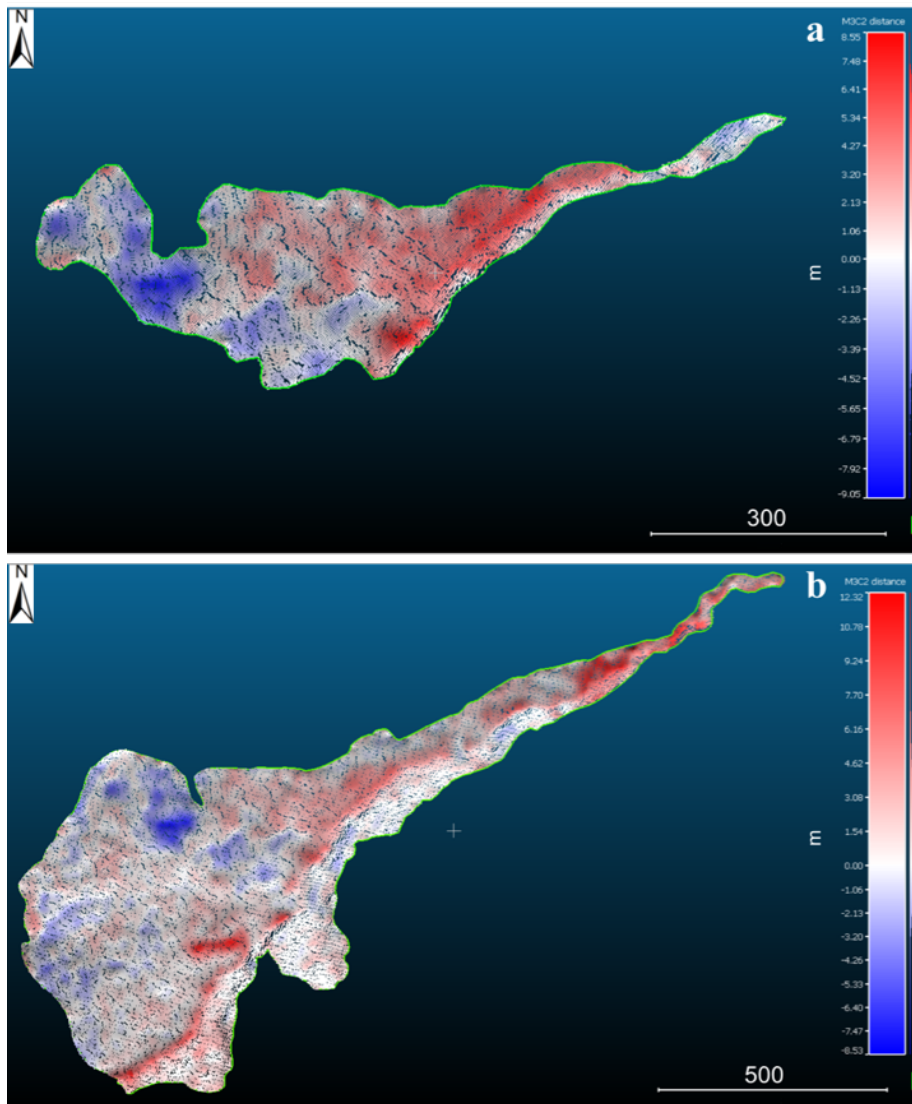


Fig. 5.9 - Difference in volume between the reconstructed 3D Points Clouds of 1945 and of 2003 segmented on the boundary of the landslide that occurred in 2003 (a) and on the contour of the landslide traced in 2016 (b).

Considering the present contour of the landslide, the right lobe involved in an old event occurred before 1945, year of the first set of examined images of this area, is recognizable. It shows an important region with hot colour, indicating areas where increment of volume occurred. This is due to the analysis conducted starting from the 1945 set of images shot after an important landslide. In this way, the volume recorded as increment in that area can be probably related to some interventions executed successively between 1986 and 1991, as recognizable by the respective set of historical aerial photos (Fig. 5.10).



Fig. 5.10 - Orthomosaic of the CL-PO landslide referred to 1991 with highlighted in the red circle the fulfilled works between 1986 and 1991.

The evolution of the recent years was assessed by means of several field campaigns aimed at surveying the displacement affecting 8 trihedral Corner Reflectors⁹ located inside the landslide body and to map principal landslide structural features as main and secondary scarps. The displacement, estimated using GPS measurements (**Table 5.6**), allowed to display the movement that occurred on each still available today Corner Reflector. During the field surveys was notice as, during the monitoring period, one of them (CR8) was removed and another one (CR2) was, with high probability, moved or distorted losing its usefulness.

The last reading in 2016 was conducted with a new instrument not needing the reading of the bases to ensure precise measurements. As for some benchmarks, several readings carried out for Corner Reflectors were used to assess their displacements (**Fig. 5.11**).

⁹**Corner Reflectors:** passive instruments composed by three perpendicular intersecting flat surfaces, reflecting back the waves directly towards the source. The three intersecting surfaces often have square shapes, made of metal used to reflect radio waves from radar sets. This causes them to show a strong "return" on radar screens.

Table 5.6 - Summary of the GPS measurements conducted for the CL-PO landslide.

	Reading "0"	Reading "1"	Reading "2"	Reading "3"	Reading "4"	Reading "5"
Base_1	Nov-2010	Feb-2011	Nov-2011	Mar-2012	May-2013	no surveyed
Base_2	Nov-2010	Feb-2011	Nov-2011	no survey	no survey	no surveyed
Base_3	Nov-2010	Feb-2011	Nov-2011	Mar-2012	May-2013	no surveyed
CR1	Nov-2010	Feb-2011	Nov-2011	Mar-2012	May-2013	16/07/16
CR2	Nov-2010	Feb-2011	Nov-2011	Mar-2012	lost	(16/07/16)
CR3	Nov-2010	Feb-2011	Nov-2011	Mar-2012	May-2013	16/07/16
CR4	Nov-2010	Feb-2011	Nov-2011	Mar-2012	May-2013	16/07/16
CR5	Nov-2010	Feb-2011	Nov-2011	Mar-2012	May-2013	16/07/16
CR6	Nov-2010	Feb-2011	Nov-2011	Mar-2012	May-2013	16/07/16
CR7	Nov-2010	Feb-2011	Nov-2011	Mar-2012	May-2013	16/07/16
CR8	Nov-2010	Feb-2011	Nov-2011	Mar-2012	lost	lost

The information of the displacements measured on benchmarks and on Corner Reflectors are important because they allow a better understanding of ground movements inside the landslide body.

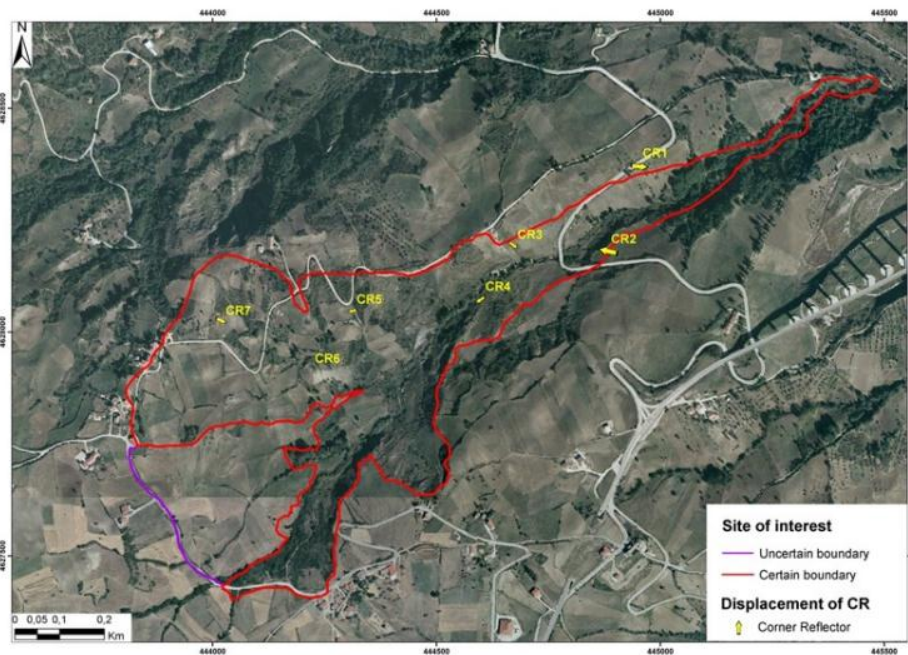


Fig. 5.11 - Displayed displacement for the Corner Reflector located into the body of the CL-PO landslides map measured by means of GPS campaigns from 2010 to 2016. The dimension and the orientation of the arrows reflect the value of the displacement.

A geomorphological mapping of the landslide surroundings, in addition to the recognition of the main and secondary scarp of the mass-movement, was realized by means of on-site observations and evidences (Fig.

5.12) in order to map the numerous scarps and counter-slopes, mainly recognized during the last field surveys of July 2016, behind and close to the top of the landslide.

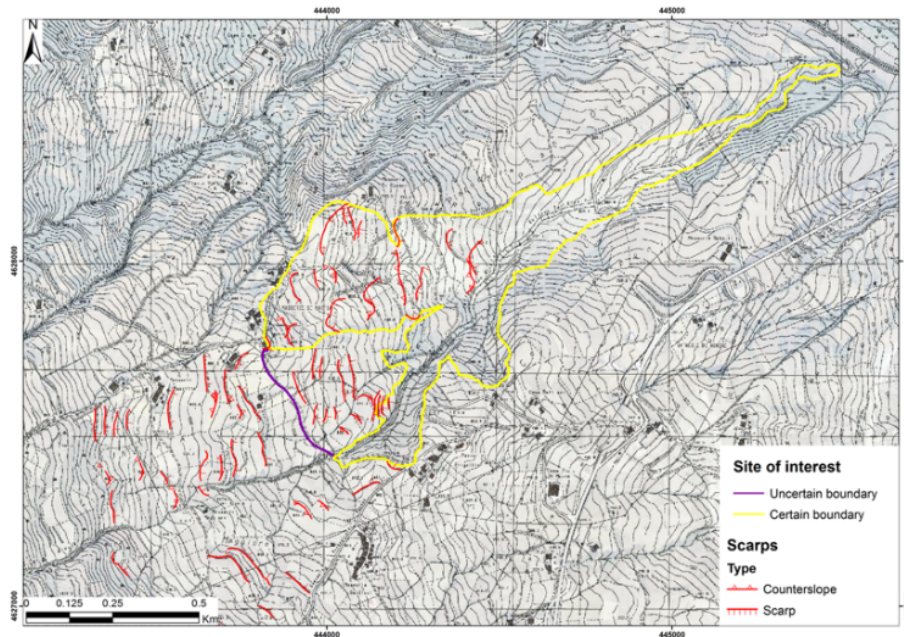


Fig. 5.12 - Geomorphological map of the landslide area and its uphill region.

The numerous recognized scarps indicate that the mass-movement affected causing geomorphological changes into the body of the landslide and in the uphill area. Their localization and mapping could help understanding the influencing of the phenomenon and the possible future evolution of the landslide. Furthermore, the geomorphological map indirectly shows the continuous evolution of the slope also after the known main reactivations. Some scarps and counter-slopes were visible in the area between the two lobes of the mass-movement, where no important phenomena occurred, but they are indicative of further involvement of this area. The evidences induced to trace the “probable boundary” even if no important active signs were recognized along the investigated time-span. It is worthy to note that most part of the recognized scarps, mainly far from the boundary of the landslide, are smoothed. This could suggest no recent movements in those areas, but possible older ones. This hypothesis is in accordance with the probability that the area was involved in some paleo-landslide on which the investigated mass-movement is superimposed.

Furthermore, the improvement of the remote sensing approaches allows to investigate the recent evolution of the landslide by means of the use of Persistent Scatterer Interferometry (PSI) data. The available Persistent Scatterers (PS) radar benchmarks from 1992 to 2000, ERS1/2 satellite (**Fig. 5.13a**), from 2002 to 2010, ENVISAT platform (**Fig. 5.13b**), and from 2012 to 2015, COSMO-SkyMed sensor (**Fig. 5.13c**), confirm the temporal evolution and the acceleration in some periods, when the main reactivation occurred. The main problem of this technique for the CL-PO area is the low density of radar points due to the rare outcropping and/or urban facilities and high presence of vegetation.

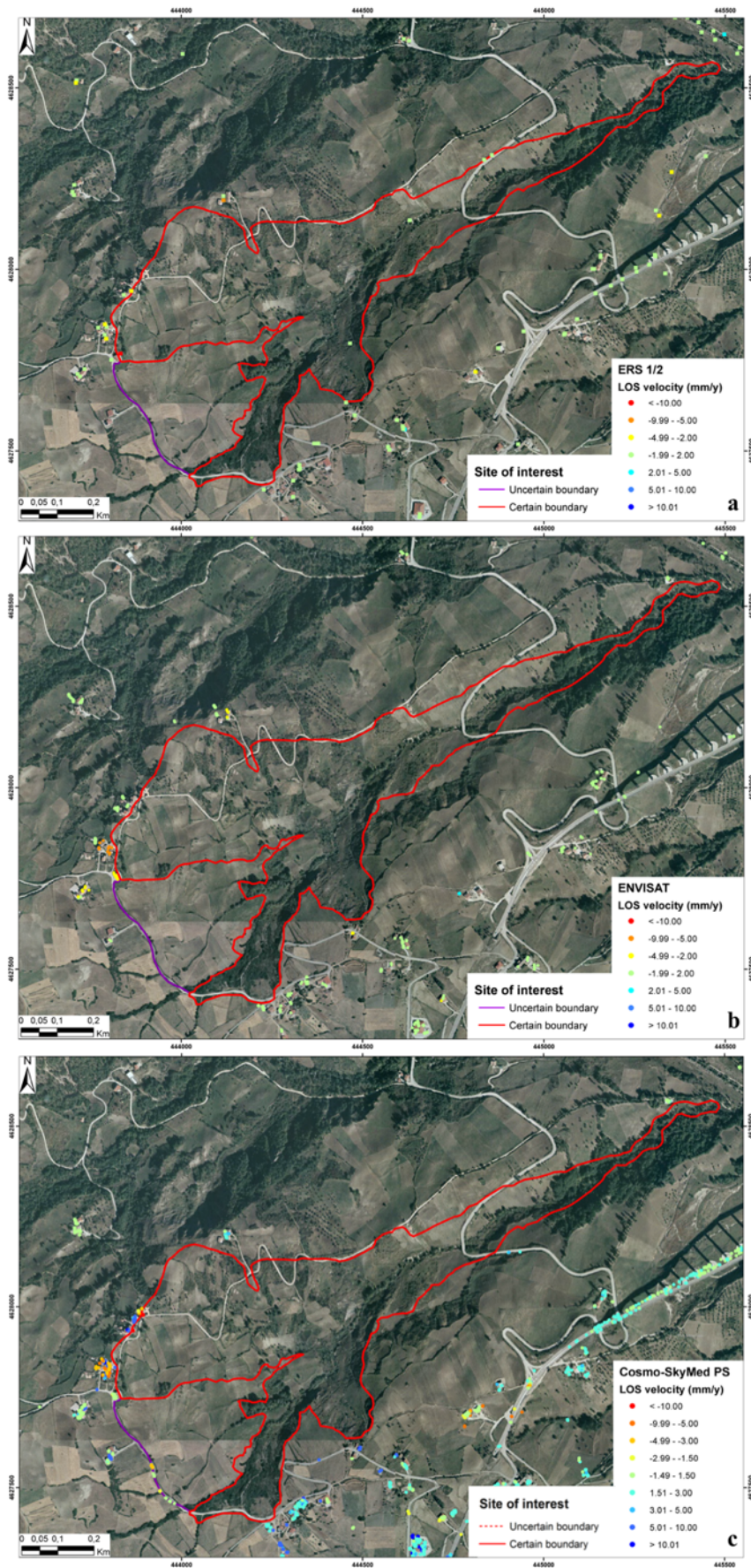


Fig. 5.13 - PS covers the CL-PO landslide acquired by ERS (a), ENVISAT (b) and COSMO-SkyMed (c) sensors.

An unusual sample time series (**Fig. 5.14**) extracted on a structure sited on the crown of the landslide, representing a graph displacement-time including all data from ERS, ENVISAT and COSMO-SkyMed sensors, shows the important movement affecting the investigated region and the periods of main activity of the landslide. The main period of movement affecting the crown area is well visible and confined from 2003, when the first main reactivation occurred, to 2010. Using a small scale, the different reactivations are not easy to recognize. It is worthwhile noticing that the velocities of shown displacement were measured along the LOS in ascending orbits. Furthermore, the plotted data are a sample of the backscattered PS on a building located on the actual crown, that in 2003 were far from the landslide. The territory in front of this building was influenced by important geomorphological modifications that smoothed the landscape.

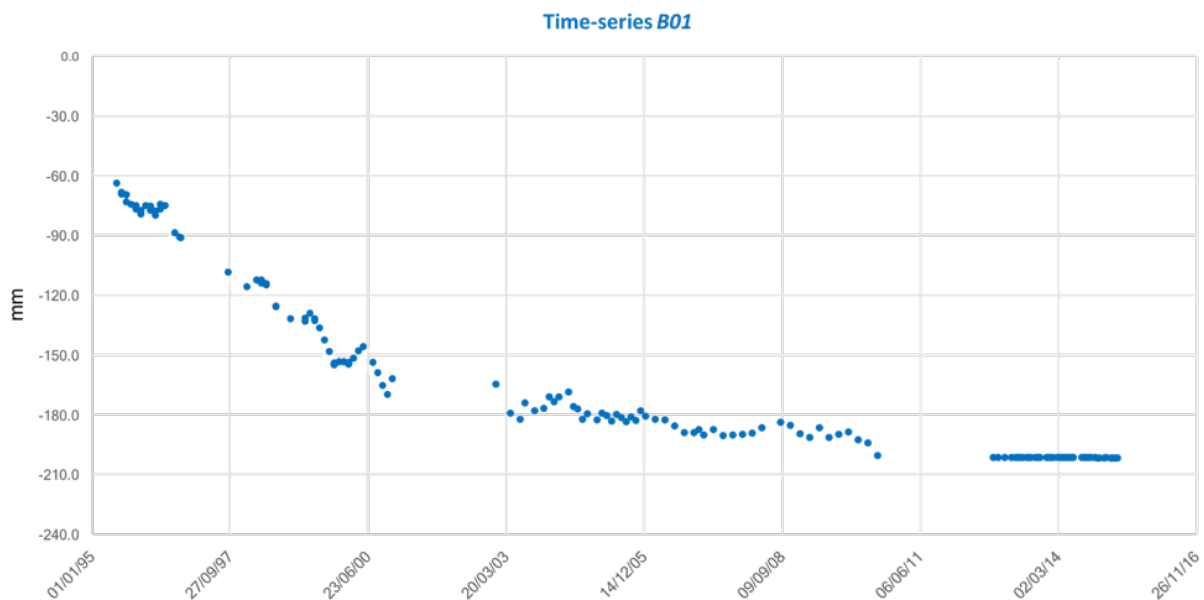


Fig. 5.14 - Complete time-series merging the data of all sensors showing and confirming the most important period of movement due to the main reactivations that occurred between 2003 to 2007. Data are taken on the Build_01 located close to the landslide crown.

The Persistent Scatterers Interferometry (PSI) time series of each sensor for both acquisition geometries into and close to the landslide were analysed and classified by the Notti et al. (2015) approach and classified by means of the automated method of Berti et al. (2013), respectively. In this way, the time series were corrected removing the regional trend, in order to better visualize and analyse the trend. Furthermore, they were categorized in six target trends: *uncorrelated*, *linear*, *quadratic*, *bilinear*, *discontinuous with constant velocity* and *discontinuous with variable velocity*. To help the localization and description of the PS time series analysed, four areas were identified (**Fig. 5.15**): structures on the crown of the landslide (*Area 1*), three neighbour buildings above the crown (*Area 2*), a built up area close to the crown of the mass-movement (*Area 3*) and two constructions on the left flank of the landslide (*Area 4*).

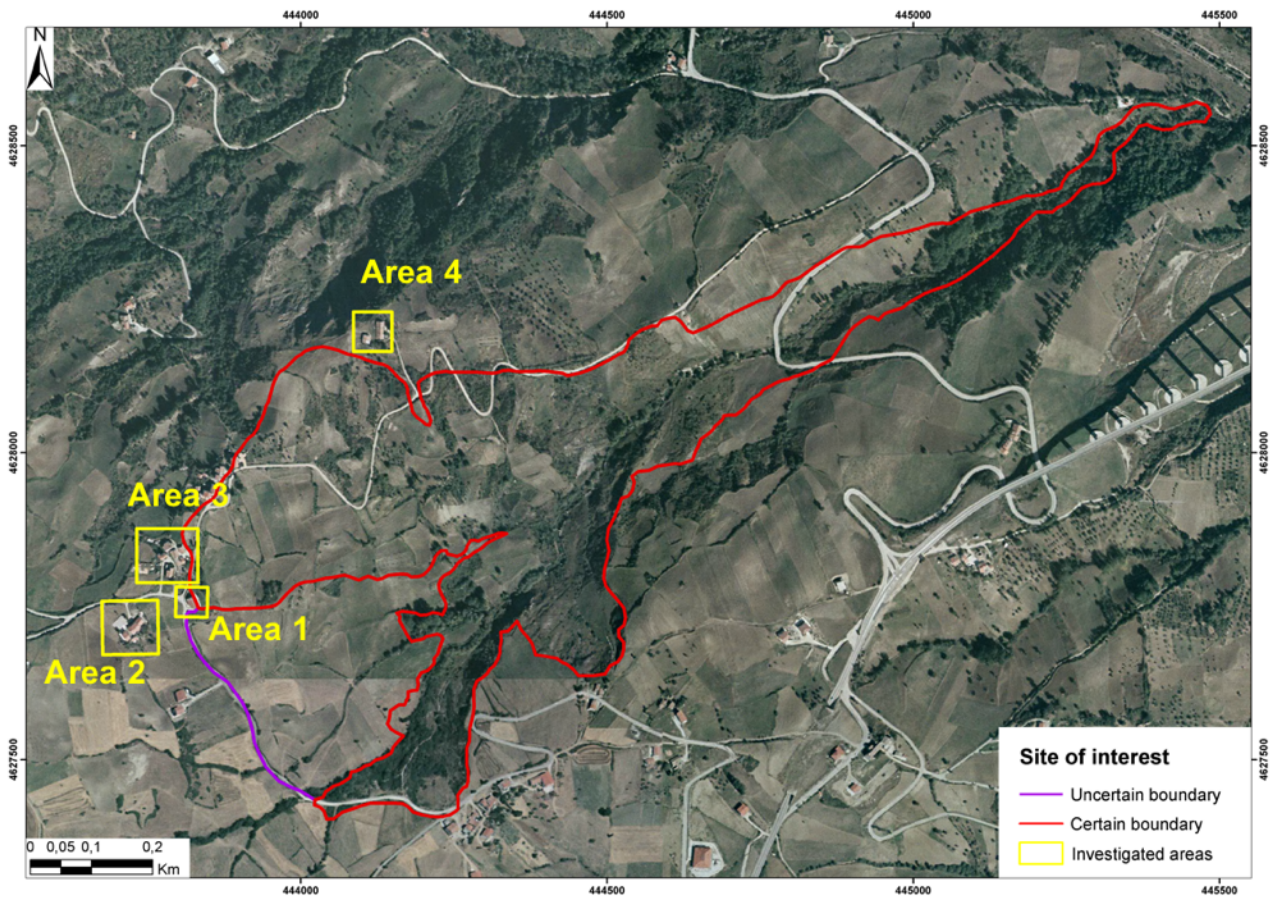


Fig. 5.15 - Areas where the time series were separately examined.

The ERS data, even if few, in ascending orbit show time series with breakpoint in autumn 1995 for PS in *Area 1*, *Area 2* and *Area 3*. This information indicates that already in 1995 the left lobe of the landslide, where actually the crown of the mass-movement is sited, was affected by displacements. Furthermore, analysing the ascending PS data into the investigated area, the time series were classified (Berti et al., 2013) in four types (Fig. 5.16): *uncorrelated* (65%), time series of PS external from the landslide; *linear* (17%), time series of few points backscattered by buildings in *Area 3*; *quadratic* (11%), time series scattered external to the mass-movement; *bilinear* (6%), time series with breakpoints in *Area 1* and some constructions in *Area 3*.

The ERS descending data give back very few information and the classification of Berti et al. (2013) categorizes quite all the PS of the area as *linear* (70%), but no more points are present close to the landslide. (Fig. 5.16).

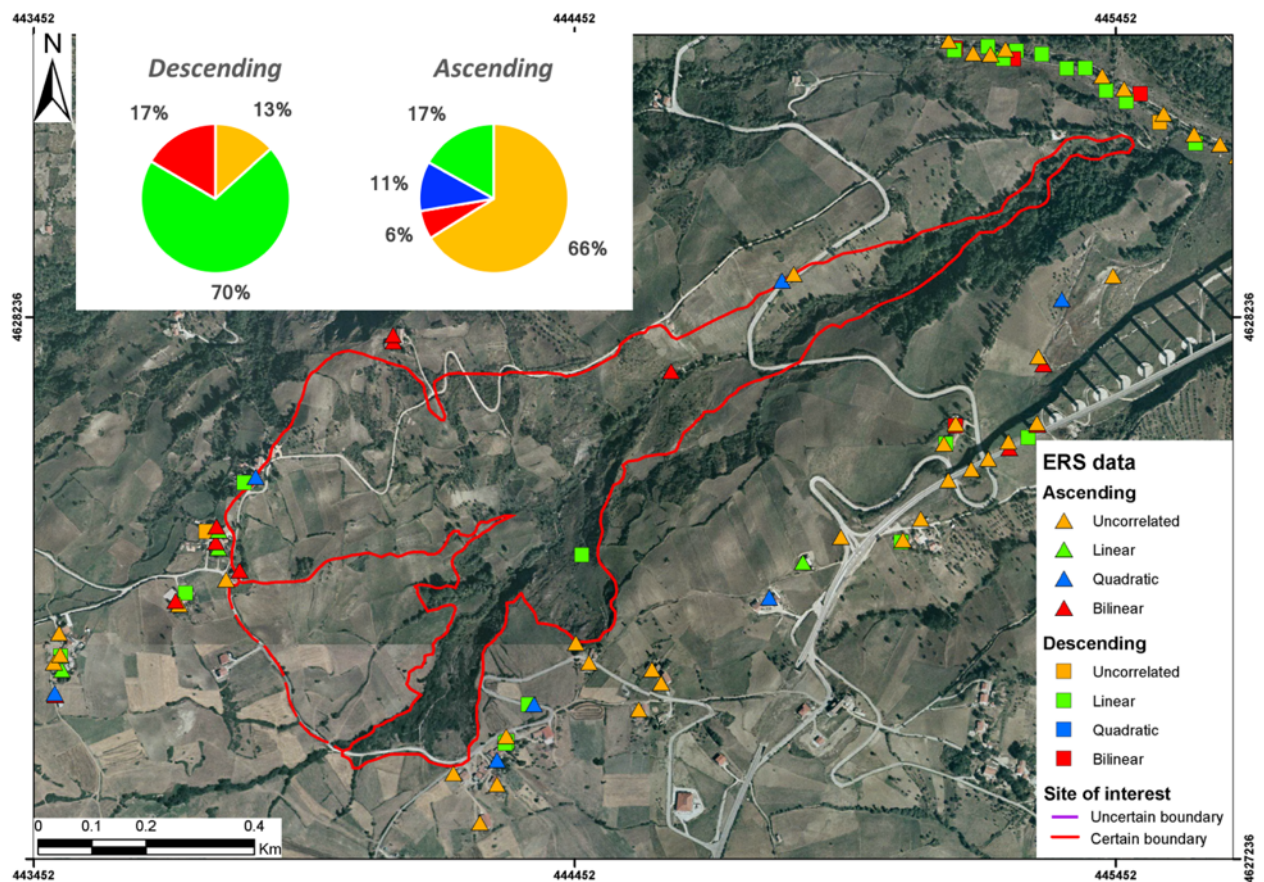


Fig. 5.16 - Categorization of the ERS ascending and descending PS time series of the surrounding of the CL-PO landslide.

For the subsequent period, the ENVISAT data were investigated with the same method (Fig. 5.17). The PS time series acquired in ascending orbit were analysed individuating three breakpoints in three different years: in spring and autumn 2005 on buildings located in the built up region of *Area 3* and uphill with respect to the crown; in 2006 PS backscattered by the structure in *Area 1*; in 2007, a little number of PS with breakpoint were individuated on different areas confirming the continue slow displacement affecting the landslide-prone area. The categorization of Berti et al (2013) of the ENVISAT PS time series show four classes: *uncorrelated* (55%), *linear* (18%), *quadratic* (17%) and *bilinear* (10%). Also the ENVISAT descending data were categorized with the same approach, but no significant information were carried out because the major number of PS time series result classified as *uncorrelated* (94%).

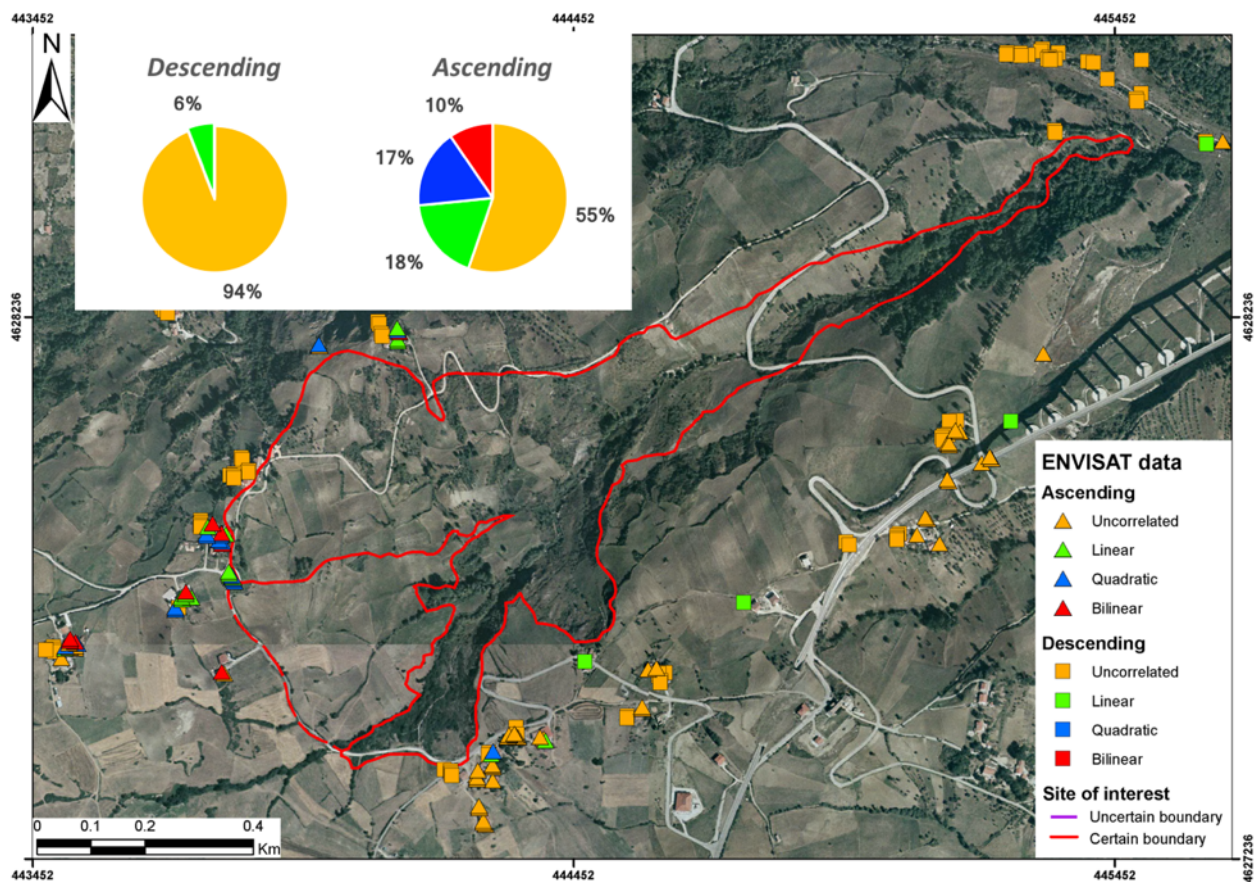


Fig. 5.17 - Classification of ENVISAT ascending and descending PS time series of the surrounding of the CL-PO landslide.

The same method was applied for the data acquired by COSMO-SkyMed (Fig. 5.18). Analysing the time series two set of breakpoints were individuated: few points located in Area 3 shows the breakpoint in spring 2013; in autumn 2014 PS time series with breakpoints were localized along and uphill with respect to the actually crown. In both ascending and descending orbits the classification of Berti et al. (2013) on this dataset gave back a categorisation spreads on six classes, two more with respect to what happened for the C-band data. The descending data are quite noisy, for this reason the main part of the PS time series was ranked as *discontinuous with constant velocity* (70%), the 21% in the *quadratic* class and the remaining percentage is divided in the other categories.

The ascending PS show time series in all possible classes: *uncorrelated* (12%) uphill with respect to the crown; *linear* (18%) in the crown or close to the boundary; few *quadratic* (4%) for some buildings in Area 2 and for the construction in Area 3 built in the crown; *bilinear* (62%) for quite all points backscattered by structures sited in the crown and in Area 2 and 3; *discontinuous with constant velocity* (only 1%) for few points in Area 3; *discontinuous with variable velocity* (3%) for some sparse points in the surrounding of the landslide.

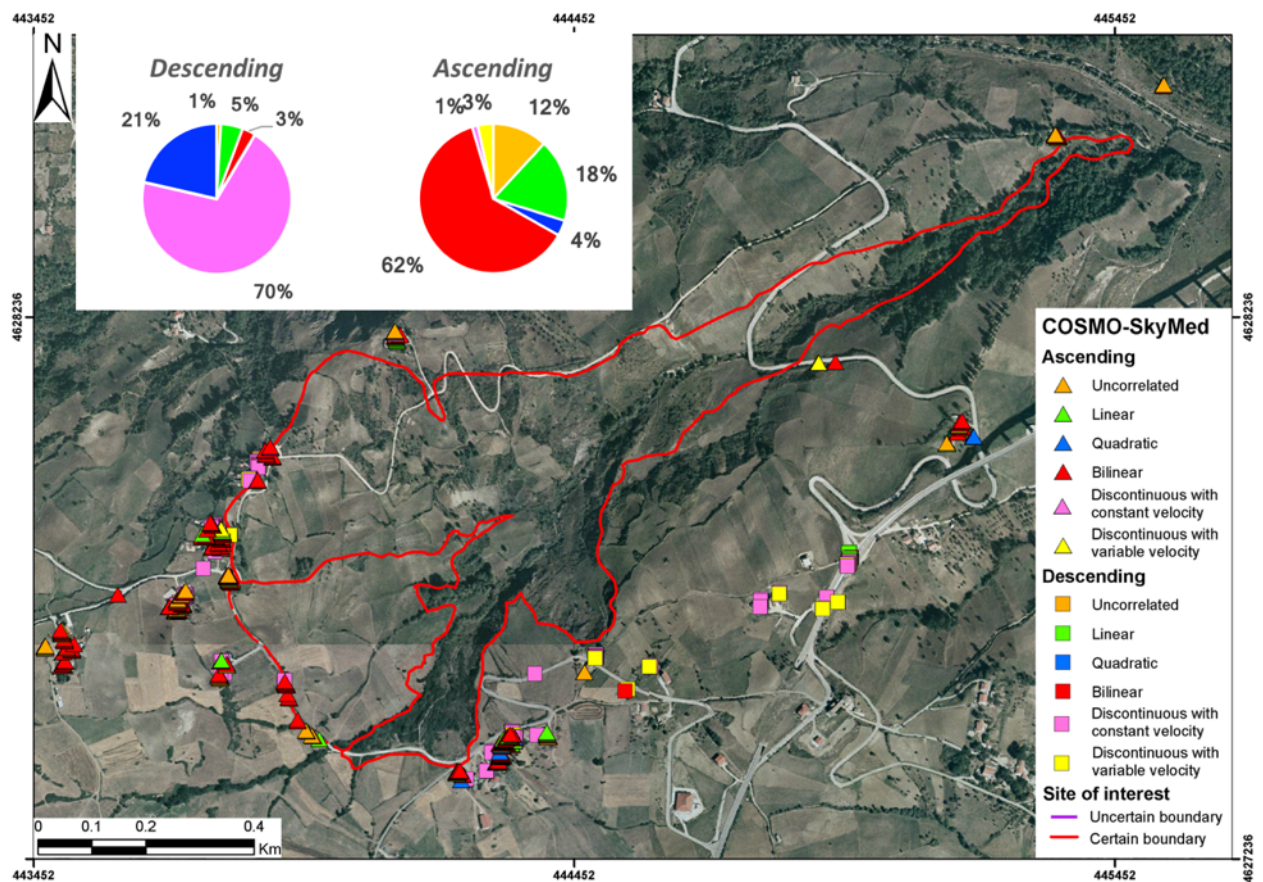


Fig. 5.18 - Categorization of the COSMO-SkyMed ascending and descending PS time series of the surrounding of the CL-PO landslide.

Furthermore, to better understand the development of this landslide, some time series were extracted and individually analysed for each satellite sensor in order to separately examined the displacement affecting the structures. All Time Series were investigated by means of the User-Oriented Methodology for DInSAR Time Series Analysis and Interpretation of Notti et al. (2015). In this way, the analysis conducted on the Time Series made cleaning them by the regional trend in order to eliminate possible noise and to focus the attention on the real displacement. The ERS1/2 data are very sparse, noisy and they do not cover all constructions, in fact for only one of the chosen areas the PS resulted reliable. Constructions sited on the right side of the landslide were not taken into consideration in this analysis because recent movements caused by sliding involved only the left lobe. All time series were recorded along the Line Of Sight in ascending geometries.

For *Area 1*, the displacement affecting a building with a concrete sidewalk around it is analysed by means of PS of all satellite sensors. The period 1993-2000 was investigated by the data acquired by ERS1/2, but it is worthy noticing that the gap between the first two acquisition is about 2 years and this is visible in the time series as a linear displacement (black circle in Fig. 5.19a) instead is only a lacking of information. For this

period, only few points sited close to the actual crown of the landslide were recognized but, already at that time, showing a high displacement along the Line Of Sight of the satellite. The depured time series with respect to the regional trend (Notti et al., 2015) **Fig. 5.19a** shows important movements (about 120 mm were registered) with cyclically repeats, even if no important reactivations and damage was advised before the main event of January 2003. This area was affected by important displacement during and post the main event occurred in January 2003, after that several interventions to drainage were made. The time-series of the following period, acquired by ENVISAT satellite, are too noisy. Subsequently, also in the period 2010-2015, the COSMO-SkyMed PS recorded on this construction showing cyclical little movements. During the winter period, between November and February, little displacements were registered, probably related to rainy and snowy precipitations (**Fig. 5.19b**).

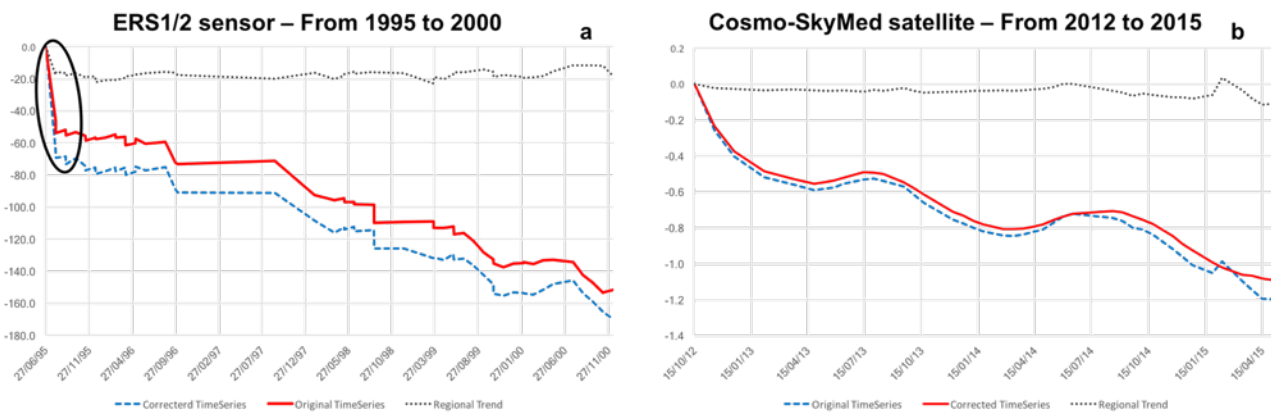


Fig. 5.19 - Sample time series registered by the ERS1/2 (a) and COSMO-SkyMed (b) satellites on Area 1.

Area 2, sited behind Area 1, based on the damage surveys and on several campaigns, it seems stable. The PSs of all sensors, ERS1/2, ENVISAT and COSMO-SkyMed, confirm this idea of stability, even if the analysed time-series are very noisy. They do not show important displacement, but only some fluctuations contained in the stability range, even if with trend, due to the snowy periods that create some problems of reflection of the radar signal (**Fig. 5.20**) not removable correcting the time series to the regional trend (notti et al., 2015).

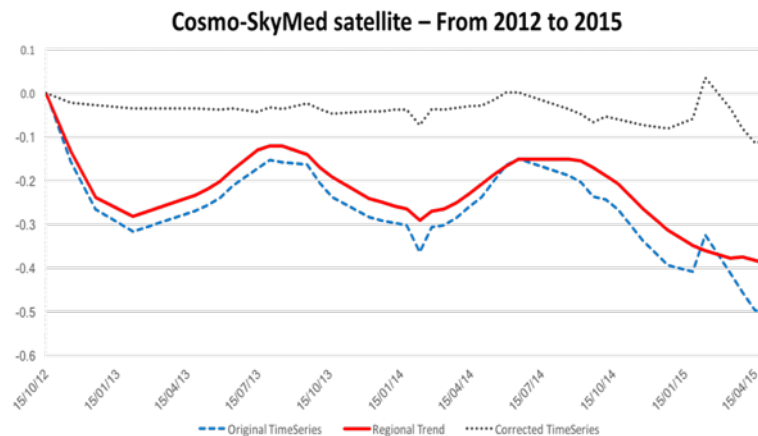


Fig. 5.20 - Sample time series registered by the COSMO-SkyMed satellites on Area 2.

Area 3 is one of the most populated, in which almost all buildings were evacuated after the main event. Even if not all structures are severely damaged, the PS guarantee that important movement affected those structures. The ERS data are too few and noisy to be reliable to investigate displacements, while ENVISAT PS, even if also in this case result noisy also removing the regional trend to the original time series (Notti et al., 2015), by means of a sample time-series (Fig. 5.21) registered on the built up Area3 is cyclical and influenced displacement in the winter period by the covering snow interfering with the radar measurements. The main reactivation of the CL-PO mass-movement occurred in January 2003 is not well recognizable by the time-series. This is probably due to the occurred displacement bigger than the possible recognizable or because the satellite did not gather good images in that precise period, in fact as visible in the first black circle in Fig. 5.21, only points indicating an important displacement are visible. The same problem affects the reactivation that occurred between December 2004 and January 2005, while the displacements of June and July 2006 (the second black circles in Fig. 5.21), as well testified by the inclinometers data, are recognizable. Furthermore, an important increase of displacement is detectable from November 2009.

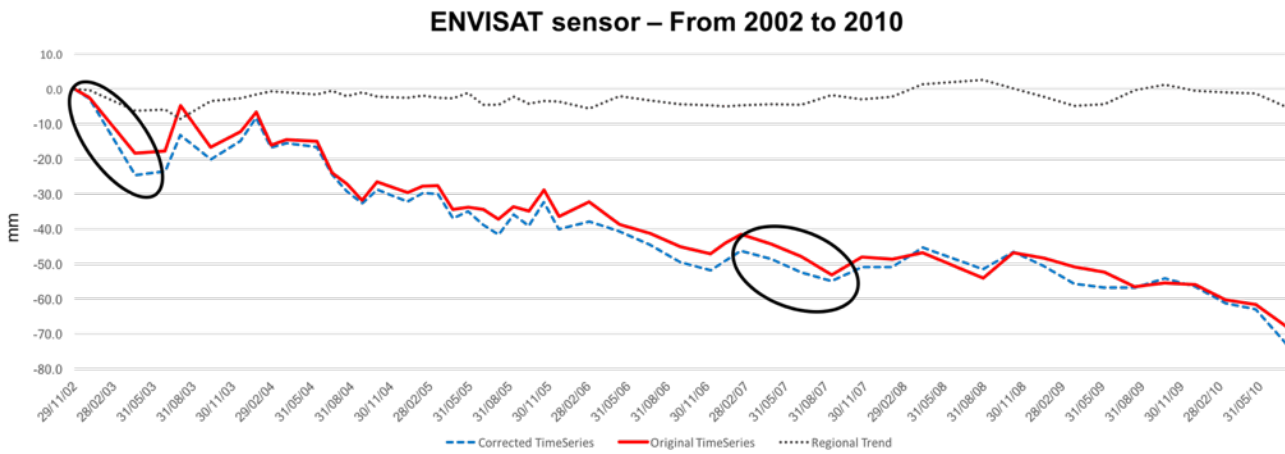


Fig. 5.21 - Sample of a time series of the Area3 recorded by the ENVISAT sensors from 2002 to 2012.

After 2 years’ gap of PS information, COSMO-SkyMed data (Fig. 5.22) indicated a continuous movement affecting this area. It is worthy noticing that the referring scale is much different, but the cyclical displacement is also visible also deparating the time series by the little trend affecting the entire framework.

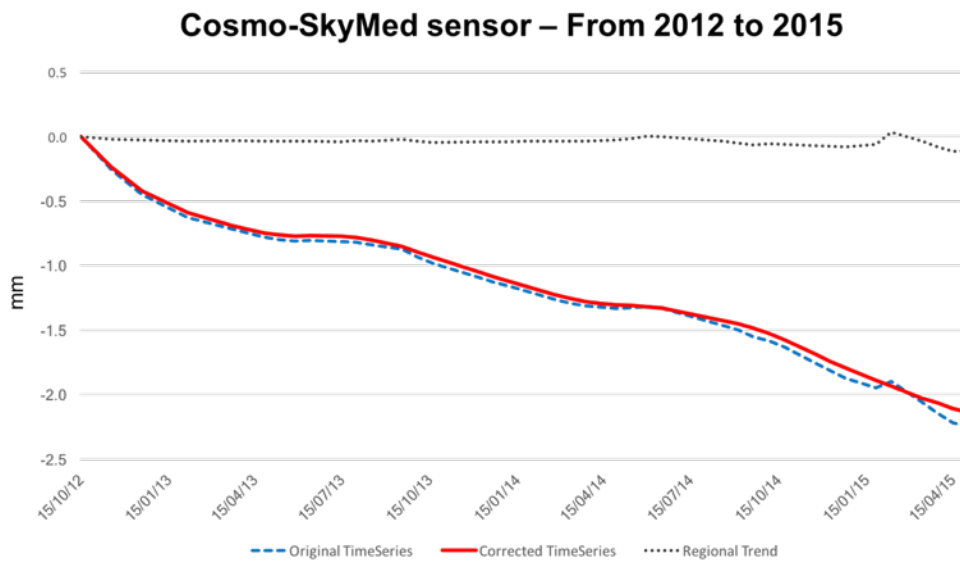


Fig. 5.22 - Sample of the time-series recorded for the Area 3 by the COSMO-SkyMed sensors for the period 2012-2015.

Displacements detected for Area 4 allowed investigating deformations affecting two constructions each one composed by two connected structures. The ERS data are not backscattered and the ENVISAT PS resulted very noisy also applying the Notti et al. (2015) method to remove the regional trend affecting the time series, but they show a trend of important movements (green traced line in Fig. 5.23). In this graph, displacements caused by several reactivations occurred in the analysed period are difficult to isolate due to the noise caused by atmospheric and snow interferences.

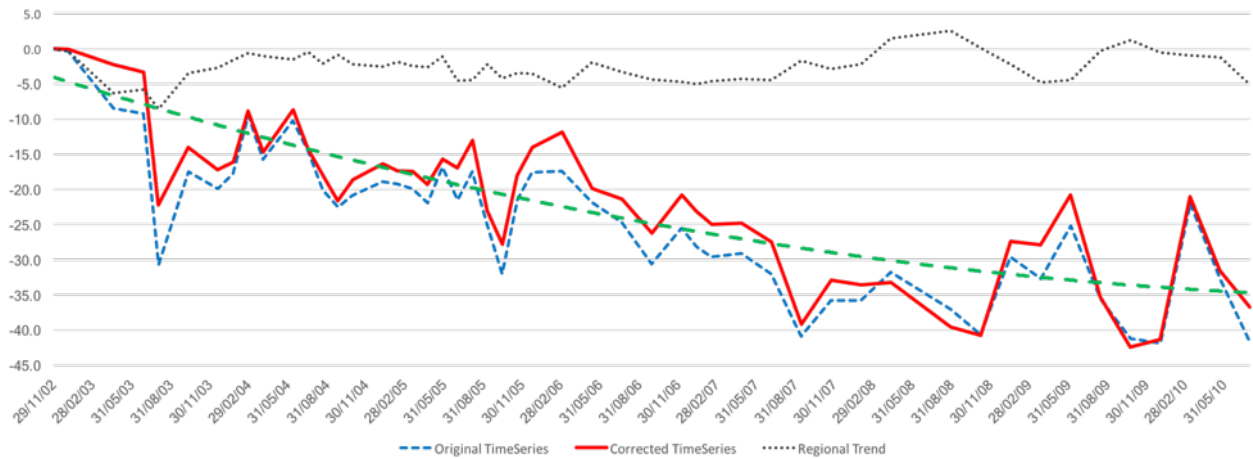


Fig. 5.23 - Sample of a time series of the Area 4 recorded by the ENVISAT sensors from 2002 to 2012.

COSMO-SkyMed PS data elaborated and corrected by the regional trend for this area showed a different tendency of movement. Until about the middle of 2012, data showed a movement away from the satellite, instead in the following the signal exhibits a continuous decreasing of the distance respect to the sensor (Fig. 5.24). By means of orthophotos and field surveys conducted in this region, another landslide close to the CL-PO, but having a different direction, i.e. NE, was recognized (Fig. 5.25a). The increasing of dimension of this mass-movement could have caused an inversion of the displacement measured on the investigated construction due to the involving by its retrograde effects. It is important noticing that the amount of these values is small, close to the instrumental error, but it is interesting to be mentioned.

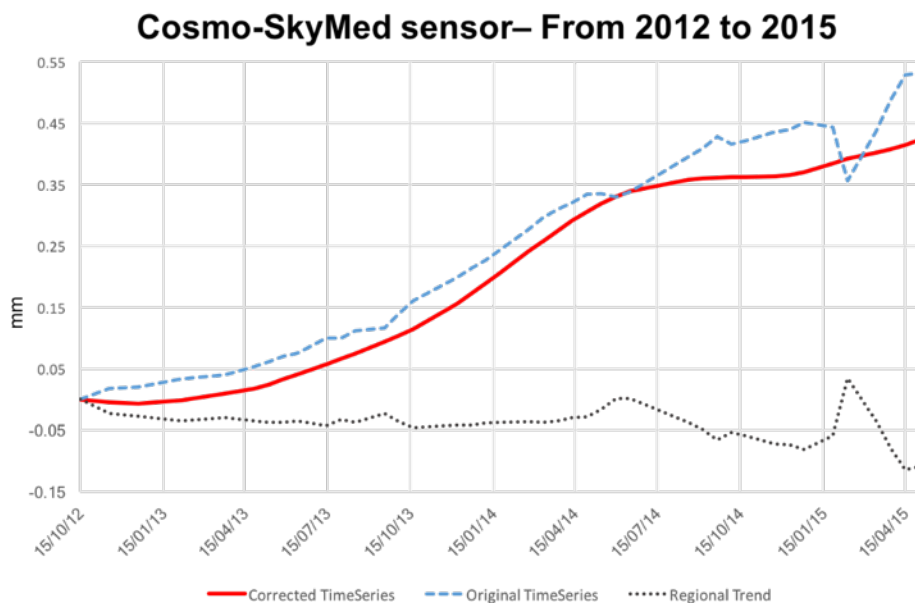


Fig. 5.24 - Sample of the time-series recorded for the Area 4 by the COSMO-SkyMed sensors for the period 2012-2015.

In the middle of the two adjacent buildings, constituting the monitored structures, a vertical open crack, characterized little aperture in the bottom and bigger in the upper part close to the roof (Fig. 5.25b) was recognized during the field campaign, probably caused by the different direction of movement which affected them. Furthermore, cyclical rates of movements were possible to recognize also in this graph supporting the hypothesis about the influence of the snow and the atmospheric conditions, or problems affecting acquisition or elaboration of the raw data.

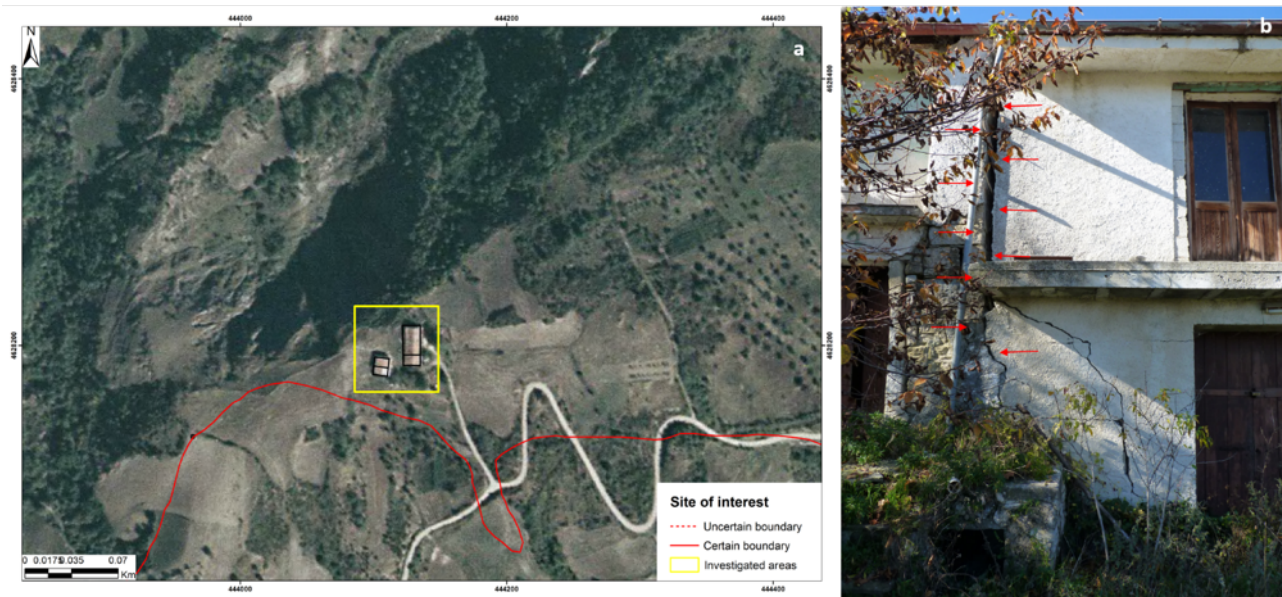


Fig. 5.25 - Localization of the structures of the Area 4 and their proximity to the closer landslide (a). Open cracks visible between two adjacent constructions (b).

In spite of the conducted works to stabilize the area and the knowledge on this landslide, it is impossible to say if the movement has been arrested. As explained by means of the PS data and confirmed by several surveys the landslide seems still now active with several consequent problems and damage regarding facilities as well as indirect economic losses due to the abandonment of the agricultural terrains.

5.2.2 Damage classification of facilities

The reactivation of the landslide occurred in January 2003 and its continuous evolution caused serious damage to facilities and buildings chiefly related to the loss of support to structures due to a downward and outward movement of the foundation zone (Hunt, 2005). The buildings sited close to the body and on the crown of the increasing mass-movement, were subjected to some restrictive measures by local municipal administrator, e.g. precautionary evacuation. In November 2015 and July 2016 34 buildings, 2 walls and 3 concrete nearby anthropogenic surfaces were surveyed and the individuated and characterized damage classified. Moreover, the same buildings, with others close to the mass movements, were investigated and

monitored using the remote sensing techniques by means of the Persistent Scatterers. During the field campaigns the external damage on the structures were surveyed adopting a developed regular scheme (Fig. 5.2). The phase of the identification of the damage requests attention because same openings, or similar cracks, could mean different answers of the structures depending on several factors e.g. different material construction.

Some examples of different typologies of damage affecting the facilities:

- hairline cracks (Fig. 5.26a);
- open ruptures on external walls (Fig. 5.26b and c);
- fractures and open cracks between walls and external sidewalk (Fig. 5.26d and e);
- rare, but possible collapse of roof (Fig. 5.26f).



Fig. 5.26 - Example of cracks and rupture identified on structures. a) hairline cracks on plaster of masonry wall; b) open crack on reinforced concrete walls; c) open crack of masonry building walls; d) open crack between wall and external sidewalk; e) open crack between external wall and ground surface; f) collapsed roof in a masonry building (Del Soldato et al., under review_a)

In concrete sidewalks and walls, the following elements were investigated:

- hairline cracks (Fig. 5.27a and the red arrow in Fig. 5.27c);
- open cracks (Fig. 5.27b, c and d).



Fig. 5.27 - Fine (a) and open (b) cracks recognizable on pavement of sidewalks slab; hairline (highlighted by means of red arrows) and open fractures on concrete (c) and masonry walls (d).

The performed in situ investigation allowed to collect qualitative and quantitative information on the damage to provide an assessment of the studied elements, according to literature classifications (Burland, 1977; Alexander, 1986; Chiochio et al., 1997; Cooper, 2008; Baggio et al., 2009) described in the paragraph 4.2.1.1 and by means of the newly developed approach (paragraph 5.1) (Del Soldato et al., under review_b). Although landslide damage classifications known in literature were devised for categorizing only buildings, they were applied to rank also different man-made elements (i.e. an electricity pole, two walls and three concrete areas) strongly affected by damage. The application of these different approaches gave back five categorizations of the building base on the affecting damage.

Chronologically, the first classification adopted for the structures was that of Burland (1977) which investigates only damage of external façades, although important displacement could affect the foundation system. Considering this ranking about a half of the buildings, were classified from *Slight* to *Very severely* levels of damage (Fig. 5.28). Furthermore, several rural constructions resulted abandoned and strongly affected by damage or partially collapsed. Few buildings show low levels of damage. In fact, according to this approach only two structures resulted in the *Negligible* class and four in *Very slight* class, mainly observed in recent-built structures and in small constructions probably slightly recently renovated.

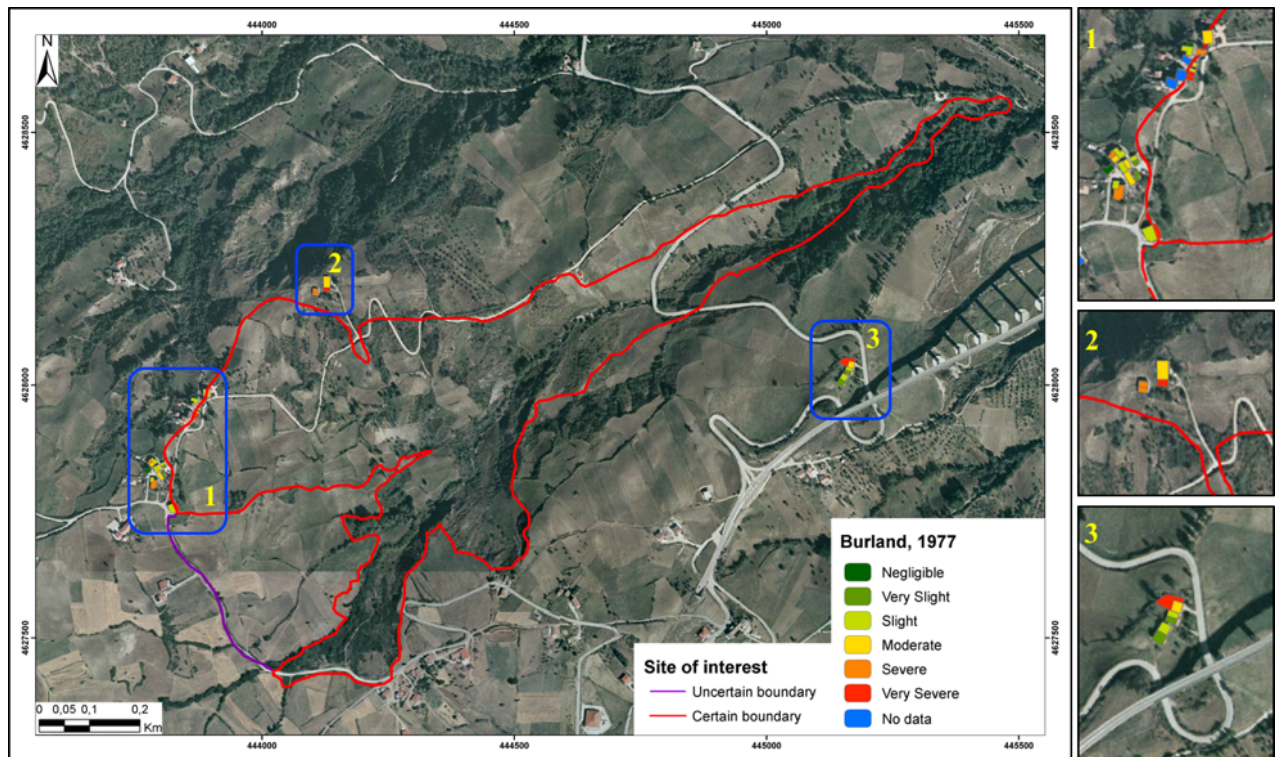


Fig. 5.28 - Classification of the facilities close to the CL-PO landslide according to Burland, 1977.

The methodology of Alexander (1986), estimating the crack aperture in centimetres, instead of millimetres, as the previous one, implies less sensitivity for construction affected by low levels of damage. This difference provoked the classification of many structures in *Light* and *Moderate* classes (Fig. 5.29). It is worthy noticing that, to support these differences, already in *Moderate* class of damage the “evacuation and rapid attention to ensure” is suggested. Another noteworthy thing is due to the improvement respect to the previous approach by adding *Partial collapse* and *Total collapse* categories for buildings strongly affected by damage. Nine buildings classified in the maximum grade of damage according to Burland (1977) classification, in Alexander’s (1986) ranking are categorized in three different high level classes of damage: three in *Very Serious*, five in *Partial collapse* and one in *Total collapse*.

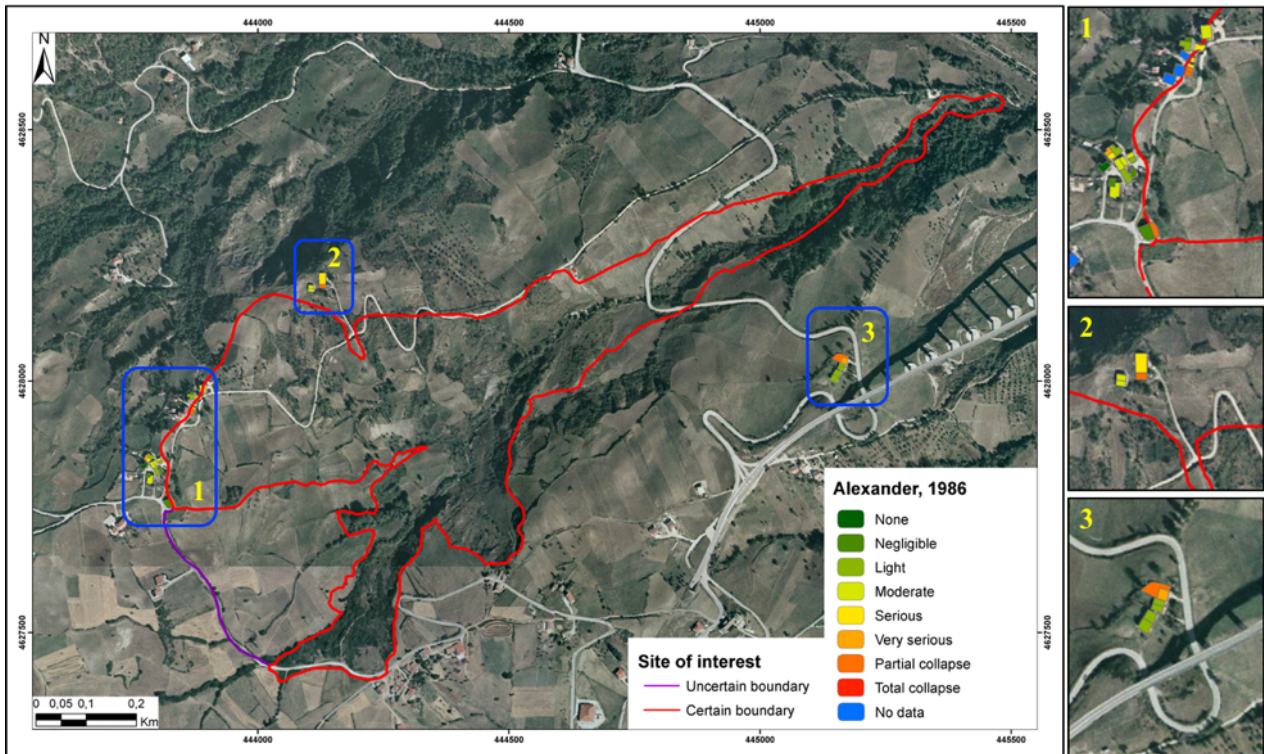


Fig. 5.29 - Classification of the facilities close to the CL-PO landslide according to Alexander, 1986.

The categorization made by Chiocchio et al. (1997), with respect to the previous older classifications, adds the distinction between masonry and reinforced concrete into the level of gravity of damage. By means of this improvement, structures affected by important rigid settlements, previously classified as low levels of damage, resulted grouped in more severe classes (Fig. 5.30). Then main part of the structures shows *Light* and *Moderate* levels of damage and already for *Moderate* category the evacuation is suggested by the Authors. The high ranks, i.e. *Partial collapse* and *Total collapse*, include six buildings probably abandoned several years ago before the main event, as happened for the categorization made by Alexander (1986) approach.

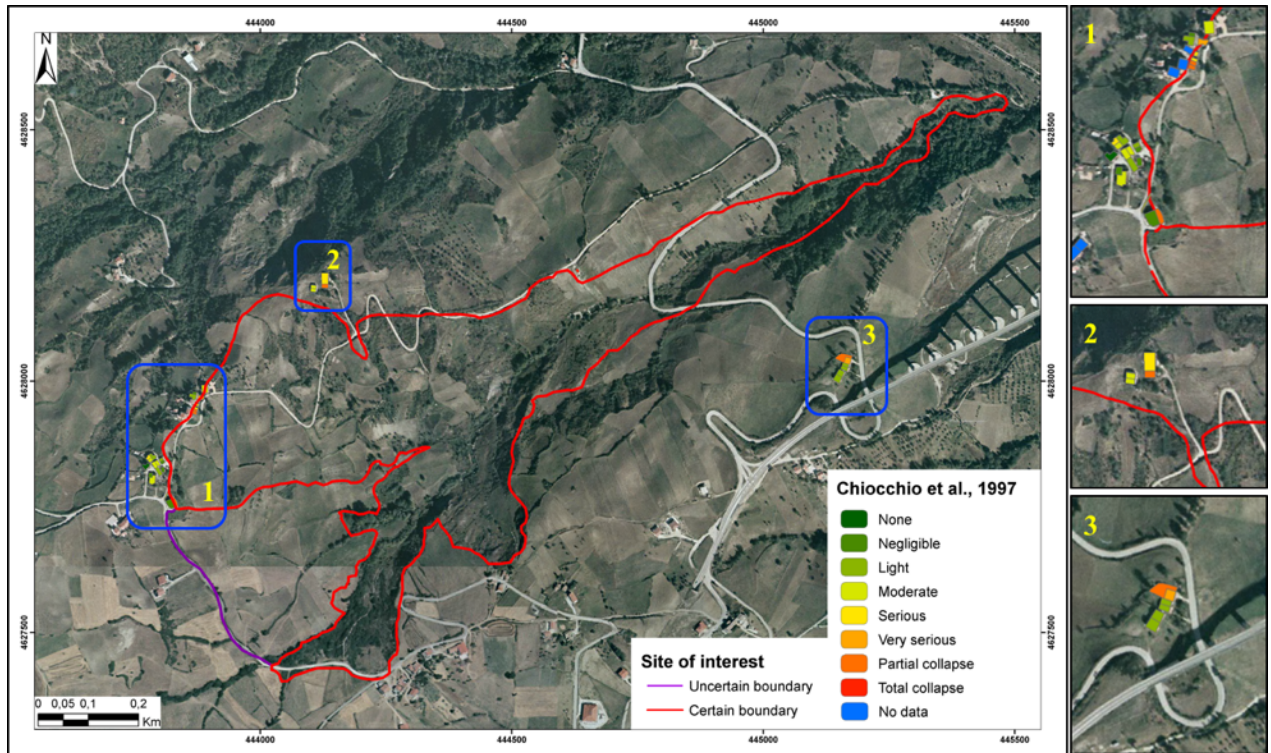


Fig. 5.30 - Classification of the facilities close to the CL-PO landslide according to Chiocchio et al. (1997).

For the first time, the description and categorization of the landslide ground damage was added to the facilities and buildings damage classification by Cooper (2008). The values used to characterize the recognizable opening of cracks on the investigated elements are evaluated in millimetres as for Burland (1977). This could be a reason whereby a greater number of facilities are ranked into highest levels of damage if comparing result with those previously shown. This methodology, and the scale to recognize damage, result to be more appropriate in classifying ruptures affecting different facilities, not only buildings, as pillars, walls and concrete sidewalks. Several buildings are classified into *Class 2* and *Class 3*, compatible respectively with the *Slight* and *Moderate* categories, to confirm the good applicability of this approach (Fig. 5.31).

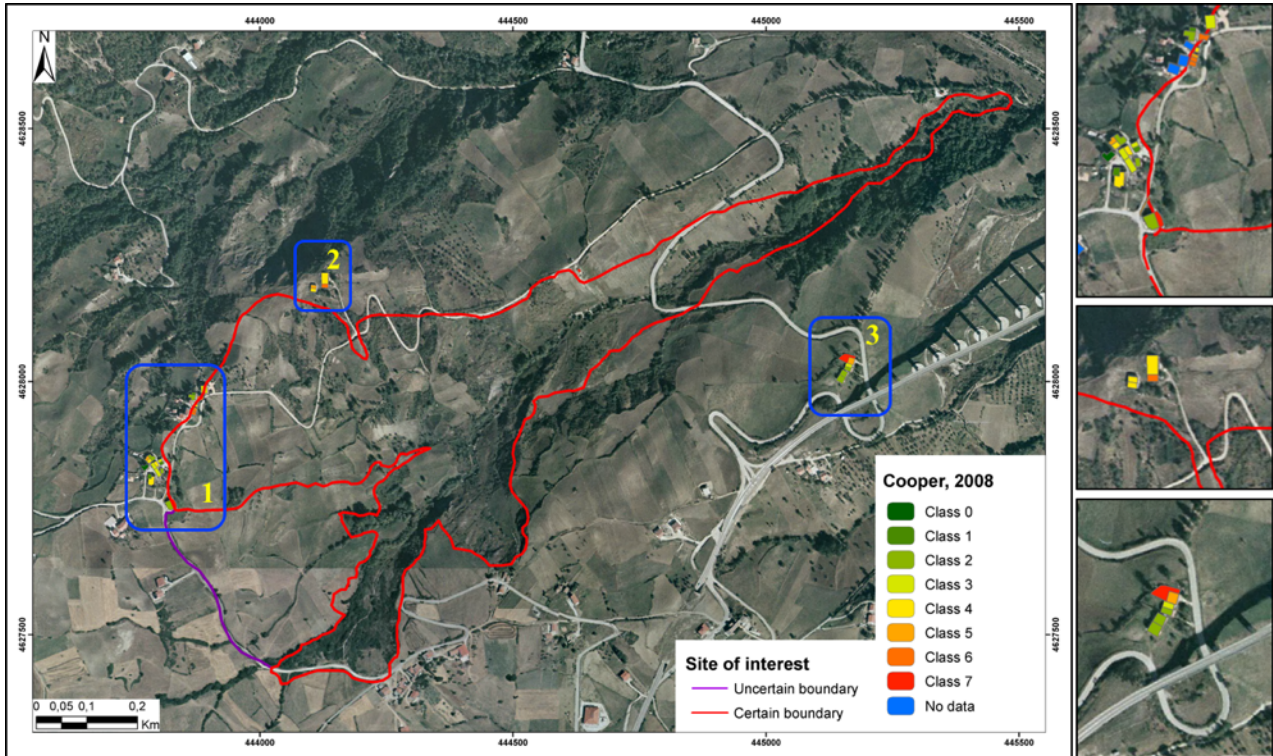


Fig. 5.31 - Classification of the facilities close to the CL-PO landslide according to Cooper (2008).

At the end, in spite of the DPC approach (Baggio et al., 2009), which shows only four ranks to categorize the level of damage, they were subdivided in eight classes to allow a comparison with the others: two low levels (*None* and *Negligible*), four categories of important damage (*Severe*, *Very severe*, *Partial* and *Total collapse*) and two intermediate grades (*Slight* and *Moderate*). Result of the classification (Fig. 5.32) is a more homogeneous ranking of the buildings damage, than the previous described and applied approaches, involving all classes. Besides the little number of facilities located in the study area, it is possible to identify a concentration of the number of structures in *Severe* and *Very severe* classes of damage. The DPC methodology is though for paying more attention to buildings with visible damage because its original aim is to evaluate the suitability for human habitation of the construction after the occurrence of a seismic event.

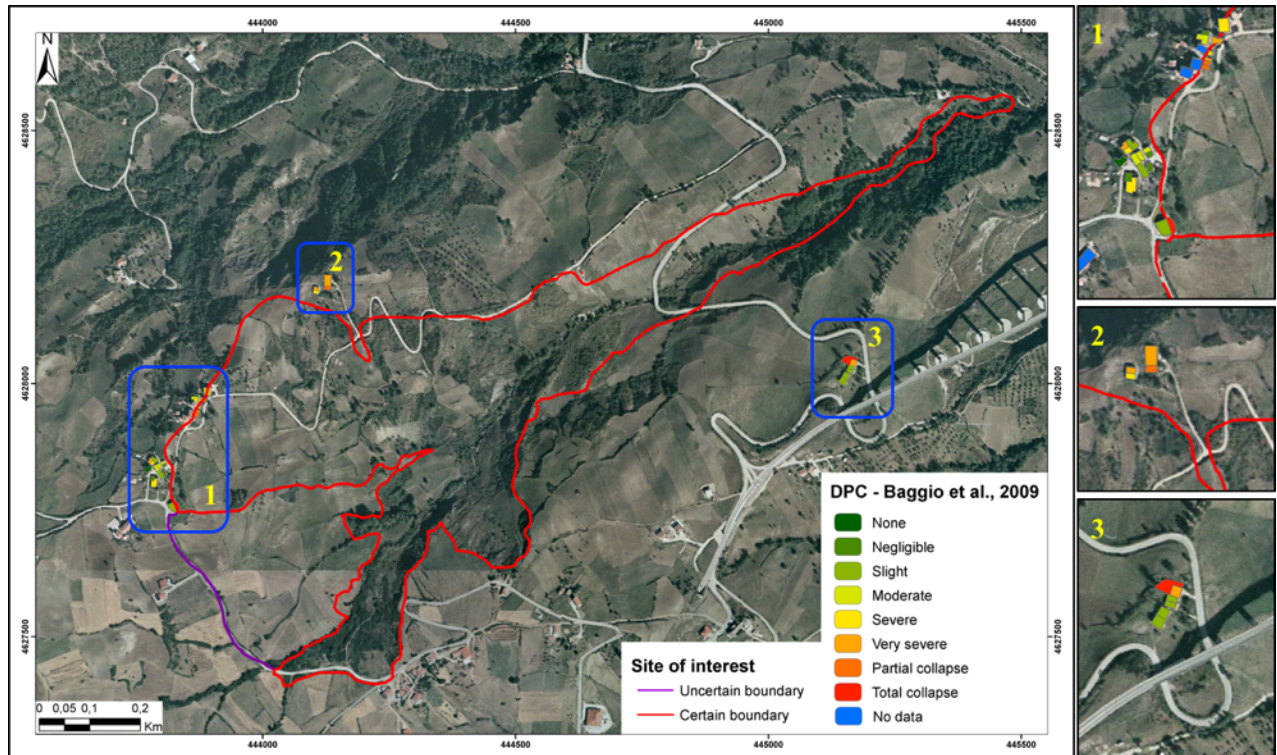


Fig. 5.32 - Classification of the facilities close to the CL-PO landslide according to the DPC approach (Baggio et al., 2009).

To follow the application of the literature ranking, a new methodology was developed and applied to the same site. Del Soldato et al. (under review_b) approach results to be a complete method to investigate the cracks affecting the ground surfaces, as in Cooper (2008), the structures and, *a posteriori*, the facilities in *sensu stricto* allowing a more precise categorization (Fig. 5.33). The classification of the buildings in the surrounding of the CL-PO is well distributed and represents all categories. An important number of them are classified in *Negligible* and *Weak* ranks, as seen for the others approach. Furthermore, an important number of structures, probably mainly represented by rural and abandoned constructions, fall into the *Potential Collapse*. This approach results to be applicable for buildings as well as for other facilities, in fact the damage situation for some walls and concrete sidewalks investigated and ranked was also represented with good precision.

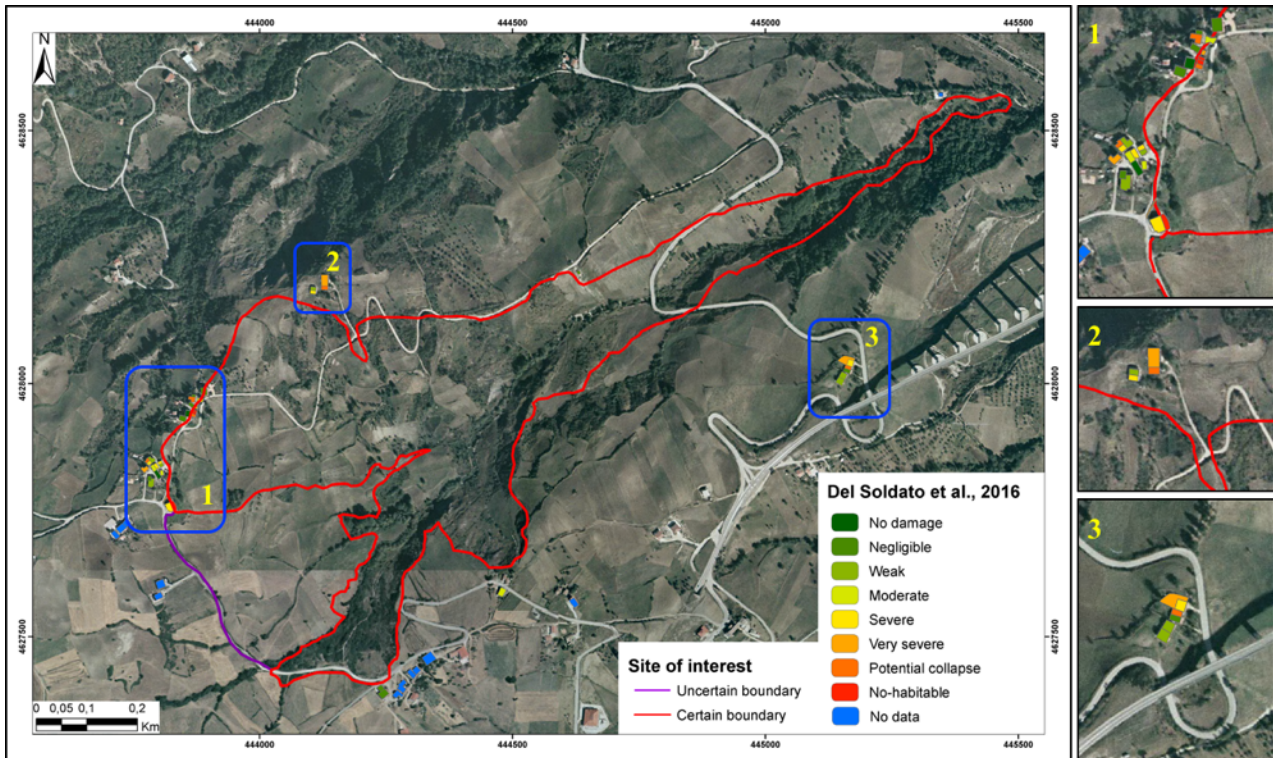


Fig. 5.33 - Classification of the facilities close to the CL-PO landslide according to the Del Soldato et al. (NewApproach_under review) approach.

It is curious and interesting noticing as, for all the applied and shown categorizations, the buildings located on the probable current crown of the landslide (B01 in Fig. 5.34c) is classified in low or very low level of damage. This reflects the real situation of the damage visible on the external façades of the construction, affected by very few and tight visible cracks (Fig. 5.34a), despite a possible very important rupture involving its foundations. This hypothesis is justified and supported by important visible ruptures affecting the front concrete sidewalk (S01 in Fig. 5.34c), partially collapsed into the landslide (Fig. 5.34b).

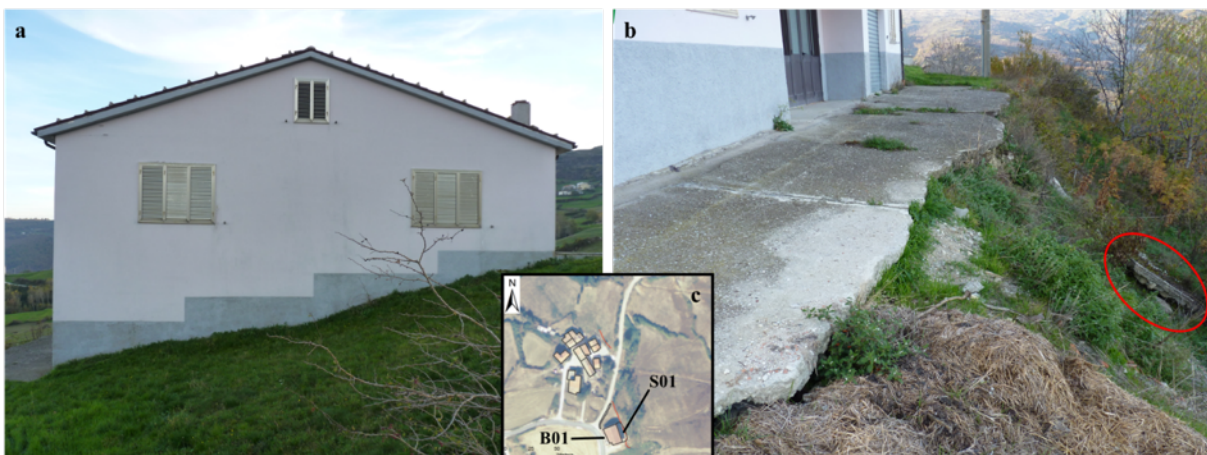


Fig. 5.34 -North façade (a) of the building (B01) located on the crown of the landslide with in front a several damage concrete sidewalk (b) partially collapsed (red circle).

Furthermore, two concrete walls and other two sidewalks were investigated and classified because affected by several open cracks or showing distortion. Also in this case, the applied categorization reflected the situation of the structures. The application of the rankings developed by Cooper (2008) and Del Soldato et al. (under review_b) demonstrated to be the more suitable methods adaptable also for different facilities, besides of buildings. The same ranking approach was applied to classify the ruptures on anthropic surfaces and on the ground (Fig. 5.35). The possibility to add this information on a map, to investigate and to classify the grade of damage visible on the ground surfaces could be interesting due to their probably relation with the propagation of the movement and the increasing of the dimension of the mass movement. On the crown area of landslide some fractures, that indicate the possible retrogression of the boundary of the landsliding zone, are visible. Laterally of the body of the mass-movement some cracks are recognizable in the soils inducing to the possible continuous movement of the landslide. During several field campaigns, it was possible identifying the continuous retrogression of the landslide crown, enlarging its boundaries and dimensions. Some cracks were simple to recognize by means of manifestations of new opening tension cracks or the partial collapses of border sidewalks, made of reinforced concrete. Their severity was classified by analysing their linear extension, their displacement and their location (i.e. in soils or on rigid material).

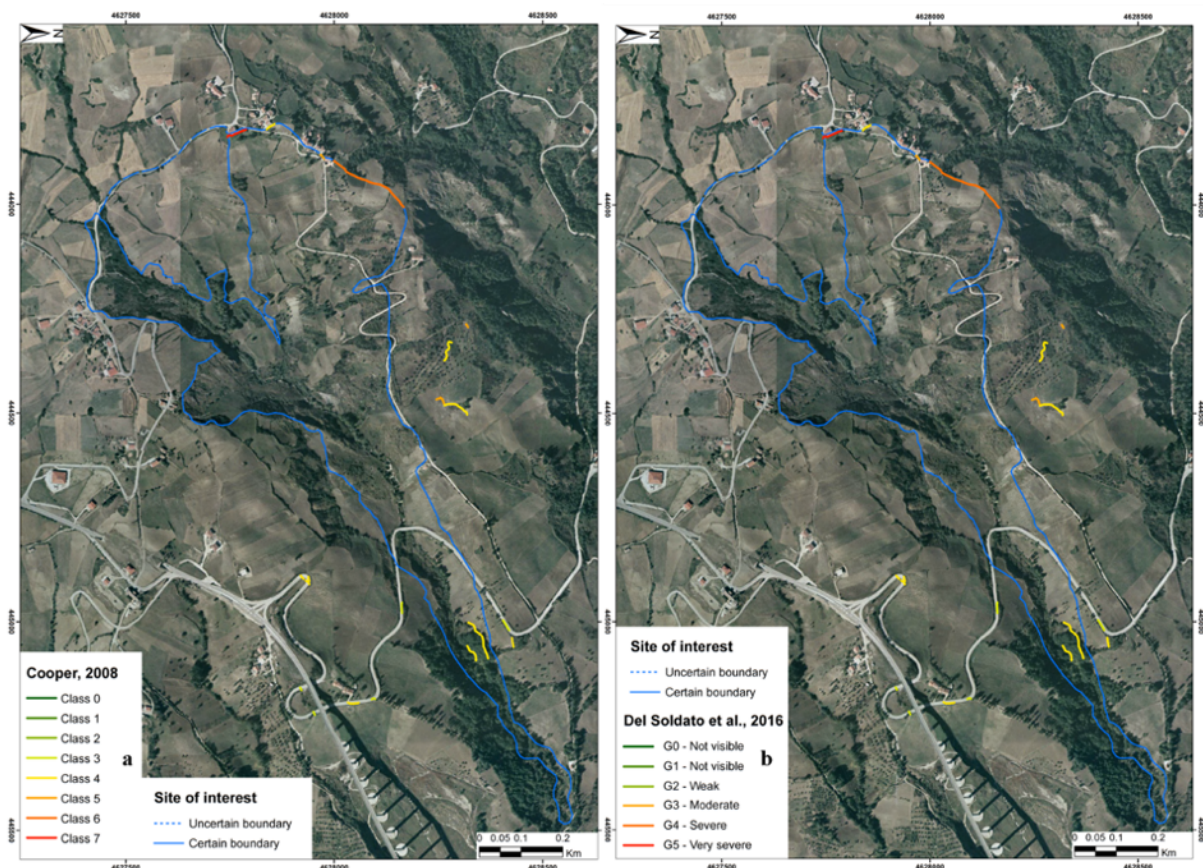


Fig. 5.35 - Classification of fracture and ruptures recognizable in soil and man-made surfaces by the methods proposed by Cooper (2008) (a) and Del Soldato et al. (under review_b) (b).

In addition to the classifications of the recognized damage during field surveys, structures were categorized also by means of the use of the remote sensing analysis. The Persistent Scatterers, reflected by structures, were analysed and elaborated to extract the velocity maximum displacement measured along the LOS and the for both ascending and descending geometries. Furthermore, the mean velocity and average displacement, reprojected along the slope, affecting each construction were assessed to categorize them. The ENVISAT data extracted from the National Cartographic Portal (PCN) of the PST-A Project (*Piano Straordinario di Telerilevamento*, Italian Ministry of the Environment and Protection of Land and Sea - MATTM; National Cartographic Portal) cover the area, but the high vegetation caused a low density of PS. Several structures resulted no covered by PS data, even considering the combination of the data of both geometries. Furthermore, the same analysis was conducted using the PS derived from the elaboration by the CPT algorithm on COSMO-SkyMed images covering the span period from February 2012 to May 2015. The number of Persistent Scatterers elaborated using this sensor is higher than of ENVISAT and with both geometries, ascending and descending, almost all structures are monitored and classifiable.

The velocity and the displacement measured along the Line of Sight (LOS) for each building were assessed, separately for ascending and descending orbits, taking into account only the PS reflected by the structures. Once isolated the PS on the buildings for each orbit, the average by means of *Summary statistics* tools of ArcGIS® of the LOS velocity and the maximum displacement were calculated and used to classify structures. First of all, it is important to notice that the higher velocities are recorded in the crown region of the landslide, even if not for all construction PS data were available. The colours of the buildings were assigned according to the scale of colours used for the velocity, while the threshold values were chosen combining the quality of the data with the possible response of the structures. As visible in **Fig. 5.36**, low velocities not always indicate no displacement, in fact, some buildings affected by low velocity, recognizable in green in **Fig. 5.36a**, after eight years show a cumulated displacement of different millimetres, exhibited in yellow or orange colours in **Fig. 5.36b**.

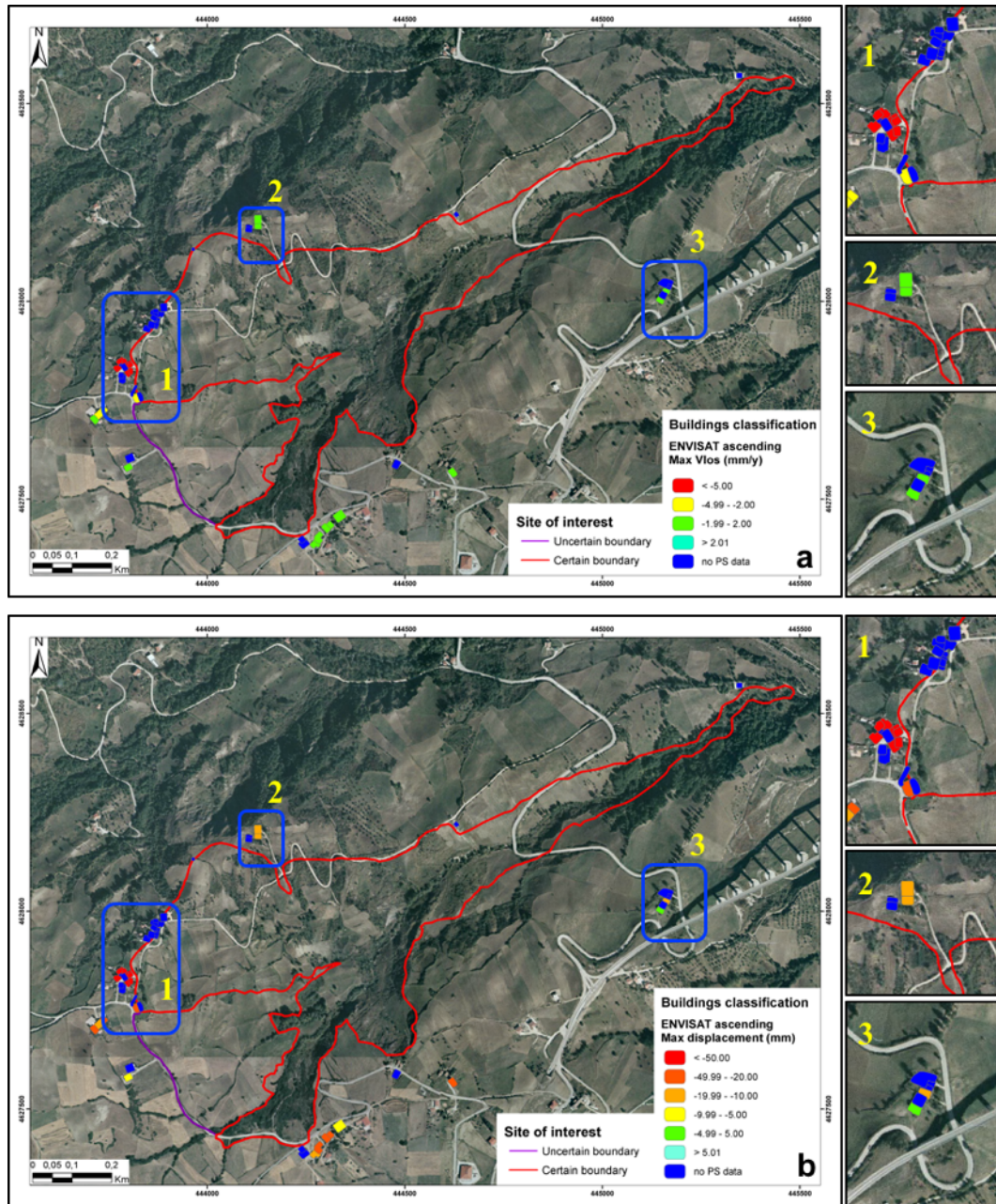


Fig. 5.36 - Building classification conducted based on the Velocity (a) and the cumulated displacement (b) recorded along the Line of Sight of the ascending orbit of ENVISAT sensor.

The same work was carried out with difficulty on the descending PS due to the very low density. The results were shown in Fig. 5.37a and b, but only five structures were classified, three of which are not so close to the landslide.

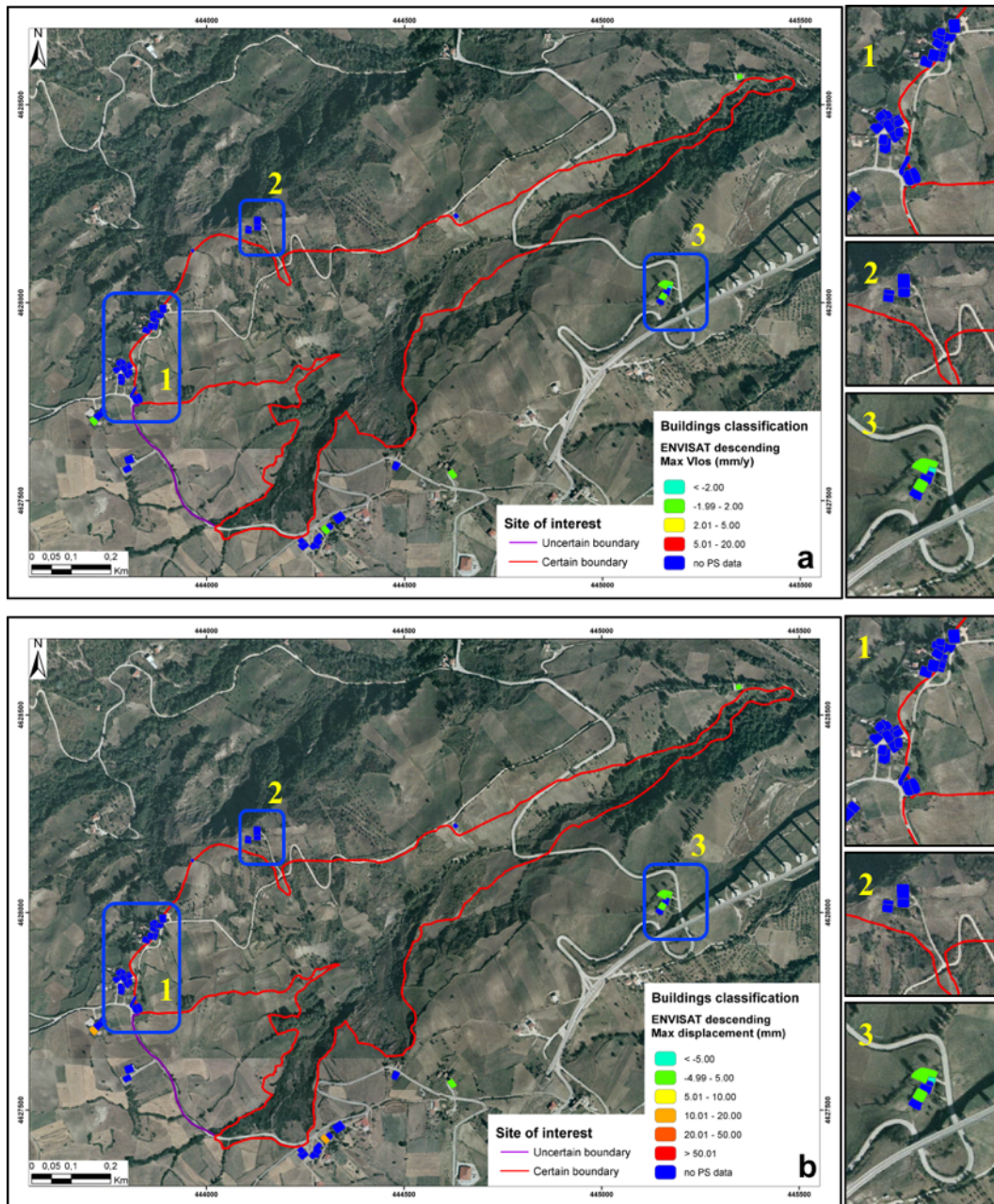


Fig. 5.37 - Building classification conducted based on the Velocity (a) and the cumulated displacement (b) recorded along the Line Of Sight of the descending orbit of ENVISAT sensor.

Using the X-band data from COSMO-SkyMed the same type of work was conducted taking advantage from the better spatial distribution and the higher precision of the measurements. The colours used to classify the buildings by means of the analysis of the CSK data are the same used for the ENVISAT data, but the threshold values are different based on precision of the available data. The velocity and the cumulated displacement assessed using the ascending data along the LOS, are shown in **Fig. 5.38a**. The LOS velocity, coming inbound to the sensor, and the cumulated displacement, for the period 2012 - 2015, exhibit a relative calm situation for all constructions, except for a built up area on the left side of the crown (**Fig. 5.38b**) where some movements were recorded. Some aspects are worthy to be pointed out:

- the building located on the actual crown of the landslide, **B01**, is not affected by important velocity and neither by cumulated displacement. This confirms the surveys conducted during the field campaigns, where negligible damage on this construction were recognized.
- a different situation affects the external sidewalk, as mentioned before, but unfortunately no PS data are available on this structure due to its little dimensions;
- the only area affected by important velocity and cumulated displacement (> of 1.5 mm) is that built close to the crown. The damage recorded in this area during the surveys conduct in different periods, show an increasing of cracking;
- the building severely affected by damage in the foundation sited on the left side of the crown of the mass-movement (yellow in box 1 in **Fig. 5.38a**) show a moderate velocity, but negligible displacement. The displacement in this area pertain to the terrain in front of the construction affects its foundation but, until now, not harshly involving the structure;
- maximum displacement measured for several structures is lower than the expected based on the LOS velocity. This is justified by the cyclical velocity as above shown in the time-series that smooth the cumulated displacement.

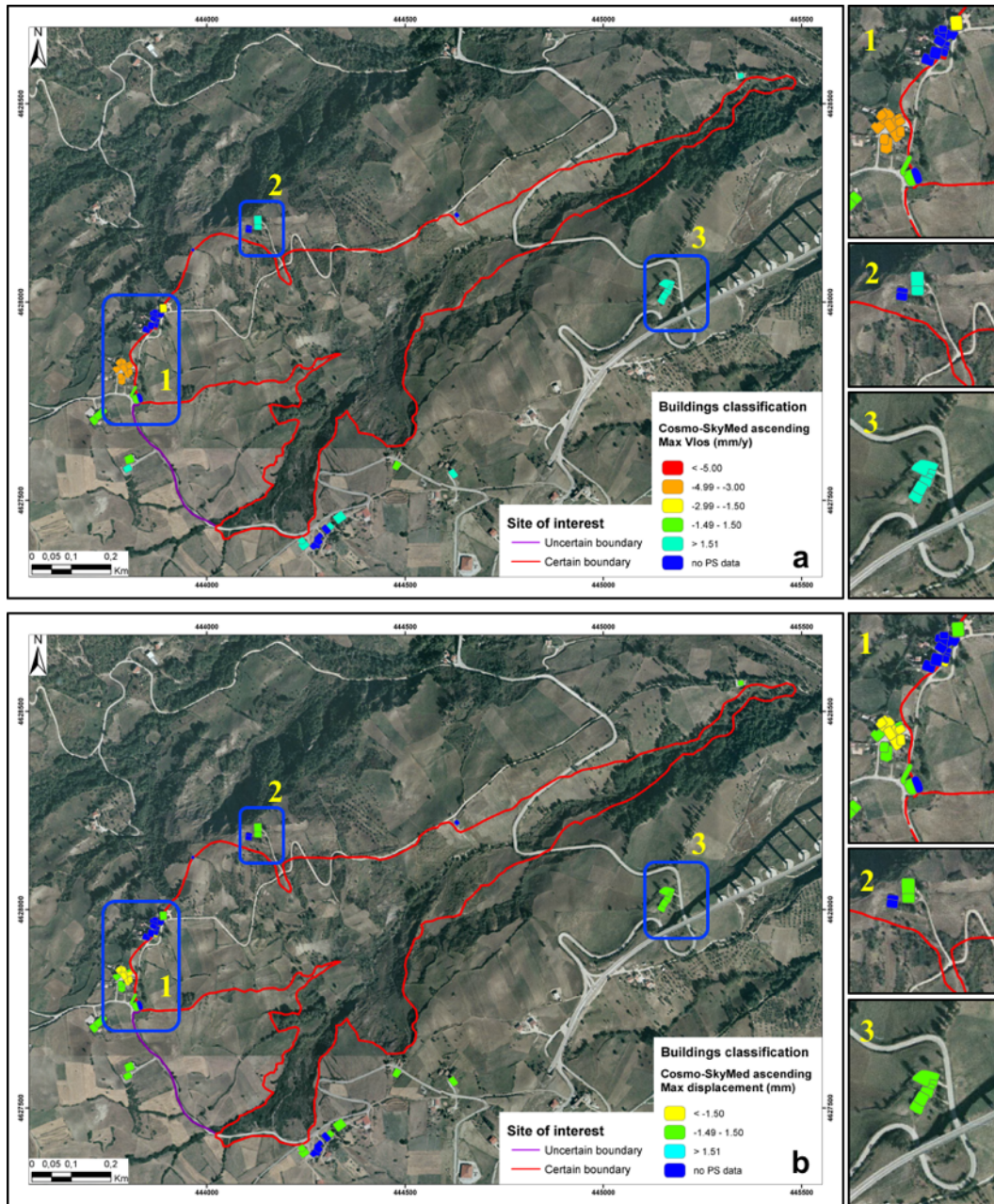


Fig. 5.38 - Building classification conducted based on the Velocity (a) and the cumulated displacement (b) recorded along the Line of Sight of the ascending orbit of COSMO-SkyMed sensor.

Using the same threshold values, the classifications of the buildings based on the LOS velocity and the cumulated displacement were conducted also by means of the descending PS data (Fig. 5.39). The displacement measured moving away from the ascending orbit, in the descending geometries is registered moving toward the sensor, therefore with positive values. For this reason, and for a simpler comprehension of the images, the scale of colours was maintained the same, but using the absolute value. In this way, the classification is visually comparable with that carried out by the ascending PS. First of all, it is worthy noticing that the ranked buildings are mainly present in the crown area than in other regions of the landslide. Furthermore, it is important remembering that the descending data are affected by a bigger imprecision due

to the difficulty encountered during the elaboration of the raw data. In spite of this, the LOS velocity and the cumulated displacement registered on the constructions located on the crown of the left side of the landslide result comparable with that carried out by the other orbit. The main differences are recorded in the structures located out of the landslide boundary that, with high probability, are subjected to errors due to the difficult processing of the descending images. The attention during the processing was paid on structures located very close to the landslide in order to find out, as well as possible, reliable information about them.

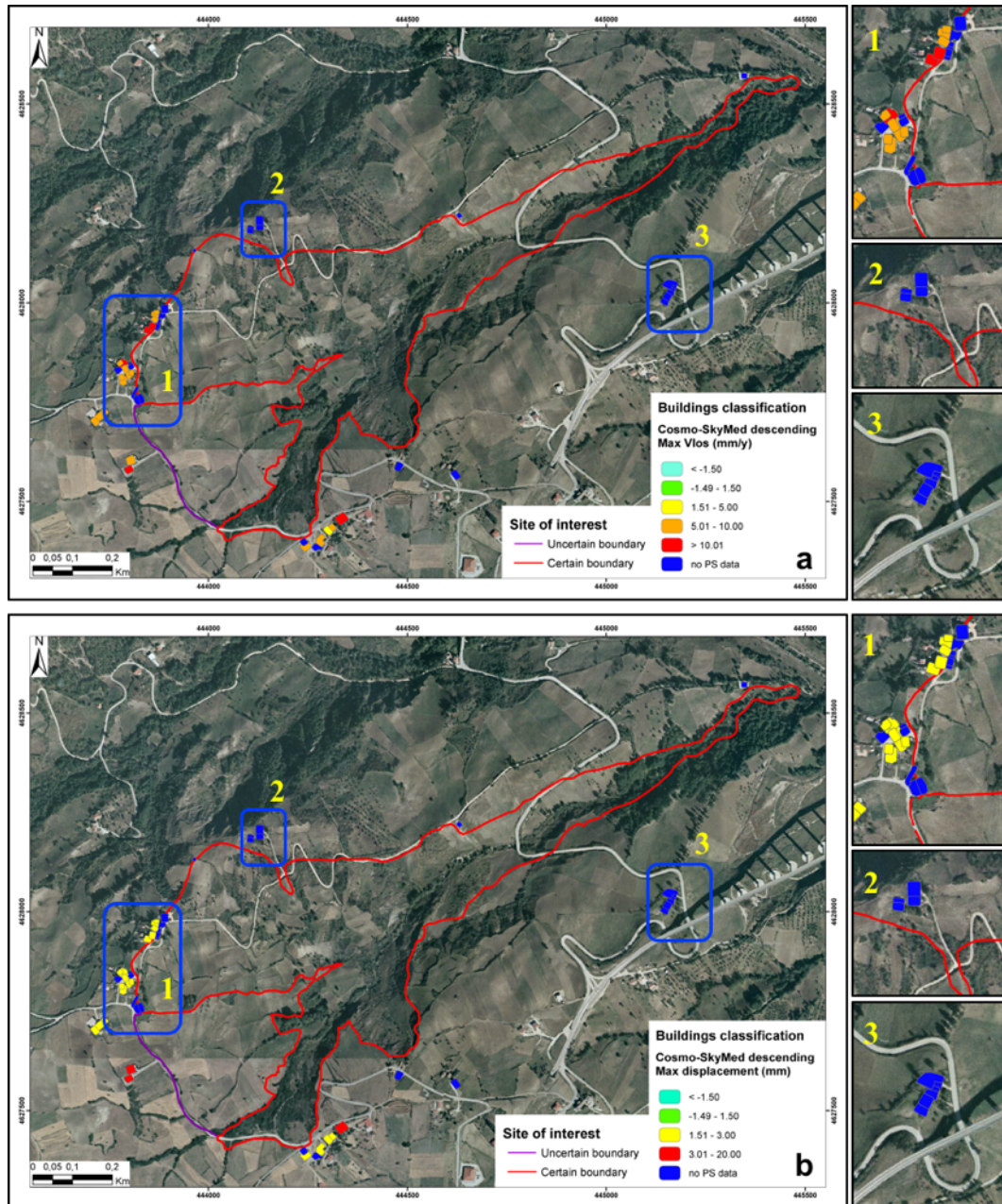


Fig. 5.39 - Building classification conducted based on the Velocity (a) and the cumulated displacement (b) recorded along the Line of Sight of the descending orbit of COSMO-SkyMed sensor.

Even if the landslide is E-W oriented, and thus suitable to be visible from both orbits of the satellite sensors, the descending PS data, both ENVISAT and COSMO-SkyMed, are affected by uncertainty and scarce spatial distribution. To overcome this problem, ascending and descending orbits were combined to better classify the building, reprojected LOS velocities and cumulated displacements along the direction of the local steepest slope of the PS intersecting the constructions. Then, the structures were classified through the analysis of the velocity and the maximum displacement projected along the slope (V_{slope} and D_{slope} , respectively) derived from ENVISAT and COSMO-SkyMed sensors.

For the case study of Agnone, the projection of the velocity and the cumulated displacement along the steepest slope was conducted using the DEMs with 5-m and 10-m cell resolution. This was done to verify the suggestion by Notti et al. (2010) about the use of a DEM with low resolution to reach better results.

Using the available PS dataset, the projection conducted with both DEM (**Fig. 5.40a** with 5-m cell resolution DEM and **Fig. 5.40b** with 10-m cell resolution DEM), shows little differences in the classification of structures. Some differences were carried out only analysing the relationship between the classification of the buildings and the D_{slope} parameter. For categorization conducted with the velocity projected along the slope was increased the stability range due to the elaboration that adds a possible error to the values. For this reason, the “stability” threshold was enlarged to ± 5 mm/year, also because the used value is an average of all the PS data reflected by each structure. The major part of the structures far from the landslide are classified as not influenced by high displacement and only the constructions located on the actual crown results affected by high rate of displacement. It is worth noticing that the span of investigation of the ENVISAT is between November 2002 and July 2010 period during which two main reactivations, in January 2003 and between December 2004 and January 2005, involved the central region of the landslide where no PS data and construction were recorded. However, the high average annual rates on buildings sited on the actual crown are a good indicators for the location, extension and intensity of the phenomenon.

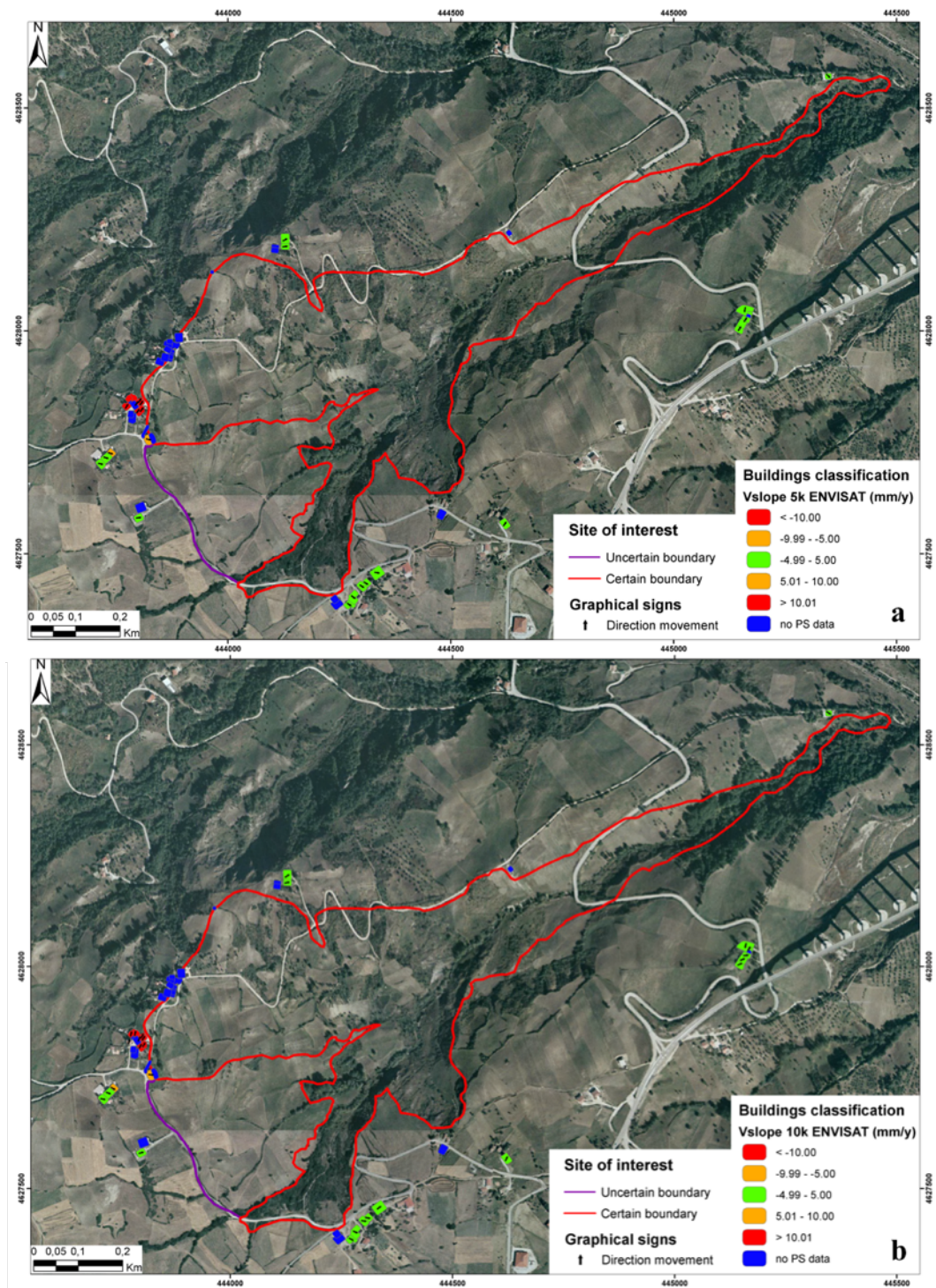


Fig. 5.40 - Building classification by means of the velocity projected along the slope and averaged assessed with ENVISAT sensors for each construction using DEM with 5-m cell resolution (a) and 10-m cell resolution (b).

The same comparison and typology of classification were conducted also by means of the cumulated displacement projected along the slope. In this case the values of cumulated displacement affecting the constructions explain better the important movements involving the area during the two main reactivation events. The same buildings, which by the V_{slope} were classified with high velocity, also using the D_{slope} resulted ranked in high category to confirm the importance of the reactivations occurred during the ENVISAT acquisition period influencing also the buildings located on the actual crown. Furthermore, several buildings located further from the landslide classified as “stable” by means of the V_{slope} , because with a low average annual velocity, reach noticeable cumulated displacement (some examples in **Table 5.7**).

Table 5.7 - Example of buildings located in different place respect to the landslide that show a low average annual velocity (V_{slope}) but reach noticeable cumulated displacements. The same results were carried out using both the DEM with 5-m cell resolution and 10-m cell resolution.

Building	Location	ENVISAT V_{slope} 5k (mm/y)	ENVISAT V_{slope} 10k (mm/y)	ENVISAT D_{slope} 5k (mm)	ENVISAT D_{slope} 10k (mm)
B_01	Crown	-6.07	-5.61	-71.29	-65.82
B_30	Out of crown	-3.78	-3.52	-48.47	-44.78
B_04N	Left flank	-4.59	-4.23	-48.22	-44.57

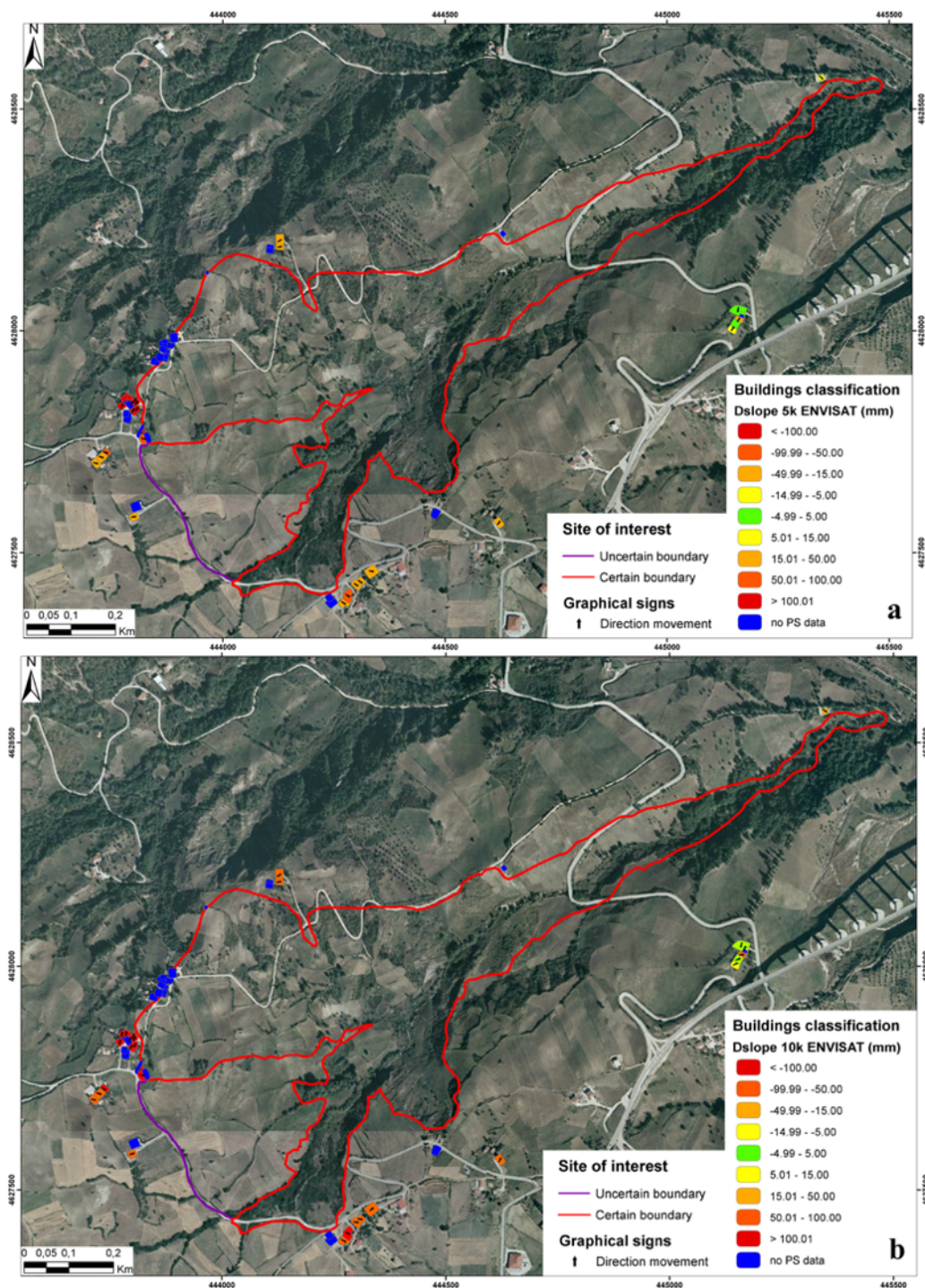


Fig. 5.41 - Building classification using the cumulated displacement projected along the slope and averaged evaluated by ENVISAT sensors for each construction using DEM with 5-m cell resolution (a) and 10-m cell resolution (b).

In the period investigated by D_{slope} calculated for CSK data (Fig. 5.42a and Fig. 5.42b, respectively realized by the use of DEM 5-m and 10-m cell resolution) no important reactivations were observed, but the movements continue to increase the dimension of the CL-PO landslide. Using X-band sensor more PS were recognized for the structures under investigation and as stability condition was established at ± 2 mm/year.

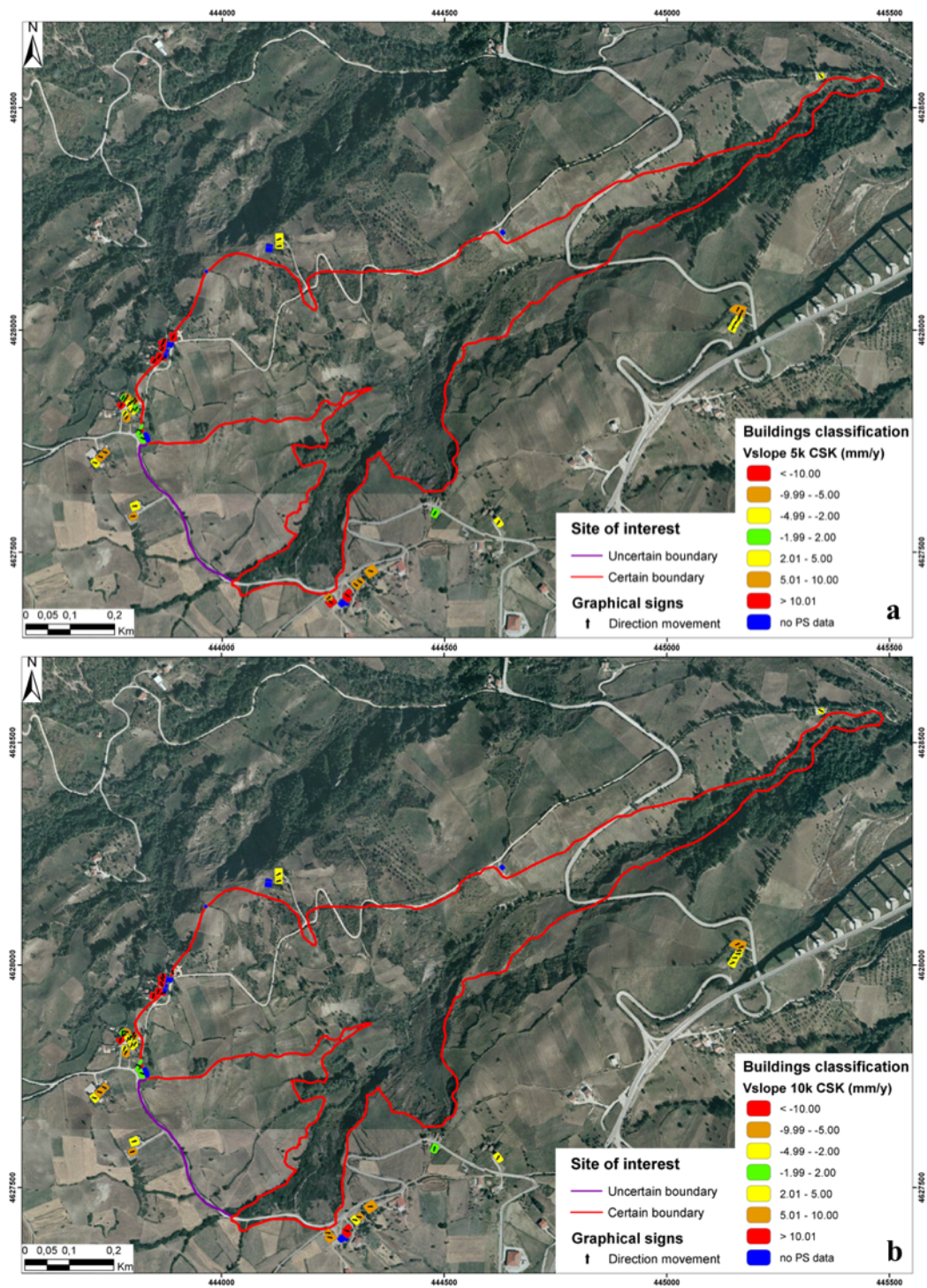


Fig. 5.42 - Building classification by means of the velocity projected along the slope and averaged assessed with COSMO-SkyMed sensors for each construction using DEM with 5-m cell resolution (a) and 10-m cell resolution (b).

The structure classification map appears visually different from that realized using ENVISAT data because the used scale is different, but some buildings show interesting behaviour to take into consideration. One of the most interesting cases to examine is the building located on the crown of the landslide (**B01**) that appears completely stable, differently to the previous period when it was ranked in a class characterized by high

velocity. Beside its external concrete sidewalk is completely cracked and partially collapsed with respect to the 2005 (**Fig. 5.34**), recent field surveys revealed that at the moment the construction does not show important cracks or damage on the external façades.

Another important evidence carried out analysing the building deformation maps by means of COSMO-SkyMed PS (**Fig. 5.42**) comparing it with that obtained by ENVISAT PS (**Fig. 5.40**), is the propagation of the deformation in the surrounding of the landslide body. The velocity along the slope measurement on structure behind the traced crown could indicate possible future continuous evolutions of the phenomenon with retrogressive development that could cause an increment of the dimension of the landslide area.

The map of cumulated displacement, calculated with two DEM with different cell resolution (**Fig. 5.43**) shows some differences in the classification of several constructions located in the left part of the crown of the landslide and in the right surrounding. Some of them have value close to the threshold and, in fact, using the DEM with cell resolution of 5-m (**Fig. 5.43a**) the built-up area of buildings in the left region of the crown are classified by means of the cumulated D_{slope} under the 5 mm, while employing the DEM with low resolution, 10-m cell, they are classified above the threshold value in red (**Fig. 5.43b**). This confirms as the spatial resolution of the initial data and the choices done by the users are important to reach good and reliable results. Furthermore, this example demonstrates the key role of the field survey to validate the remote sensing analysis and investigations.

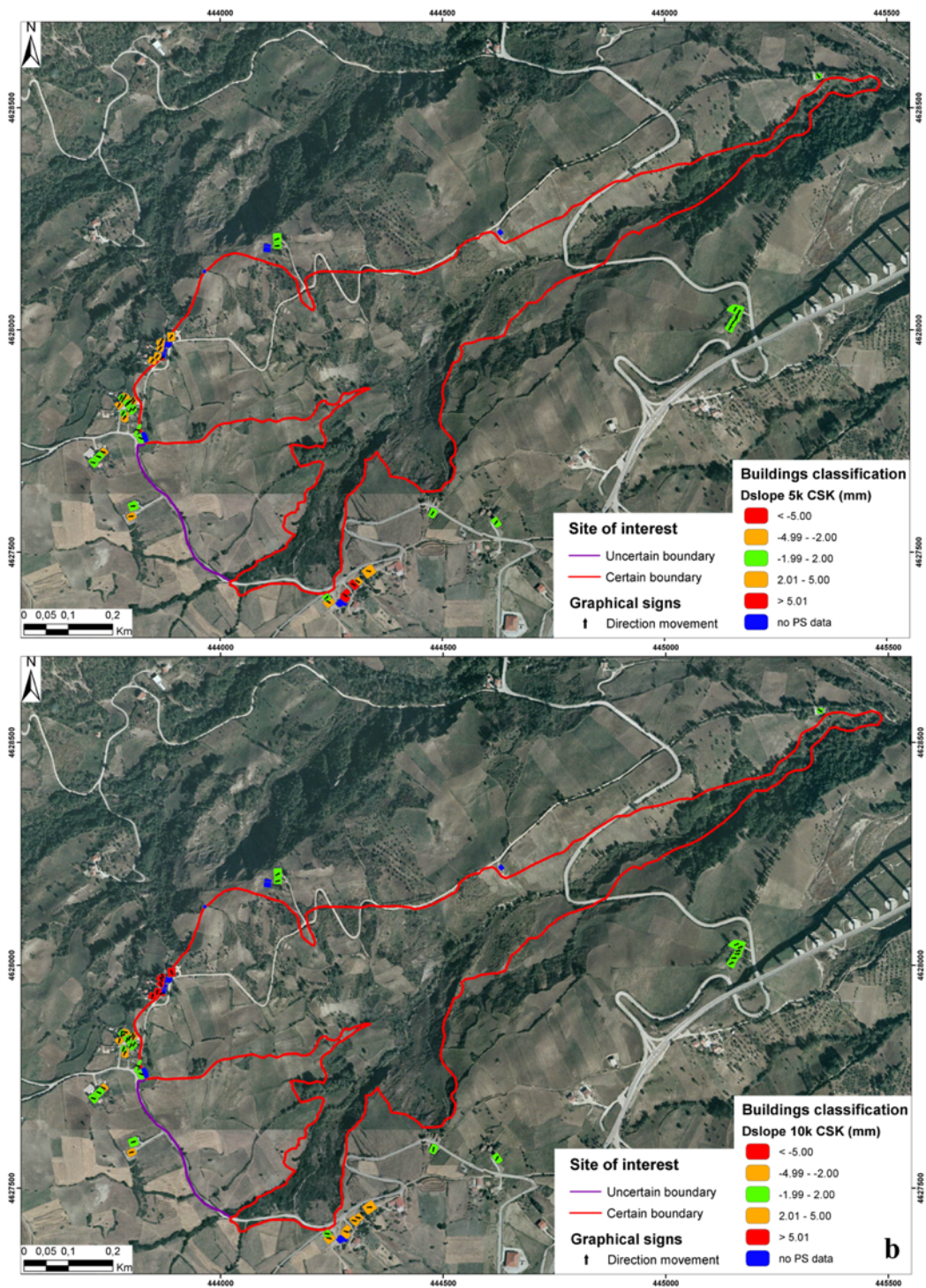


Fig. 5.43 - Building classification by means of the cumulated displacement projected along the slope and averaged evaluated by COSMO-SkyMed sensors for each construction using DEM with 5-m cell resolution (a) and 10-m cell resolution (b).

5.3 Volterra landslide (Tuscany region)

5.3.1 Evolutionary stages and monitoring of the landslide

No more historical information about the ground instability affecting the southwestern sector of Volterra (Tuscany region, central Italy) were found, differently from the Colle Lapponi-Piano Ovetta. The area of interest is located between the rural zone and the southwestern sector of the city centre, characterized by middle urban fabric density and partially affected by landslides. The boundary of the mass-movements affecting these areas are very difficult to detect due to the anthropic influence obliterating geomorphological shapes and slide surfaces. The constructions involved and damaged by landslide were mainly built in different typologies, such as masonry structures and concrete frameworks, in the 19th century. The studied landslides are placed in a partially urbanized region of the southwestern sector where part of the cultural and historical heritage of Volterra town is present. 35 m long and 9.5 m high portion of the Etruscan fortification walls embracing the urban fabric of Volterra suddenly collapsed in the southwestern side in January 2014. After the collapses of part of the historical walls to monitor and demonstrate that no displacement occurred on the buildings by Ground-Based Interferometric SAR (GB-InSAR) (Pratesi et al., 2015).

After the emergency, in 2014-2015 the Department of Earth Sciences of the University of Florence analysed the ground instability of the whole Volterra territory in order to update the pre-existing landslide inventories (e.g. *IFFI* and *PAI* projects). Furthermore, the state of activity and the typology of mass-movements were characterized (**Fig. 5.44**). Several phenomena affecting the area, some of these active, are shallow phenomena involving thick colluvial debris and underlying clayey lithotypes, causing damage to localized buildings and facilities.

An analysis of the historical aerial images allowing the investigation of the geomorphological evolution of the region of interest, as made for the Colle Lapponi - Piano Ovetta landslide in Agnone, was developed. By the application of the Structure for Motion technique, 3D models for different years were reconstructed. Five 3D reconstructions were realized for each different set of images by means of the analysis of aerial historical images shot by the Italian IGM (*Istituto Geografico Militare*). Furthermore, the area was investigated by means of the remote sensing technique, i.e. through Persistent Scatterers Interferometry.

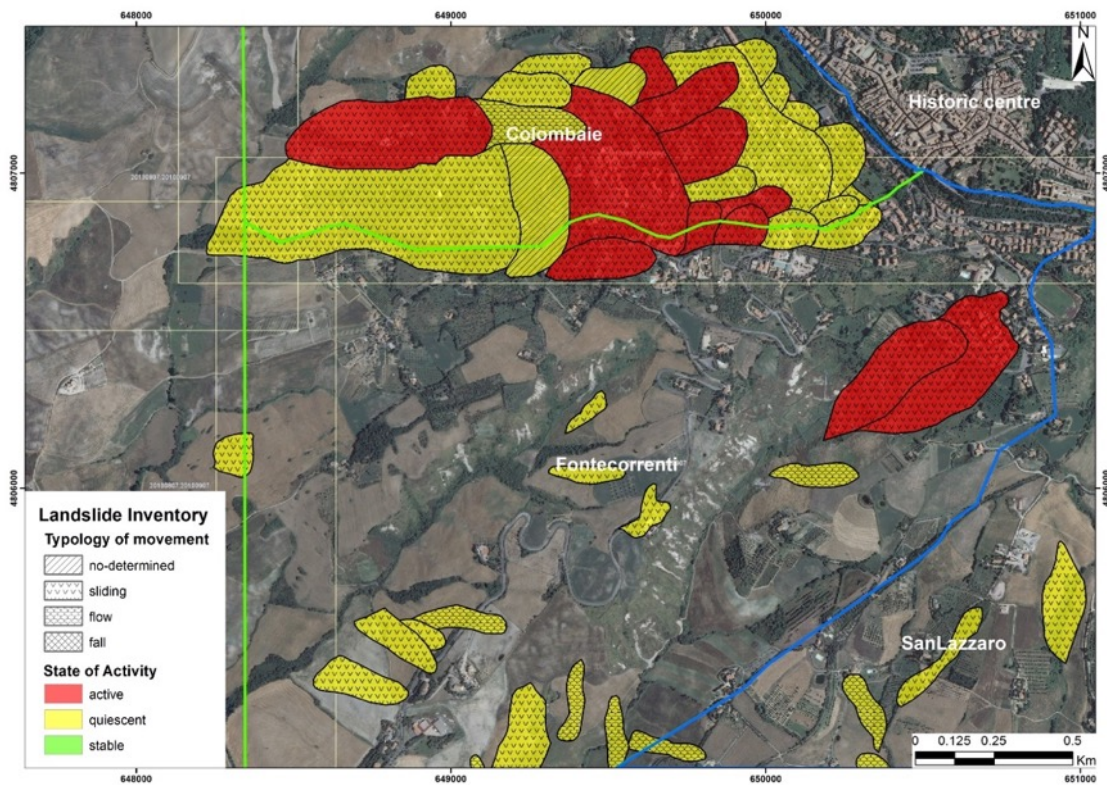


Fig. 5.44 - Landslide inventory in the studied southwestern portion of the municipality of Volterra.

Landslide geomorphological signatures are not simple to recognize by field investigations due to the diffusion of the fabrics. In the same way, the recognition of little and often obliterated forms on historical images with not high resolution, results difficult. Taking advantage from the use of the reconstructed 3D models allowing to zoom and virtually fly inside the reconstructed model, some geomorphological forms are better recognizable. The 3D models reach errors lower than 5 m despite the high number of fabrics in the northeastern zone causing difficulties to find reliable points with good precision. Analysing the evolution in time for *Le Colombaie* and *Fontecorrenti* areas, some scarps and counterslopes were identified from the 1954 reconstruction (**Fig. 5.45a**). The same shapes result in continue increment in 1965 (**Fig. 5.45b**) and 1982 (**Fig. 5.45c**) 3D Points Clouds. In these regions, mainly in *Fontecorrenti*, also badland shapes are well-defined and easily to recognize. Furthermore, their evolution is easily recognizable analysing the subsequent 3D reconstructions. The main evolution of geomorphological features of landslides is localized in the upper portion of *Le Colombaie* area, where the crown of several landslides is traced (**Fig. 5.44**). In 1986 and 1995 reconstructions (**Fig. 5.45d** and **f**, respectively) geomorphological signatures are too difficult to identify due to the spread of new buildings in the sectors under investigations.

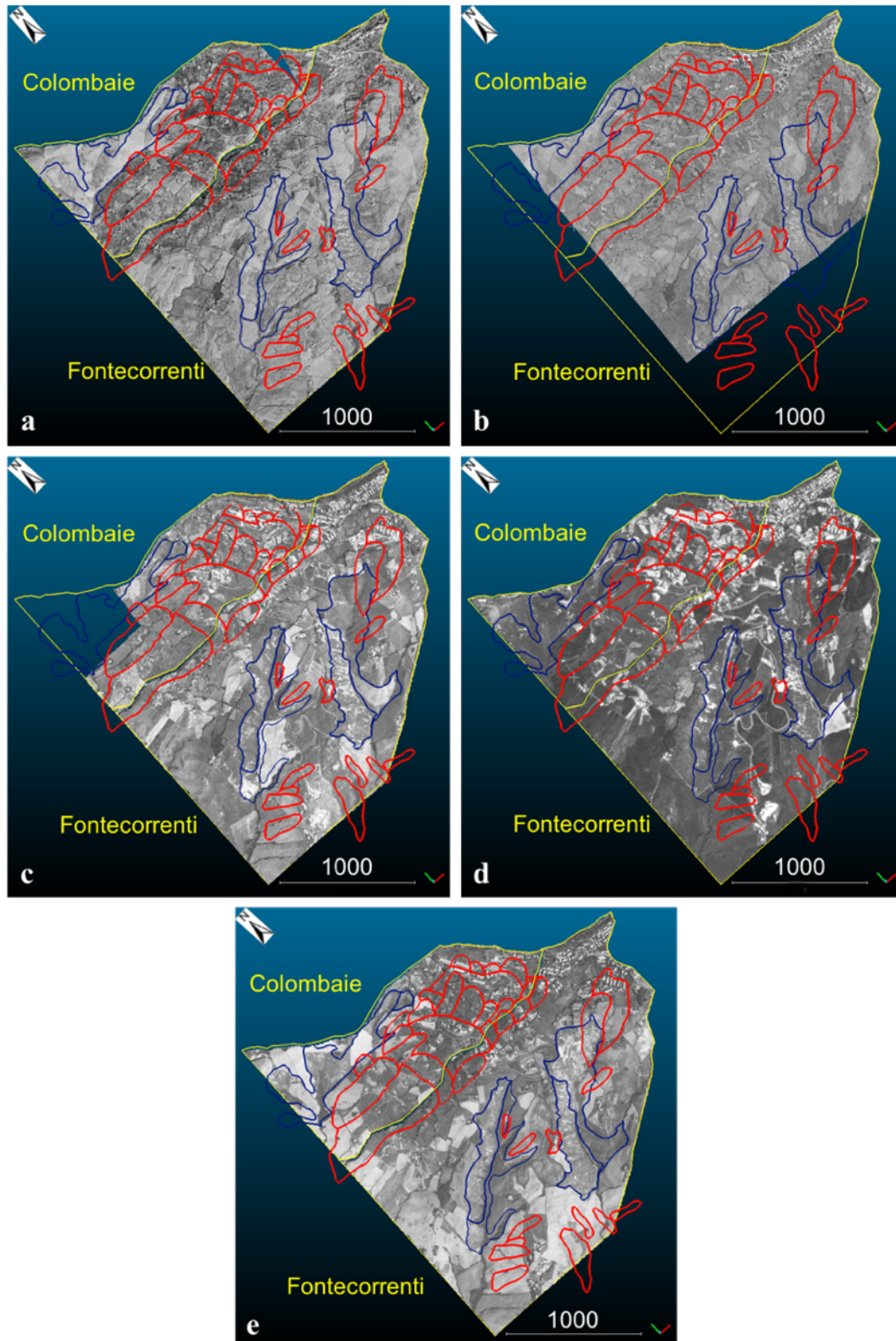


Fig. 5.45 - Evolution of the *Le Colombaie* and *Fontecorrenti* areas affected by both landslides (in red) and badlands (in dark blue) reconstructed 3D Point Clouds by means of the *SfM* techniques applied on historical aerial imagery of 1954 (a), 1965 (b), 1982 (c), 1986 (d) and 1995 (e). The boundaries of the landslides and of the badlands, derive from the inventories of the municipality strategic plan of Volterra (2005).

Some geomorphological signatures were recognized by means of the 3D reconstructions made using historical images, i.e. 1954 and 1995. Some of them were identified in sites in which during the '80s several constructions were build. Comparing the zoom of an area reconstructed in 1965 (**Fig. 5.46a**) and in 1995 (**Fig. 5.46b**), new constructions are recognizable in the uphill of a possible geomorphological scarp. Some of these buildings, mainly that close to the geomorphological shape, are actually affected by important damage.

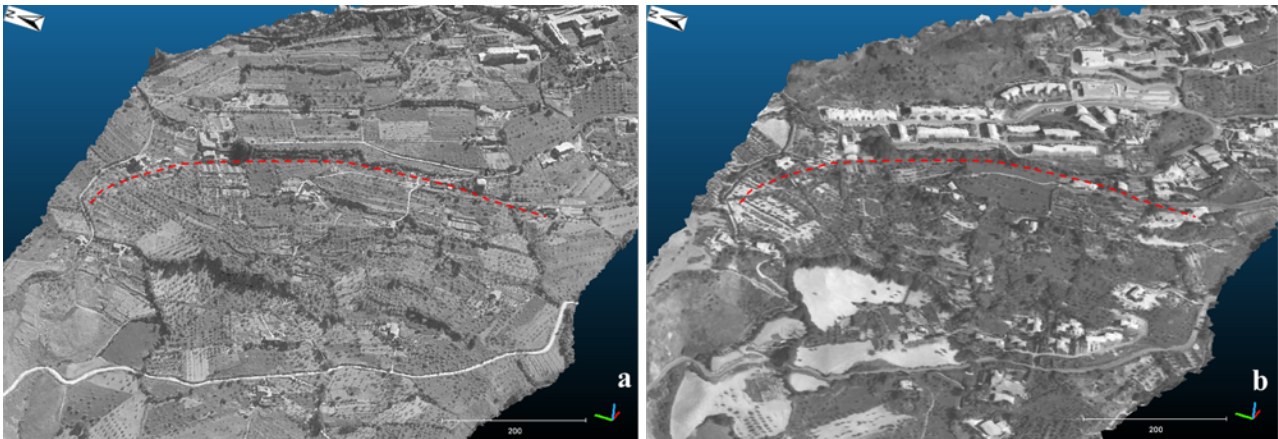


Fig. 5.46 - Particular in *Colombaie* sector of the 3D reconstructions of 1965 (a) and 1995 (b) where new buildings uphill of a possible geomorphological shape, in red, were built.

Furthermore, exploiting the 3D reconstructions carried out by the *SfM* technique, the difference in volume between the Points Clouds of 1954 and of 1995 was developed. An algorithm to compute the distance in each direction between two clouds, present in *CloudCompare* software, was used to manage the georeferenced points clouds and to calculate the changes of volume. The analysis was conducted for *Le Colombaie* and *Fontecorrenti* areas affected by slope movements (**Fig. 5.47**). It is important to consider that the error in regions very close to the boundary are bigger than in the centre due to the location of the GCPs. In spite of this inconvenience, the qualitative assessment results in accord to the literature and with the displacement measured by other remote sensing techniques and the site investigations. To support the quality of the result, some buildings located in the crown of a group of shallow landslides affecting *Le Colombaie* area erected in the '80s, in the 3D points clouds are recognizable as increment of volume (orange circle in **Fig. 5.47**). In the upper part of the reconstruction a little portion not covered by the 3D reconstruction of 1954 create and increment of error, in fact the highest and the lowest values are concentrated there.

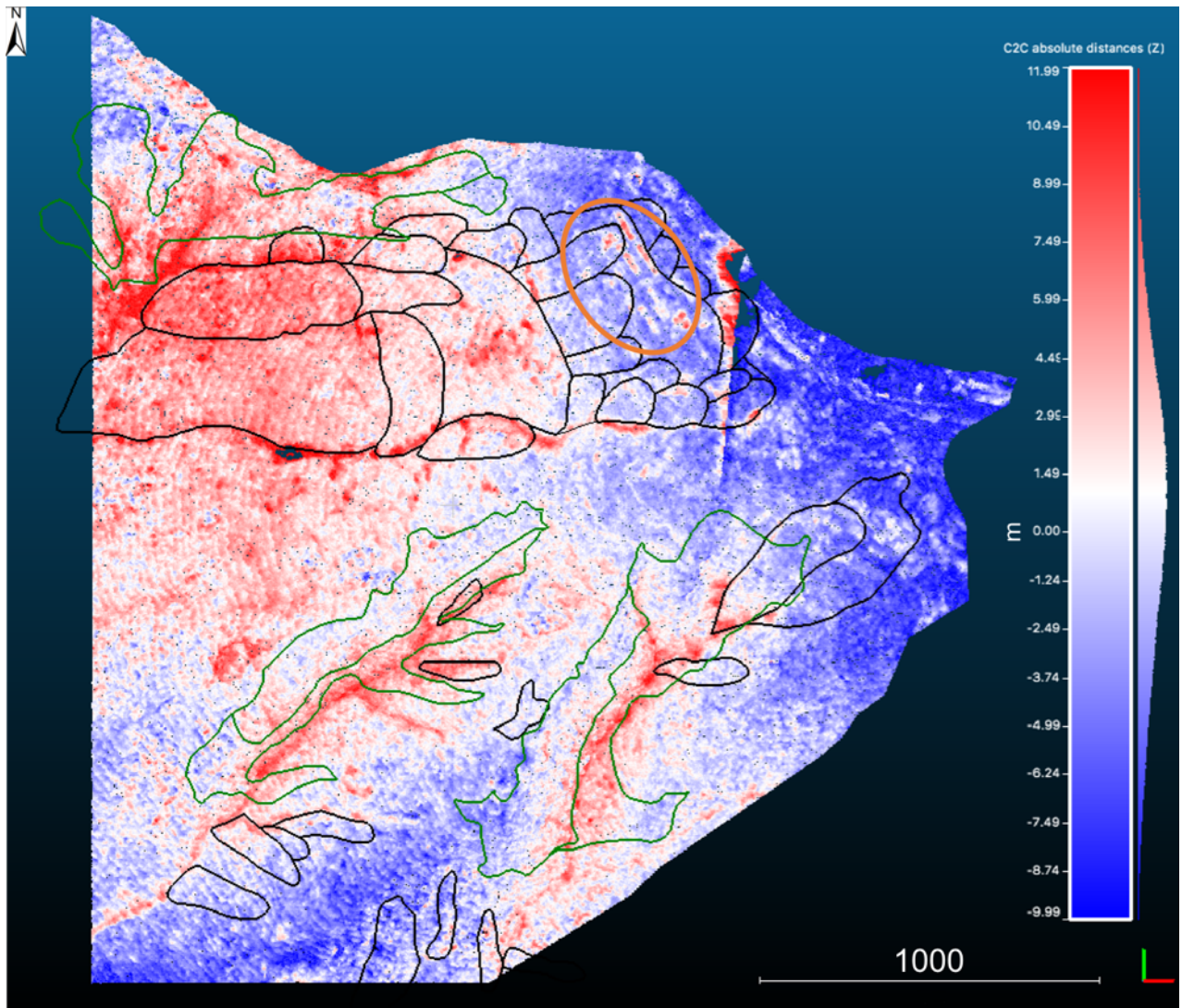


Fig. 5.47 - Detection of changes of volume for *Le Colombaie* and *Fontecorrenti* areas affected by both landslides (in black) and badlands (in green). The orange circle indicates some buildings build between the 1954 and 1995 were visible as increase of volume.

The hot colours of **Fig. 5.47** indicate areas where the volume increased, thus regions affected by accumulation of material eroded, displaced by the movements of the entire landslide or by shallow slope-moving (traced in black). In blue are recognizable regions affected by down-moving or where erosional processes are present due to shallow landslides phenomena. Moreover, some badlands phenomena (traced in green) affect few slopes causing further erosional and accumulation areas.

To confirm the hypothesis carried out by the investigation conducted on the historical set of images from 1954 to 1995 and to monitor the recent evolution of the landslide, remote sensing technique, field investigations and direct measurements in situ were adopted. The Persistent Scatterers of the study area, derived from the images acquired in C-band by ERS1/2 and ENVISAT sensors, processed by the PSInSARTM

methodology (Ferretti et al., 2000, 2001), were available on the *Portale Cartografico Nazionale* (PCN) of the Italian Environmental Ministry (<http://www.pcn.minambiente.it/>). Furthermore, X-band COSMO-SkyMed (CSK) constellation acquired by during the emergency of 2014 by the DPC, were elaborated by means of the SqueeSAR™ techniques (Ferretti et al., 2011) by TRE-ALTAMIRA company.

The available ERS data acquired for the period 1992 - 2000 only in descending geometry (**Fig. 5.48**) are few despite they show stability for the historic Volterra town and instability for some regions of the southwestern study sectors. The stability threshold for the C-band data was assigned at ± 2 mm and the common scale of colour (i.e. hot colours for data moving away from the sensor and cold colours for displacement coming toward the satellite) were used.

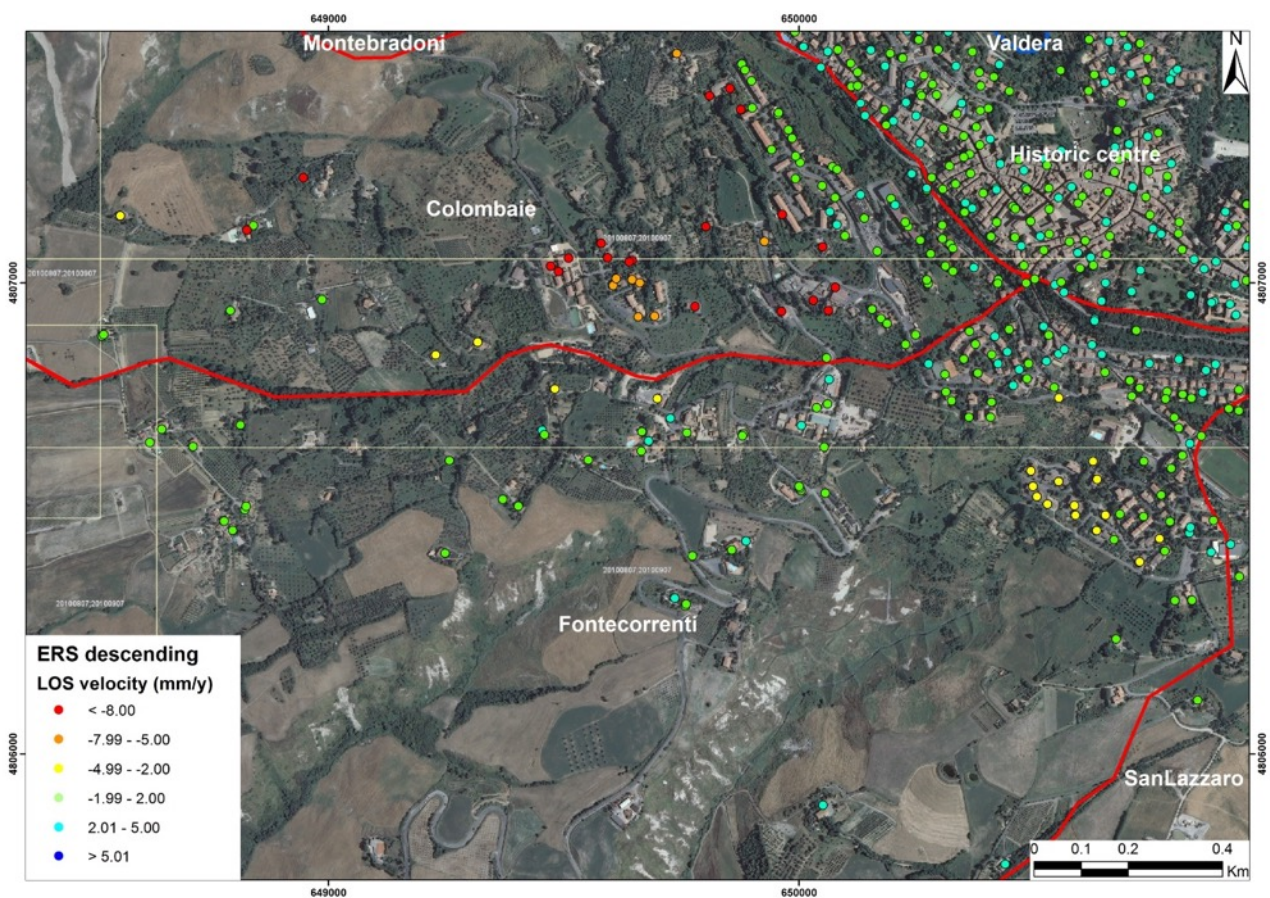


Fig. 5.48 - ERS data in descending orbit backscattered for the southwestern sector of Volterra town.

The ENVISAT data, gathered between 2002 and 2010, were registered for ascending (**Fig. 5.49a**) and descending (**Fig. 5.49b**) geometries and a higher number of Persistent Scatterers benchmarks can be detected. For the data collected by the ENVISAT satellites, the colours and the stability values assigned, i.e. ± 2 mm, are the same of that used for the ERS data.

Analysing the PSInSAR™ products from ERS and ENVISAT satellites, the Volterra town results stable while in the southwestern regions, *Le Colombaie* and *Fontecorrenti*, several zones affected by instabilities are

identifiable. They are characterized by light-blue and blue points in ascending orbits and while by yellow, orange and red in descending geometry.

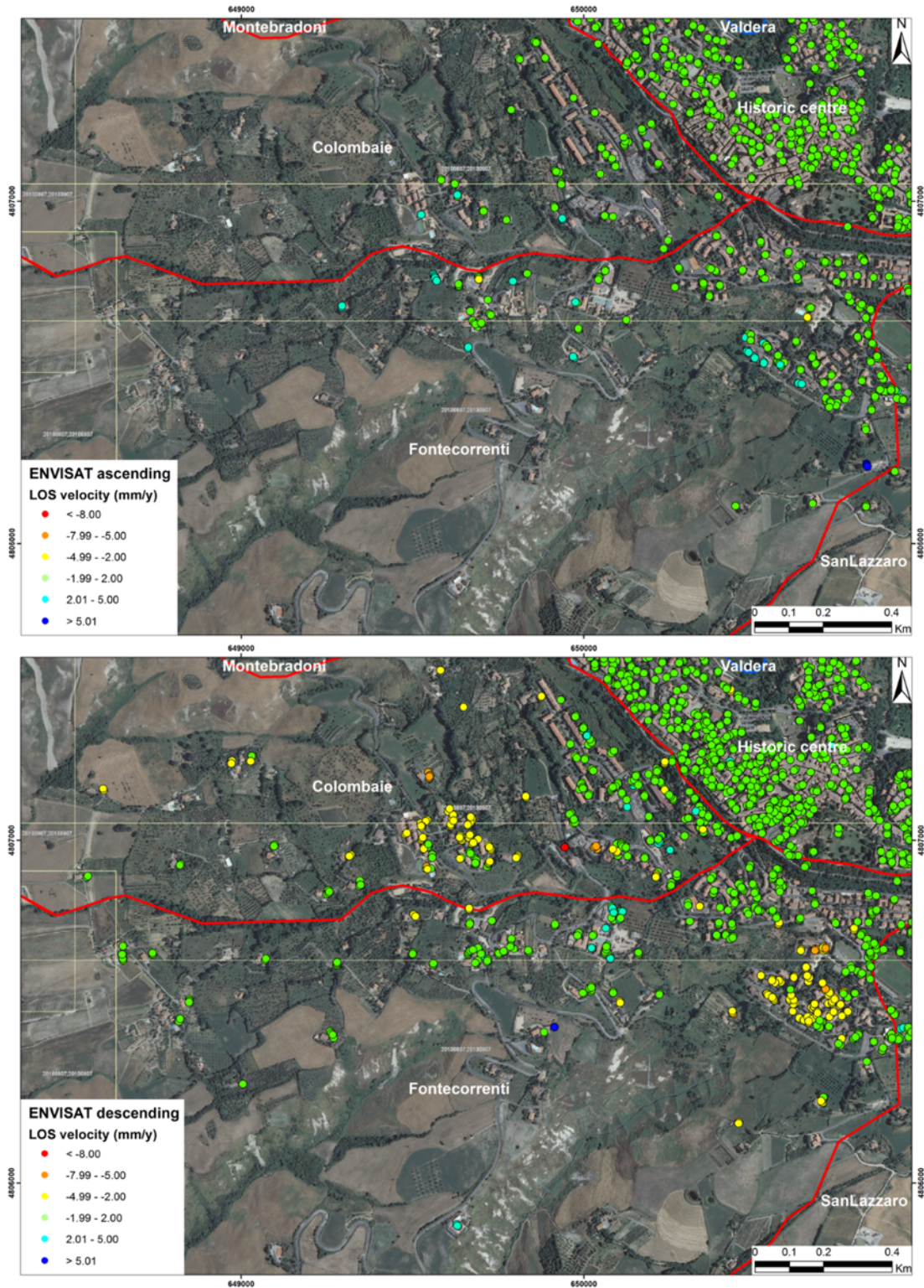


Fig. 5.49 - ENVISAT products acquired in the ascending (a) and the descending (b) geometries for the southwestern sector of Volterra.

In the same period, due to some damage affecting buildings and facilities, seven inclinometers were installed to monitor the evolution of the slope from January 2009 (measure considered “read zero”) until February 2010 after four campaigns of measurement. Two of them located in *Le Colombaie* and in *Fontecorrenti* sites, respectively, were destroyed due to very high ground motions (**Fig. 5.50**).

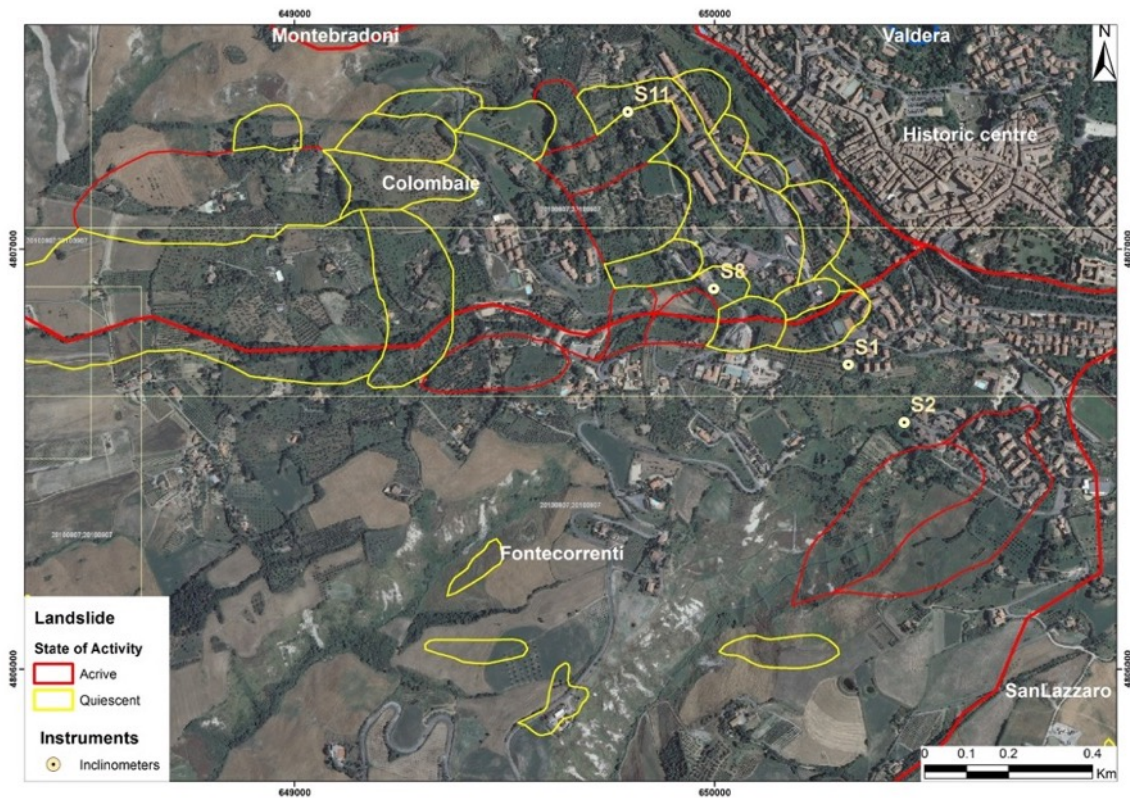


Fig. 5.50 - Localization of the inclinometers in the southwestern sectors of Volterra.

The readings made about each three months were plotted in a scheme (**Fig. 5.51**), showing important information about the slip surfaces of the investigated landslide.

Starting from the East to the West:

- the inclinometer placed in the borehole S11 (**Fig. 5.51a**), did not show important movement, even if some displacement occurred at the bottom of the hole at 20 m depth were recognized;
- the instrument sited in the soil drilling S8 (**Fig. 5.51b**) highlighted an evident slip surface at 18 m depth with a velocity of movement of 22 mm per year classifiable from very slow to slow (Cruden and Varnes, 1996);
- the inclinometer located in the borehole S1 (**Fig. 5.51c**) did not show a clear surface of rupture, but annual cyclical movement of about 4 mm at depth of 12 m, where there is a change of clay consistency. Moreover, several little movements were registered at different depths with low importance;
- the instrument installed in the hole S2 (**Fig. 5.51d**) highlighted a rupture surface with movement from very slow to slow (Cruden and Varnes, 1996) similar to that measured in S8 at 16 m depth;

- inclinometers placed in the boreholes S6 and S7 (Fig. 5.51e and f) did not show important movement recognizable as indicators of a rupture surface.

The measurements collected by the inclinometer confirmed that, between January 2009 and February 2010, the instability affected the southwestern sector of Volterra in *Le Colombaie* and *Fontecorrenti* areas, where the instruments S11, S8, S1 and S2 are localized, but does not involve the close *San Lazzaro* area, where S6 e S7 were located.

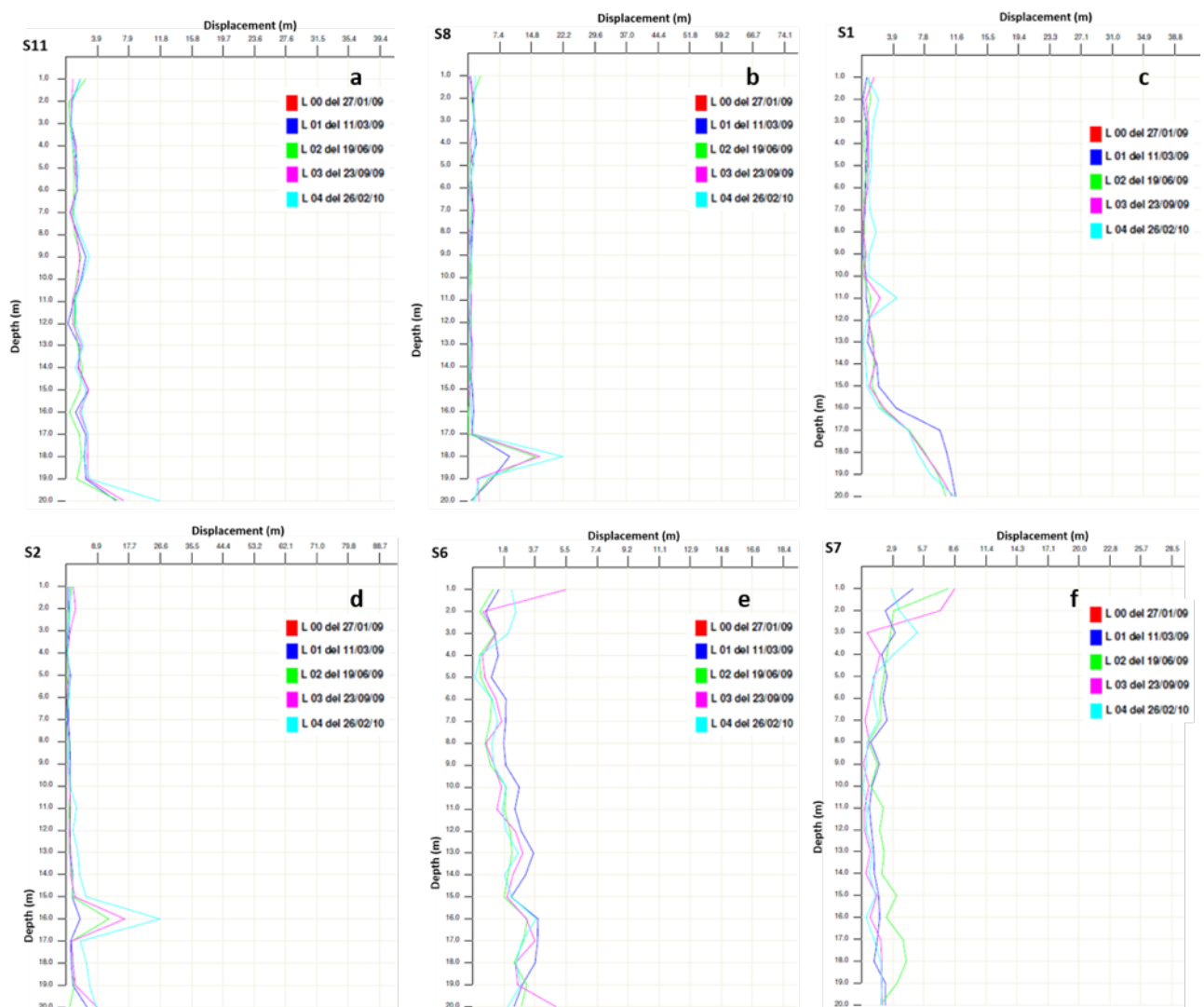


Fig. 5.51 - Temporal sequences of inclinometer measures of five instruments located in the southwest sector of Volterra (GEOSER s.c.r. & GEOPROGETTI).

In the following period the monitoring of the instability was pursued by means of the Persistent Scatterers gathered in both orbits by COSMO-SkyMed constellation (ascending and descending in Fig. 5.52a and b,

respectively). PS extrapolated by SqueeSAR™ technique (Ferretti et al., 2011) allowed a better spread of points also in areas cover by diffuse vegetation as in the southwestern region of Volterra.

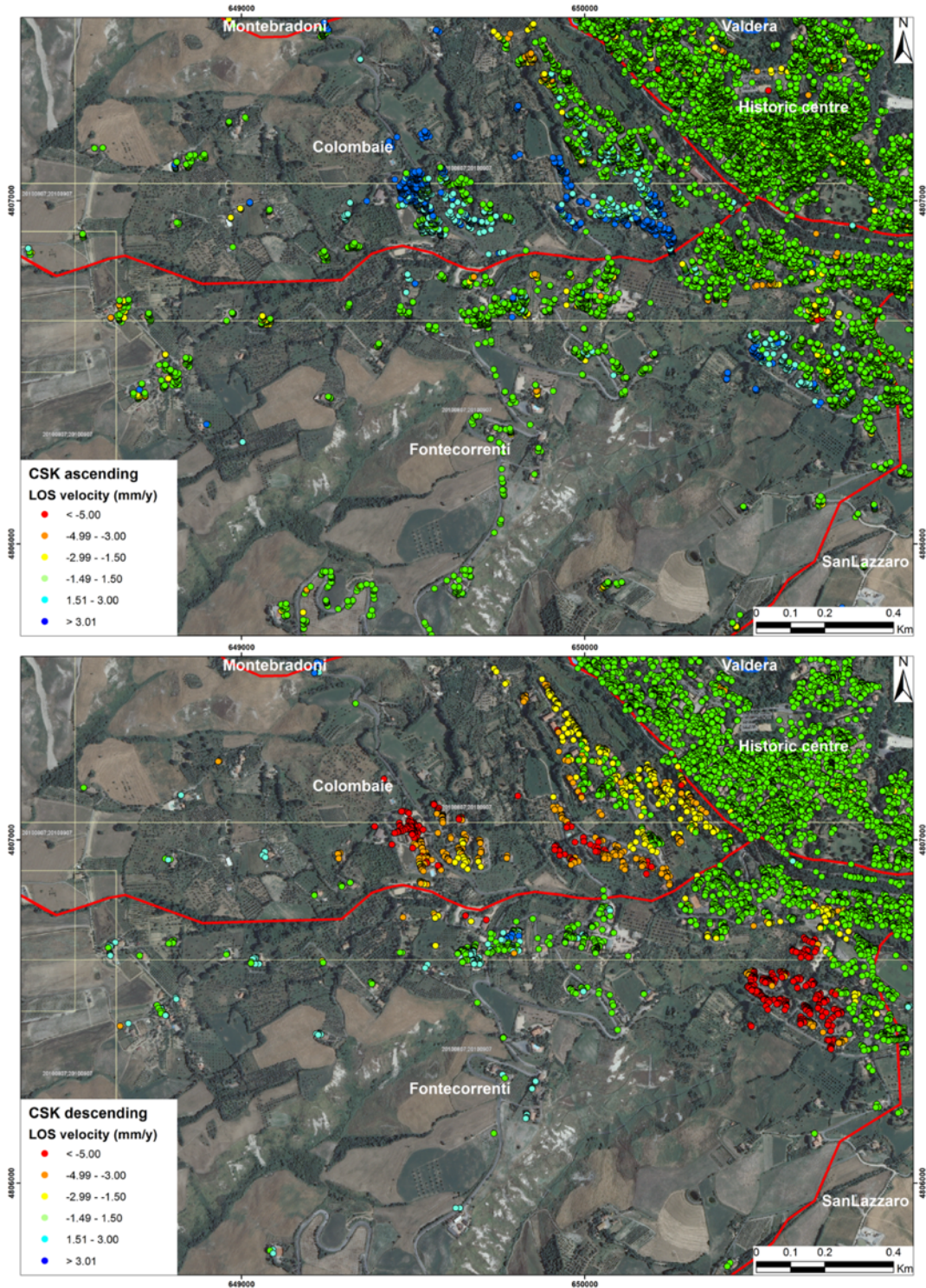


Fig. 5.52 - COSMO-SkyMed products acquired in the ascending (a) and the descending (b) geometries for the southwestern sector of Volterra.

The areas affected by ground instability are easily visible and recognizable by means of the interpretation of the usual scale colours related to the orbit. The phenomena affecting the study area are identifiable by cold colours in the ascending geometry and featured by hot colours in the descending one. The landslides that occurred in the southwestern sector of the Volterra's municipality and damage affecting buildings in this area were localized by movements detected for existing PSs. By means of PS data, the ground movements caused by the evolution of badlands are not easily visible if not involving some structures. Only using the descending data, both ENVISAT and COSMO-SkyMed, some little displacements affecting some constructions in the crown of a badlands were detectable.

As for the first case study of Agnone, the Persistent Scatterers Interferometry (PSI) time series of ENVISAT and COSMO-SkyMed satellites acquired in both acquisition geometries for the entire southwestern sector of the municipality of Volterra, were analysed corrected to the regional trend by the Notti et al. (2015) method. Furthermore, they were automatically categorized by means of the approach of Berti et al. (2013) in six target trends. In order to better understand and monitor the evolution of the slope instability across time, three areas (**Fig. 5.53**) were chosen to be investigated separately in detail. For each one, a sample time-series was extracted and displayed for each sensor recording displacements. The analyses conducted for the chosen landslides areas were executed using data acquired in the descending orbit. This choice was done because this geometry shows better displacements and is the only one recorded for all sensors allowing to investigate a long period covered by ERS, ENVISAT and COSMO-SkyMed sensors.

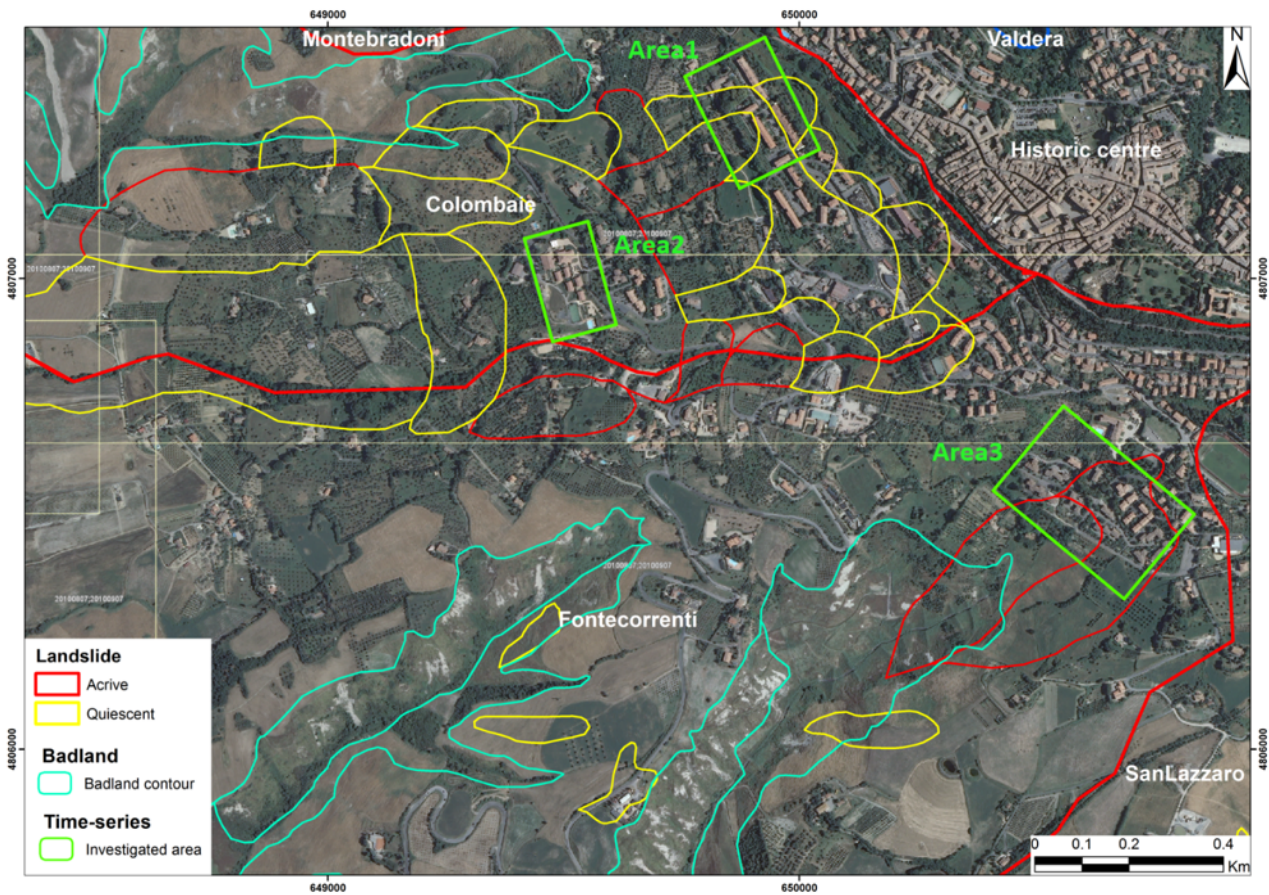


Fig. 5.53 - Study areas by means of the extraction of the time-series for each satellite that recorded data.

For the three areas, the ENVISAT PS time series were categorized according to the Berti et al. (2013) method. The analysis was conducted for the wall area (Fig. 5.54a) and subsequently also for the area of main interest (Fig. 5.54b). Important differences were recorded between the percentage of distribution of the classes of Berti et al. (2013), in both ascending and descending orbits. This is due to the considerable effect of the several stable points on the historical centre of Volterra resulting, according the used method, categorized as *uncorrelated* because not showing any trend. In fact, the percentage of the PS time series for this category in both descending and ascending decreases from 69.8% to 13.8% and from 76.9% to 49%, respectively, while the *linear* classes increase in both orbit from 20.8% to 71.0% in descending and from 19.4% to 47% in ascending. The other ranks, *quadratic*, *bilinear*, *discontinuous with constant velocity* and *discontinuous with variable velocity*, in ascending and descending varies too, but with no significant changes.

It is interesting noticing as quite all the time series recorded in Area2 and Area3 by ENVISAT sensors are linear, so with a constant trend.

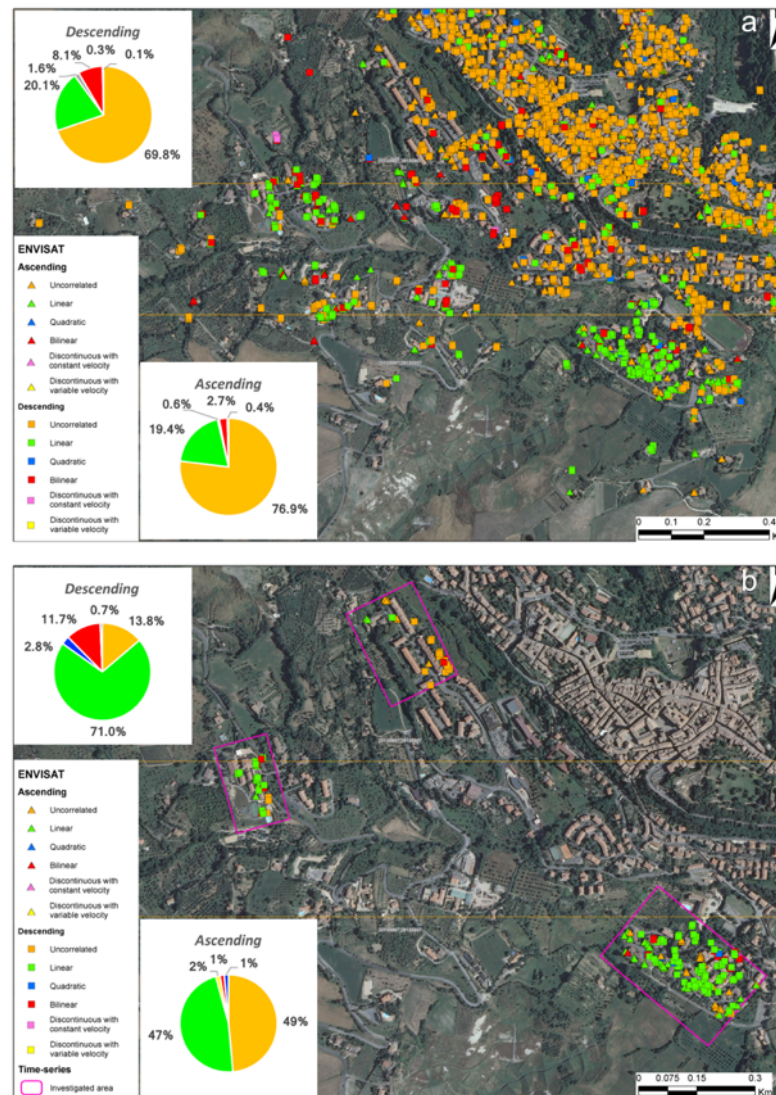


Fig. 5.54 - Categorization of the ENVISAT ascending and descending PS time series of the whole southwester sector of Volterra town (a) and for the three area of interest (b).

The same type of analysis was conducted for the COSMO-SkyMed time series for the whole southwestern sector (Fig. 5.55a) and for the three areas of major interest (Fig. 5.55b) too. As for the investigation covering the period 2003-2010, the time series recorded on the centre of Volterra town by the COSMO-SkyMed constellation for the period 2012-2015 are categorized as *uncorrelated* due to them stability in both ascending and descending orbit. For this reason, the major part of the PS time series (58.3% in descending and 58.2% in ascending geometries) falls down in this class, while only the 1% and 16.1%, respectively, considering only the three areas of interest. The *linear* class shows, both in descending and ascending orbits, frequencies with similar values indifferently from the area of the investigation (from 26.9% to 32% and from 22.1% to 27.2%, respectively). Important differences are recognizable comparing the percentage of the

quadratic categories for the entire southwester sector of the Volterra municipality and analysing only the areas where buildings with more damage were recorded: this class increase in descending from 6.4% to 38% and in ascending from 10.1% to 33.2%. The same behaviour is recorded for the *bilinear* rank showing an increment in descending from 8.0% to 26% and in ascending from 9.1% to 22.8%. About the other classes, *discontinuous with constant velocity* and *discontinuous with variable velocity*, no important variations were visible.

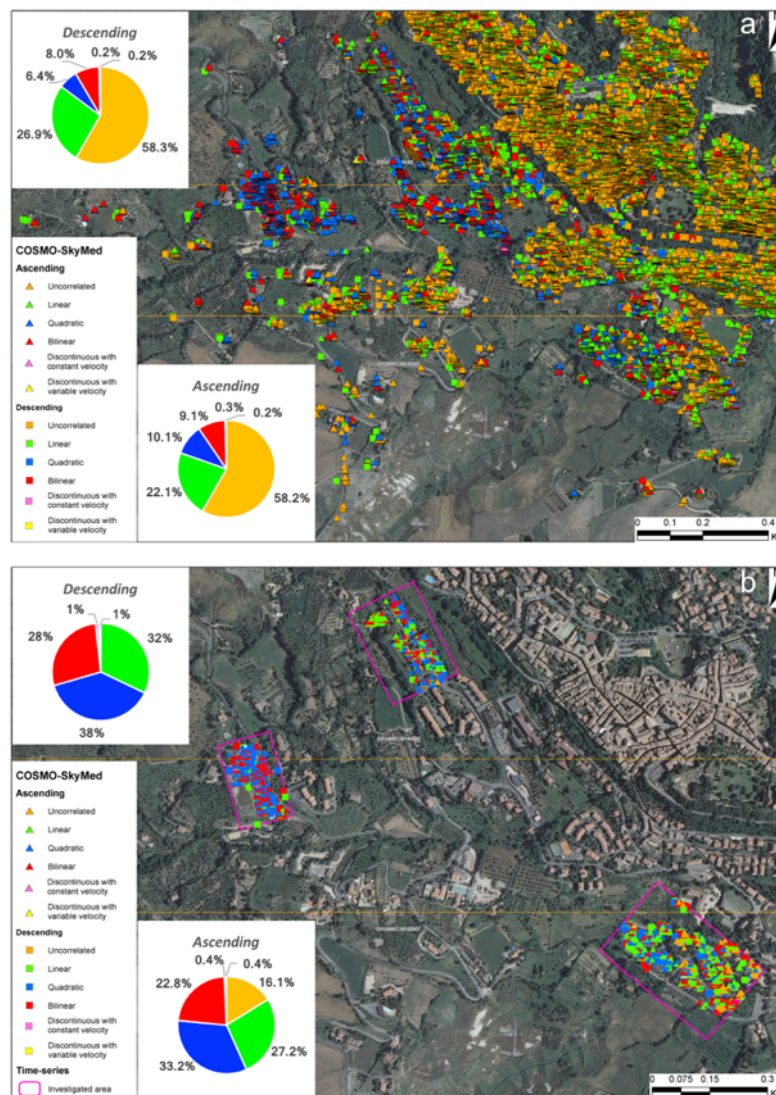


Fig. 5.55 - Classification of the COSMO-SkyMed ascending and descending PS time series of the whole southwester sector of Volterra town (a) and for the three area of interest (b).

For the three areas with constructions affected by damage, a sample time series representing them was shown. To better interpreted the displacement occurred, the time series were deperated by the region trend according to the Notti et al. (2015) approach and for each one are shown the original trend, the regional

trend and the corrected time series.

Area1 is in the crown of important a big landslide and some shallow landslides affecting the slope causing important damage to numerous constructions. The buildings of this area were built during the '80s except for two of them. This makes meaningful analyses made by PS and the time-series extracted for of all sensors from the constructions on this zone given that the time period covered by the ERS1/2, ENVISAT and COSMO-SkyMed sensors is quite comparable with the age of them. The data recorded in descending geometry show instability for the entire investigated period from 1992 to 2013 with a consequent increment of dimensions of the involved region. The ERS (**Fig. 5.56a**) and the CSK (**Fig. 5.56b**) data show an important trend moving away from the sensors and a low regional trend to confirm the reliability of the time series. Despite the time series of ENVISAT data are very noisy a trend in accord to that of ERS and CSK is recognizable.

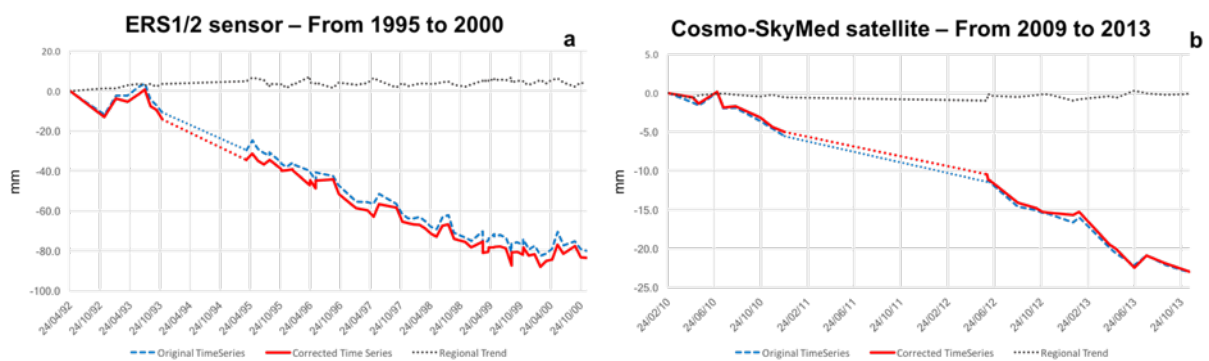


Fig. 5.56 - Sample of time-series of ERS (a) and COSMO-SkyMed (b) sensors acquired in the *Area1*.

Area2 was chosen sited downhill with respect to *Area1*, inside a landslide complex. In this portion, several buildings are affected by different grades of damage and the investigation, made by means of the time-series covers the period between 1992 and 2013. All investigated constructions in this area were built in 2003, even if the few points previously acquired by C-band of ERS1/2 satellites (**Fig. 5.57**) already shown displacement not influenced by the regional trend. Comparing the time series of this area with that of *Area1*, it is possible noticing the increment of displacement affecting the constructions of *Area2*. The difference can be ascribable to the combination of the displacement caused by the landslide activity with the local shallow movements.

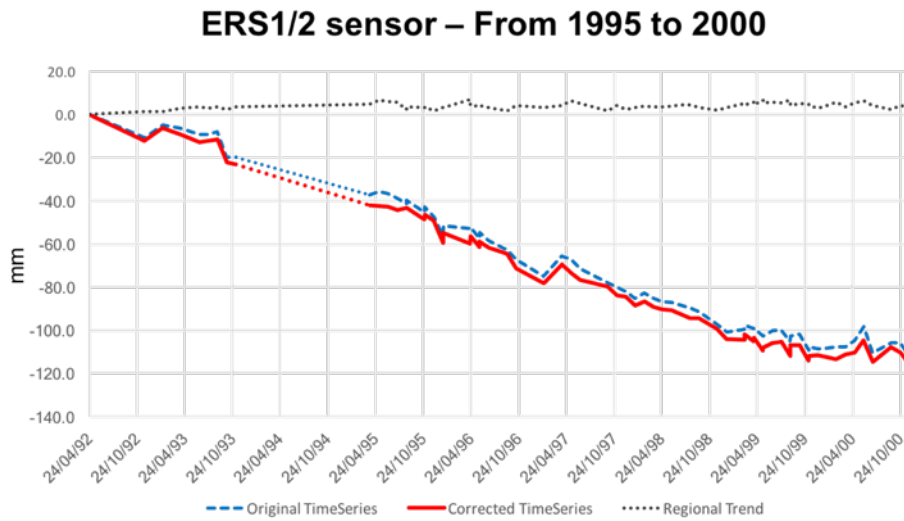


Fig. 5.57 - Sample time-series of ERS data reflecting the situation of the Area2.

From 2002 to 2010 and between 2010 and 2013 the PS number increased due to the anthropic constructions. The time-series of ENVISAT (Fig. 5.58b) and COSMO-SkyMed (Fig. 5.58c) respectively, exhibit a continuous moving away from the satellite, even if the ENVISAT data result to be noisy also corrected by the regional trend (Notti et al., 2015). Comparing the data with those recorded in the crown of Area1, also ENVISAT and COSMO-SkyMed PS show displacement bigger.

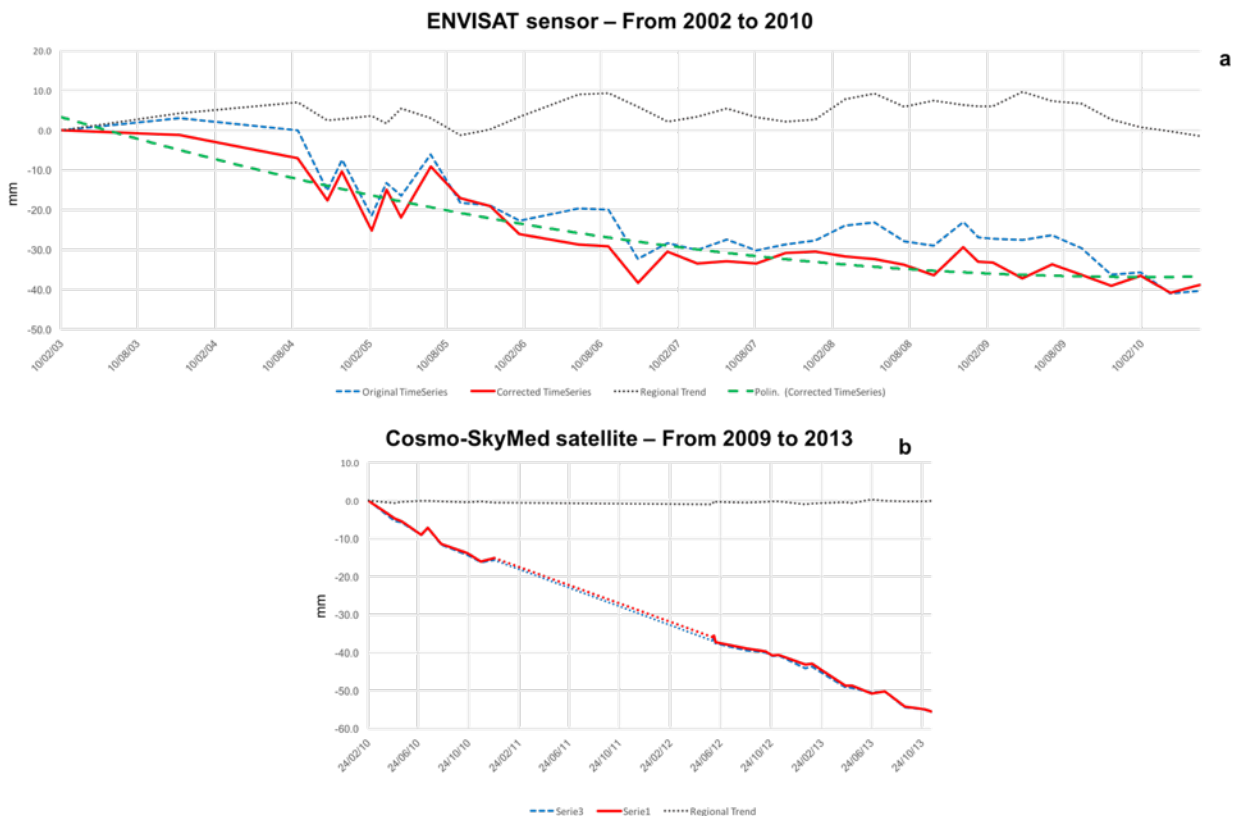


Fig. 5.58 - Sample of time-series of ENVISAT (a) and COSMO-SkyMed (b) data of the Area2.

In *Fontecorrenti* sector only *Area3* were separately investigate due to the less number and little dimension of the landslides affecting this region. Several buildings, erected in the '70s in brick, are partially located in the crown of a landslide affecting the upper part of the sector. The constructions of the study area reflected for all sensors allowing the acquisition of the data from 1992 to 2013. The sample ERS corrected time series recorded on the structure (**Fig. 5.59**) shows displacements reaching 50 mm in ten years.

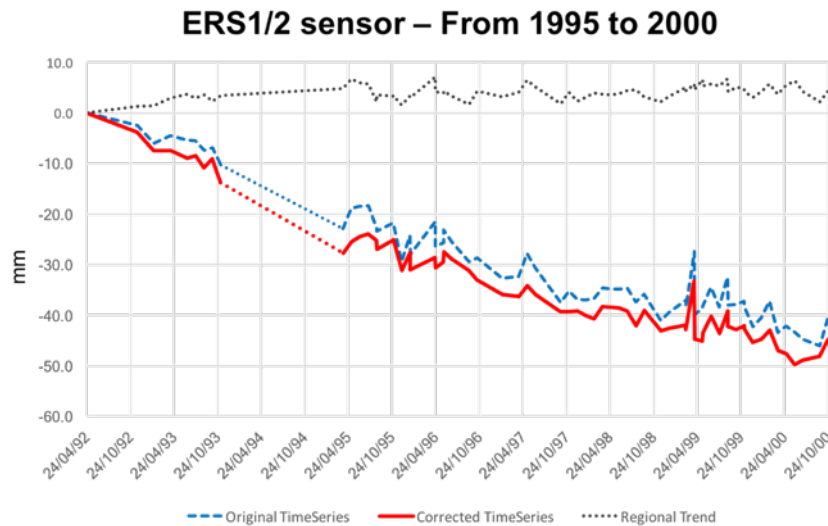


Fig. 5.59 - Sample of time-serieses of ERS sensor acquired in *Area3* in *Fontecorrenti* sector.

Despite the constructions in *Area3* are not all affected by damage, ENVISAT (**Fig. 5.60a**), even if also in this case noisy, and COSMO-SkyMed (**Fig. 5.60b**) time series confirm the continuous movement away from the satellite. Also in this case the investigated time series were subjected to the Notti et al. (2015) approach in order to analyse the trend depurated to the regional trend.

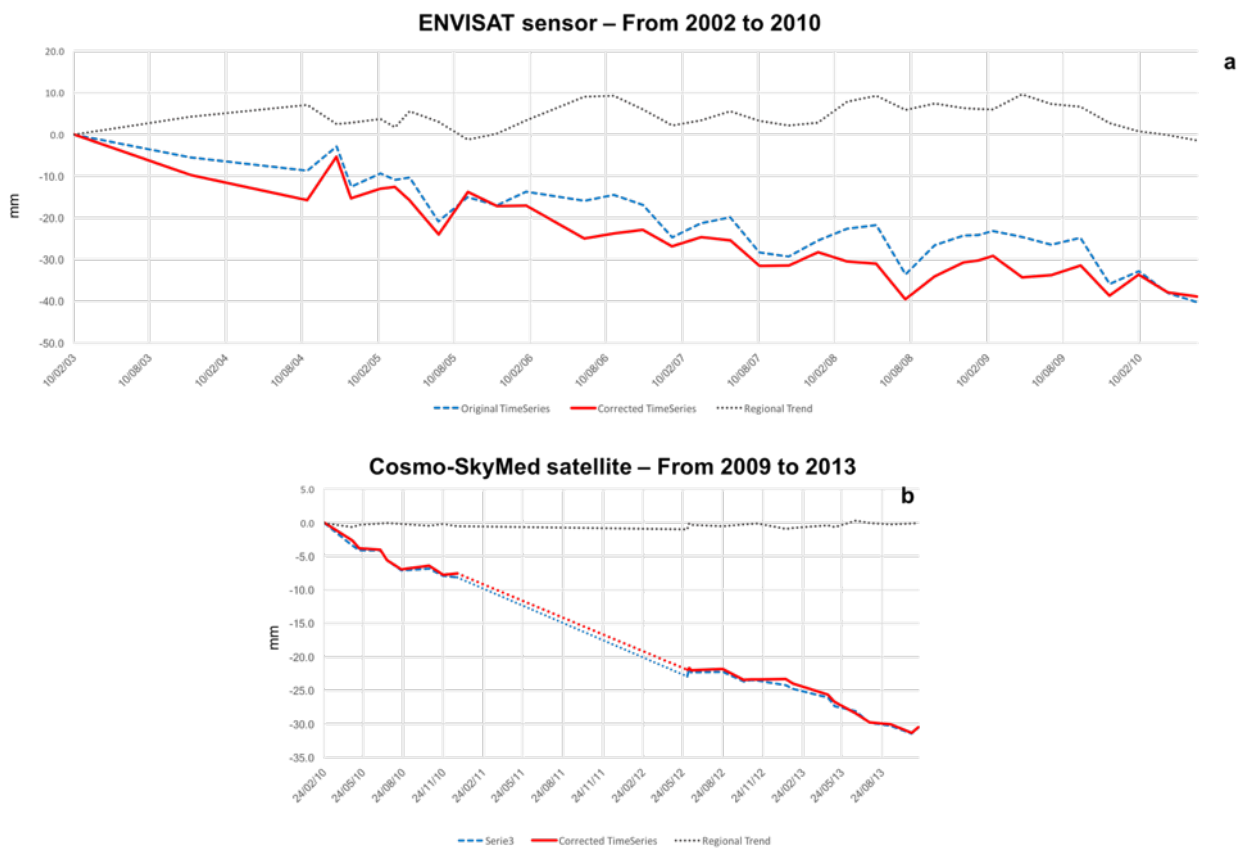


Fig. 5.60 - Sample of the time-series of ENVISAT (a) and COSMO-SkyMed (b) data of Area3.

The ascending data, showing the displacement moving toward the sensors, confirm the recorded movements. Furthermore, the ascending data acquired by COSMO-SkyMed were registered since 2015 instead of 2013, and show a similar trend of movement of that displayed above by the sample time-series.

5.3.2 Damage classification of buildings

The displacement affecting the southwestern sector of Volterra caused damage on several constructions. The damage, related to the differential movement of the slope due to several shallow slope-movements (Bianchini et al., 2015b), are mainly concentrated in areas located in the crown of two big landslides and one inside of the big slope-movement affecting *Le Colombaie* sector. In the Volterra case study only buildings were classified because facilities did not show important damage to be categorized. The only exception was the collapse of a part of the walls enclosing Volterra town (Pratesi et al., 2015) not due to a landslide, therefore it was not considered in the following damage classification maps. The field investigations were performed in order to individuate the damage affecting constructions in *Le Colombaie* and *Fontecorrenti* sectors for categorizing them by means of one recent proposed damage classification (Cooper, 2008) and the new developed ranking during the PhD thesis (Del Soldato et al., under review_b). As mentioned before in *Le Colombaie* sector, several constructions are recent and localized into areas affected by active or quiescent

landslides (**Fig. 5.61a**). *Fontecorrenti* area was partially urbanized already in the '60s, but the constructions sited in the upper part of the active landslide affecting this sector was realized in the '80s (**Fig. 5.61b**).

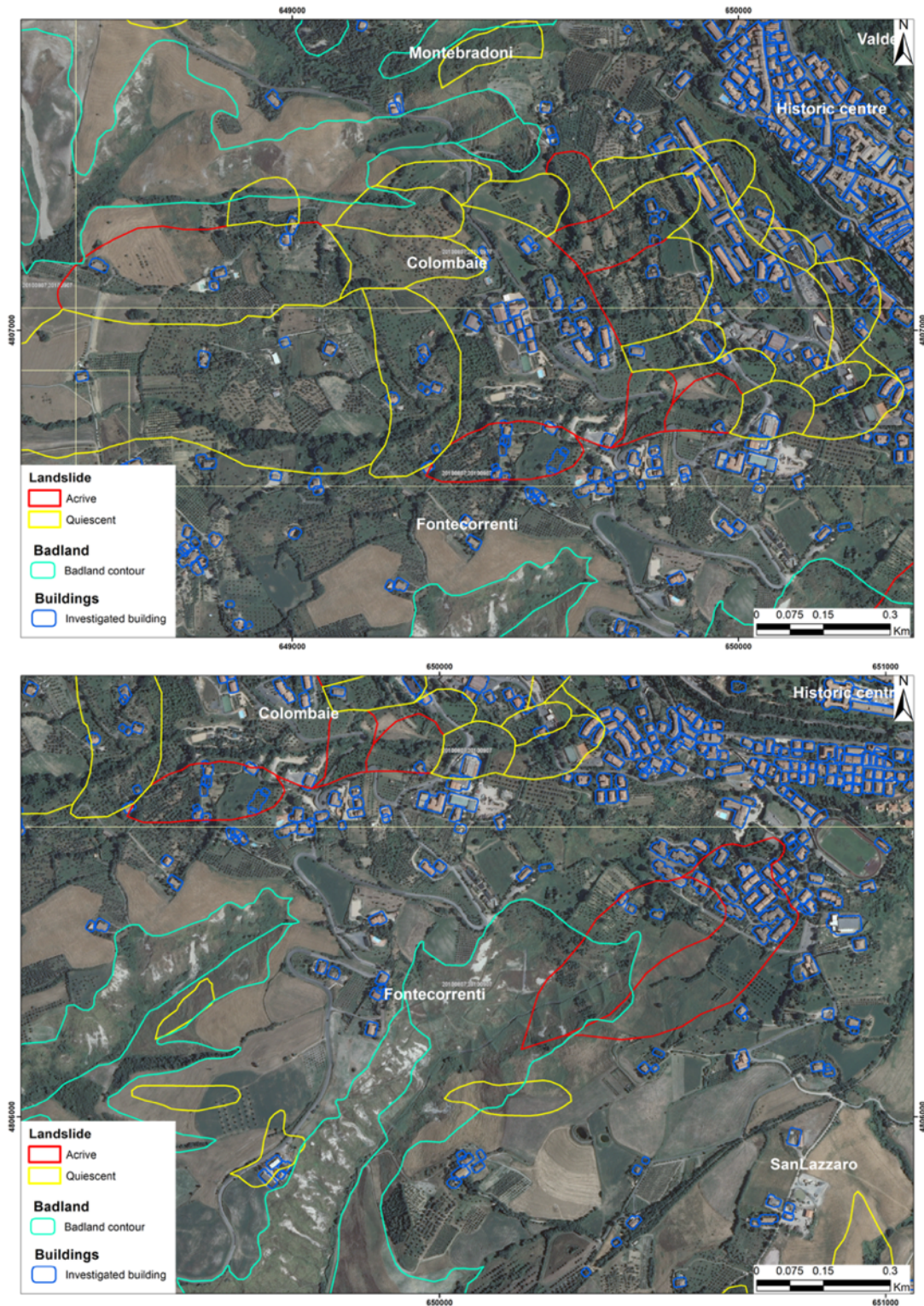


Fig. 5.61 - Le Colombaie (a) and Fontecorrenti sectors with the investigated buildings, the landslide and the badlands contours.

In these urban regions, little damage, as fine plaster cracks, were generally quickly restored, differently for the more rural territory of the Agnone landslide (CL-PO landslide). In the surveyed sectors rarely weak or negligible damage (red arrows in **Fig. 5.62a**) and some constructions with important cracks (red arrows in **Fig. 5.62a, b** and **c**) and tilting (blue arrows in **Fig. 5.62**) were recognized.



Fig. 5.62 - Different types of damage (red and blue arrows) recognized during field surveys on buildings in the southwestern sector of Volterra. a) plaster cracks restored; b) weak and moderate fractures on plaster; c) numerous severe fractures; d) important cracks plunging about 45° and open fractures between the two structures; e) important tilting between two parts of the same buildings.

During the field surveys the recording scheme suggested in the new developed approach (**Fig. 5.2**) was used to reveal damage affecting the buildings of the study area (an example in **Fig. 5.63** of a building sited close to the *Area3*). The use of this scheme, as mentioned before, was useful to survey different damage, cracks, fractures and tilting affecting a construction to categorize their severity singularly and, in a second moment, to assess their effect on the entire construction.



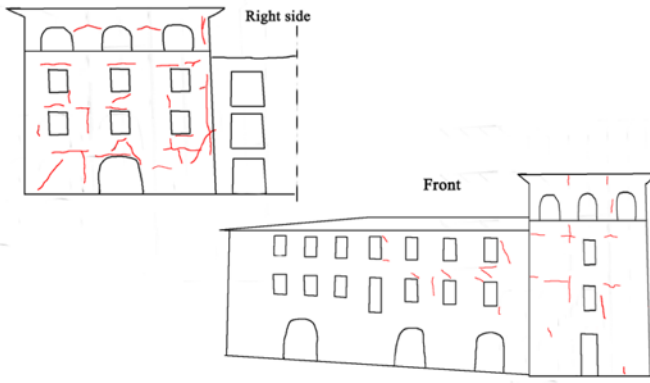
DAMAGE RECORDING SCHEME						
Data	16	october	2016	ID	Build 20	1369/1370
Site	Via di Fontecorrenti, 2			Corners coordinates		
Municipality	Volterra	Prov.	PI	X	Y	Z
Type of construction	Building			N		
Load-bearing material	Concrete			E		
Date of construction	2004			S		
Floors	3/4	Position respect to the landslide			Landslide Crown	
				Thin and open vertical, horizontal and diagonal cracks; local crushing with or without losing of material; fissure and cracks in plaster and intersection of walls; distortion of services; unstable wedge and bended or collapse roof; open and thin crack between the wall and sidewalk; open (sometimes filled) and thin parallel and perpendicular cracks in horizontal structures; propagation of landslide crown; minor or major scarps; fractures and thin fissure in ground surfaces; piece of structure fall along the scarp		
Description and sketch of the damage				Extension of the damage		
				G0	G1	G2
				G3	G4	G5
				< 1/3		X
				1/3 < damage < 2/3		
				> 2/3	X	
						
Observations: The right side shows some visible damages and the back façade was no accessible. Pictures shot: P1100149 - P1100150 - DMG211016151651 - DMG211016151646						



Fig. 5.63 - Sample of the recording scheme (Del Soldato et al., under review_b) compiled (a), with two images (b and c) of the investigated buildings, used for the recognition of the damage affecting the several surveyed structures in the southwestern sector of Volterra.

Quite all constructions of both *Le colombaie* and *Fontecorrenti* sectors, except for some isolated structure, were categorized (Fig. 5.64) based on the damage recorded on them during several field surveys. According to Cooper (2008) buildings on which damage recognized were mainly categorized in *Class 2* and *Class 3*. Only three buildings were classified in *Class 5*, rank reflecting important damage. The major part of the buildings is not affected by fractures and several negligible fine plaster cracks are, with high probability, not related to the landslide movements, but to the weather conditions or to the age of the structures.

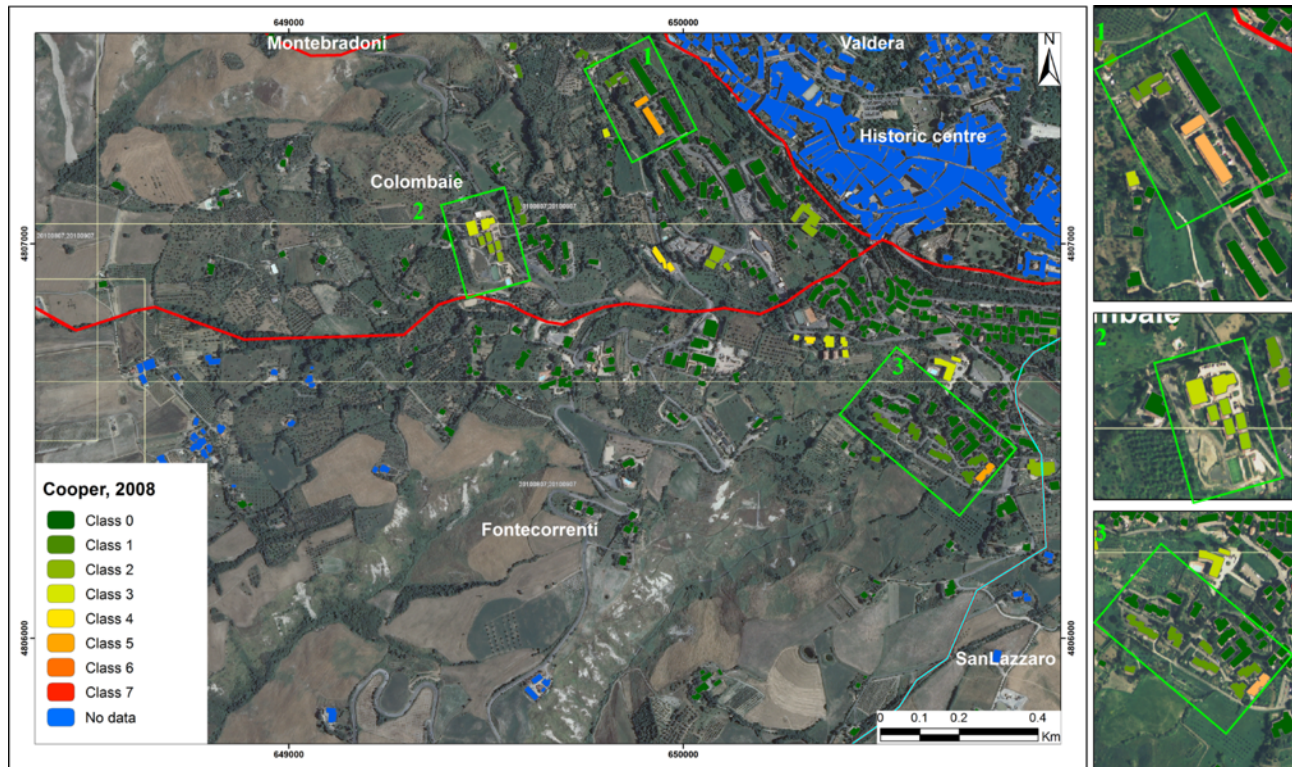


Fig. 5.64 - Classification of buildings damage according to Cooper (2008).

According to the approach developed during the thesis (Del Soldato et al., under review_b), the buildings classified by the surveyed damage were differentiated in more classes than in Cooper (2008) (Fig. 5.65). This ranking, not considering the collapse during the investigation and classification of the cracks, allows more possibility to categorize the low levels of damage affecting the structures. Comparing the classifications of Cooper (2008) and Del Soldato et al. (under review_b) it is possible pointing out the influence of this difference mainly for *Area2* and in *Area3*. These built up areas erected in the '80s, are affected by different levels of damage due to their position respect to the occurring shallow movements. It is worthy noticing that for both classifications, the constructions affected by important cracks (e.g. the two big buildings in *Area1* and the ones in the right of *Area3* or others structures sparse in the territory) were categorized as severely damaged.

To confirm the efficiency of the developed approach by Del Soldato et al. (under review_b) to rank better the difference of the damage on the structures, in *Area1* the two buildings were categorized differently (one in the "Potential collapse" and one in "Severe" classes), while Cooper (2008) ranked them both as "Class 5". The differentiation between the two structures is in accord with the legislative restrictions promulgated by the municipality administrators that decided to revoke the habitability for one of them.

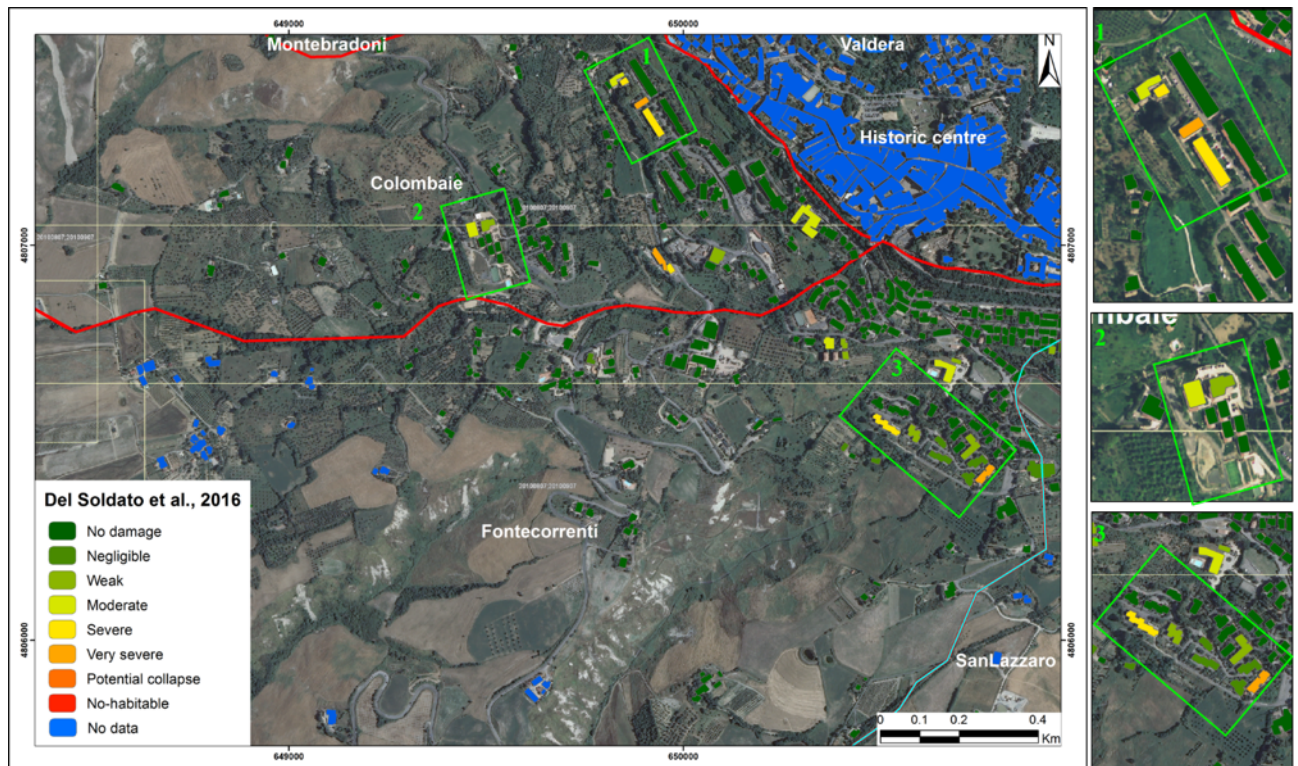


Fig. 5.65 - Classification of constructions damage according to Del Soldato et al. (under review_b).

Besides of the classification of the constructions through surveying recognizable damage, structures were categorized also taking advantage of the remote sensing techniques. The Persistent Scatterers gathered by ENVISAT and COSMO-SkyMed, elaborated by means of PSInSARTM and SqueeSARTM respectively, were used to classify structures according to their velocity measured along the Line of Sight (V_{LOS}) and the maximum displacement (D_{max}). Furthermore, velocity and displacement were reprojected along the local steepest slope, in order to homogenize the rates recorded by the ascending and the descending orbits (V_{slope} and D_{slope} , respectively).

The categorizations based on the V_{LOS} and D_{max} of the ENVISAT PS data were conducted separately for ascending and descending orbits. The ascending ENVISAT data allowed the categorization only for some construction of the southwestern sector by the V_{LOS} (Fig. 5.66a) and the D_{max} (Fig. 5.66b) parameters. The velocities recorded along the Line Of Sight show stability, assigned as for the PS data at ± 2 mm, for almost all the constructions where the PS were reflected, except for few constructions. In Area3 three constructions are affected by high velocity that could indicate the state of activity of the landslide, which causing damage during the period 2000 - 2010. The maximum displacement, showing high values to the construction in the Volterra town although is note that is stable (Bianchini et al., 2015b), it suggests that the noise revealed in the time-series create problems in the assessment of the maximum displacement affecting buildings.

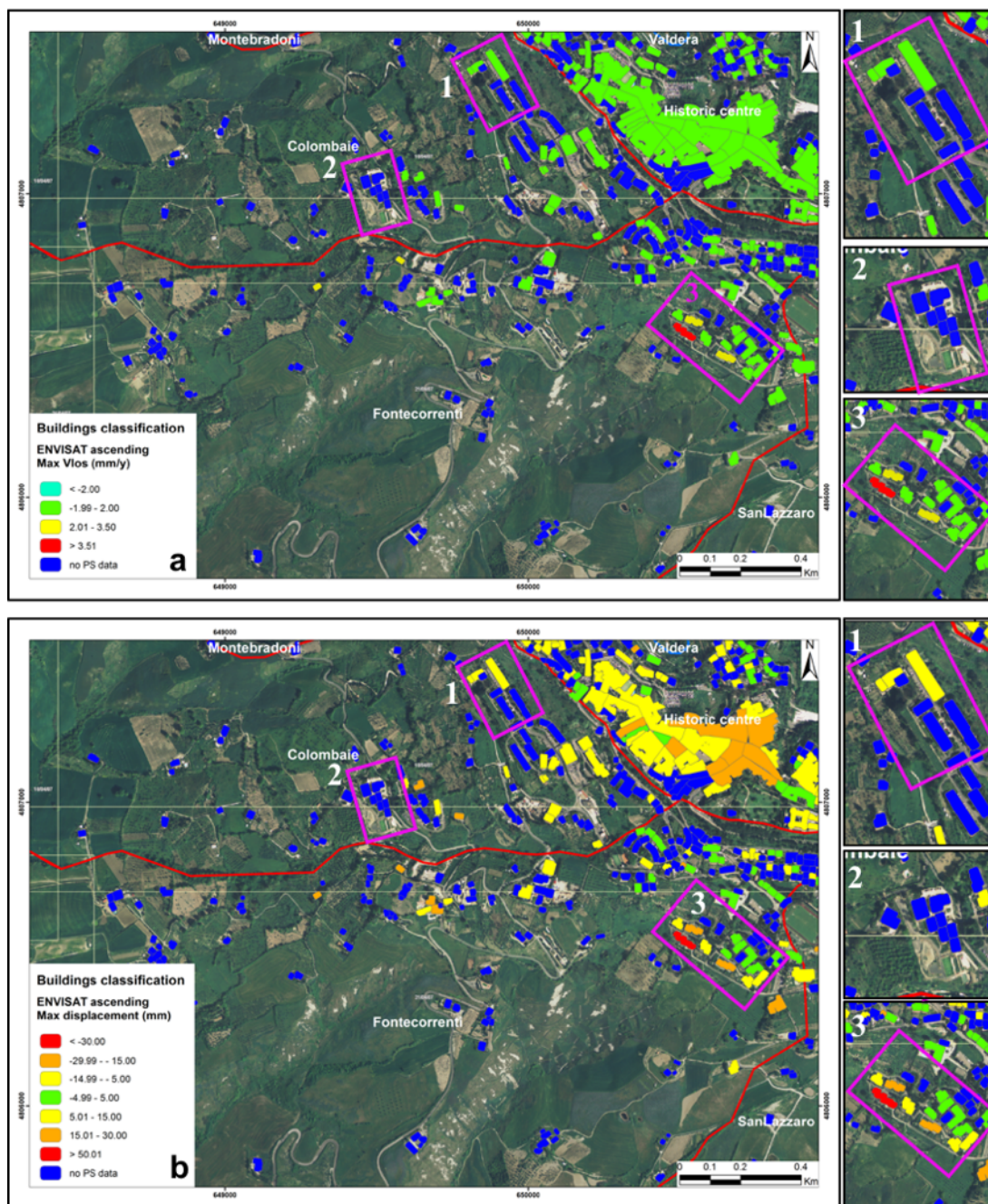


Fig. 5.66 - Buildings classifications based on the analysis of the velocity (a) and the maximum displacements (b) measured along the Line of Sight of the ascending orbit by ENVISAT sensors.

The descending orbit better allows recognizing the real values of the parameters affecting the slope due to its orientation. Investigating the PS recorded in this orbit, the categorization of the buildings reveal more structures affected by velocity (Fig. 5.67a). It is important noticing that the major part of the displacement affecting this area is identified for the Area3, as for the ascending geometry. Furthermore, some constructions showing high velocity are recognizable also in Area2 in Le Colombaie sector. About the maximum displacement (Fig. 5.67b), the map suggests, as for the above mentioned ascending data, that the noise create mistakes in the evaluation of the D_{max} recorded by ENVISAT sensor.

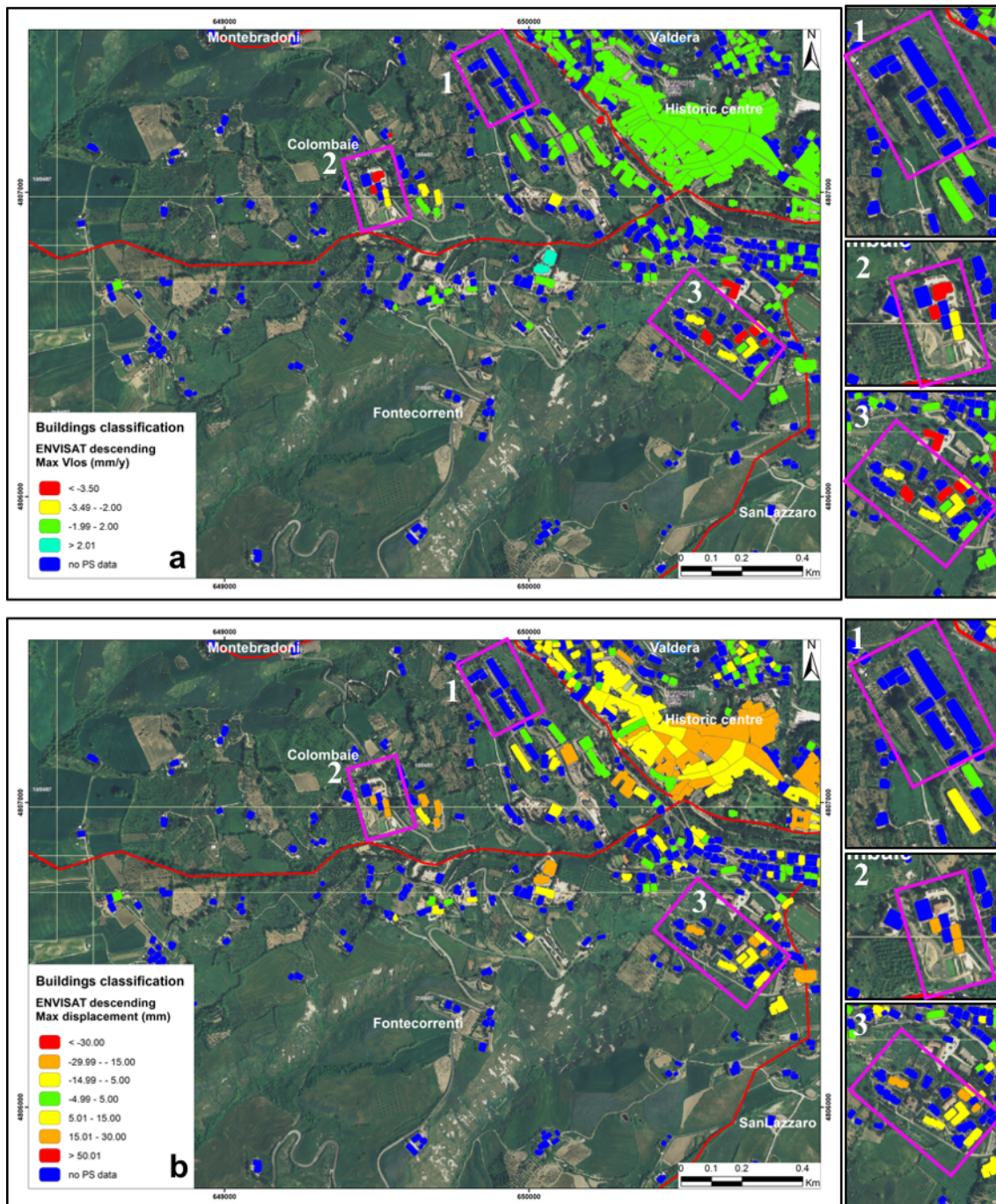


Fig. 5.67 - Buildings classifications conducted considering the velocity (a) and the maximum displacements (b) measured along the Line of Sight of the descending orbit by ENVISAT satellites.

The same analyses were made for the period 2010 - 2015 using the X-band data, by COSMO-SkyMed constellation. First of all, the applied modern technique (SqueeSARTM) to elaborate the raw data allowed to cover by the PS almost all the structures located in these study sectors. The colours used for the classification of structures were maintained the same, changes were made only the thresholds in accord to the improved

quality of the data that allowed to increase the precision of the investigation and to assign ± 1.5 mm as stability range.

The CSK data recorded in the ascending orbit (**Fig. 5.68a**) allows several considerations:

- *Area1*, no shows important velocities besides its location in the crown portion of landslides;
- in *Area2* important velocities were recorded along the LOS for the landslide involving the *Le Colombaie* sector;
- in *Fontecorrenti* region, the velocity recorded in correspondence to *Area3* indicates activity to the landslide affecting this zones;
- the cumulated displacements (**Fig. 5.68b**) acquired by the CSK sensors reflect the recorded velocity, but reveals also a strange displacement affecting the urban fabric of Volterra;

Some strangenesses are due to the intersection between the Line Of Sight of the satellite during its ascending orbit and the little NE dipping of the town of Volterra that create errors affecting the cumulated displacement. This is the reason why the buildings of Volterra town were classify affected by displacement, even if the stability of the city is known (Bianchini et al., 2015b; Pratesi et al., 2015).

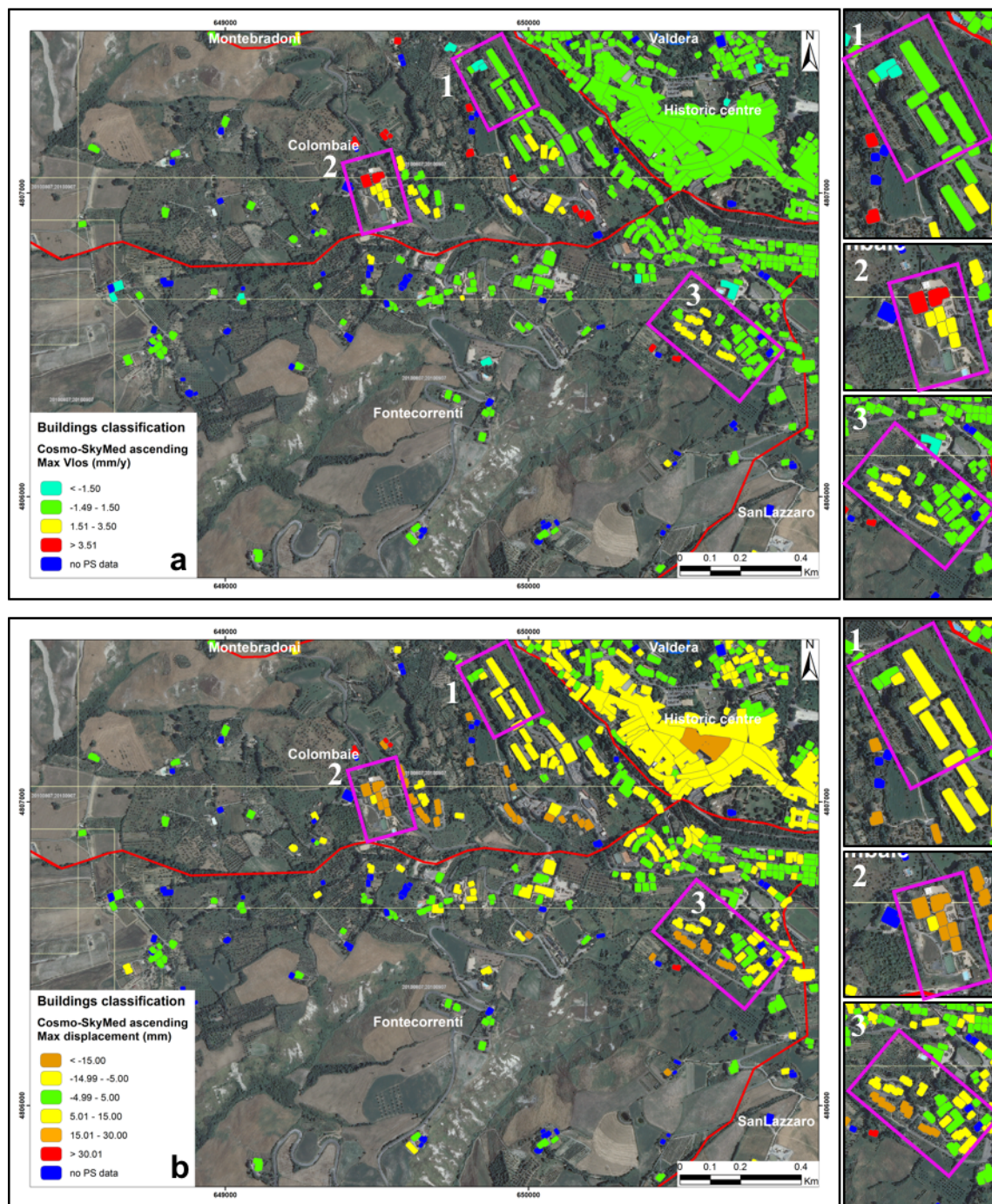


Fig. 5.68 - Structures categorization based on the velocity (a) and the maximum displacement (b) recorded along the Line of Sight of the ascending orbit of COSMO-SkyMed sensors.

The COSMO-SkyMed data of the descending orbit covers almost all the structure allowing to categorize them by means of the V_{LOS} (Fig. 5.69a) and the D_{max} (Fig. 5.69b) acquired along the Line Of Sight. This geometry is better than the ascending one to record interferometric parameters for the study area. For the three separate investigated areas the recorded velocity along the LOS confirmed the actual activity of the landslide. Some of the damaged buildings in Area1, are not covered by the PS, but all the region is affected

by moderate velocity and cumulated displacement. Furthermore, both velocity and cumulated displacement show the stability of the Volterra town, confirming the good quality of the data and the problems due to the inclination of Volterra town affecting the acquisition in the ascending geometry.

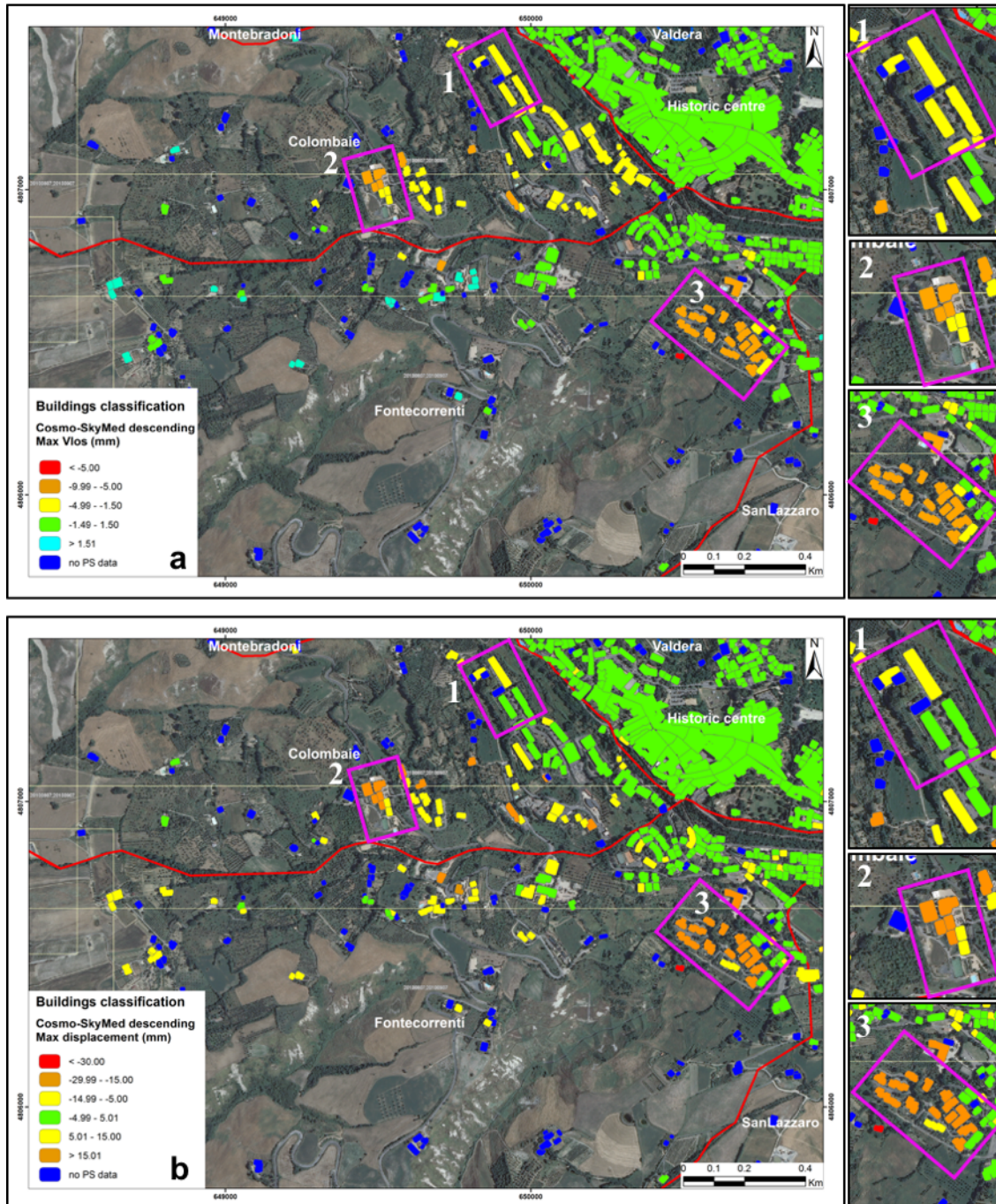


Fig. 5.69 - Buildings categorization according to the velocity (a) and the maximum displacement (b) measured along the Line of Sight of the descending geometry of COSMO-SkyMed constellation.

To combine ascending and descending data, in order to cover more buildings as possible, the velocity and the maximum displacement measured along the slope for each orbit were reprojected along the slope (Notti

et al., 2014). This procedure was done for both ENVISAT and COSMO-SkyMed data.

The ENVISAT data were sparse and even if the two orbits were combined, several buildings were not ranked. As for the velocity along the LOS, the V_{slope} values result reliable to classify constructions (**Fig. 5.70a**) showing important value of velocity for the three individuated areas, mainly for *Area2* and *Area3*, while only three buildings are covered by PS in *Area1*. It is important noticing the hotel built after 2000 close to *Area3* affected by high velocity due to its proximity to an active landslide. Other velocities are recognizable for spare structures close to landslides, partially quiescent and partially active, affecting *Le Colombaie* sector. Another important thing that have to be noted is the constructions in *Area2*, not revealing important damage, but characterized by high V_{slope} . They were built after 2003 then the velocity and the displacement measured for them in this period can be influenced by the construction phase of these buildings.

The same situation can be carried out analysing the classification map by the D_{slope} (**Fig. 5.70b**) even if the noise observed in the time-series have to be taken into consideration. In fact, almost all the buildings in the investigated three areas show important displacements. The same situation is recognizable for the hotel close to *Area3*. In spite of the ascending and the descending data were merged and the values for each structure averaged, the noise affecting all data did not allow to overpass the problems caused by the interference between the dipping of Volterra town and the LOS.

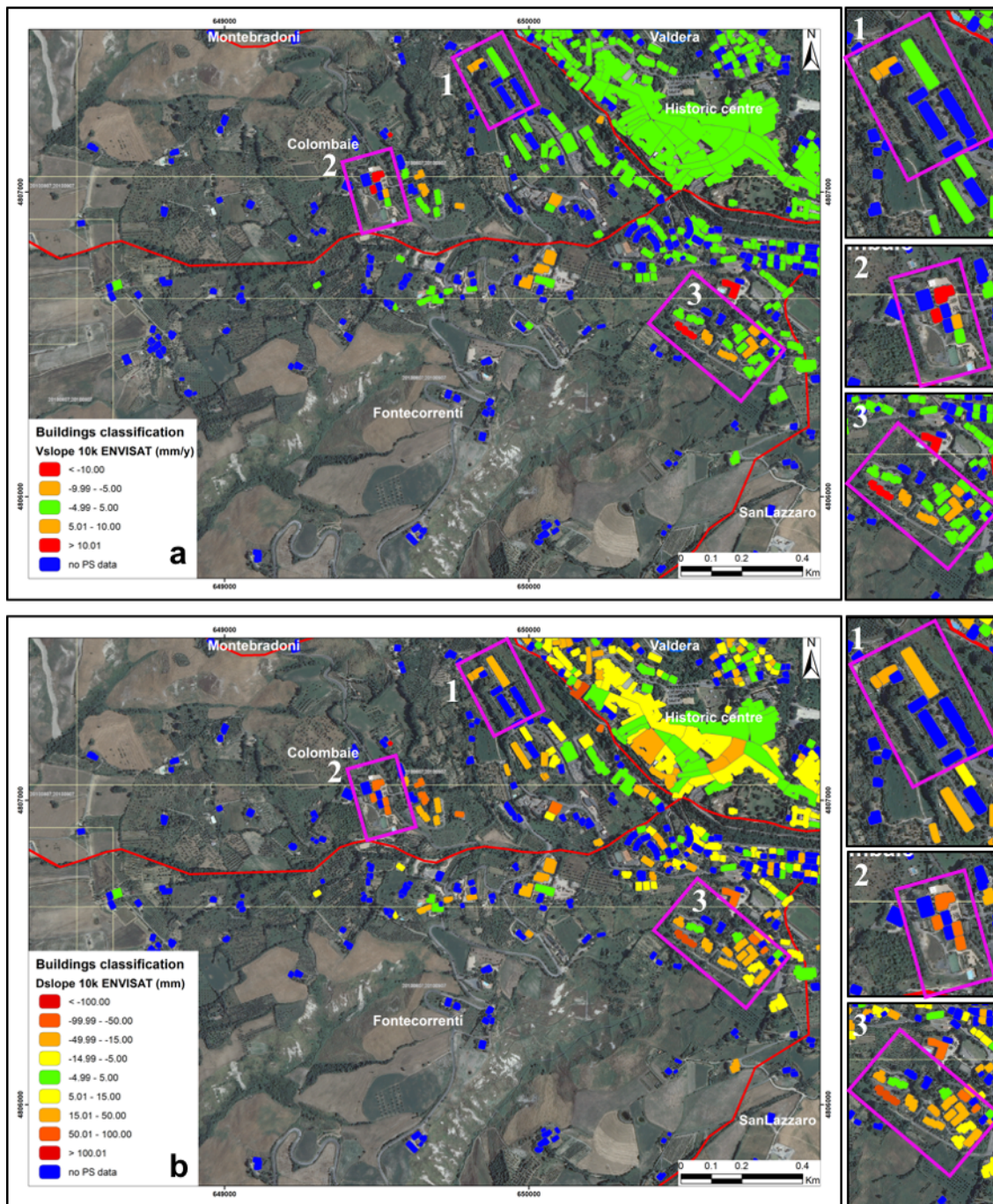


Fig. 5.70 - Building classification conducted by the velocity (a) and the maximum displacement (b) projected along the slope and averaged for each construction, acquired by ENVISAT sensors.

The same procedure was conducted to the COSMO-SkyMed data reprojecting the velocity and the maximum displacement along the slope. The result allowed classifying almost all the buildings of the two study sectors. Furthermore, the classifications obtained by both V_{slope} (Fig. 5.71a) and D_{slope} (Fig. 5.71b) showed the situation according to the mapped landslides. The buildings affected by damage in Area1 show moderate velocity, the other exhibits stability. This situation is due to a different lithology between the two series of parallels construction, one affected by displacement, the other one stable. The same is confirmed

also by the D_{slope} ranking and the high displacement measured for the construction built perpendicularly respect to the street. Concordance between the V_{slope} and the D_{slope} is recognizable also in Area2 and Area3, even if the damage surveyed on the buildings in these areas are not diffuse as the velocity and the cumulated displacement by the satellites.

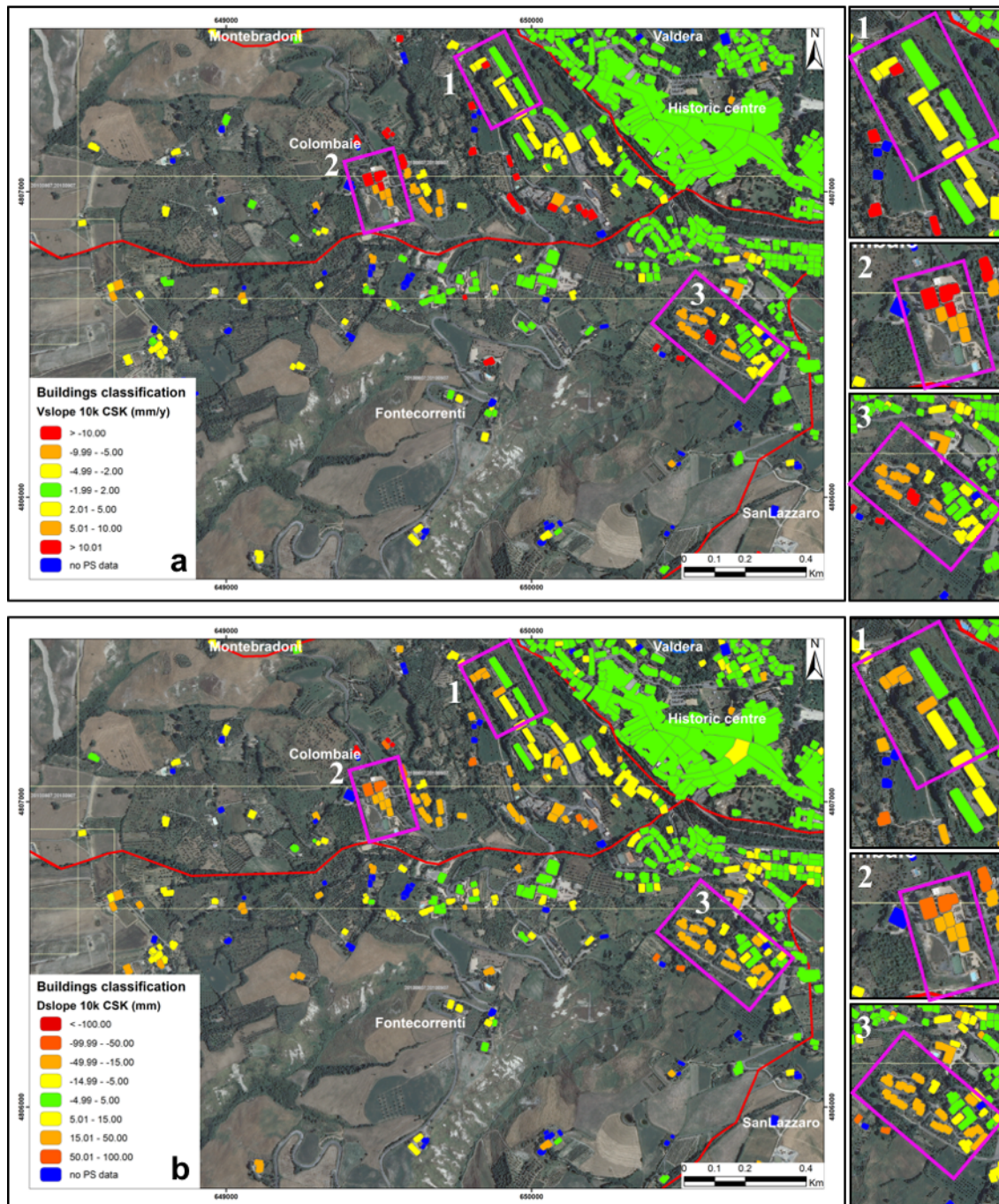


Fig. 5.71 - Constructions classification based on the velocity (a) and the maximum displacement (b) projected along the slope and averaged for each structure, acquired by COSMO-SkyMed satellite.

5.4 Relationship damage-displacement

Given that the main damage on structures in landslide-prone areas are due to the differential settlement, in this area the low presence of PS benchmarks for structures did not allow a detailed analysis. For this reason, a potential relationship between the damage on structures recorded by means of several surveys (**Fig. 5.2**), and the kinematic parameters for each entire construction gathered by ENVISAT and COSMO-SkyMed PS data was investigated. A correlation was searched by plotting the classification of the severity of damage affecting buildings and facilities, categorized by Cooper (2008) and Del Soldato et al. (under review_b) combined with velocity and cumulative ground displacement measured by ENVISAT and COSMO-SkyMed satellites. It is important to highlight that the analysis on displacement rates and on damage was performed for each whole building, paying attention to discriminate the landslide-induced damage from the other causes. Low velocities or displacements can provoke relevant damage on structures and facilities if they are affected by differential settlement, but in this case, due to the low number of PSs, the investigation was made to understand the behaviour of entire structures subject to displacements. The mean yearly velocity (V_{LOS}) and the maximum displacement (D_{max}) measured along the satellite Line Of Sight, maintained separated for ascending and descending geometries, and velocity and cumulated displacement reprojected along the local steepest slope (V_{slope} and D_{slope} , respectively) were used. These last parameters, being a value projected along the slope direction, were plotted using the absolute values to look for a relation, assuming that the detected movements cannot be upwards with respect to the slope.

The first analyses were conducted for structures surveyed in the surrounding area of the CL-PO landslide, in the Agnone municipality (Molise region, central Italy), involving the average values of V_{LOS} and D_{max} of ENVISAT PS acquired in ascending geometry backscattered by each structure. These values do not show a clear correlation combined with the ranking of damage neither according to Cooper (2008) nor to Del Soldato et al. (under review_b) (**Fig. 5.72**). The same investigation was impossible to conduct for descending data because the velocity and the maximum displacement were recorded for few facilities, only for seven structures.

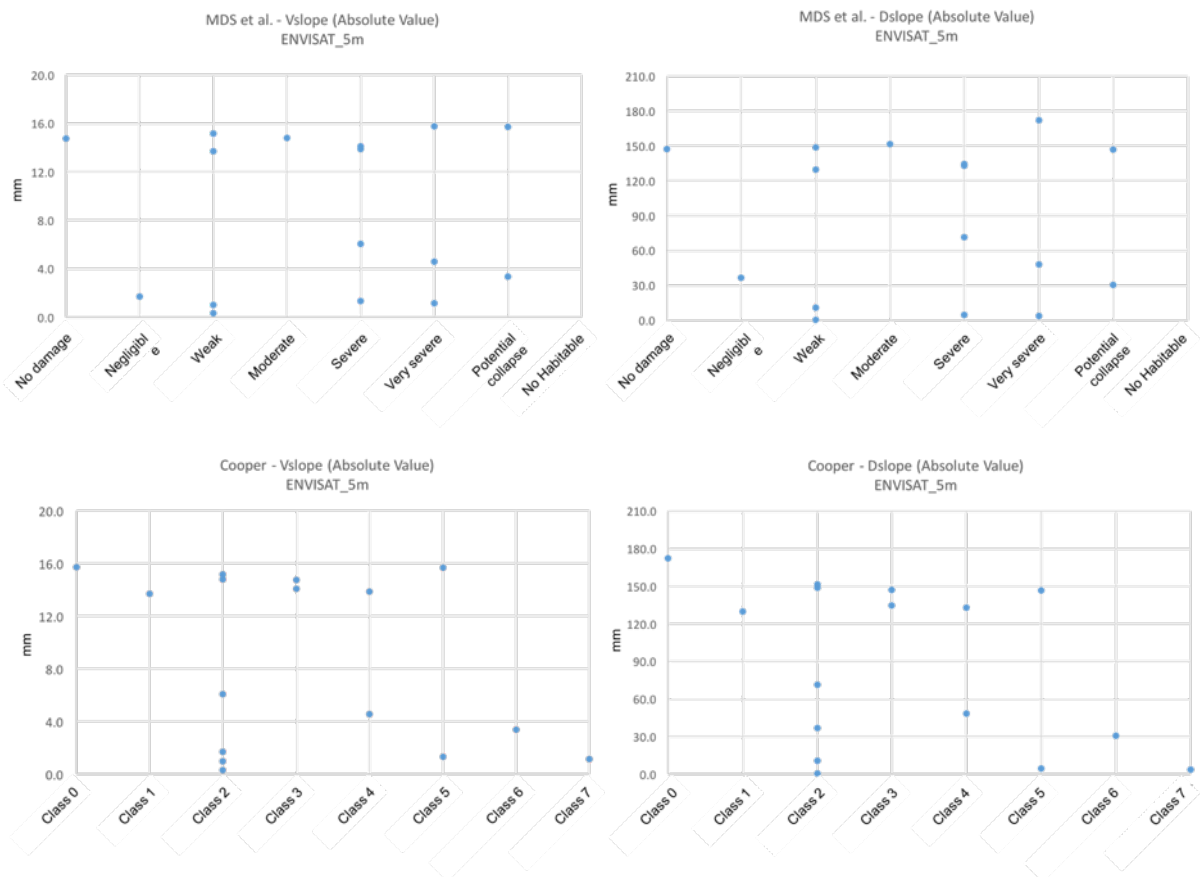


Fig. 5.72 - Graphs between the values of velocity and maximum displacement acquired along the Line Of Sight in the ascending orbit of the ENVISAT sensors and the damage classification of buildings made by Cooper (2008) and Del Soldato et al. (under review_b) for the CL-PO in Agnone.

To improve the number of the investigated facilities, ascending and descending data were combined by means of the reprojection, to look for a relationship between V_{slope} and D_{slope} and the damage levels ranked by Cooper (2008) and Del Soldato et al. (under review_b). The analyses were conducted for both reprojecton made by the use of 5-m and 10-m cell resolution DEMs, in order to verify the suggestion of Notti et al. (2014) regarding to this procedure.

The analyses of the V_{slope} and the D_{slope} data by the ENVISAT sensor, projected by the use of the DEM with high resolution, were plotted in absolute values on a graph with the classes of damage detected by Cooper (2008) and Del Soldato et al. (under review_b). No relations were detected, but different velocity rates were recorded on structures with low and high level of damage, indifferently (Fig. 5.73).

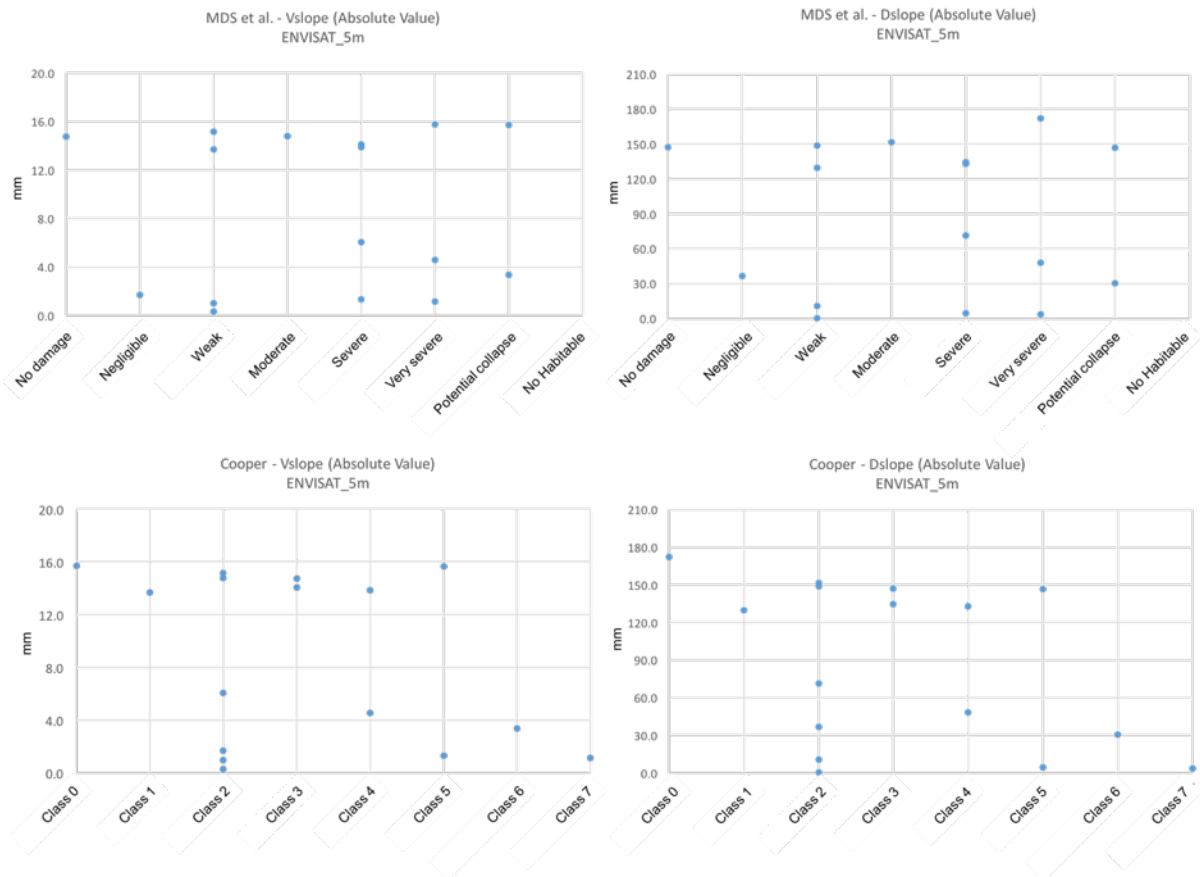


Fig. 5.73 - Plots of values of the velocity and the maximum displacement reprojected, using a 5-m cell resolution DEM, along the slope recorded by ENVISAT satellites respect to the facilities damage ranks by Cooper (2008) and Del Soldato et al. (under review_b) for the CL-PO in Agnone.

In Fig. 5.74 the absolute values of V_{slope} and D_{slope} acquired by ENVISAT satellites, reprojected calculating the C factor for the DEM with low resolution (10-m cell resolution), were combined with the raking of damage levels revealed by Cooper (2008) and Del Soldato et al. (under review_b) classifications. As for the V_{slope} and D_{slope} calculated by using the 5-m cell resolution DEM, no relationships or correlations were recognized also for V_{slope} and D_{slope} , using the reprojection conducted on a 10-m cell resolution DEM. This happened for both categorization approaches of Cooper (2008) and Del Soldato et al. (under review_b).

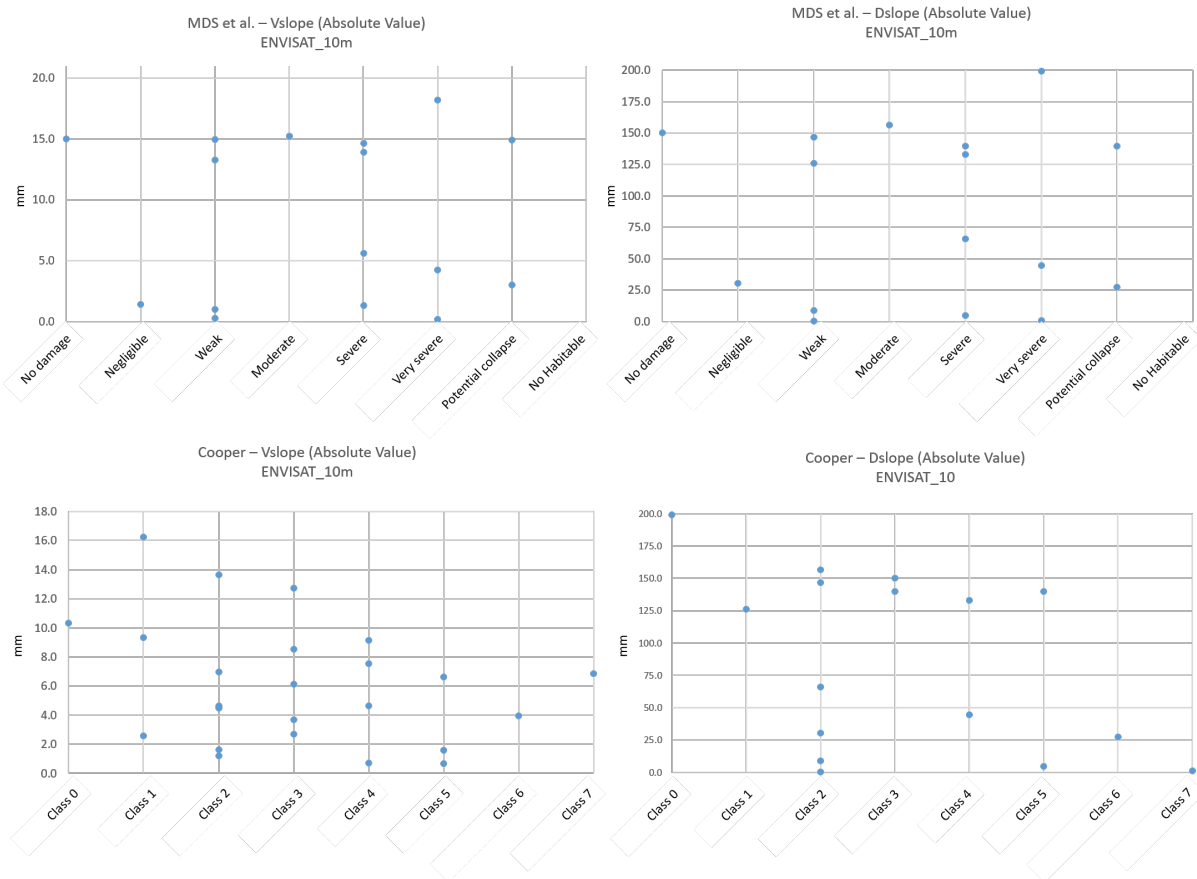


Fig. 5.74 - Graphs showing the values of velocity and maximum displacement measured by ENVISAT satellites and reprojected along the slope using a 10-m cell resolution DEM, combined to facilities damage ranked by Cooper (2008) and Del Soldato et al. (under review_b) for CL-PO in Agnone.

The same analyses, considering V_{LOS} and D_{max} measured along the Line Of Sight for both geometries separately, as well as V_{slope} and D_{slope} acquired by COSMO-SkyMed constellation, combined to the damage ranks of buildings, were conducted. These sensors, working in X-band, allowed to investigate more structures by means of a better PSs distribution and precision of the assessed velocity and displacement than C-band.

Velocity and cumulated displacement measured along the ascending Line Of Sight were plotted in combination with the categorized damage ranks by Cooper (2008) and Del Soldato et al. (under review_b) (Fig. 5.75) no revealing evident relations, as for the ENVISAT data. No alignments of the plotted points are recognizable, in all graphs the point are plotted sparsely or without meaningful clear dispositions.

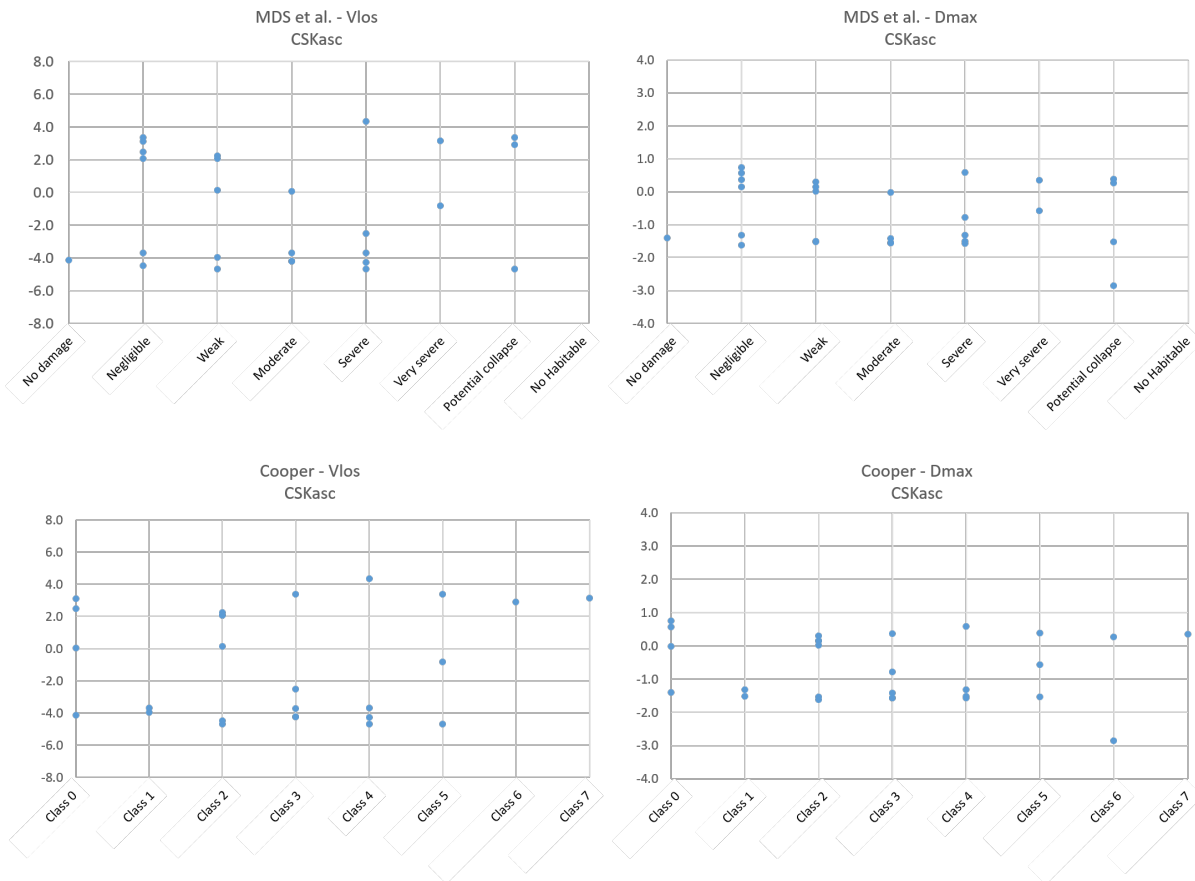


Fig. 5.75 - Graphs showing the values of velocity and maximum displacement acquired along the LOS in the ascending orbit of COSMO-SkyMed constellation related to the damage classification of buildings conducted by Cooper (2008) and Del Soldato et al. (under review_b) for CL-PO in Agnone.

The investigation on the data recorded along the descending orbit of COSMO-SkyMed, even if few with respect to the ascending, was conducted no exhibiting correlation by plotting them in a damage classes - V_{los} or D_{max} graphs. Moreover, the points are too scattered and few to be meaningful (Fig. 5.76) for assess a relationship. Furthermore, in both graphs of ascending and descending data, high values of velocity along the LOS for each rank of damage was exhibited.

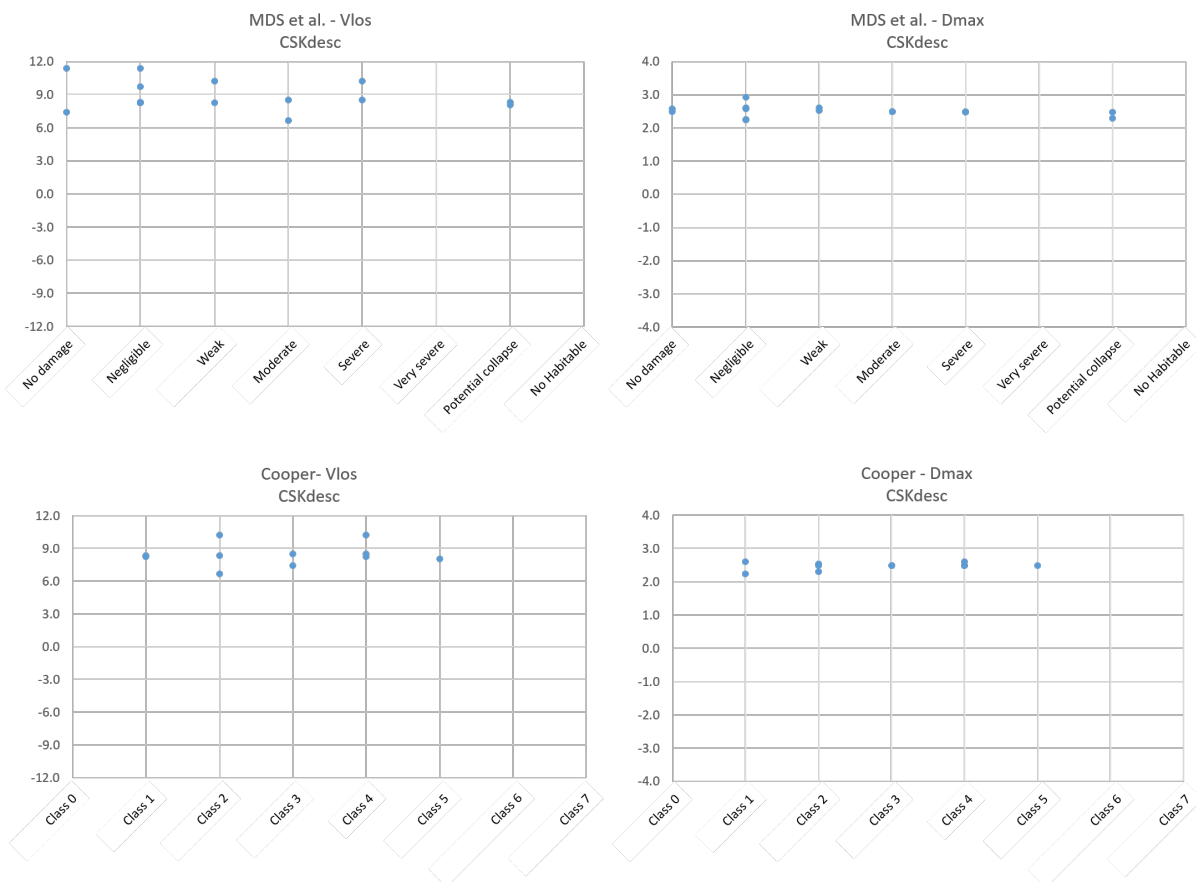


Fig. 5.76 - Plots of the values of velocity and maximum displacement acquired along the Line Of Sight in the descending orbit by COSMO-SkyMed satellites and the classes of damage recorded on buildings classified by the approach of Cooper (2008) and Del Soldato et al. (under review_b).

The low number of buildings and facilities in the landslide area of Colle Lapponi - Piano Ovetta, combined with the difficulty to extract several PS due to few reflectors and high density of vegetation also using the X-band, push likewise in this case to combine the data by means of the reprojection of velocity and maximum displacement along the slope. The investigation between remote sensing parameters, V_{slope} and D_{slope} values reprojected by means both 5-m and 10-m cell resolutions DEMs, with respect to the damage levels recorded by Cooper (2008) and Del Soldato et al. (under review_b), were made. Differently from that occurred for ENVISAT data, using COSMO-SkyMed data, the reprojection made with both DEMs gave back good results. Using the 5-m cell resolution DEM to reproject, a possible correlation between the damage categorised by Del Soldato et al. (under review_b) and the highest absolute values of V_{slope} and D_{slope} is visible (Fig. 5.77). Upper envelopes between the maximum V_{slope} (α in Fig. 5.77) or the cumulated D_{slope} (β in Fig. 5.77) and the damage classes were identified.

The highest detected values of damage for each class describe a regression line with respect to the absolute values of V_{slope} and D_{slope} . This observation means that structures with the same deformation velocity

do not show an equivalent damage degree, therefore the differential ground movements affecting them cause different effects on structures, depending on several factors, e.g. typology, age of construction, type of foundation. Structures falling close to the regression line are characterized by important damage caused by compact displacement, while construction that are under the envelope are featured by different effect of differential settlements or they are subjected to no landslide-induced damage (e.g. abandoned buildings). Some points, in both case of V_{slope} and D_{slope} , representing structures mainly affected by low levels of damage, are outliers.

Considering the Cooper (2008) ranking no correlations are recognizable neither with V_{slope} , nor for D_{slope} .

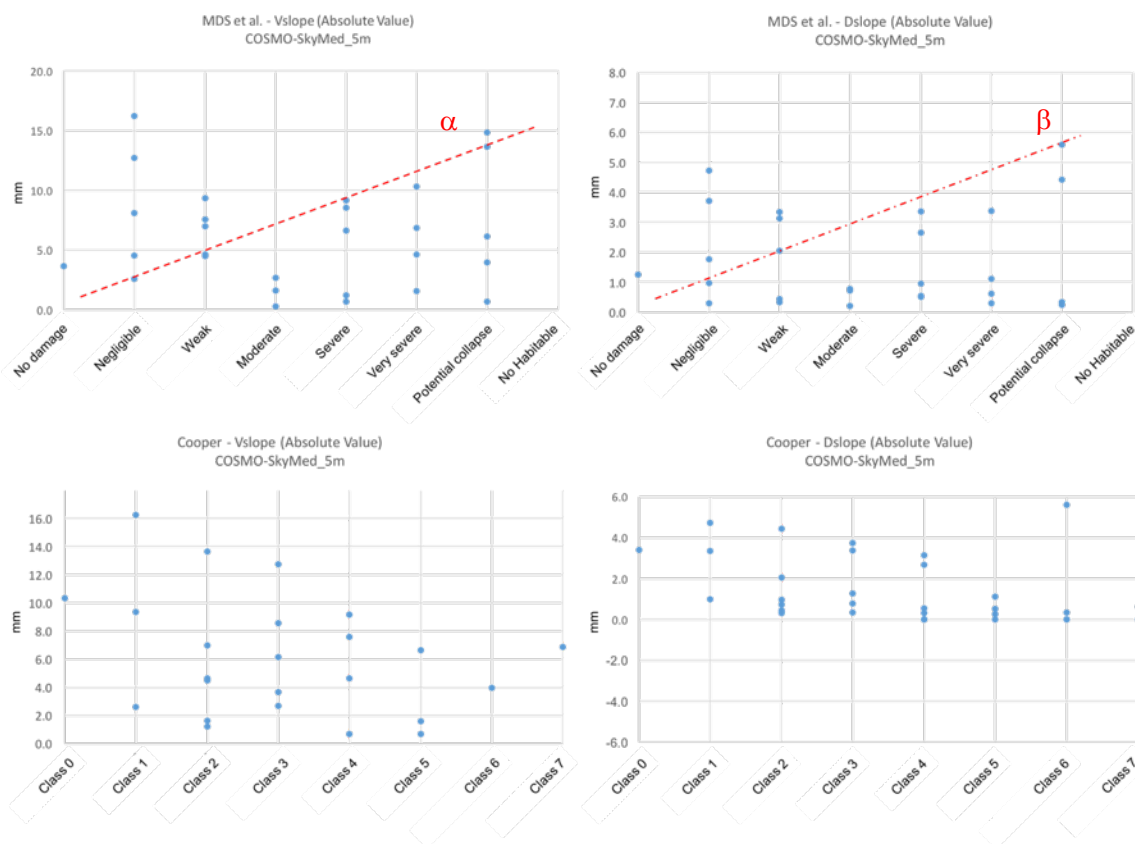


Fig. 5.77 - Graphs showing the values of velocity and maximum displacement value acquired by COSMO-SkyMed sensors, reprojected along the slope using a DEM with 5-m cell resolution, compared to the structures damage classified by Cooper (2008) and Del Soldato et al. (under review_b) for the CL-PO in Agnone.

The same investigation conducted on the damage levels with respect to the reprojected velocity data, by means of the 10-m cell resolution DEM, exhibit a similar plot. The correlation is visible for the damage recorded with the classification of Del Soldato et al. (under review_b), showing main differences for high rates of V_{slope} recorded for some constructions with *Negligible* damage. An upper envelope was traced to define a correlation, mainly valid for the high classes of damage, between the velocity of displacement of the entire structure and the damage classes. As visible in **Fig. 5.78**, from low classes of damage (i.e. *Weak*) the

absolute V_{slope} value increase for higher levels of damage, while for lower damage grades (i.e. *No damage* and *Negligible*) the structures are mainly outliers. To understand the reason an individually investigation was conducted and quite all result to be constructions recently built or renovated. The same typology of relation is recognizable, even if with more noise, with the same outliers for structures affected by low levels of damage, between the Del Soldato et al. (under review_b) classification and the D_{slope} parameter. The same consideration cannot be carried out for damage levels recorded by Cooper's (2008) classification.

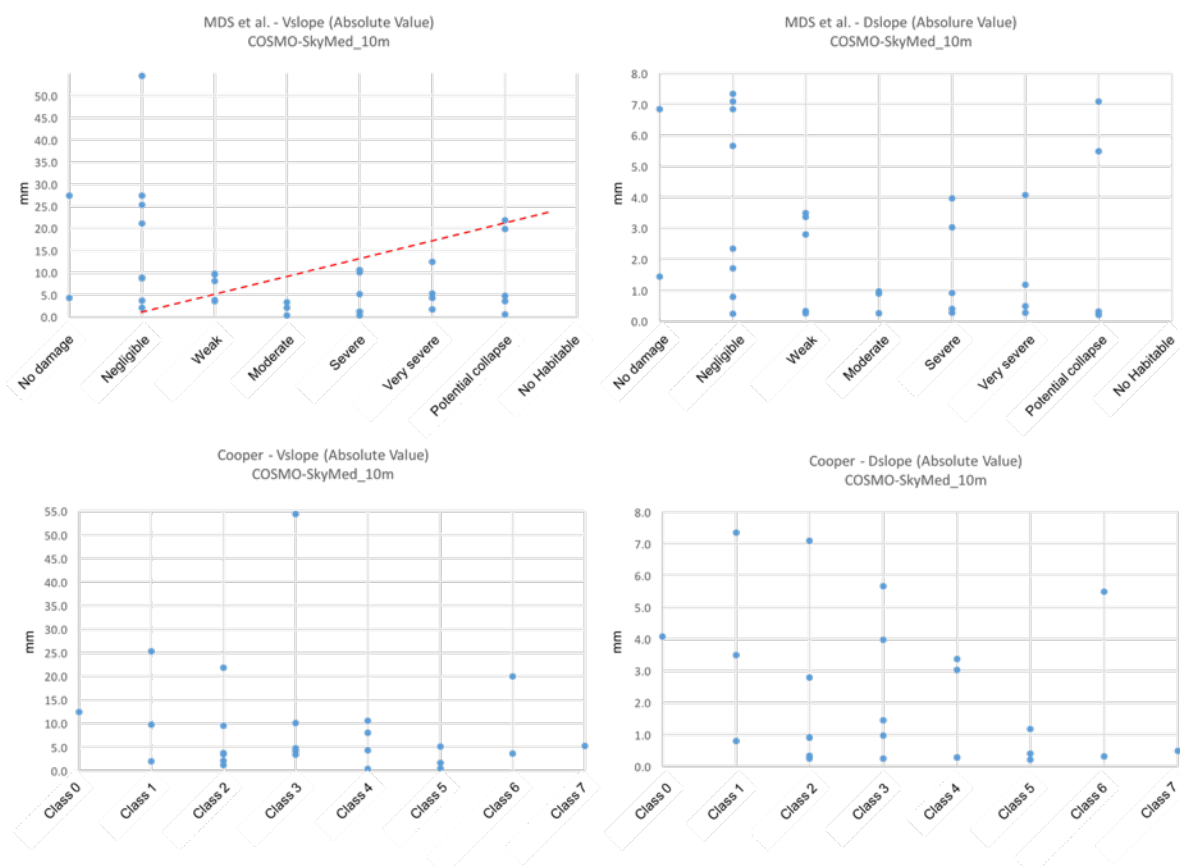


Fig. 5.78 - Plots of velocity and maximum displacement reprojected along the slope using a 10-m cell resolution DEM values gathered by COSMO-SkyMed satellites related to the buildings damage ranked by Cooper (2008) and Del Soldato et al. (under review_b) for the CL-PO in Agnone.

Despite the difficulties due to the low number of artificial and natural reflectors and the high rate of vegetation in the study area of Colle Lapponi - Piano Ovetta landslide in the municipality of Agnone (southern Italy), a correlation between classes of damage and V_{slope} values was carried out. For COSMO-SkyMed data also the D_{slope} values traced an upper envelope, but the distribution of the points resulted a little noisier than for V_{slope} . For this reason, V_{slope} values were taken into account in order to develop a symmetric matrix to categorize the reliability of the recorded data with respect to the classes of the surveyed damage. This matrix

was realized considering a relationship between the severity of the damage recognizable on structures and the absolute value of the averaged velocity projected along the slope for each construction. Four classes of velocity were considered and, consistently, the grades of damage were aggregated in four categories, in order to have a symmetric matrix. Once that the values of the stability range were assigned, i.e. ± 2 mm for the C-band and ± 1.5 mm for the X-band, the classes of V_{slope} , distinguished as *low*, *medium* and *high* based on its values have to be defined differently for each case. The threshold should be meaningful and it has to be made in order to cover all the investigated structures. The levels of damaging recorded by Del Soldato et al. (under review_b) were grouped in this way:

- In *LOW* class *No damage* and *Negligible* categories of damage were grouped;
- in *MEDIUM* rank *Weak* and *Moderate* classes of damage were unified;
- in *SEVERE* category *Severe* and *Very severe* levels of damage were assembled;
- in *HIGH* type *Potential collapse* and *No-habitable* were gathered.

The same procedure was made for the classification of Cooper (2008) assembling:

- In *LOW* rank *Class0* and *Class1* categories of damage class were grouped;
- in *MEDIUM* category *Class2* and *Class3* ranking of damage rank were unified;
- in *SEVERE* type *Class4* and *Class5* levels of damage were assembled;
- in *HIGH* category *Class6* and *Class7* ranks were gathered.

In this way, a table of category of reliability of the V_{slope} related with the damage affecting the structures was elaborated (**Table 5.8**).

Table 5.8 - Reliability categories of the relationship between absolute value of V_{slope} and surveyed levels of damage.

	ND	LOW level of damage	MEDIUM level of damage	SEVERE level of damage	HIGH level of damage		
ND							High Reliability
STABILITY							Medium Reliability
LOW V_{slope}							Low Reliability
MEDIUM V_{slope}							Very Low Reliability
HIGH V_{slope}							ND one parameter
							ND both parameters

First of all, this matrix was applied on the data recorded in Agnone by the COSMO-SkyMed constellation, area in which it was developed after the investigation of possible relations.

Combining the velocity reprojected along the slope with the damage classes categorized by Del Soldato et al. (under review_b) (**Fig. 5.79a**) and Cooper (2008) (**Fig. 5.79b**), two maps exhibiting the reliability of the correlation, were generated. Critically comparing and analysing the maps carried out, some considerations can be made:

- in *Area1* two different situations for the northern and southern built-up areas, respectively exhibiting high and very low value of reliability of the correlations, are recognizable;
- *Area2* exhibits only one buildings ranked, due to the lacking of PS information;
- *Area3*, even is further than the other investigated regions, shows very high level of reliability for all constructions.

It is interest noticing as, despite the low number of buildings in this area, more of them shows high rate of reliability, indifferently from their location. Low reliability is exhibited for some buildings in the crown and some structures in the southwest crown of the landslide close to the nearest valley. This is justifiable considering the effect of the landslide affecting the closest basin influencing the velocity of displacement of the PS backscattered to this structures.

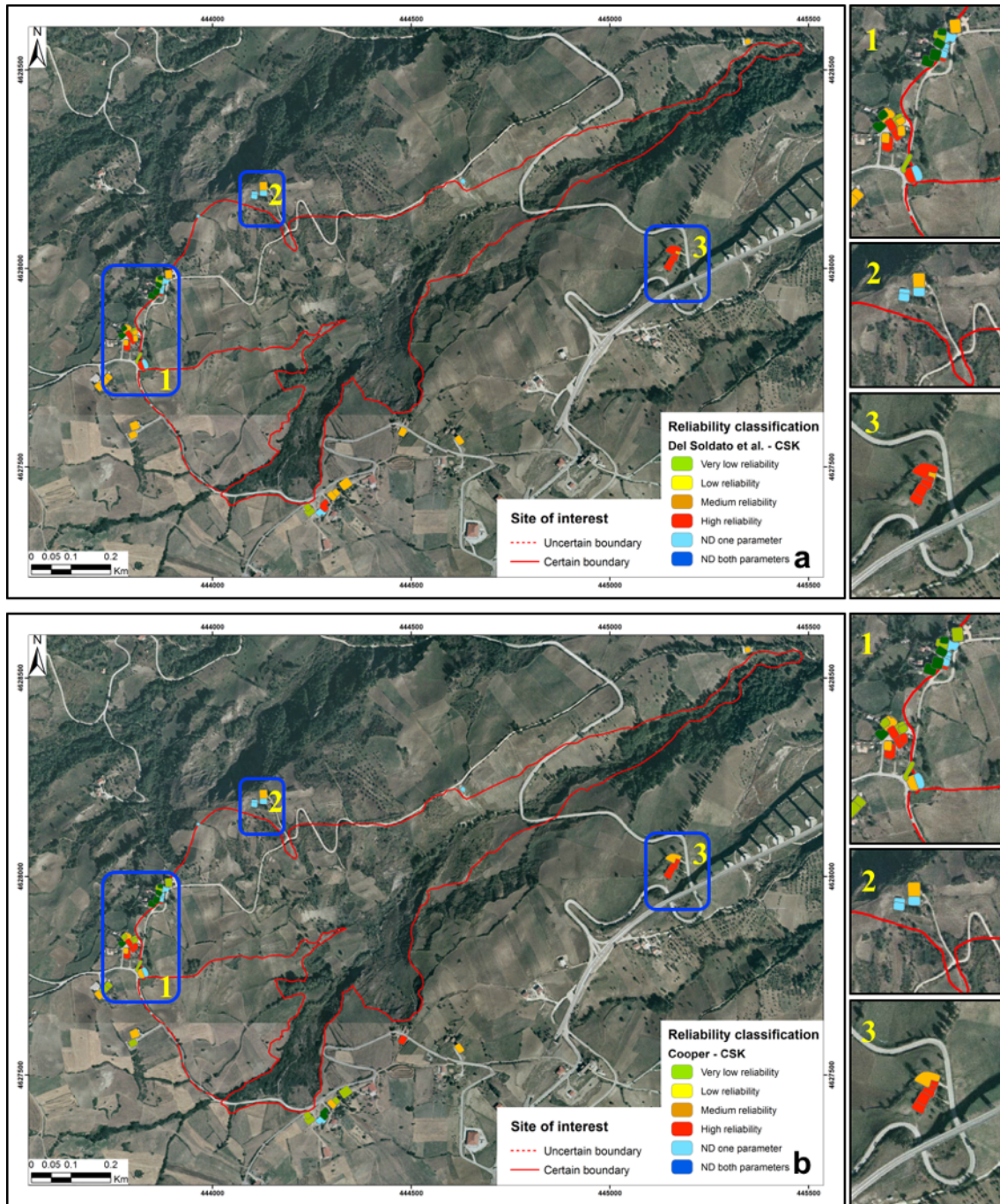


Fig. 5.79 - Reliability categorization between the levels of damage recorded by Cooper (2008) and Del Soldato et al. (under review_b) and V_{slope} recorded by COSMO-SkyMed satellite for CL-PO in Agnone.

The validation of the reliability categorization between V_{slope} and the recorded damage on structures was conducted in the study site of Volterra municipality. This case study offers more buildings and structures on which the efficiency of the developed matrix can be investigated. The relation between V_{slope} data and the damage levels categorized by Del Soldato et al. (under review_b) and Cooper (2008), as made for the CL-PO landslide, was analysed. This relation shows that to the increment of the detected V_{slope} , the severity of the surveyed damage also increases. A similar relation is exhibited for the D_{slope} with respect to the ranked

damage by Del Soldato et al. (under review_b). The Cooper classification allows a similar interpretation only for the V_{slope} parameter, while for the D_{slope} no alignment is identifiable. In both cases the reliability shows low correlation for low damage levels, i.e. *No damage* or *Negligible* classes, while good correspondence for categories of severely damaged buildings.

The reliability matrix to investigate the V_{slope} - damage classes relations was applied on the constructions of the southwestern *Fontecorrenti* and *Le Colombaie* sectors of Volterra (**Fig. 5.80a**). The same approach was adopted to evaluate the reliability of the relationship between the CSK V_{slope} and the damage classification of Cooper (2008) (**Fig. 5.80b**).

The maps of reliability categorization show undefined category due to the missing data about the damage for the historic centre of Volterra because the damage in that area were not investigated. While for the two southwestern sectors the categorizations cover almost all the constructions, except some isolated structures. The area close to the centre exhibits structures characterized by *High* and *Medium reliability* classes. Some differences are visible in the middle of *Le Colombaie* sector, where an agglomerate of buildings exhibits *Low reliability* values, as well as for some constructions in the upper region of *Fontecorrenti*. It is important noticing as few constructions ranked as *Very low reliability* are present, thus featured by no agreement between the measured V_{slope} by the satellite and the recorded damage categories.

Analysing separately the three areas, different situations were visible due to the age of building construction and the severity of the damage affecting them. Furthermore, problems to access to some private areas influence the accuracy of the damage assessment:

- *Area 1* shows high rate of reliability exhibiting a good efficiency for damage recently occurred and then well recorded by the CSK;
- *Area2* displays a medium rate of reliability due to the low level of damage recorded on these recent constructions affected by high velocity of displacement. Some damage was recorded on the external areas, steps, but *Negligible* on the façades;
- in *Area3*, there are different level of reliability due to the discrepancy between the differentiate levels of damage recorded and the quite constant medium velocity affecting the whole area.

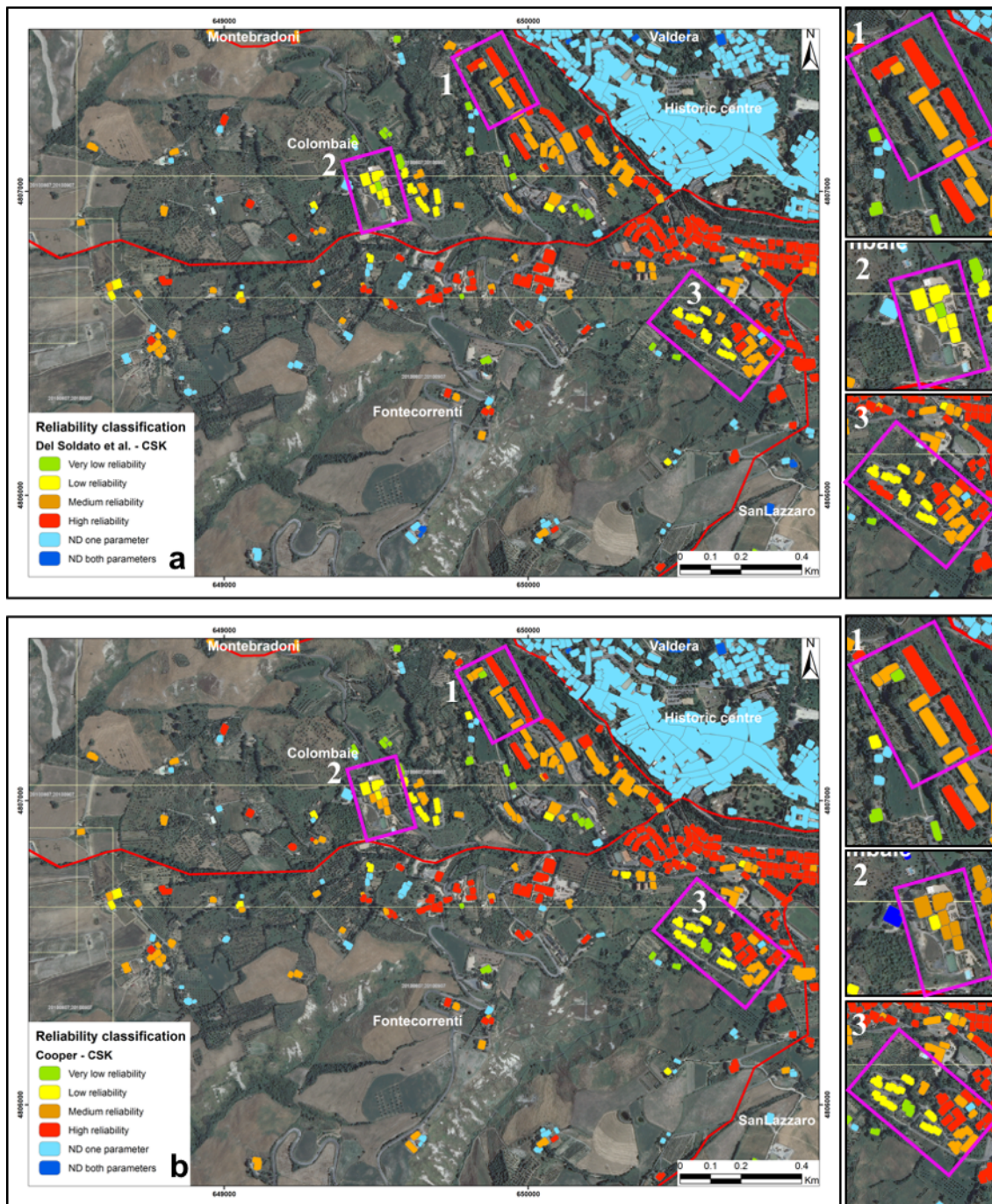


Fig. 5.80 - Categorization of the reliability of the V_{slope} of COSMO-SkyMed and the relieved damage for both classification of Del Soldato et al. (under review_b) (a) and Cooper (2008) (b) in the southwestern sectors of Volterra.

In spite of a lower density of the data recorded, the same ranking was applied on V_{slope} of C-band ENVISAT sensors (Fig. 5.81). The categorization of the reliability of the relationship between the V_{slope} parameter and the rate of surveyed damage shows that almost all the constructions are ranked in *High* and *Medium reliability* categories. For both classification, based on the buildings damage classification of Del Soldato et al. (under review_b) (Fig. 5.81a) and Cooper (2008) (Fig. 5.81b), the most part of the constructions that exhibit high rates of reliability are located in the same sites where occurs for the V_{slope} data of X-band COSMO-

SkyMed. It is interesting noticing as *Area3* shows highest category of reliability with respect to the previously categorization made by the COSMO-SkyMed data. This can be justified considering that the main damage affecting the structures in that area where caused in period covered by the ENVISAT data.

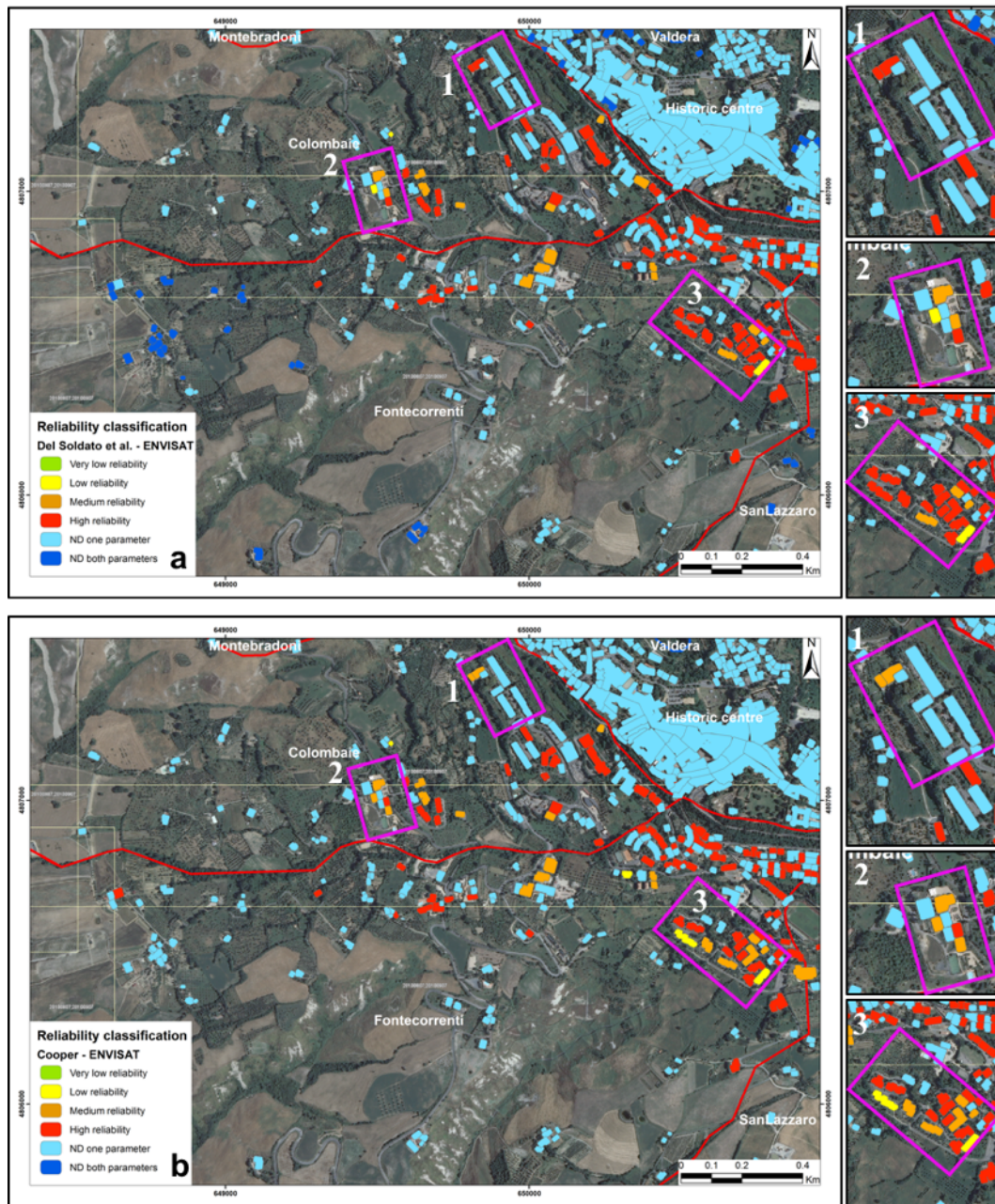


Fig. 5.81 - Classification of the reliability of the Vslope of ENVISAT and the relieved damage for both ranking of Del Soldato et al. (under review_b) (a) and Cooper (2008) (b) in the southwestern sectors of Volterra.

6 Discussion

The first outcome of the PhD work was the investigation of the evolution in time of two landslide areas by means of remote sensing and traditional data. For several available sets of historical images of different years, the CL-PO landslide of Agnone (Molise region, southern Italy) and for *Le Colombaie* and *Fontecorrenti* sectors of Volterra (Tuscany region, central Italy), 3D reconstructions were developed by means of the *Structure from Motion* algorithm, Photoscan Pro and CloudCompare software. Usually these techniques, as well as the above-mentioned software, are widely used for the analysis in geosciences with scenarios shot by UAV instruments. In this PhD thesis, these techniques were employed to create 3D Points Clouds and models based on sets of aerial historical images dating from 1945 and 1954 for Agnone and Volterra, respectively. The precision and the efficiency of the models obtained depend on several factors. The number of images, state of preservation and accuracy used during the scanning process play a key role. The number of images influences the superimposing of the images and, consequently, the dimension and the future reliability of 3D reconstructions of the investigated area. Some scratches or strokes traced by pen traced on the physical old images, were the cause of some problems to the *SfM* algorithm even if the scan process was carried out with attention and a very high resolution. Furthermore, the visibility of the scene using optical sensors could be influenced by the weather, for instance clouds that hide the territory. These are some inconveniences caused by using historical sets of images with some negative consequences on the precision of the results. Moreover, in the old images recorded by IGM, strategic and military areas are masked or erased. These regions, as well as wide water areas (i.e. big lake or the sea close to coastal area), create some problems to the *SfM* algorithm during the modelling because they are recognized as areas with no information. A high resolution of the digitalized images, allows to obtain more details, that help the identification of points to use as Ground Control Points (GCPs) and TiePoints. The precision of the resulting georeferenced 3D model depends on the number and the spatial distribution of GCPs and TiePoints. The accuracy of the input coordinates is based on the attention paid during the identification of the same points on historical aerial images, on recent aerial images and on DEM. Furthermore, the input process should cover the wall area under investigation, following as much as possible a regular cell-grid. This was not simple to pursue for areas completely influenced by a phenomenon, as the analysed region in Agnone, and for very old images, as used in both case studies, due to their low resolution. DEM or DTM are used to find the coordinates and the height of each GCP and TiePoint, as well as the Web Mapping Service. The correct identification of the GCPs place on to the historical images is fundamental to create a georeferenced model with good accuracy. Obviously, the precision of the model depends on the resolution of the terrain model (DEM, DTM, or WMS, indifferently) used to derive the input coordinates of the points. It is fundamental to notice that the buildings are affected by distortion due to the Line Of Sight of the shooting camera, consequently causing

shadow effect for elements in elevation such as constructions. The use of the LiDAR data should be an improvement, giving attention to the above-mentioned differences between the DEM and the DTM, but still today it is not available for all Italian territory. In both case studies, a DEM with 5-m cell resolution was used to obtain the coordinates and the height of each point. Consequently, the maximum precision of the realized models was 5-m, even if the software, in some cases, gave back higher resolution for the elaborations.

The oldest and the youngest reconstructed 3D Points Clouds and models were used to assess the morphological changes through a qualitative analysis of volume differences between them. The possible error of this evaluation could be higher than the accuracy of the models used, thus not allowing a quantitative interpretation of the result. For this reason, in both test sites, the resulting map of differences of volume were understood as qualitative. The outcomes can be considered a good result taking into account that the investigation involves sets of images about 70 years old. In this way, the areas influenced by accumulation or loss of material can be singled out.

In the CL-PO landslide the reactivation of 2003, affecting the left-side of the basin, determined a characteristic depletion of material in the upper part of the landslide and an accumulation of the mobilized material in the river basin as visible by the differences between the 3DPCs. The same “classical” situation is not recognizable in the right-side of the mass-movements, an area historically affected by landslides. This is due to the age of the landslide with respect to the first available images; in fact the set of images of 1945 already recorded the occurred mass-movement. As a consequence, the changes of volume recognized by the algorithm, highlight an increment of volume due to the fulfilment interventions made to mitigate the possibility of recurrences on that side. Another interesting facet to highlight in the CL-PO area is the uphill portion of territory, where alternations of reduction and increment of volume were evident. These changes could be interpreted as movements due to the accommodation of the big displacement caused by the important mass-movement that occurred in January 2003. To support this theory, several scarps and counterslopes were recorded in that area, as shown in the geomorphological map produced by several field surveys. This interpretation, even if qualitative and not quantitative, can be helpful to understand the possible effects of future reactivations and as a support to realize mitigation plans, susceptibility maps and other products useful to the local administrators.

In the southwestern sector of Volterra, analyses showed two main separated regions of accumulation and loss of material. Only a qualitative interpretation was possible due to the high difficulty to insert several Ground Control Points as a regular grid. This inconvenience caused huge errors in the area close to the town, because the high density of constructions causes important shadow effects, and close to the border of the investigated region, due to the lack of site localized with high accuracy in both sets of images. The reliability of the model and the consequent qualitative analysis are confirmed by means of some constructions in *Le Colombaie* area, close to the town, built in the investigated period of the volume changes analysis, shown as

increment of volume. A concentration of error in a north-eastern portion is due to a little area where the overlapping of the images of 1954 shows an empty space and consequently in the 3D reconstructed model. For this area, extensively affected by gully erosion, the analysis could support the investigation and help also in the understanding of the badlands evolution. The collected data did not allow a precise interpretation due to the high difficulty to find several GCPs or TiePoints close to the phenomena. This is a limitation of the historical images, but important qualitative considerations on the local phenomena affecting an area are allowed to support the presence of shallow displacements.

The investigation of the recent evolution was made using Persistent Scatterers data, supported by direct measurements and field surveys. By means of the PCN, the coverage and the reliability of the PS for both areas were checked: C-band products are spread in the southwestern sector of Volterra, while in the CL-PO landslide-prone area the presence of high vegetation and the few natural reflectors prevent many PS to be retrieved. Beside some inconveniences, the data results reliable when compared with direct measurements, field surveys and damage recognizable in those areas where important velocity was recorded. For each individuated area, in both investigated sites, sample time series were analysed. To better inspect them reliability and evolution the time series were corrected to the regional trend (Notti et al., 2015) and automatically categorized (Berti et al., 2013). First of all the time series were visualized and deperated to the regional trend. Furthermore, an estimation of data of abrupt changes into the time series was attempted. For the CL-PO landslide was possible individuate some effects, determined by breakpoints in the time series, uphill with respect to the mobilized areas. They could be attributed to the several reactivation of the mass-movement individuated also by means the classification of the time series even if no precise time of abrupt changes of velocity involving all the landslide were recognized, but different data involving selected areas. Regarding the Volterra sample site, it was possible to highlight as some areas, by means the *linear* classification of the time series (Berti et al., 2013), resulted active already in the past and during the recent period they shown an increment of displacement, as individuated also by the *quadratic* rank of Berti et al. (2013). It is interesting noticing the change of percentage values between the investigations conducted on the entire southwestern sector of Volterra and the results obtained focusing only on the chosen areas. The percentage of *uncorrelated* time series significantly decrease due to the stability of the historic centre of Volterra. Also in this case no abrupt changes involving big area at the same time was individuated.

Given that the main aim of the thesis is to look for a relationship between landslide-induced damage recorded on buildings and the velocity of displacement, the structures close to the CL-PO landslide and the constructions in the *Le Colombaie* and *Fontecorrenti* sectors of Volterra were classified by means of several damage approaches and kinematic satellite parameters. Different categorizations were based on similar parameters, but some differences were observed, i.e. different reference unit. The comparison between the different classifications shows that the oldest approaches (Burland 1977; Alexander 1986; Chiocchio et al. 1997) concentrate the categorization of the structures mainly in classes representing the medium damage

levels, while the newest rankings (Cooper 2008; Baggio et al. 2009) result a little bit precautionary with more constructions in the most severe classes of damage.

The analysis of drawbacks and benefits of five different existing approaches in literature, developed in 50 years of research, attempting to overcome their disadvantages and exploit advantages. The different existing methods were firstly applied and critically examined throughout the experience acquired in several case studies, in order to smooth their weakness and homogenise the features that have to be considered. Therefore a new methodology to classify the landslide-induced damage was developed (Del Soldato et al., under review_b). It is a well-structured approach to categorize structures, facilities and ground damage in landslide-prone and -affected regions. The approach is divided into two phases: the first one concerns the identification, investigation and classification of cracks and fractures on structures, facilities and ground surfaces; the second one regards an *a posteriori* categorization of the man-made structures in *sensu stricto*, in their complexity. The approach could appear complicated due to the two phases, despite its simplicity of application. Furthermore, the new method is suitable also to characterize and classify the fractures affecting natural and anthropogenic ground surfaces. This possibility derives from the effort to identify and categorize the severity of damage affecting structures and natural and anthropogenic ground surfaces, indifferently. The whole structures, i.e. buildings and facilities, have to be taken into consideration secondarily, analysing the ranking of the damage and their extension. The classes of damage, the thresholds of the crack width and the descriptions of different damage for each category were carried out from the previous models. The union of the features of several existing approaches was critically realized and improved by means of the accumulated experience on field.

One of the main problems of the classification of landslide-, subsidence- or earthquake-induced damage, is the subjectivity of the operator who possesses few values and too general descriptions of the possible damage. To limit this drawback, a sketch with function of referring scheme of the possible damage that can affect structures and grounds, as well as a recording scheme requiring several information, were suggested to be used during field surveys. Such supplementary material, in addition to the improvement of the objectiveness of the investigation, allow operators with little experience in this field to perform a good damage survey and to achieve good results.

A further important characteristic of this approach is that it does not require accessibility to internal portions of the structures. This philosophy was already considered in one of the last developed methods. The experience accumulated during field surveys in landslide-prone areas conducted to consider that this fundamental thought has to be taken into account in the new approach. Moreover, this facet plays a key role in the interpretation of the resulting classification maps by the application of the ranked damage.

The detection, description and categorization of cracks and fractures affecting ground surfaces can help to interpret the severity of the damage occurring on neighbours' constructions. Furthermore, information of

ground damage supports the identification of the types of displacement, their evolution and any increment of dimension, as well as a better interpretation of the landslide boundaries.

It is worth noticing that in the proposed damage ranking, classes concerning the collapse are absent, differently to the existing approaches in literature. In this way, maintaining the same number of classes the possibility to discretize the severity of the cracks identifiable on the façades improves. The same consideration is true also for the categorization of fractures identifiable on ground surfaces. This improvement was an indirect consequence derived by the division of the methodology in two distinct phases.

The new approach was validated in different sites, two of them were the case studies of this PhD thesis. The chosen sites exhibit a good accuracy in the resulting classifications of buildings and facilities. In addition to the landslide-prone areas of the Colle Lapponi-Piano Ovetta in Agnone municipality (Molise region, southern Italy) and in the southwestern sector of Volterra (Tuscany region, central Italy), the method was also proved on buildings in other sites abroad, e.g. in Finestrat (Alicante province, southwestern Spain). Different landslides-prone and -affected regions were chosen to verify the possibility to investigate the application of the new approach on different typologies of mass-movements with good accuracy. For instance, roto-translational slides and flows, deep-seated slow-movements, rock falls and shallow landslides were taken into consideration during the validation process.

The applications of the new developed method (Del Soldato et al., under review_b) allowed the understanding of the importance of the framework of the suggested damage recording scheme and the sketch of the possible damage affecting structures, natural and anthropogenic surfaces. A drawing of possible damage leads to the identification and the recognition on the investigated sites. This helped also to assess the severity of the damage during the surveys in the validation sites, therefore the sketch was included in the recording scheme with a short description of each possible damage. Despite the little time spent during field surveys, the resulting classification is more precise than the obtainable with other existing methods.

The newly developed approach, which does not include the collapse classes in the phase of categorization of cracks and fractures, allows a more precise distribution of the severity of the damage. The CL-PO site is a rural area causing consequences on the categorization of some constructions classified with high levels of damage, but not affected by landslide-induced damage. For instance, there are three buildings close to the boundary of the mass-movements that clearly as had been abandoned for several years and were ranked as collapsed or in-habitable. For these structures the relation between damage and V_{slope} could not be verified. Beside this, in such case, the categorization of buildings and facilities of CL-PO reflects, with acceptable precision, the preventive restrictions promulgated by the municipality administrator, after the main reactivation of 2003. On the other hand, one building sticks out as affected by *Very slight* or *Negligible* damage, according to all categorizations used, despite its position respect to the boundary of the landslide and the restrictive measurements effective also for it. This construction does not show damage on the façades, even if it is located on the present-day crown of the landslide, while several open cracks and a partial

collapse affect its sidewalk. With high probability, its foundations are also affected by damage. This case is a good example to understand the importance of investigating the facilities, in addition to buildings, in order to help promulgate restrictive measure by local administrators. Furthermore, this type of analysis can also help the investigation of the phenomenon.

In Volterra test site, only the categorizations of Cooper (2008) and Del Soldato et al. (under review_b) were applied. More than 500 structures affected by several quiescent and active slope instabilities were classified in *Le Colombaie* and *Fontecorrenti* sectors. The main damaged buildings are located in areas where superficial displacements, due to colluvial debris, are concentrated: severe damage was recorded on buildings in the upper portion of active or quiescent landslides and others in a central portion of the big *Le Colombaie* landslide, with high probability active. Constructions in the historic centre were excluded by the investigations that were concentrated on the regions where PSI data show high velocity in both ascending and descending geometries.

In the upper portion of *Le Colombaie* complex of landslides, several constructions show different situations based on their locations with respect to a street. The four constructions in the downhill portion of the road, two of these built in the '90s and other two older and now probably abandoned, show severe damage. The other structures on the opposite side of the street do not exhibit any damage. With high probability, this effect is due to the lithological change between the upper stable Villamagna sands, the lower clayey material (Argille Azzurre Formation) and colluvial debris. This contrast causes important damage and differential displacement affecting constructions in the downhill portion of the street. The severity of the damage forces the local administrator to promulgate restrictions to one of these, in addition to an instinctive abandonment of the oldest damaged structures. To support this hypothesis two inclinometers confirmed the occurring displacement exhibiting a clear sliding surface and afterwards were broken to the high terrain motion. It is interesting to notice that the structure, highly damaged and put under restriction, is located perpendicularly respect to the geolithological boundary.

Another region, where meaningful velocity of displacement and damage on the constructions were recorded, is the urban area built after 2000 inside a landslide complex in the *Le Colombaie* sector. Differently from the previous structures, diffuse and fine cracks were recorded in subsequent field survey. The causes can be probably attributed to the filling material compaction, even if PSI velocities derived from ERS, ENVISAT sensors recorded between 1993 and 2010, also show high values. The X-band PS and DS data derived from the COSMO-SkyMed constellation, confirmed the hypothesis made by the ERS and ENVISAT data. Further investigation and future field survey should be conducted to monitor the situation and the evolution of the damage in this area.

In the *Fontecorrenti* sector, constructions affected by damage was built in the 70's and they are sited in the upper region of two active landslides. Furthermore, a building recently built uphill respect to the

landslide, is partially affected by important damage confirming a continuous retrogressive evolution of the landslide and growth of the area involved. Damage affecting structures is not homogeneously distributed. The classification show few constructions exhibiting very important damage, several structures with *Weak* fractures and others that do not present any problems. Also for this area a contribution of the local geology in the distribution of the movements provoking differential displacement is presumed.

In order to combine buildings categorized by the damage with the displacement affecting the structures, constructions and facilities of the CL-PO landslide in Agnone and of the southwestern sectors of Volterra were categorized by means of several parameters derived from the PS. Velocity and displacement recorded along the Line Of Sight, and velocity and cumulated displacement reprojected along the slope, were used to categorize the structures. The damage classification and their categorization based on the satellite parameters were analysed. Plotting all the used kinematic parameters combined with the classes of damage recorded by Cooper and Del Soldato et al. (under review_b), a relationship was pursued. Between V_{slope} and the classes of damage recorded by Del Soldato et al. (under review_b) a disposition along a linear regression describing an upper envelope was recognized for some constructions. Some constructions characterized by low level of damage, but high velocities, result outliers. These are probably justified considering that some constructions close to the landslide area were recently renovated or under construction. The points aligned on the regression line describe a good correlation between the velocity affecting the whole construction and the recorded damage. Structures characterized by lower velocities, plotted under the envelope, the causes can be attributed to the different effects of differential displacement due to several factors, e.g. age and typology of the constructions, or causes not related to the landslide, e.g. the abandonment of the construction. The ENVISAT data for both sites result very noisy and the accumulated displacements result unreliable to analyse in order to find another possible relation. The correlation was previously investigated and carried out for the Agnone test site, where the reprojection of the data were conducted using two DEM with a different resolution. It was surprising because the reprojection conducted with both high and low resolution DEM, 5-m and 10-m cell resolution, show a similar relation. This occurred investigating both ENVISAT and COSMO-SkyMed data. This is a little bit in contrast with the thesis of Notti et al. (2014) according to whom a lower DEM resolution works better in the reprojection process. Considering that the area of the CL-PO landslide, where several reactivations influenced a very big area with geomorphological local changes of the topography, smoothed with DEM with low resolution, differences affecting the reprojection of velocities along the slope were expected. The uniformity of the data is justifiable considering that the PSs are not recorded on natural ground surfaces or outcropping, but only on man-made structures.

Despite the few targets investigated in Agnone, a reliability matrix of the relationship between the V_{slope} acquired by COSMO-SkyMed and the levels of damage was developed. Applying it on the constructions close to the CL-PO landslide some interesting situations were identified. In the boundary of the landslide different reliability classes were identified for the two neighbouring built-up areas. The northern one exhibits high

values, while in the southern one very low classes, except for one building, were shown. These discrepancies were due mainly to the characteristics of the buildings: southern buildings, old structures built by masonry frameworks, registered all movements affecting the area; the northern structures, including some abandoned constructions, collapsed or destroyed, and others under construction or renovation. Only one building shows high reliability in this sector, affected by important damage and high velocities because built on the present-day boundary cracks of the landslide.

The procedure was validated applying the reliability matrix on the southwestern sectors of Volterra for both satellite ENVISAT and COSMO-SkyMed. The data and the field surveys imply that the more correct maps are those derived from the V_{slope} recorded by the COSMO-SkyMed constellations, despite high correspondence between recorded damage and V_{slope} acquired by ENVISAT satellites were visible. Analysing the obtained reliability classification maps is evident as generally the high reliability is diffused indifferently to the sensors used. Considering the area where high velocities were recorded, some considerations can be done. *Area1* shows *High* and *Moderate* values of reliability for all structures indifferently to the used damage classification approach. The ENVISAT data for these structures are too spread to make any considerations. In *Area2* and *Area3* similar considerations can be made. For both areas, the reliability results higher between damage and ENVISAT V_{slope} , indifferently to the applied classification approach. Investigating the possible relationship between COSMO-SkyMed V_{slope} and levels of damage recorded by Cooper (2008) and Del Soldato et al. (under review_b) methods, some differences were recognizable. This could be justified considering that the damage recorded in the recent field surveys had probably occurred, showing high correlation, in the period in which the ENVISAT satellite recorded the displacement velocity. The velocity recorded by the COSMO-SkyMed constellation for *Area2* results higher respect to the level of low damage degrees affecting the structures surveyed during the field campaigns. The constructions in this sector were built recently, approximatively in 2003, on level-off filling material. The consolidation of this material could justify the velocity of displacement recently recorded with no relevant damage. Furthermore, damage revealed on the constructions during field surveys appear increasing, by which an influence of slope movements can be taken into consideration. This hypothesis is supported by the ERS data that already exhibited displacement when the constructions were absent. The same circumstance in *Area3* can be justified by taking into consideration the V_{slope} for both sensors. The levels of damage are well correlated with high rates of V_{slope} recorded by ENVISAT data. This allows to assume that the main damage in this area occurred in the period 2003 - 2010, when high rates of V_{slope} were recorded. To support this interpretation no important increment of the severity of the damage was recorded during the several field campaigns. Uphill, close to *Area3*, a hotel, built around the year 2000 shows high reliability for COSMO-SkyMed V_{slope} , while no data were recorded by the ENVISAT satellites. The high rate of reliability of this construction with the CSK V_{slope} and the recent recorded damage on it, can confirm the mass-movement activity and the consequent effects caused to the structures.

The abovementioned considerations allow to determine that the categorization of the level of damage and their correlation with the velocity of displacement recorded by remote sensing data can support and update the ground movements interpretation and help the planning of mitigation measures by authorities. The reliability categorization made for different sensors, between the damage and the velocity of displacement is a fundamental support to better interpret different influences of the damage on structures. Moreover, involving ENVISAT and CSK satellites, it is possible to understand the period in which the main damage occurred, even if they were recently surveyed. Furthermore, information obtained can help hypothesize the possible future damage when high rates of velocity were recorded in structures with similar features considering the position respect to the regression line described by the data recorded in the study area. Obviously, the interpretation must be done considering also collected and ancillary data in order to avoid errors. Some examples of low reliability, justifiable only analysing also the traditional data, of the correlation between the recorded damage and V_{LOS} are shown for some buildings in Volterra where damage recently surveyed was caused by old displacements. The same applies to few collapsed/abandoned structures in Agnone. In this case, the exhibit reliability is low because the recorded damage, with high possibility, is the outcome of abandonment rather than by the landslide.

7 Conclusions

The PhD work was developed on two test sites, Colle Lapponi-Piano Ovetta (CL-PO) in the municipality of Agnone (Molise region, southern Italy) and the southwestern sector of Volterra (Tuscany municipality, central Italy), both affected by landslides. The evolution of the phenomena affecting the study areas were investigated using several direct and indirect methods including the analysis, by means of the *Structure from Motion* algorithm to reconstruct 3D Point Clouds and models, of sets of historical aerial images of different years and the investigation conducted by DInSAR techniques. C-band data, ERS1/2 and ENVISAT, acquired from 1992 to 2010, and X-band data, COSMO-SkyMed, covering the period 2010 - 2015 were used to investigate the recent evolution of the phenomena in order to classify the buildings by means of different kinematic parameters.

For both sites, the difference between the oldest and the newest 3D Points Clouds were made in order to evaluate the occurred changes of volume. The investigation of the CL-PO landslide, involving the period between 1945 and 2003, years of the last important reactivation show an interesting clear distinction between the area of loss and the region of accumulation of material. Furthermore, some perturbations exhibited in the uphill regions were recognized, justifiable considering that the area behind the crown of the landslide was influenced by displacement caused by the reactivation of the mass-movement that occurred in January 2003. The same analysis was conducted between the 3D Points Cloud of 1954 and 1995 of the southwestern sector of Volterra allowing to carry out important characteristics and information about the studied phenomena. For the CL-PO landslide area the geomorphological features recognized by means of the 3D reconstruction of several years and the difference between the 3D Points Clouds, were controlled and validated conducting several field surveys and creating a geomorphological map on the landslide area and its uphill surrounding.

The evolution of the phenomena helped also to interpret their effect on the structures, and to distinguish the damage caused by the displacement due to the mass-movement or other causes. The damage on the structures and facilities into and close to the landslides were surveyed by means of several field campaigns and their severity was categorized applying several damage classification approaches. Buildings and facilities located in the CL-PO area in Agnone were initially classified according to five literature categorizations. The different damage classifications of the structures were compared and discussed allowing to carry out benefits and drawbacks in order to improve a new classification approach. The developed categorization was tested and validated on several sites including the CL-PO landslide area and the southwestern sector of Volterra. The new classification method was developed merging the good quality of the existing schemes, correcting some drawbacks encountered in the application and using a new idea to simplify the classification process.

The developed classification approach was divided into two phases, the identification of the damage and the categorization of the constructions in *sensu stricto*. This procedure allows a better recognition and classification of the damage in addition to the assessment of the condition of the entire structure with more precision. Furthermore, it is applicable on buildings and facilities, and moreover it includes features to rank the ground fractures. The importance of a map made by the classification of the damage affecting structures, facilities and ground surfaces is fundamental for understanding the extension of the phenomena, but also to support the local administrators.

A relationship between damage and kinematic parameters recorded by a remote sensing technique was inquired into. Structures and facilities of both investigated sites were categorized by means of V_{LOS} and D_{max} , separated for ascending and descending geometries, and V_{slope} and D_{slope} extracted by ENVISAT and COSMO-SkyMed data. The velocity and the cumulated displacement recorded along the Line Of Sight both by ENVISAT and COSMO-SkyMed sensors, for each orbit separately, showed no important relationship. A linear regression characterising an upper envelope was identified combining the damage levels with the averaged value of the velocity reprojected along the deepest local slope (V_{slope}) for both ENVISAT and COSMO-SkyMed data. Once identified for the CL-PO landslide case study, the same was applied to the southern sector of Volterra, classifying the constructions according to the V_{slope} and D_{slope} .

At the end, the quality of the correlation study was investigated generating a matrix involving the severity of damage and the rate of displacement. To make a symmetrical matrix, four classes of the V_{slope} (i.e. stability, low, medium and high velocity) and the eight levels of the damage agglomerated in four categories (i.e. low, medium, severe, high level of damage) were plotted. In both cases, except for some buildings for which some considerations were made, the reliability of the correlation resulted high.

8 Future research topics

Some consideration on the possible ideas to improve the issues take on during the PhD work have to be done.

An improvement to identify and recognize the damage on the structures could be the use of the Infrared Thermographic (IRT) technique during the field surveys. In this way, cracks or fractures masked by slight surficial renovations made on the façades can be recognized in order to better assess the real situation of the damage affecting the structures (Avdelidis and Moropoulou, 2004; Nolesini et al., 2016). The new damage classification approach, developed for landslide-induced damage, should be tested also in areas affected by subsidence to increase the possible application of this new method. In addition, it would be interesting investigate the possibility to have three different grades of damage in the same construction, but the difficulty to create a scheme with three axes has to be considered.

Furthermore, for the CL-PO landslide, given that the PS data are few due to several factors, to resolve some problems it could be apply the *pixel offset technique* to analyse the landslide movement (Singleton et al., 2014) This technique allow to overcome the D-InSAR limitation on the spatial displacement gradient using just two images acquired at different time and measuring the displacement vectors along the LOS. In this way for recognizable points, i.e. the Corner Reflectors that result not visible by the DInSAR techniques, it possible obtain the 2-dimensional displacements by measuring the row and column offsets as defined intervals in range/azimuth (Singleton et al., 2014).

Another possibility to identify and assess the recent effect of the mass movement could be work on the satellite raw data to apply the *change detection* technique working on the intensity of the signal (e.g. Wadge et al., 2002; Wadge et al., 2011; Bignami et al., 2013; Whelley et al., 2014). This methodology can be applied in both CL-PO and Volterra landslide in order to individuate with more precision areas where changes and displacement occurred.

At the end, it could be interesting to improve the resolution of differences in volume estimations, in order to reach a quantitative result, for instance working on the precision of the location of the input GCPs and their coordinates (Riquelme et al., under review).

9 List of publications

9.1 Proceedings

Del Soldato M, Di Martire D and Tomas R (2016) Comparison of different approaches for landslide-induced damage assessment: The case study of Agnone (southern Italy). *Rendiconti Online Societa Geologica Italiana* 41: 139-142.

Del Soldato M, Tomas R, Pont J, Herrera G, Garcia Lopez-Davalillos JC and Mora O (2016) A multi-sensor approach for monitoring a road bridge in the valencia harbor (se spain) by sar interferometry (insar). *Rendiconti Online Societa Geologica Italiana* 41: 235-238.

Del Soldato M, Segoni S, De Vita P, Pazzi V, Tofani V and Moretti S (2016) Thickness model of pyroclastic soils along mountain slopes of campania (southern italy). *Landslides and Engineered Slopes Experience, Theory and Practice: Proceedings of the 12th International Symposium on Landslides (Napoli, Italy, 12-19 June 2016)*, CRC Press, pp 797-804

Bianchini S, Pratesi F, Nolesini T, Del Soldato M and Casagli N (2016) A psi-based analysis of landslides in the historic town of volterra (italy). *Landslides and Engineered Slopes Experience, Theory and Practice: Proceedings of the 12th International Symposium on Landslides (Napoli, Italy, 12-19 June 2016)*, CRC Press, pp 411

9.2 Journals

Bianchini S, Del Soldato M, Solari L, Nolesini T, Pratesi F and Moretti S (2016) Badland susceptibility assessment in volterra municipality (tuscany, italy) by means of GIS and statistical analysis. *Environmental Earth Sciences* 75: 1-14. doi: 10.1007/s12665-016-5586-5

Del Soldato M, Di Martire D, Bianchini S, Tomàs R, De Vita P, Ramondini M, Casagli N and Calcaterra D (under review_a) An assessment of landslide induced damage to structures: Agnone (southern Italy) case study. *Engineering Failure Analysis*.

Del Soldato M, Bianchini S, Calcaterra D, De Vita P, Di Martire D, Tomàs R and Casagli N (under review_b) New approach for preliminary landslide-induced damage assessment. *Geomatics, Natural Hazard and Risk*.

Riquelme A, Del Soldato M, Tomàs R, Cano M, Jorda L and Moretti S (under review) Digital surface reconstruction using open access old and recent digital nadir aerial imagery: application for anthropogenic changes detection. *Geomorphology*

10 Acknowledgments

I would like to thank my advisors of the University of Naples Federico II Prof. Pantaleone De Vita and Prof. Domenico Calcaterra to welcoming me and to follow me during the PhD period. I am also thankful to Prof. Nicola Casagli, my co-advisor at University of Firenze, for his constructive suggestions and constant support during this research, giving me the possibility to follow a dream.

I am grateful to have met the research group “Ingeniería del Terreno y sus Estructuras (EnTerEs)” of the University of Alicante (Spain) for the support, the help and the transfer of knowledge during the PhD abroad period, in particular to Prof. Roberto Jover Tomàs and Dr. Adrian Riquelme. It was a pleasure to meet nice colleagues at the University of Alicante. They are wonderful people and their contribution makes this research work possible.

An important thanksgiving has to be made to my colleagues at the group of the university of Florence, especially to Silvia, to a continue support during all period of my doctorate in which I had several difficult moments overpassed also thank to them.

Finally, I am in special debt to my parents and my grandmother for their consistent support, advice and respect to letting me make my own decisions, in many detailed aspects. Moreover, a grateful to all my friends in Florence, Naples and Lavagna (Genoa province) for the support along this way.

At the end, a thanks to COSMO-SkyMed Product - ©ASI - Agenzia Spaziale Italiana - 2016 (All Right Reserved), to give me the possibility to use the data for the research in Agnone, in addition to “GEOPROGETTI - Studio associato” (geologists Francesca Franchi and Emilio Pistilli) for making the geological and geotechnical data on Volterra available.

11 References

- Abellan A, Derron M-H and Jaboyedoff M (2016) "Use of 3d point clouds in geohazards" special issue: Current challenges and future trends. *Remote Sensing* 8: 130.
- Alexander D (1983) The landslide of 13 december 1982 at ancona. Central Italy: Report to the International Disaster Institute, London.
- Alexander D (1986) Landslide damage to buildings. *Environmental Geology and Water Sciences* 8: 147-151.
- Aliaga DG, Funkhouser T, Yanovsky D and Carlbom I (2002) Sea of images. Proceedings of the conference on Visualization'02, IEEE Computer Society, pp 331-338
- Almagià R (1910) Studi geografici sulle frane in italia. Vol. li. L'apennino centrale e meridionale. Conclusioni generali. Società Geografica Italiana
- AMI—Servizio Meteorologico dell'Aeronautica Militare Italiana (2011) Tabelle climatiche 1971–2000 della stazione meteorologica di Volterra dall'Atlante Climatico 1971–2000. <http://clima.meteoam.it/AtlanteClimatico/pdf/%28164%29Volterra.pdf>. Accessed 7 Sept 2015
- Annual Disaster Statistical Review (2015) The numbers and trends. Debarati Guha-Sapir, Philippe Hoyois and Regina Below. Centre for Research on the Epidemiology of Disasters (CRED) Université catholique de Louvain, Brussels (Belgium).
- Antonello G, Casagli N, Farina P, Leva D, Nico G, Sieber A and Tarchi D (2004) Ground-based sar interferometry for monitoring mass movements. *Landslides* 1: 21-28.
- Baggio C, Bernardini A, Colozza R and Corazza L (2009) Manuale per la compilazione della scheda di 1 livello di rilevamento danno, pronto intervento e agibilità per edifici ordinari nell'emergenza post-sismica. Editrice Italiani nel Mondo srl-Roma.
- Baltzer A (1875) Über bergstürze in den alpen. Caesar Schmidt,
- Bazzoffi P, Boscagli A, Brandi G, Busoni E, Calzolari C, Chiarucci A, Chiaverini I, Chisci G, Colica A and De Dominicis V (1997) Badland processes and significance in changing environments. *Supplementi di Geografia Fisica e Dinamica del Quaternario* 3: 151-166.
- Berardino P, Fornaro G, Lanari R and Sansosti E (2002) A new algorithm for surface deformation monitoring based on small baseline differential sar interferograms. *Geoscience and Remote Sensing, IEEE Transactions on* 40: 2375-2383.
- Berti M, Corsini A, Franceschini S and Iannacone J (2013) Automated classification of persistent scatterers interferometry time series. *Natural Hazards and Earth System Sciences* 13: 1945-1958.
- Bianchini S, Ciampalini A, Raspini F, Bardi F, Di Traglia F, Moretti S and Casagli N (2015) Multi-temporal evaluation of landslide movements and impacts on buildings in san fratello (italy) by means of c-band and x-band psi data. *Pure and Applied Geophysics* 172: 3043-3065.
- Bianchini S, Cigna F, Righini G, Proietti C and Casagli N (2012) Landslide hotspot mapping by means of persistent scatterer interferometry. *Environmental Earth Sciences* 67: 1155-1172.
- Bianchini S, Del Soldato M, Solari L, Nolesini T, Pratesi F and Moretti S (2016) Badland susceptibility assessment in volterra municipality (tuscany, italy) by means of gis and statistical analysis. *Environmental Earth Sciences* 75: 1-14. doi: 10.1007/s12665-016-5586-5
- Bianchini S, Herrera G, Mateos RM, Notti D, Garcia I, Mora O and Moretti S (2013) Landslide activity maps generation by means of persistent scatterer interferometry. *Remote Sensing* 5: 6198-6222.
- Bianchini S and Moretti S (2015) Analysis of recent ground subsidence in the sibari plain (italy) by means of satellite sar interferometry-based methods. *International Journal of Remote Sensing* 36: 4550-4569.
- Bianchini S, Pratesi F, Nolesini T and Casagli N (2015) Building deformation assessment by means of persistent scatterer interferometry analysis on a landslide-affected area: The volterra (italy) case study. *Remote Sensing* 7: 4678-4701.
- Bianchini S, Tapete D, Ciampalini A, Di Traglia F, Del Ventisette C, Moretti S and Casagli N (2014) Multi-temporal evaluation of landslide-induced movements and damage assessment in san fratello (italy) by means of c-and x-band psi data. *Mathematics of planet earth, Springer*, pp 257-261
- Blanco-Sanchez P, Mallorquí JJ, Duque S and Monells D (2008) The coherent pixels technique (cpt): An advanced dinsar technique for nonlinear deformation monitoring. *Pure and Applied Geophysics* 165: 1167-1193.

- Bonnard C, Noverraz F and Dupraz H (1996) Long-term movements of substabilized versants and climatic changes in the swiss alps. VIth International Symposium on Landslides, Trondheim, Norway, pp 1525-1530
- Borgatti L, Corsini A, Barbieri M, Sartini G, Truffelli G, Caputo G and Puglisi C (2006) Large reactivated landslides in weak rock masses: A case study from the northern apennines (italy). *Landslides* 3: 115-124.
- Boscardin MD and Cording EJ (1989) Building response to excavation-induced settlement. *Journal of Geotechnical Engineering* 115: 1-21.
- Brasington J, Rumsby B and McVey R (2000) Monitoring and modelling morphological change in a braided gravel-bed river using high resolution gps-based survey. *Earth Surface Processes and Landforms* 25: 973-990.
- Bressani L, Pinheiro R, Bica A, Eisenberger C and SOARES J (2008) Movements of a large urban slope in the town of santa cruz do sul (rgs), brazil. CHEN, Z; ZHANG, J; LI, Z: 293-298.
- Brodu N and Lague D (2012) 3d terrestrial lidar data classification of complex natural scenes using a multi-scale dimensionality criterion: Applications in geomorphology. *ISPRS Journal of Photogrammetry and Remote Sensing* 68: 121-134.
- Bru G, Herrera G, Tomás R, Duro J, De la Vega R and Mulas J (2013) Control of deformation of buildings affected by subsidence using persistent scatterer interferometry. *Structure and infrastructure engineering* 9: 188-200.
- Brückl E, Brunner F and Kraus K (2006) Kinematics of a deep-seated landslide derived from photogrammetric, gps and geophysical data. *Engineering Geology* 88: 149-159.
- Burland JB (1977) Behavior of foundations and structures on soft ground. *Proc 9th ICSMFE*, pp 495-546
- Calcaterra D, Di Martire D, Ramondini M, Calò F and Parise M (2008) Geotechnical analysis of a complex slope movement in sedimentary successions of the southern apennines (molise, italy). *Landslides and Engineered Slopes*: 299-305.
- Calò F, Ardizzone F, Castaldo R, Lollino P, Tizzani P, Guzzetti F, Lanari R, Angeli MG, Pontoni F and Manunta M (2014) Enhanced landslide investigations through advanced DInSAR techniques: the Ivancich case study, Assisi, Italy. *Remote Sensing of Environment*, 142: 69-82.
- Campbell RH (1975) Soil slips, debris flows, and rainstorms in the santa monica mountains and vicinity, southern california. US Govt. Print. Off.,
- Carrara A, Crosta G and Frattini P (2003) Geomorphological and historical data in assessing landslide hazard. *Earth Surface Processes and Landforms* 28: 1125-1142.
- Cascini L, Peduto D, Pisciotta G, Arena L, Ferlisi S and Fornaro G (2013) The combination of dinsar and facility damage data for the updating of slow-moving landslide inventory maps at medium scale. *Nat Hazards Earth Syst Sci* 13: 1527-1549.
- Casu F, Manzo M and Lanari R (2006) A quantitative assessment of the sbas algorithm performance for surface deformation retrieval from dinsar data. *Remote Sensing of Environment* 102: 195-210.
- Chandler J (1999) Effective application of automated digital photogrammetry for geomorphological research. *Earth Surface Processes and Landforms* 24: 51-64.
- Chiocchio C, Iovine G and Parise M (1997) A proposal for surveying and classifying landslide damage to buildings in urban areas. *Engineering Geology and the Environment*: 553-558.
- Ciampalini A, Bardi F, Bianchini S, Frodella W, Del Ventisette C, Moretti S and Casagli N (2014) Analysis of building deformation in landslide area using multisensor psinsar™ technique. *International Journal of Applied Earth Observation and Geoinformation* 33: 166-180. doi: <http://dx.doi.org/10.1016/j.jag.2014.05.011>
- Cigna F, Tapete D and Casagli N (2012) Semi-automated extraction of Deviation Index (DI) from satellite Persistent Scatterers time series: tests on sedimentary volcanism and tectonically-induced motions. *Nonlinear Processes in Geophysics* 19: 643-655.
- Cigna F, Bianchini S and Casagli N (2013) How to assess landslide activity and intensity with persistent scatterer interferometry (psi): The psi-based matrix approach. *Landslides* 10: 267-283. doi: 10.1007/s10346-012-0335-7
- Cigna F, Bianchini S, Righini G, Proietti C and Casagli N (2010) Updating landslide inventory maps in mountain areas by means of persistent scatterer interferometry (psi) and photo-interpretation: Central calabria (italy) case study. *Mountain risks: bringing science to society*, Florence: 24-26.
- Colesanti C, Ferretti A, Prati C and Rocca F (2003) Monitoring landslides and tectonic motions with the permanent scatterers technique. *Engineering Geology* 68: 3-14.

- Colesanti C and Wasowski J (2006) Investigating landslides with space-borne synthetic aperture radar (sar) interferometry. *Engineering geology* 88: 173-199.
- Confuorto P Di Martire D Ramondini M and Calcaterra D (2014) Differential SAR interferometry for slow- moving landslide monitoring in Crotona Province (Italy). Proceedings of 'the Analysis and Management of Changing Risks for Natural Hazards conference', Padua, 18-19 November.
- Cooper AH (2008) The classification, recording, databasing and use of information about building damage caused by subsidence and landslides. *Quarterly Journal of Engineering Geology and Hydrogeology* 41: 409-424.
- Costa JE (1984) Physical geomorphology of debris flows. *Developments and applications of geomorphology*, Springer, pp 268-317
- Crescenzi E, Iovine G and Parise M (1994) Analysis of landslide damage in a village in southern Italy: A preliminary report. *Incontro Internazionale dei Giovani Ricercatori in Geologia Applicata*, Lausanne Suisse: 68-72.
- Crosetto M, Biescas E, Duro J, Closa J and Arnaud A (2008) Generation of advanced ers and Envisat interferometric sar products using the stable point network technique. *Photogrammetric Engineering & Remote Sensing* 74: 443-450.
- Crosetto M, Monserrat O, Iglesias R and Crippa B (2010) Persistent scatterer interferometry. *Photogrammetric Engineering & Remote Sensing* 76: 1061-1069.
- Cruden DM (1991) A simple definition of a landslide. *Bulletin of Engineering Geology and the Environment* 43: 27-29.
- Cruden DM and Varnes DJ (1996) Landslides: Investigation and mitigation. Chapter 3-landslide types and processes. *Transportation research board special report*.
- D'Elia B (1991) Deformation problems in the Italian structurally complex clay soils. *Proc, 10th Europ Conf on Soil Mech and Found Eng*, pp 1159-1170
- Del Soldato M, Di Martire D and Tomás Jover R (2016a) Comparison of different approaches for landslide-induced damage assessment: The case study of Agnone (southern Italy). *Rendiconti Online Società Geologica Italiana* 41: 139-142. doi: 10.3301/ROL.2016.113
- Del Soldato M, Segoni S, De Vita P, Pazzi V, Tofani V and Moretti S (2016c) Thickness model of pyroclastic soils along mountain slopes of Campania (southern Italy). *Landslides and Engineered Slopes Experience, Theory and Practice: Proceedings of the 12th International Symposium on Landslides (Napoli, Italy, 12-19 June 2016)*, CRC Press, pp 797-804
- Del Ventisette C, Righini G, Moretti S and Casagli N (2014) Multitemporal landslides inventory map updating using spaceborne sar analysis. *International Journal of Applied Earth Observation and Geoinformation* 30: 238-246.
- Dewitte O, Jasselette J-C, Cornet Y, Van Den Eeckhaut M, Collignon A, Poesen J and Demoulin A (2008) Tracking landslide displacements by multi-temporal dtms: A combined aerial stereophotogrammetric and lidar approach in western Belgium. *Engineering Geology* 99: 11-22.
- Di Martire D, De Rosa M, Pesce V, Santangelo MA and Calcaterra D (2012) Landslide hazard and land management in high-density urban areas of Campania region, Italy. *Natural Hazards and Earth System Sciences* 12: 905-926.
- Di Martire D, Iglesias R, Monells D, Centolanza G, Sica S, Ramondini M, Pagano L, Mallorquí JJ and Calcaterra D (2014) Comparison between differential sar interferometry and ground measurements data in the displacement monitoring of the earth-dam of Conza della Campania (Italy). *Remote Sensing of Environment* 148: 58-69.
- Doneus M, Verhoeven G, Fera M, Briese C, Kucera M and Neubauer W (2011) From deposit to point cloud—a study of low-cost computer vision approaches for the straightforward documentation of archaeological excavations. *Geoinformatics FCE CTU* 6: 81-88.
- Duro J, Inglada J, Closa J, Adam N and Arnaud A (2004) High resolution differential interferometry using time series of ers and Envisat sar data. *FRINGE 2003 Workshop*, pp 72
- Esu F (1977) Behaviour of slopes in structurally complex formations. *Proceedings of the international symposium on the geotechnics of structurally complex formations*, pp 292-304
- Farina P, Colombo D, Fumagalli A, Marks F and Moretti S (2006) Permanent scatterers for landslide investigations: Outcomes from the esa-slam project. *Engineering Geology* 88: 200-217.
- Farr TG (1993) Radar interactions with geologic surfaces. *Guide to Magellan Image Interpretation*, pp 45
- Ferretti A, Fumagalli A, Novali F, Prati C, Rocca F and Rucci A (2011) A new algorithm for processing interferometric data-stacks: Squeesar. *IEEE Transactions on Geoscience and Remote Sensing* 49: 3460-3470.
- Ferretti A, Prati C and Rocca F (2000) Nonlinear subsidence rate estimation using permanent scatterers in differential sar interferometry. *IEEE Transactions on Geoscience and Remote Sensing* 38: 2202-2212.

- Ferretti A, Prati C and Rocca F (2001) Permanent scatterers in sar interferometry. *Geoscience and Remote Sensing, IEEE Transactions on* 39: 8-20.
- Filocamo F, Roskopf CM, Amato V, Cesarano M and Di Paola G (2015) The integrated exploitation of the geological heritage: A proposal of geotourist itineraries in the alto molise area (italy). *Rend Online Soc Geol It* 33: 44-47. doi: 10.3301/ROL.2015.11
- Fisher RB, Breckon TP, Dawson-Howe K, Fitzgibbon A, Robertson C, Trucco E and Williams CK (2013) *Dictionary of computer vision and image processing*. John Wiley & Sons,
- Freeman TJ, Littlejohn GS and Driscoll RM (1994) *Has your house got cracks?: A guide to subsidence and heave of buildings on clay*. Thomas Telford,
- Funning GJ, Parsons B and Wright TJ (2007) Fault slip in the 1997 manyi, tibet earthquake from linear elastic modelling of insar displacements. *Geophysical Journal International* 169: 988-1008.
- Furukawa Y and Ponce J (2010) Accurate, dense, and robust multiview stereopsis. *Pattern Analysis and Machine Intelligence, IEEE Transactions on* 32: 1362-1376.
- Gabriel AK, Goldstein RM and Zebker HA (1989) Mapping small elevation changes over large areas: Differential radar interferometry. *Journal of Geophysical Research: Solid Earth* 94: 9183-9191.
- García-Ruiz JM, Nadal-Romero E, Lana-Renault N and Beguería S (2013) Erosion in mediterranean landscapes: Changes and future challenges. *Geomorphology* 198: 20-36.
- Giannini E, Lazzarotto A and Signorini R (1971) Lineamenti di stratigrafia e tettonica della toscana meridionale. *Rend Soc It Min Petr* 27: 75-89.
- Giordan D, Allasia P, Manconi A, Baldo M, Santangelo M, Cardinali M, Corazza A, Albanese V, Lollino G and Guzzetti F (2013) Morphological and kinematic evolution of a large earthflow: The montaguto landslide, southern italy. *Geomorphology* 187: 61-79.
- Godt J, Coe J and Savage W (2000) Relation between cost of damaging landslides and construction age, alameda county, california, USA, el niño winter storm season, 1997–98. *Landslides, Proceedings of 8th international symposium on landslides, Cardiff, Wales*, pp 26-30
- Goetz JN, Guthrie RH and Brenning A (2011) Integrating physical and empirical landslide susceptibility models using generalized additive models. *Geomorphology* 129: 376-386.
- Grünthal G (1998) *European Macroseismic Scale 1998 (EMS-98)*. European Seismological Commission, subcommission on Engineering Seismology, working Group Macroseismic Scales. Conseil de l'Europe, Cahiers du Centre Européen de Géodynamique et de Séismologie, 15, Luxembourg.
- Guadagno F, Palmieri M, Siviero V and Vallario A (1987) La frana del febbraio 1984 in località fonte griciata nel comune di agnone (isernia). *Mem Soc Geol It* 37: 127-134.
- Gullà G, Peduto D, Borrelli L, Antronico L and Fornaro G (2016) Geometric and kinematic characterization of landslides affecting urban areas: The lungro case study (calabria, southern italy). *Landslides*: 1-18.
- Guzzetti F, Mondini AC, Cardinali M, Fiorucci F, Santangelo M and Chang K-T (2012) Landslide inventory maps: New tools for an old problem. *Earth-Science Reviews* 112: 42-66.
- Hanssen RF (2001) *Radar interferometry: Data interpretation and error analysis*. Springer Science & Business Media,
- Hapke C (2005) Estimation of regional material yield from coastal landslides based on historical digital terrain modelling. *Earth Surface Processes and Landforms* 30: 679-697.
- Hartley R and Zisserman A (2003) *Multiple view geometry in computer vision*. Cambridge university press,
- Heim A (1932) *Bergsturz und menschenleben*. Fretz & Wasmuth,
- Herrera G, Davalillo J, Mulas J, Cooksley G, Monserrat O and Pancioli V (2009) Mapping and monitoring geomorphological processes in mountainous areas using psi data: Central pyrenees case study. *Nat Hazards Earth Syst Sci* 9: 1587-1598.
- Herrera G, Gutiérrez F, García-Davalillo J, Guerrero J, Notti D, Galve J, Fernández-Merodo J and Cooksley G (2013) Multi-sensor advanced dinsar monitoring of very slow landslides: The tena valley case study (central spanish pyrenees). *Remote Sensing of Environment* 128: 31-43.
- Hoek E and Bray JD (1981) *Rock slope engineering*. CRC Press,
- Hooper A (2008) A multi-temporal insar method incorporating both persistent scatterer and small baseline approaches. *Geophysical Research Letters* 35.

- Hooper A, Bekaert D, Spaans K and Arkan M (2012) Recent advances in sar interferometry time series analysis for measuring crustal deformation. *Tectonophysics* 514: 1-13.
- Hooper A, Segall P and Zebker H (2007) Persistent scatterer interferometric synthetic aperture radar for crustal deformation analysis, with application to volcán alcedo, galápagos. *Journal of Geophysical Research: Solid Earth* 112.
- Hooper A, Zebker H, Segall P and Kampes B (2004) A new method for measuring deformation on volcanoes and other natural terrains using insar persistent scatterers. *Geophysical research letters* 31.
- Hsieh Y-C, Chan Y-C and Hu J-C (2016) Digital elevation model differencing and error estimation from multiple sources: A case study from the meiyuan shan landslide in taiwan. *Remote Sensing* 8: 199.
- Hungr O, Leroueil S and Picarelli L (2014) The varnes classification of landslide types, an update. *Landslides* 11: 167-194. doi: 10.1007/s10346-013-0436-y
- Hunt RE (2005) *Geotechnical engineering investigation handbook*. Crc Press,
- Hutchinson J (1989) General report: Morphological and geotechnical parameters of landslides in relation to geology and hydrogeology: Proc 5th international symposium on landslides, lausanne, 10–15 july 1988v1, p3–35. Publ rotterdam: Aa balkema, 1988. *International Journal of Rock Mechanics and Mining Sciences & Geomechanics Abstracts*, Pergamon, pp 88
- Iovine G and Parise M (2002) Schema illustrato per la classificazione ed il rilievo dei danni da frana in aree urbane. *Memorie Società Geologica Italiana* 57: 595-603.
- Italian Ministry of the Environment and Protection of Land and Sea (MATTM) (2010) Piano Straordinario di Telerilevamento Ambientale (PSTA); Linee guida per l'analisi dei dati interferometrici satellitari in aree soggette a dissesti idrogeologici; MATTM: Rome, Italy, 2010; p. 108.
- James MR and Robson S (2014) Mitigating systematic error in topographic models derived from uav and ground-based image networks. *Earth Surface Processes and Landforms* 39: 1413-1420.
- Jebara T, Azarbajehani A and Pentland A (1999) 3d structure from 2d motion. *Signal Processing Magazine, IEEE* 16: 66-84.
- Jennings J and Kerrich J (1962) The heaving of buildings and the associated economic consequences with particular reference to the orange free state goldfields. *Civil Engineer in South Africa, Transactions of the South African Institute of Civil Engineering* 4: 221-248.
- Jongmans D, Renalier F, Knies U, Schwartz S, Pathier E, Orengo Y, Bièvre G, Villemin T and Delacourt C (2008) Characterization of the avignonet landslide (french alps) using seismic techniques. *10th International Symposium on Landslides and Engineered Slopes*, Taylor & Francis, pp 395-401
- Kampes BM and Adam N (2006) The stun algorithm for persistent scatterer interferometry. *Fringe 2005 Workshop*,
- Lacerda WA (2007) Landslide initiation in saprolite and colluvium in southern brazil: Field and laboratory observations. *Geomorphology* 87: 104-119.
- Lagios E, Papadimitriou P, Novali F, Sakkas V, Fumagalli A, Vlachou K and Del Conte S (2012) Combined seismicity pattern analysis, dgps and psinsar studies in the broader area of cephalonia (greece). *Tectonophysics* 524: 43-58.
- Lagios E, Sakkas V, Novali F, Bellotti F, Ferretti A, Vlachou K and Dietrich V (2013) Squeesar™ and gps ground deformation monitoring of santorini volcano (1992–2012): Tectonic implications. *Tectonophysics* 594: 38-59.
- Lagios E, Sakkas V, Novali F, Fumagalli A and Del Conte S (2011) Ground deformation studies in cephalonia island (western greece) based on dgps & ps interferometry. *Geoscience and Remote Sensing Symposium (IGARSS), 2011 IEEE International*, IEEE, pp 3887-3890
- Lague D, Brodu N and Leroux J (2013) Accurate 3d comparison of complex topography with terrestrial laser scanner: Application to the rangitikei canyon (n-z). *ISPRS Journal of Photogrammetry and Remote Sensing* 82: 10-26. doi: <http://dx.doi.org/10.1016/j.isprsjprs.2013.04.009>
- Lanari R, Casu F, Manzo M, Zeni G, Berardino P, Manunta M and Pepe A (2007) An overview of the small baseline subset algorithm: A dinsar technique for surface deformation analysis. *Pure and Applied Geophysics* 164: 637-661.
- Lanari R, Mora O, Manunta M, Mallorquí JJ, Berardino P and Sansosti E (2004) A small-baseline approach for investigating deformations on full-resolution differential sar interferograms. *IEEE Transactions on Geoscience and Remote Sensing* 42: 1377-1386.
- Lane S, Richards K and Chandler J (1993) Developments in photogrammetry; the geomorphological potential. *Progress in Physical Geography* 17: 306-328.
- Lee E and Moore R (1991) Coastal landslip potential assessment: Isle of wight undercliff. Ventnor. Technical Report

- prepared by Geomorphological Services Ltd for the Department of the Environment, research contract PECD 7/1/272,
- Lucieer A, de Jong S and Turner D (2013) Mapping landslide displacements using structure from motion (sfm) and image correlation of multi-temporal uav photography. *Progress in Physical Geography*: 0309133313515293.
- MacLeod I and Littlejohn G (1974) Discussion on session 5. Conf on Settlement of Structures, Cambridge, Pentech Press London, pp 792-795
- Mansour MF, Morgenstern NR and Martin CD (2011) Expected damage from displacement of slow-moving slides. *Landslides* 8: 117-131. doi: 10.1007/s10346-010-0227-7
- Manzo M, Ricciardi G, Casu F, Ventura G, Zeni G, Borgström S, Berardino P, Del Gaudio C and Lanari R (2006) Surface deformation analysis in the ischia island (italy) based on spaceborne radar interferometry. *Journal of Volcanology and Geothermal Research* 151: 399-416.
- Massonnet D and Feigl KL (1998) Radar interferometry and its application to changes in the earth's surface. *Reviews of geophysics* 36: 441-500.
- Massonnet D, Rossi M, Carmona C, Adragna F, Peltzer G, Feigl K and Rabaute T (1993) The displacement field of the landers earthquake mapped by radar interferometry. *Nature* 364: 138-142.
- Maybank S (2012) *Theory of reconstruction from image motion*. Springer Science & Business Media,
- Medvedev SV (1965) *Engineering seismology*.
- Metternicht G, Hurni L and Gogu R (2005) Remote sensing of landslides: An analysis of the potential contribution to geo-spatial systems for hazard assessment in mountainous environments. *Remote Sensing of Environment* 98: 284-303. doi: <http://dx.doi.org/10.1016/j.rse.2005.08.004>
- Mihalinec Z and Ortolan Z (2008) Landslide "granice" in zagreb (croatia). *Proceedings, 10th International Symposium on Landslides and Engineered Slopes, Xi'an, China*, pp 1587-1593
- Mills J, Buckley S, Mitchell H, Clarke P and Edwards S (2005) A geomatics data integration technique for coastal change monitoring. *Earth Surface Processes and Landforms* 30: 651-664.
- Milone G and Scepi G (2011) A clustering approach for studying ground deformation trends in Campania Region through the use of PS-InSAR time series analysis. *Journal of Applied Sciences Research* 11: 610-620.
- Mora O, Mallorqui JJ and Broquetas A (2003) Linear and nonlinear terrain deformation maps from a reduced set of interferometric sar images. *IEEE Transactions on Geoscience and Remote Sensing* 41: 2243-2253.
- Moretti S and Rodolfi G (2000) A typical "calanchi" landscape on the eastern apennine margin (atri, central italy): Geomorphological features and evolution. *Catena* 40: 217-228.
- National Cartographic Portal. Available online: <http://www.pcn.minambiente.it> (accessed on 29 March 2015).
- Nawy EG (1968) Crack control in reinforced concrete structures. *Journal Proceedings*, pp 825-836
- Niethammer U, James M, Rothmund S, Travelletti J and Joswig M (2012) Uav-based remote sensing of the super-sauze landslide: Evaluation and results. *Engineering Geology* 128: 2-11.
- Notti D, Davalillo J, Herrera G and Mora O (2010) Assessment of the performance of x-band satellite radar data for landslide mapping and monitoring: Upper tena valley case study. *Nat Hazards Earth Syst Sci* 10: 1865-1875.
- Notti D, Herrera G, Bianchini S, Meisina C, García-Davalillo JC and Zucca F (2014) A methodology for improving landslide psi data analysis. *International Journal of Remote Sensing* 35: 2186-2214. doi: 10.1080/01431161.2014.889864
- Notti D, Calò F, Cigna F, Manunta M, Herrera G, Berti M, Meisina C, Tapete D and Zucca F (2015) A user-oriented methodology for DInSAR time series analysis and interpretation: Landslides and subsidence case studies. *Pure and Applied Geophysics*, 172(11): 3081-3105.
- Ouchi K (2013) Recent trend and advance of synthetic aperture radar with selected topics. *Remote Sensing* 5: 716.
- Panet M, Vormeringer R, Vigier G and Goodman R (1969) Discussion of graphical stability analysis of slopes in jointed rock. *Journal of Soil Mechanics & Foundations Div*.
- Pascucci V, Merlini S and Martini IP (1999) Seismic stratigraphy of the miocene-pleistocene sedimentary basins of the northern tyrrhenian sea and western tuscan (italy). *Basin Research* 11: 337-356.
- Pasuto M and Soldati A (1990) Some cases of deep-seated gravitational deformations in the area of cortina d'ampezzo (dolomites). *Proceedings of the European Short Course on Applied Geomorphology* 2: 91-104.
- Patacca E, Sartori R and Scandone P (1990) Tyrrhenian basin and apenninic arcs: Kinematic relations since late

tortonian times. *Mem Soc Geol It* 45: 425-451.

Petley D (2012) Global patterns of loss of life from landslides. *Geology* 40: 927-930.

Petley DN and Allison RJ (1997) The mechanics of deep-seated landslides. *Earth Surface Processes and Landforms* 22: 747-758.

Photoscan A (2013) Agisoft photoscan user manual professional edition, version 1.0.0. St Petersburg: Agisoft LLC.

Picarelli L, Urciuoli G, Ramondini M and Comegna L (2005) Main features of mudslides in tectonised highly fissured clay shales. *Landslides* 2: 15-30.

Plank S (2014) Rapid damage assessment by means of multi-temporal sar—a comprehensive review and outlook to sentinel-1. *Remote Sensing* 6: 4870-4906.

Pollefeys M, Koch R and Van Gool L (1999) Self-calibration and metric reconstruction inspite of varying and unknown intrinsic camera parameters. *International Journal of Computer Vision* 32: 7-25.

Pollefeys M, Van Gool L, Vergauwen M, Verbiest F, Cornelis K, Tops J and Koch R (2004) Visual modeling with a hand-held camera. *International Journal of Computer Vision* 59: 207-232.

Pratesi F, Nolesini T, Bianchini S, Leva D, Lombardi L, Fanti R and Casagli N (2015) Early warning gbinsar-based method for monitoring volterra (tuscany, italy) city walls. *IEEE Journal of Selected Topics in Applied Earth Observations and Remote Sensing* 8: 1753-1762.

Radbruch-Hall DH (1978) Gravitational creep of rock masses on slopes. *Rockslides and avalanches* 1: 607-657.

Razak K, Straatsma M, Van Westen C, Malet J-P and De Jong S (2011) Airborne laser scanning of forested landslides characterization: Terrain model quality and visualization. *Geomorphology* 126: 186-200.

Righini G, Pancioli V and Casagli N (2012) Updating landslide inventory maps using persistent scatterer interferometry (psi). *International journal of remote sensing* 33: 2068-2096.

Rizzoli P and Bräutigam B (2014) Radar backscatter modeling based on global tandem-x mission data. *IEEE Transactions on Geoscience and Remote Sensing* 52: 5974-5988.

Rodolfi G, Frascati F (1979) Cartografia di base per la programmazione degli interventi in aree marginali—Area rappresentativa dell'Alta Val D'Éra. *Memorie illustrative della carta geomorfologica*. *Ann Ist Sper Dif Suolo* 10:37-80

Rosi A, Agostini A, Tofani V and Casagli N (2014) A procedure to map subsidence at the regional scale using the persistent scatterer interferometry (psi) technique. *Remote Sensing* 6: 10510-10522.

Rybár J (1997) Increasing impact of anthropogenic activities upon natural slope stability. *Proceedings of the International Symposium on Engineering Geology and the Environment*, pp 23-27

Sabelli R, Cecchi G and Esposito A (2012) *Mura etrusche di volterra. Conservazione e valorizzazione*. Bientina, Ita.: La Grafica Pisana, Italy,

Sanabria M, Guardiola-Albert C, Tomás Jover R, Herrera García G, Prieto Á, Sánchez H and Tessitore S (2014) Subsidence activity maps derived from dinsar data: Orihuela case study.

Santaloia F, Cotecchia F and Polemio M (2001) Mechanics of a tectonized soil slope: Influence of boundary conditions and rainfall. *Quarterly journal of engineering geology and hydrogeology* 34: 165-185.

Schmidt DA and Bürgmann R (2003) Time-dependent land uplift and subsidence in the santa clara valley, california, from a large interferometric synthetic aperture radar data set. *Journal of Geophysical Research: Solid Earth* 108.

Schuster RL (1996) Socioeconomic significance of landslides. *Landslides: Investigation and Mitigation* Washington (DC): National Academy Press Transportation Research Board Special Report 247: 12-35.

Schuster RL and Fleming RW (1986) Economic losses and fatalities due to landslides. *Bulletin of the Association of Engineering Geologists* 23: 11-28.

Scott K, Pringle P and Vallance J (1992) Sedimentology, behavior, and hazards of debris flows at mount ranier, washington. Available from Books and Open Files Reports Section, USGS Box 25425, Denver, CO 80225 USGS Open File Report 90-385, 1992 106 p, 21 fig, 8 tab, 123 ref, 1 plate.

Segoni S, Rossi G and Catani F (2012) Improving basin scale shallow landslide modelling using reliable soil thickness maps. *Natural hazards* 61: 85-101.

Singleton A, Li Z, Hoey T and Muller JP (2014) Evaluating sub-pixel offset techniques as an alternative to d-insar for monitoring episodic landslide movements in vegetated terrain. *Remote Sensing of Environment* 147: 133-144. doi: <http://dx.doi.org/10.1016/j.rse.2014.03.003>

Skempton AW and MacDonald DH (1956) The allowable settlements of buildings. *Proceedings of the Institution of Civil Engineers* 5: 727-768.

- Slama CC, Theurer C and Henriksen SW (1980) Manual of photogrammetry. American Society of photogrammetry,
- Snavely N, Seitz SM and Szeliski R (2008) Modeling the world from internet photo collections. *International Journal of Computer Vision* 80: 189-210.
- Stini J (1910) *Die muren*. Verlag der Wagner'shen Universitätsbuchhandlung, Innsbruck (Debris flows, English translation by M Jakob and N Skermer, 1997, EBA Engineering Consultants, Vancouver, Canada, 106p).
- Strozzi T, Wegmuller U, Keusen HR, Graf K and Wiesmann A (2006) Analysis of the terrain displacement along a funicular by sar interferometry. *IEEE Geoscience and Remote Sensing Letters* 3: 15-18.
- Szeliski R (2010) *Computer vision: Algorithms and applications*. Springer Science & Business Media,
- Tarchi D, Casagli N, Fanti R, Leva DD, Luzi G, Pasuto A, Pieraccini M and Silvano S (2003) Landslide monitoring by using ground-based sar interferometry: An example of application to the tessina landslide in italy. *Engineering Geology* 68: 15-30.
- Tarquini S, Vinci S, Favalli M, Doumaz F, Fornaciai A and Nannipieri L (2012) Release of a 10-m-resolution dem for the italian territory: Comparison with global-coverage dems and anaglyph-mode exploration via the web. *Computers & geosciences* 38: 168-170.
- Terrenato N (1998) Tam firmum municipium: The romanization of volaterrae and its cultural implications. *Journal of Roman Studies* 88: 94-114.
- Terzaghi K (1950) *Geologic aspects of soft-ground tunneling*.
- Terzaghi K and Peck RB (1948) *Soil mechanics in engineering practice*.
- Tofani V, Raspini F, Catani F and Casagli N (2013) Persistent scatterer interferometry (psi) technique for landslide characterization and monitoring. *Remote Sensing* 5: 1045-1065.
- Tofani V, Segoni S, Agostini A, Catani F and Casagli N (2013) Technical note: Use of remote sensing for landslide studies in europe. *Natural Hazards and Earth System Sciences* 13: 299-309.
- Tomás R, Cano M, García-Barba J, Vicente F, Herrera G, Lopez-Sanchez JM and Mallorquí J (2013) Monitoring an earthfill dam using differential sar interferometry: La pedrera dam, alicante, spain. *Engineering geology* 157: 21-32.
- Tomás R, Romero R, Mulas J, Marturà JJ, Mallorquí JJ, López-Sánchez JM, Herrera G, Gutiérrez F, González PJ and Fernández J (2014) Radar interferometry techniques for the study of ground subsidence phenomena: A review of practical issues through cases in spain. *Environmental earth sciences* 71: 163-181.
- Tralli DM, Blom RG, Zlotnicki V, Donnellan A and Evans DL (2005) Satellite remote sensing of earthquake, volcano, flood, landslide and coastal inundation hazards. *ISPRS Journal of Photogrammetry and Remote Sensing* 59: 185-198. doi: <http://dx.doi.org/10.1016/j.isprsjprs.2005.02.002>
- Turner D, Lucieer A and Watson C (2012) An automated technique for generating georectified mosaics from ultra-high resolution unmanned aerial vehicle (uav) imagery, based on structure from motion (sfm) point clouds. *Remote Sensing* 4: 1392-1410.
- Ullman S (1979) *The interpretation of visual motion*. Massachusetts Inst of Technology Pr,
- Uzielli M, Catani F, Tofani V and Casagli N (2015) Risk analysis for the ancona landslide—ii: Estimation of risk to buildings. *Landslides* 12: 83-100.
- Van Rooy J (1989) A new proposed classification system for dolomitic areas south of pretoria. *Contributions to engineering geology* 1: 57-65.
- Van Westen CJ (2013) *Remote sensing and gis for natural hazards assessment and disaster risk management*. Schroder JF and Bishop MP *Treatise on Geomorphology* Academic Press, Elsevier, San Diego: 259-298.
- Varnes DJ (1978) *Slope movement types and processes*. Transportation Research Board Special Report.
- Verhoeven G (2011) Taking computer vision aloft—archaeological three-dimensional reconstructions from aerial photographs with photoscan. *Archaeological Prospection* 18: 67-73.
- Verhoeven G, Taelman D and Vermeulen F (2012) Computer vision-based orthophoto mapping of complex archaeological sites: The ancient quarry of pitaranha (portugal-spain). *Archaeometry* 54: 1114-1129.
- Vezzani L, Ghisetti F, Festa A and Follador U (2004) *Carta geologica del molise*. SELCA,
- Wasowski J, Lollino P, Limoni P, Del Gaudio V, Lollino G and Gostelow P (2004) Towards an integrated field and eo-based approach for monitoring peri-urban slope instability. *Landslides: evaluation and stabilization Ninth international symposium on landslides AA Balkema Publishers, Leiden*, pp 809-816

Webster TL and Dias G (2006) An automated gis procedure for comparing gps and proximal lidar elevations. *Computers & geosciences* 32: 713-726.

Werner C, Wegmuller U, Strozzi T and Wiesmann A (2003) Interferometric point target analysis for deformation mapping. *Geoscience and Remote Sensing Symposium, 2003 IGARSS'03 Proceedings 2003 IEEE International, IEEE*, pp 4362-4364

Westoby M, Brasington J, Glasser N, Hambrey M and Reynolds J (2012) 'Structure-from-motion' photogrammetry: A low-cost, effective tool for geoscience applications. *Geomorphology* 179: 300-314.

Wood HO and Neumann F (1931) Modified mercalli intensity scale of 1931. *Seismological Society of America*

WP/WLI (1993) *Multilingual Landslide Glossary*. UNESCO, Working Party on World Landslide Inventory, Bitech Publishers, Richmond

Wu C and Qiao J (2009) Relationship between landslides and lithology in the three gorges reservoir area based on gis and information value model. *Frontiers of Forestry in China* 4: 165-170.

Wu T, Tang W and Einstein H (1996) *Landslide hazard and risk assessment*. Landslides Investigation and mitigation Transportation Research Board Special Report National Academy Press, Washington: 106-118.

Wu X, Chen X, Zhan FB and Hong S (2015) Global research trends in landslides during 1991–2014: A bibliometric analysis. *Landslides* 12: 1215-1226. doi: 10.1007/s10346-015-0624-z

Xu W and Cumming I (1996) Unwrapping the difficult sardegna interferogram. *ESA Workshop on Applications of ERS SAR Interferometry, Fringe*,

Yin J-H, Zhu H-H and Jin W (2008) Monitoring of soil nailed slopes and dams using innovative technologies. *Landslides and engineered slopes: from the past to the future Proceedings of the tenth international symposium on landslides and engineered slopes Taylor & Francis, Xi'an*, pp 1361-1366

Zaruba Q and Ménci V (1969) *Landslides and their control: Nueva york*. Landslides and their control: Nueva York: Elsevier y Academia de Ciencia de Checoslovaquia.

Zebker H and Shanker A (2008) Geodetic imaging with time series persistent scatterer insar. *AGU Fall Meeting Abstracts*, pp 02

Zhang Q, Wang L, Zhang X, Huang G, Ding X, Dai W and Yang W (2008) Application of multi-antenna gps technique in the stability monitoring of roadside slopes. *Landslides and engineered slopes: from the past to the future Proceedings of the tenth international symposium on landslides and engineered slopes Taylor & Francis, Xi'an*, pp 1367-1372